

Copyright is owned by the Author of the thesis. Permission is given for a copy to be downloaded by an individual for the purpose of research and private study only. The thesis may not be reproduced elsewhere without the permission of the Author.

SMART ELECTROCHEMICAL SENSING SYSTEM FOR THE REAL TIME DETECTION OF ENDOCRINE DISRUPTING COMPOUNDS AND HORMONES

A thesis presented in partial fulfilment of the
requirements for the degree of
Doctor of Philosophy
in
Electronics Engineering
at Massey University, Manawatu,
New Zealand

ASIF IQBAL ZIA

**30th October,
2014**

Dedications

In the name of Allah the most beneficent and the most merciful

To my parents

Mr Sher Afzal Zia

Mrs Shamim Akhter

To my wife

Mrs Nazia Asif

&

To my boys

Muhammad Shaheryar Asif

Muhammad Asfandyar Asif

Muhammad Abdur-Rehman Bin Asif

Abstract

Presented research work has not only provided a real-time tool to perform week-long chemical and bio-chemical assays in minutes yet, it had been operating as a source of community awareness about the said chemicals that we keep ingesting knowing or unknowingly. Phthalates are the most ubiquitous chemicals that pose a grave danger to the human race due to their extraordinary use as plasticizer in consumer product industry. All contemporary detection methods require high level of skills, expensive equipment and long analysis time as compared to the technique presented in this research work that introduces a real time non-invasive assay. A novel type of silicon substrate based smart interdigital sensor fabricated by employing thin film micro-electromechanical system semiconductor device fabrication technology. Electrochemical Impedance Spectroscopy was used in conjunction with the fabricated sensor to detect hormones and phthalates in deionized water. Various concentrations of phthalates as low as 2 parts per billion to a higher level of 2 parts per million in deionized water were detected distinctively using new planar ID sensor based EIS sensing system. The sensor was functionalized by a self-assembled monolayer of 3-aminopropyltriethoxysilane with embedded molecular imprinted polymer to introduce selectivity for the phthalate molecule. Spectrum analysis algorithm interpreted the experimentally obtained impedance spectra by applying complex nonlinear least square curve fitting in order to obtain electrochemical equivalent circuit and corresponding circuit parameters describing the kinetics of the electrochemical cell. Principal component analysis was applied to deduce the effects of surface immobilized molecular imprinted polymer layer on the evaluated circuit parameters and its electrical response. The results obtained by the testing system were validated using commercially available high performance liquid chromatography diode array detector system.

Research Outputs

The research outputs which have been published are listed below. The research outputs are in conjunction with the author's PhD candidacy:

Journals

1. **A. I. Zia**, S. C. Mukhopadhyay, P.-L. Yu, I. Al-Bahadly, C. P. Gooneratne, and J. Kosel, "Rapid and molecular selective electrochemical sensing of phthalates in aqueous solution," *Biosensors and Bioelectronics*, **2014**.
<http://www.sciencedirect.com/science/article/pii/S0956566314006460>
2. **A. Zia**, S. Mukhopadhyay, P. Yu, I. Al-Bahadly, C. Gooneratne, and J. Kosel, "Post Annealing Performance Evaluation of Printable Interdigital Capacitive Sensors by Principal Component Analysis," *Sensors Journal, IEEE*, vol. 67, pp. 342-349, **2014**.
3. **A. I. Zia**, M. S. A. Rahman, S. C. Mukhopadhyay, P.-L. Yu, I. Al-Bahadly, C. P. Gooneratne, J. Kosel, and T.-S. Liao, "Technique for rapid detection of phthalates in water and beverages," *Journal of Food Engineering*, vol. 116, pp. 515-523, **2013**.
4. **A. I. Zia**, A. M. Syaifudin, S. Mukhopadhyay, P. Yu, I. Al-Bahadly, C. P. Gooneratne, J. Kosel, and T.-S. Liao, "Electrochemical impedance spectroscopy based MEMS sensors for phthalates detection in water and juices," *Journal of Physics*: vol. 439, p. 012026, **2013**.

Proceedings and Conference Papers

1. **A. I. Zia**, S. C. M. P.L.Yu, I. H. Al Bahadly, "Development and evaluation of portable low cost testing system for phthalates ," in *eighth International Conference on Sensing Technology (ICST)*, 2014, S2IS, vol. 7, pp. 385 – 391

2. **A. I. Zia**, S. C. Mukhopadhyay, P.-L. Yu, I. Al-Bahadly, C. P. Gooneratne, and J. Kosel, Poster presentation for "Rapid and molecular selective electrochemical sensing of phthalates in aqueous solution," 24th Anniversary World Congress on Biosensors, 27-30 May 2014, Melbourne, Australia.
3. **A. I. Zia**, S. Mukhopadhyay, I. Al-Bahadly, P. Yu, C. P. Gooneratne, and J. Kosel, "Introducing molecular selectivity in rapid impedimetric sensing of phthalates," in *Instrumentation and Measurement Technology Conference (I2MTC) Proceedings, 2014 IEEE International*, 2014, pp. 838-843
4. **A. I. Zia**, A. R. Mohd Syaifudin, S. C. Mukhopadhyay, I. H. Al-Bahadly, P. L. Yu, C. P. Gooneratne, J. Kosel, and T.-S. Liao, "MEMS based impedimetric sensing of phthalates," in *Instrumentation and Measurement Technology Conference (I2MTC), 2013 IEEE International*, 2013, pp. 855-860.
5. **A. I. Zia**, S. C. M. P.L.Yu, I. H. Al Bahadly, "Ovarian Hormone Estrone Glucuronide (E1G) Quantification- Impedimetric Electrochemical Spectroscopy Approach," in *Seventh International Conference on Sensing Technology (ICST), 2013*, 2013, pp. 22 - 27.
6. A. Syaifudin, **A. I. Zia**, S. Mukhopadhyay, P. Yu, C. P. Gooneratne, and J. Kosel, "Improved detection limits of bacterial endotoxins using new type of planar interdigital sensors," in *Sensors, 2012 IEEE*, 2012, pp. 1-4.
7. **A. I. Zia**, A. Mohd Syaifudin, S. Mukhopadhyay, P. Yu, I. Al-Bahadly, J. Kosel, and C. Gooneratne, "Sensor and instrumentation for progesterone detection," in *Instrumentation and Measurement Technology Conference (I2MTC), 2012 IEEE International*, 2012, pp. 1220-1225.

8. **Asif. I. Zia**, A.R. Mohd Syaifudin, S.C. Mukhopdhyay, I. H. Al-Bahadly and P.L. Yu, C.P. Gooneratne and Jürgen Kosel. “*Development of Electrochemical Impedance Spectroscopy Based Sensing System for DEHP Detection*”. Proceeding of 5th International Conference on Sensing Technology (ICST 2011), Palmerston North, New Zealand. pp. 703 – 711. 28th Nov – 1st Dec 2011. IEEE Catalog Number: CFP1118E-CDR. ISBN: 978-1-4577-0167-2.

Seminars

- 1 “Real-time low-cost assay for the selective detection of endocrine disrupting compounds and hormones.” Programme of Massey University Pakistani Students Association, Postgraduate Student Presentations, 28th – 29th October, 2014, Massey University, Palmerston North New Zealand.
- 2 “Development and evaluation of portable low cost testing system for the selective detection of endocrine disrupting compounds and hormones” Programme of IEEE Central Section, New Zealand Chapter IEEE Student Presentations, 18th September, 2014, Victoria University, Wellington, New Zealand.
- 3 “Post anneal performance evaluation of interdigital capacitive sensors for the selective detection of endocrine disrupting compounds and hormones” Electronics, Information and Communication System (EICS) Seminar, 30th July 2014. School of Engineering and Advanced Technology, Massey University, Palmerston North. New Zealand.
- 4 “Electrochemical Impedance Spectroscopy; a rapid detection tool for reproductive hormones and toxins” Electronics, Information and Communication System (EICS) Seminar, 15th September 2013. School of Engineering and Advanced Technology, Massey University, Palmerston North. New Zealand.
- 5 “Electrochemical capacitive sensing of alcohol in human breath ” Programme of IEEE Instrumentation and Measurement Society New

Zealand Chapter Workshop on Smart Sensors, 18th -19th February, 2013, University of Waikato, Hamilton, New Zealand.

- 6 “Detection of Phthalates in water and beverages; interdigital sensors based electrochemical impedance spectroscopy approach” Programme of IEEE Central Section, New Zealand Chapter IEEE Student Presentations, 7th September, 2012, Massey University, Palmerston North New Zealand.
- 7 “Phthalates detection in using interdigital sensors based system” Electronics, Information and Communication System (EICS) Seminar, 2nd August 2012. School of Engineering and Advanced Technology, Massey University, Palmerston North. New Zealand.
- 8 “Improvements in detection limits for phthalates in aqua baverages ” Programme of IEEE Instrumentation and Measurement Society New Zealand Chapter. Workshop on applications to agriculture and environment monitoring, 11th -12th April, 2012, Lincoln University, Christchurch, New Zealand.
- 9 “Smart sensing system for detection of reproductive hormones and toxins” PhD confirmation seminar. 20th October 2011. School of Engineering and Advanced Technology, Massey University, Palmerston North. New Zealand.
- 10 “A review of Smart materials and sensors for energy harvesting applications” Programme of IEEE Instrumentation and Measurement Society New Zealand Chapter Workshop on Sensors and Instrumentation in Environmental Health and Agriculture Applications, 1st ,2nd September, 2010, Massey University, Wellington.

Awards

1. HEC, Govt. of Pakistan Doctoral Scholarship Award, January 2010
2. Cash Award US\$750 travel grant for paper presentation, "Introducing molecular selectivity in rapid impedimetric sensing of phthalates," in *Instrumentation and Measurement Technology Conference (I2MTC) held in Montevideo, Uruguay 12-15 May 2014.*

Acknowledgements

All praises and thanks are for Allah the All-Mighty for His blessing and benevolence.

I wish to acknowledge the people who have helped and supported me throughout the Ph.D program and also their contributions towards the completion of the thesis.

I would like to express my deepest gratitude to Professor Dr Subhas Chandra Mukhopadhyay, Associate Professor Dr. Pak-Lam Yu and Associate Professor Dr. Ibrahim Al-Bahadly for their support and supervisions. Thank you for the invaluable guidance, constructive criticisms and opinions and constant encouragement throughout this study.

I would like to express my sincere thanks to Dr. Chinthaka Gooneratne, Dr. Jürgen Kosel, Dr. Amri Mohd Yunus, Dr. Muhammad Syaifuddin, Mr. Hemant Ghayvat , Mrs. Li (Shelly) Xie, Miss Apeksha Rao and Mr. Anindya Nag for their active collaborations in the research. Also, to Mrs. Michele Wagner, Ms. Trish O’Grady, Mrs. Ann-Marie Jackson, Mrs. Judy, Ms. Julia Good, Mr. Ken Mercer, Mr. Collin Plaw, Mr. Bruce Collins, Mr. Doug, Mr. John Sykes, Mr. John Edwards, Mr. Ian Thomas, Mrs. Lisa Lightband, Mr. Conal Hodgetts and Mr. Brendon, for your assistance and support during my research were most appreciated.

I want to pay special gratitude to my beloved parents Mr. Sher Afzal Zia and Mrs. Shamim Akhter, siblings Gulnaz, Atif Zia, Iram and Wajahat for their selfless and fruitful prayers, family and friends for their unconditional love and support for my success. Also, I would like to thank Massey University, Higher Education Commission of Pakistan (HEC) and COMSATS University for the financial support and assistance.

Last but not the least; I am indebted to my wife Mrs. Nazia Asif, who has sacrificed her time accompanying me in New Zealand. Thank you for your love, support, patience and encouragement throughout my study. To my lovely and my wonderful boys Sherry, Muhammad and Abdur-Rehman, thank you for your patience and being such wonderful companies through my years of study in New Zealand.

Table of Contents

Abstract.....	iii
Acknowledgements.....	ix
Table of Contents	xi
Table of Figures.....	xv
List of Tables	xix
Abbreviated Terms	xx
Chapter 1 Introduction	1
1.1 Hormones and Endocrine Disrupting Compounds	1
1.2 Receptor–ligand binding assays.....	4
1.2.1 Radio Receptor Assay (RRA)	5
1.2.2 Scintillation Proximity Assay (SPA)	5
1.2.3 Fluorescence Resonance Energy Transfer (FRET).....	6
1.2.4 Fluorescence Polarization (FP)	8
1.2.5 Fluorometric Micro volume Assay (FMAT).....	8
1.2.6 AlphaScreen TM	9
1.2.7 Flow Cytometry	9
1.2.8 Fluorescence Correlation Spectroscopy (FCS)	10
1.3 Immunoassay	10
1.3.1 Surface Plasmon Resonance (SPR).....	12
1.3.2 Total Internal Reflection Fluorescence (TIRF).....	13
1.3.3 Ellipsometry	14
1.3.4 Nuclear Magnetic Resonance Spectroscopy	14
1.3.5 Amperometric Immunosensors	15
1.3.6 Conductimetric Immunosensors.....	15
1.3.7 Surface Acoustic Wave Immunosensors (SAW)	16
1.3.8 Enzyme-linked Immunosorbent Assay (ELISA)	16
1.4 Conclusions	19
1.5 Research Contributions	20
1.6 Organization of the Thesis	21
Chapter 2 Impedance Spectroscopy and Experimental Setup.....	23
2.1 Introduction	23

2.2	Electrochemical Impedance Spectroscopy.....	23
2.2.1	AC bridges	24
2.2.2	Lissajous Curves	24
2.2.3	Fast Fourier Transforms (FFT)	25
2.2.4	Phase Sensitive Detections (PSD).....	25
2.2.5	Frequency Response Analysis (FRA).....	25
2.2.6	Electrochemical Impedance Spectroscopy; Theory and Analyses	27
2.2.7	‘Nyquist’ and ‘Bode’ plots for Impedance Data Analysis.....	30
2.2.8	Randle’s Electrochemical Cell Equivalent Circuit Model.....	31
2.3	Experimental Setup.....	36
2.3.1	Equipment and Instrumentations	36
2.3.2	Fixture and Test Probe Connections	38
2.3.3	RS-232C Interface for 3522-50/3532-50 LCR Hi Tester	39
2.4	Conclusions.....	40
Chapter 3	Novel Interdigital Sensors’ Development	41
3.1	Introduction to Interdigital Sensors.....	41
3.2	Novel Planar Interdigital Sensors	44
3.3	Finite Element Modelling using COMSOL Multiphysics®	45
3.4	Sensors’ Fabrication.....	56
3.5	Sensors’ Profiling and Problem Definition.....	60
3.5.1	Connection Pads Soldering	61
3.6	Performance Evaluation.....	62
3.6.1	Experimental Evaluation.....	62
3.7	Achieving Stability in Sensors’ Performance	64
3.7.1	Post-fabrication Anneal of ID Sensor	65
3.7.2	Results’ Validation.....	67
3.7.3	Complex Nonlinear Least Squares Curve Fitting	69
3.7.4	Principal Component Analysis (PCA)	72
3.7.5	PCA analysis – ECI (30°C – 90°C) anneal	72
3.7.6	PCA analysis – EC2 (91°C – 150°C) anneal.....	74
3.7.7	PCA analysis – EC3 (151°C – 210°C) anneal.....	76
3.8	Conclusions.....	79
Chapter 4	Electrochemical Detection of Hormones.....	81

4.1	Introduction	81
4.2	Detection of Ovarian Hormone Estrone Glucuronide (E1G).....	82
4.2.1	Motivation	82
4.2.2	Point-of-care Methods.....	83
4.2.3	Basal Body Temperature method (BBT)	83
4.2.4	Billings Ovulation Method.....	83
4.2.5	Symptothermal Method (STM).....	83
4.2.6	Ovarian Monitor.....	84
4.2.7	Materials and Methods to Detect E1G	84
4.2.8	Results and Discussions	86
4.2.9	Electrochemical Impedance Spectroscopy Analyses for E1G	88
4.2.10	E1G Sensitivity Analysis	90
4.3	Electrochemical detection of Progesterone Hormone.....	92
4.3.1	Motivation	92
4.3.2	Materials and Methods for Progesterone Detection.....	94
4.3.3	Electrochemical Impedance Analyses for Progesterone	95
4.4	Conclusions	99
Chapter 5	Detection of Endocrine Disrupting Compounds	101
5.1	Introduction	101
5.2	Impedimetric Detection of DEHP and DINP.....	103
5.2.1	Motivation	104
5.2.2	Materials and Methods.....	105
5.2.3	DEHP Detection Test in Deionized Water.....	106
5.2.4	Experimental Data Analyses by CNLS Curve Fitting	108
5.2.5	Sensitivity Analysis – DEHP	110
5.2.6	DEHP Detection in Commercially Sold Energy Drink.....	111
5.2.7	Impedance Measurements of DINP-spiked Ethanol Samples	113
5.2.8	Impedance Measurements of DINP-Spiked Orange Juice.....	115
5.2.9	Conclusions	118
Chapter 6	Inducing Analyte Selectivity in the Sensing System	119
6.1	Introduction	119
6.1.1	Materials and Methods.....	121
6.1.2	Synthesis of DEHP imprinted polymer.....	122

6.1.3	EIS for detection of DEHP in MilliQ.....	125
6.1.4	Results and Discussions	127
6.1.5	Adsorption studies of DEHP to MIP	127
6.1.6	Static Adsorption of DEHP to MIP.....	128
6.1.7	Uptake Kinetics of MIP Coated Sensor to DEHP.....	129
6.1.8	Data Analyses Using Non-linear Least Square Curve fitting	130
6.1.9	Results validation by HPLC.....	132
6.1.10	DEHP in Energy Drink – MIP Coated Sensor	134
6.1.11	Conclusions.....	136
Chapter 7	Conclusions and Future Research	139
7.1	Conclusions.....	139
7.2	Future Work	144
7.2.1	Sensitivity and selectivity Improvement.....	144
7.2.2	Thick Film Electrodes	144
7.2.3	Substrate Type.....	145
Bibliography	147

Table of Figures

Figure 1.1 The endocrine system in human body	1
Figure 1.2 Leaching of DEHP and DEP from tetra packaging within expiry date of orange packaged orange juice[11]	3
Figure 1.3 Types of phthalates used in industrial sector as plasticizers	4
Figure 1.4 Basic concept of FRET as photophysical process. (A) The plot shows the dependence of the FRET efficiency on the proximity of the donor-acceptor pair. (B) shows the effect of angle between donor fluorochrome and acceptor molecule on FRET [25]	7
Figure 1.5 Detection principle of SPR technique[38]	13
Figure 1.6 Schematics of a SAW immunosensor [57]	16
Figure 2.1 Formation of Lissajous Figure	25
Figure 2.2 I-V curve for a non-linear system. Pseudo-linearity of the system is achieved by considering a small part of the curve	27
Figure 2.3 Phase shift in current I_t as a response to excitation potential E_t in a linear system	28
Figure 2.4 Flow chart for the measurement and characterization of a material-electrode system by EIS [77]	31
Figure 2.5 Kinetic processes taking place at electrode-electrolyte interface (Randle's cell model)	32
Figure 2.6 Randle's electrochemical cell equivalent circuit model	32
Figure 2.7 Nyquist plot for Randle's electrochemical cell model [79]	34
Figure 2.8 Bode plot for Randle's electrochemical cell model[79]	35
Figure 2.9 Extraction of component parameters from Bode plot[79]	35
Figure 2.10 Laboratory Test bench with Hioki Hi Precision LCR and data acquisition system.	36
Figure 2.11 Hioki (Japan) 3522-50 LCR Hi-tester	37
Figure 2.12 Connecting LCR3522-50/3532-50 to the 9262 Test fixture and developed interdigital sensing system	38
Figure 3.1 Planar interdigital sensor geometry	42
Figure 3.2 Concept of transformation (a) parallel plate capacitor (b) transformation to planar geometry (c) coplanar structure.	43

Figure 3.3 The penetration depth of electric field lines is proportional to the electrode spatial period λ	44
Figure 3.4 Excitation pattern for multi sensing electrode ID sensor geometry	45
Figure 3.5 COMSOL geometric models of ID sensors with 25 μm pitch length	47
Figure 3.6 COMSOL geometric models of ID sensors with 50 μm pitch length	48
Figure 3.7 1-5-50 Sensor structure; Silicon substrate (bottom) MUT (top)	48
Figure 3.8 Potential distribution modelling in COMSOL for (a) 1-5-25, (b) 1-5-50	50
Figure 3.9 Potential distribution modelling in COMSOL for (c) 1-11-25 and (d) 1-11-50 ID sensors	51
Figure 3.10 Modelled Capacitance for ID sensors	52
Figure 3.11 Modelled Capacitance of single ID capacitor feature on each sensor	53
Figure 3.12 Electric field and penetration depth simulation using COMSOL (a) 1-5-25, (b) 1-5-50	54
Figure 3.13 Electric field and penetration depth simulation using COMSOL (c) 1-11-25 and (d) 1-11-50 ID sensors	55
Figure 3.14 1-5-25 sensor: basic design geometry and dimensions	57
Figure 3.15 Interdigital electrode fabrication configurations	57
Figure 3.16 Fabrication process for all four types of sensors	58
Figure 3.17 Steps involved in coating 1 μm passivation layer of Parylene C	59
Figure 3.18 (a) 36 Workable sensors fabricated on one wafer (b) Individual sensor shown against scale	60
Figure 3.19 Impedance characteristics using same sensor before (a) and after (b) soldering	62
Figure 3.20 Cole-Cole plot for 1-1-50B ‘as is’ fabricated sensor’s test in air at 44% humidity and 23.3°C temperature at different times	63
Figure 3.21 Cole-Cole plot for 1-1-50A sensor’s test in air at 44% humidity and 23.3°C temperature at different times	63
Figure 3.22 SEM image of the fabricated electrode shows roughness of electrodes due to DC magnetron sputtering process	65
Figure 3.23 Annealing sensors in vacuum oven in Micro-Suit	67
Figure 3.24 Nyquist plot for EIS during annealing process at 30, 60, 90, 120, 150, 180, and 210 ° C	68
Figure 3.25 Nyquist plot for improved performance annealed sensors at initial temperature and humidity conditions	68

Figure 3.26 SEM image of electrode before (a) and after (b) anneal	69
Figure 3.27 EC1 CNLS equivalent circuit for 30-90°C	71
Figure 3.28 EC1 fitted curve (30-90°C)	71
Figure 3.29 EC2 CNLS equivalent circuit for 91-150°C	71
Figure 3.30 EC2 fitted curve (91-150°C)	71
Figure 3.31 EC3 CNLS equivalent circuit for 151-210°C	71
Figure 3.32 EC3 fitted curve (151-210°C)	71
Figure 3.33 Component Plot ECI (30°C – 90°C) anneal	73
Figure 3.34 Scree Plot ECI (30°C – 90°C) anneal	74
Figure 3.35 Component Plot EC2 (91°C – 150°C) anneal	75
Figure 3.36 Scree Plot EC2 (91°C – 150°C) anneal	76
Figure 3.37 Component Plot EC3 (151°C – 210°C) anneal	77
Figure 3.38 Scree Plot EC3 (151°C – 210°C) anneal	78
Figure 4.1 Mean hormonal values of estrone glucuronide (EIG) (-•-), LH (-□-), and pregnanediol glucuronide (PG) (-△-) by cycle day throughout 78 ovulatory cycles from 25 women [107]	82
Figure 4.2 Dip test method for EIG testing	85
Figure 4.3 Laboratory test bench for EIG testing	86
Figure 4.4 Real and imaginary parts of the measured impedance for EIG	87
Figure 4.5 Nyquist (Cole-Cole) plot for the impedance measurements of EIG	88
Figure 4.6 Electrochemical equivalent circuit extracted by CNLS curve fitting	89
Figure 4.7 CNLS curve fitting of Nyquist plot by spectrum analyser for the highest concentration of EIG 33.33nmol/L.	89
Figure 4.8 %age sensitivity of the real part of impedance (Re).	91
Figure 4.9 %age sensitivity of capacitive reactance (X).	91
Figure 4.10 Progesterone concentration level during 21 days reproductive cycle of dairy cows [12]	92
Figure 4.11 Real and Imaginary Impedance (reactance) characteristics	95
Figure 4.12 Bode plot for progesterone detection in deionized water	96
Figure 4.13 Nyquist plot for progesterone detection in DI water	97
Figure 4.14 $Z_{\text{imag}}(X)$ %Sensitivity	98
Figure 4.15 $Z_{\text{real}}(R_s)$ %Sensitivity	98
Figure 5.1 Molecular structure DEHP	104
Figure 5.2 Molecular structure DINP	104

Figure 5.3 Test bench setup	105
Figure 5.4 Dip-test (bulk)	105
Figure 5.5 Imaginary and real parts of impedance measurements for DEHP dip-test	106
Figure 5.6 Nyquist plot for detection of DEHP in DI water	107
Figure 5.7 Equivalent circuit proposed by CNLS curve fitting	108
Figure 5.8 CNLS curve fitting plot for absolute value of Impedance.	109
Figure 5.9 CNLS curve fitting plot for imaginary value of Impedance.	109
Figure 5.10 CNLS curve fitting plot for phase shift (θ)	109
Figure 5.11 Reactance percentage sensitivity for DEHP in DI water	111
Figure 5.12 Test bench setup for DEHP-spiked energy drinks	112
Figure 5.13 Z_{real} and Z_{imag} for DEHP dip-test of spiked energy drink	112
Figure 5.14 Bode plot showing measured spectra for the spiked drink	113
Figure 5.15 Nyquist plot for DINP concentration test in EtOH	114
Figure 5.16 Real part of impedance for DINP-in-EtOH	115
Figure 5.17 Imaginary Part of Impedance for DINP-in-EtOH	115
Figure 5.18 Real part of measured impedance for DINP in orange juice	116
Figure 5.19 Reactance plot for DINP-in-Orange juice	117
Figure 6.1 Synthesis process of Molecular Imprinted Polymer	120
Figure 6.2 Extraction of template molecule forming molecular recognition site in MIP	120
Figure 6.3 Polymerisation reaction	122
Figure 6.4 Polymerized MIP	122
Figure 6.5 Soxhlet Extraction	123
Figure 6.6 Filter caplet 0.22 μm	123
Figure 6.7 DEHP extracted MIP	124
Figure 6.8 MIP coated sensor using SAM of APTES	124
Figure 6.9 Confocal micrograph image of MIP coated sensor	124
Figure 6.10 Dip Coating process	125
Figure 6.11 Drying in nitrogen flow	125
Figure 6.12 Laboratory test bench setup for MIP coated sensor	126
Figure 6.13 Isotherm for the static adsorption studies of DEHP to MIP	128
Figure 6.14 Isotherm for adsorption uptake kinetics of DEHP to MIP	129
Figure 6.15 Nyquist plot for EIS testing of MIP coated Sensor	130
Figure 6.16 Equivalent circuit estimated by CNLS analysis	131
Figure 6.17 DIONEX-Ultimate 3000 HPLC apparatus	132

Figure 6.18 Absorption spectrum of DEHP	133
Figure 6.19 MIP eluent tested with HPLC for EIS results validation	133
Figure 6.20 DEHP eluent extracted from MIP immobilized on ID sensor	134
Figure 6.21 Nyquist plot for DEHP spiked drink by MIP coated sensor	135
Figure 6.22 HPLC chromatogram showing the DEHP peaks in the eluent extracted out of the functionalized MIP	136
Figure 7.1 New sensor design to overcome heat and stray capacitance problems	145

List of Tables

Table 1.1 Endocrine system's glands, hormones and their function	2
Table 1.2 Advantages and disadvantages of contemporary techniques used for biochemical analytes	18
Table 2.1 Hioki Hi Precision LCR 3522-50 and 3532-50 Specifications	37
Table 2.2 Hioki Hi Precision LCR test terminals description	38
Table 2.3 LCR testing parameters and calculation equations	39
Table 3.1 Geometric design parameters for all four types of modelled ID sensors	46
Table 3.2 Calculated values of capacitance and total electrical energy stored for all four sensors using COMSOL Multiphysics®	52
Table 3.3 Component parameters for the best fit circuit	70
Table 3.4 Table of variance ECI (30°C – 90°C) anneal	73
Table 3.5 Table of variance EC2 (91°C – 150°C) anneal	75
Table 3.6 Table of variance EC3 (151°C – 210°C) anneal	77
Table 4.1 Equivalent circuit components' parameters deduced by CNLS curve fitting technique for electrochemical spectrum analysis	90
Table 4.2 Progesterone in deionized water- Samples' nomenclature and concentration	95
Table 5.1 List of the most ubiquitous EDCs	101
Table 5.2 Risk assessment of phthalates by world agencies [130].	103
Table 5.3 Equivalent circuit parameters evaluated by CNLS algorithm	110
Table 6.1 CNLS curve fitted equivalent circuit parameters	131
Table 6.2 Equivalent circuit parameters evaluated by CNLS fitting for DEHP detection in 'Lift Plus' drink by MIP functionalized sensor	135

Abbreviated Terms

AC	Alternating Current
AFM	Atomic Force Microscope
Alumina-Al₂O₃	Aluminium Oxide
APTES	3-aminopropyltriethoxysilane
Au	Gold
BBP	Butylbenyl phthalate
Bode	Data presentation as a function of frequency
BSA	Bovine serum albumin
C	Capacitance
<i>C_{ad}</i>	Adsorption capacitance
<i>C_{dl}</i>	Double-layer capacitance
CNLS	Complex Non-linear Least Square
CPE	Constant Phase-Element
Cr	Chromium
D	The electric displacement
DBP	Di- <i>n</i> -butyl phthalate
DEHP	Di-(2-ethylhexyl) phthalate
DEP	Di-ethyl phthalate
dH₂O	Distilled water
DINP	Di-isononyl phthalate
DMF	dimethyl formamide
DMP	Di-methyl phthalate
DNA	Deoxyribonucleic Acid
DOP	Di- <i>n</i> -octyl phthalate
DUT	Device Under Test
E	The electric field intensity
EC	Electrolyte Conductivity
EDCs	Endocrine Disrupting Compounds
EDs	Endocrine Disruptors
EIS	Electrochemical Impedance Spectroscopy
ELISA	Enzyme Linked Immunosorbent Assays
EtOH	Ethanol
EU	Endotoxin Unit
<i>f</i>	Frequency
FDA	United States Food and Drug Administration
FR4	Fiberglass reinforced epoxy laminates for PCB fabrication
FTIR	Fourier Transform Infrared Spectroscopy

GND	Electrical ground
H^+	Hydrogen ions
H_{CUR}	Carries the signal current source.
HPLC	High performance liquid Chromatography
HPLC	High Performance Liquid Chromatography
H_{POT}	Monitors the excitation potential, V.
I	Current
IDAM	Interdigitated Array Microelectrode
IDES	Interdigitated Electrode Structures
IDTs	Interdigital Transducers
IS	Impedance Spectroscopy
ISE	Ion-Selective Electrodes
ISFET	Ion-Sensitive Field Effect Transistors
LCR3522-50	Measuring instrument for impedance (inductance, capacitance and resistance) (1mHz to 100kHz)
LCR3532-50	Measuring instrument for impedance (inductance, capacitance and resistance) (42Hz to 5MHz)
L_{CUR}	Accepts the signal current return.
LOD	Limit of Detection
LOD	Limit of Detection
L_{POT}	Connected to the sensor's sensing electrodes
MEMS	Micro-electromechanical Systems
MilliQ	Ultra-pure water which undergo the proses filtration and deionisation that has been characterised in terms of resistivity (typically 18.2 MΩ·cm)
MRL	Minimal Risk Level
MUT	Material Under Test
NaCl	Sodium Chloride
NMR	Nuclear Magnetic Resonance
Nyquist	Data presentation in complex impedance plot
OH^-	Hydroxide ions
PC	Principal Component
PCA	Principal Component Analysis
PCB	Printed Circuit Board
PCR	Polymerase Chain Reaction
PDEs	Partial differential equations

PECVD	Plasma enhanced chemical vapour deposition
PETE	Polyethylene Terephthalate
pH	Potential of Hydrogen
PPB	Parts per billion
PPM	Parts per million
PR	Photo Resist
PVC	Polyvinyl chloride
Q	Charge
θ	Phase Angle, theta
QCM	Quartz Crystal Microbalance
R	Resistance
r^2	Residual mean squares
R_{ct}	Charge/electron transfer resistance
RIE	Reactive ion etching
R_s	Solution resistance
RS232	Serial communication port
SAW	Surface Acoustic Wave
SEAT	School of Engineering and Advanced Technology
SEM	Scanning Electron Microscope
Si	Silicon
Si_3N_4	Silicon Nitride
SiO_2	Silicon Dioxide
SNR	Signal to Noise Ratio
SPR	Surface Plasmon Resonance
SPSS	IBM Statistical Analysis software
σ_ω	Warburg coefficient
TDI	Tolerable Daily Intake
TEOS	Tetraethylorthosilicate
TMAH	Tetra-Methyl Ammonium Hydroxide
UV	Ultra-violet
V	Voltage
W_e	The electrostatic energy density
Z	Impedance
Z_w	Warburg impedance
ω	The angular frequency
ϵ_0	The permittivity of vacuum which sets to be 8.854×10^{-2} F/m
ϵ_r	The relative permittivity
ϵ	The permittivity

Chapter 1 Introduction

1.1 Hormones and Endocrine Disrupting Compounds

The endocrine system in living organisms is made up by the set of cells and glands that produce chemical signals called hormones. Hormones travel through the blood stream to approach respective receptors in the target cells. The major function of the endocrine system is to regulate nutrient supply to all cells, growth and reproduction. Anatomic positions of the glands of endocrine system are shown in Figure 1.1. Each set of glands relates to a specific function in the human body hence behave as a chemical control house to regulate the systematic operation of the other body organs. Table 1.1 provides a detail of the glands forming endocrine system and their function in the human body.

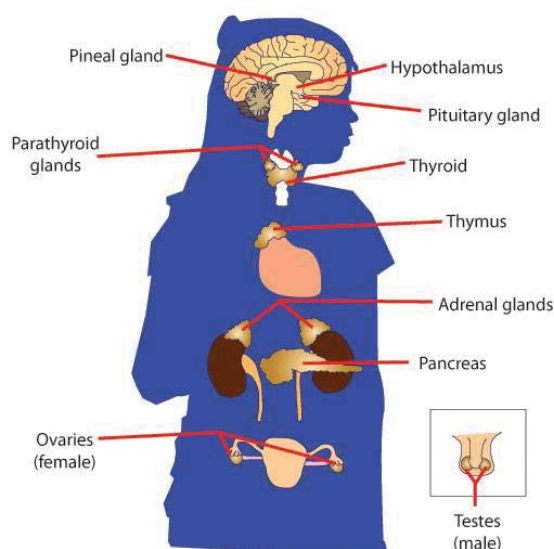


Figure 1.1 The endocrine system in human body

Endocrine Disruptors (EDs) are exogenous chemicals or mixture of chemicals that interfere in the normal functioning of endocrine system and hormones. Among the known endocrine disruptors, the most ubiquitous are esters of 1-2-Benzenedicarboxylic acid commonly known as phthalates. These industrial chemicals have a large number of

commercial uses such as lubricants, additives, solvents, softeners for plastics including food and beverage packaging, cosmetics, insecticides, paints, medical and pharmaceutical applications [1]. Since phthalate esters are not covalently attached to the polyvinyl chloride (PVC) lattice structure, they leach, migrate, and evaporate directly into foodstuffs and atmosphere exposing human beings through ingestion, inhalation and dermal routes [2]. These can directly infuse into body fluids via medication and disposable medical plastic products [3].

Table 1.1 Endocrine system's glands, hormones and their function

Gland	Hormones	Functions in human body
Hypothalamus	Releasing hormones	Stimulate pituitary activity
Pituitary	Trophic (Stimulating)	Stimulate Thyroid, gonadal and pancreatic activities
Thyroid	Thyroid	Regulates metabolism, growth and development
Adrenal	Corticosteroid hormones	Regulate metabolism and behaviour
	Catecholamine	
Pancreas	Insulin and glucagon	Regulate blood sugar level
Gonads	Oestrogens and androgens	Regulate development and growth, reproduction, immunity, onset of puberty, and behaviour

Phthalates have been declared as ubiquitous environmental pollutants and endocrine disruptors by several health monitoring agencies all over the world for carcinogenic and teratogenic effects observed as reproductive and developmental defects in rodents [4, 5]. Published research concludes that phthalates pose highest toxicity and endocrine disruptive threat to the human race, especially to young children, infants, pregnant and nursing mothers [6]. Recent researches have suggested declining trend in the human reproductive hormonal levels, damage to sperm DNA and reduced sperm count in male adults [5]; whereas, elevated risk of altered breast development and breast cancer, premature puberty and prostate changes in females [7, 8]. Leaching of phthalates into food from packaging [9]; from PET (PETE, polyethylene terephthalate) bottles into beverages and mineral water [2] and from corks of glass bottles has been published [10]. Wang et al. [11] showed that the phthalates leaching into orange juice from tetra

packaging grows 110 times higher than the safe intake limit of 6.0 $\mu\text{g/L}$ set by US EPA (United States Environmental Protection Agency) during its shelf life and until close to its expiry date (Figure 1.2). The guideline for safe drinking water published in a list of priority compounds, posing endocrine disrupting hazards to humans by World Health Organization (WHO) and European Union sets 8.0 $\mu\text{g/L}$ as a maximum safe limit for DEHP presence in fresh and drinking water [12].

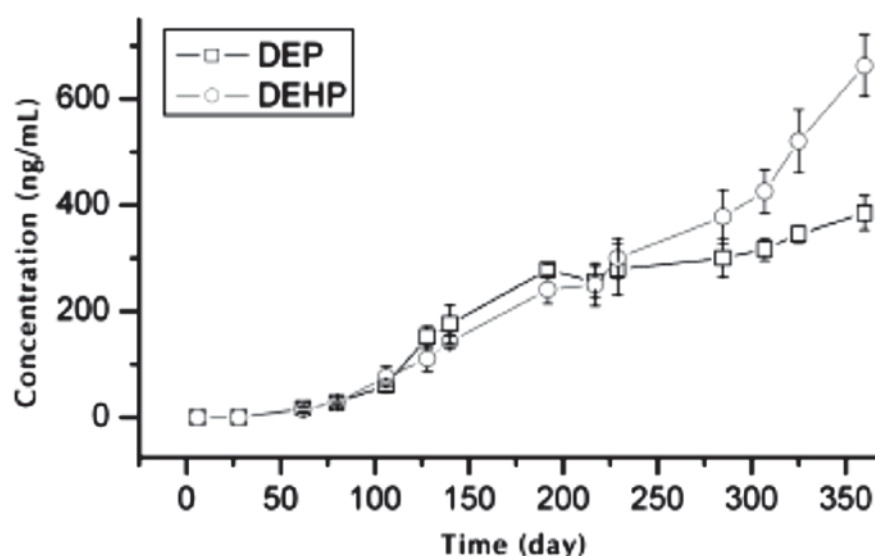


Figure 1.2 Leaching of DEHP and DEP from tetra packaging within expiry date of orange packaged orange juice[11]

The ubiquitous presence of phthalates as an environmental pollutant and containment in laboratory apparatus seriously limits minimal detection level below 2-ppb even under the most stringent conditions and controlled setup [13]. Solid phase micro-extraction (SPME) is a solvent free pre-concentration technique applied to extract phthalate metabolites from a mixture of compounds; in order to measure its quantity using Gas Chromatography (GC) and High Performance Liquid Chromatography (HPLC) [14-17]. Different types of detectors are used to measure the quantity of phthalates depending on the nature of the test sample. For example, DEHP is measured by GC using Electron Capture Detector (ECD) [18] and Flame Ionization Detector (FID) [7]. Liquid Chromatography (LC) coupled with Mass Spectrometry (MS) and UV detection are the most commonly applied well-established techniques [19].

In order to device a rapid and effective assay for hormones and EDCs, the author performed a detailed review of all the available contemporary commercial and laboratory techniques and methods used for hormone and EDCs detection. Hormone analysis is a very useful tool in pharmaceutical, medical and biological sciences. It has

been used as a diagnostic tool to confirm the disease and abnormality or to differentiate one physiological state from another. The method of hormone analysis has been changed throughout the years from bio-analysis to the more sophisticated techniques. However, every technique has its advantages and disadvantages and may be useful for different purposes. The best technique for measuring different hormones might also be different. Figure 1.3 shows all the types of phthalates used in industrial sector.

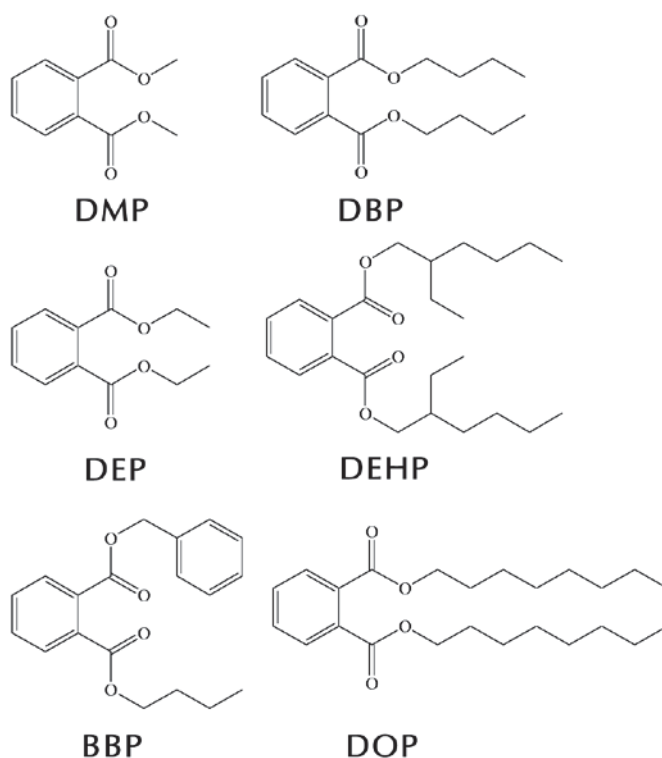


Figure 1.3 Types of phthalates used in industrial sector as plasticizers

Two major techniques used for hormone analysis are; receptor assay and immunoassay.

1.2 Receptor–ligand binding assays

In biochemistry, a **receptor** is a protein molecule found on the surface of a cell or embedded in the plasma membrane or the cytoplasm of a cell. It receives specific chemical signal from one or more specific kinds of signalling molecules that may attach to it. The signalling molecule, which binds to a receptor, is called a ligand. A ligand may be a peptide or other short molecule such as a neurotransmitter, a pharmaceutical drug, a toxin or a hormone. The ideal assay should be selective, sensitive, easy to perform, reliable, low cost, fast and adaptable for automation. Moreover, ideal assay

formats should not use any radioactive and toxic material in order to reduce health risks and environmental pollution as well as costs. Above all, the possibility to quantify multiple analytes in a single assay becomes more and more important, so the system should preferably be capable of multiplexing [20].

Receptor-ligand assays can be classified into three categories based on the detection techniques:

Heterogeneous assay uses washing; filtration, centrifuging or dialysis in order to separate the unbound fraction of the ligand from the receptor bound part of the analyte.

Homogeneous assay, on the other hand, is mix-and-measure assay. It does not require additional steps of washing, filtration, centrifuging or dialysis which induces an advantage of assay automation and miniaturization.

Non-separating homogeneous assay does not require separation procedures, rather the signal is centred or around a solid phase which contains the immobilised receptor or ligand [20].

1.2.1 Radio Receptor Assay (RRA)

Conventionally, receptor–ligand binding assays are heterogeneous and use radioactively labelled ligands for binding to a membrane-bound receptor. The principle is based on the interaction between a labelled ligand and an analyte for the same receptor binding site. After incubation of the labelled ligand, analyte and receptor it is necessary to filter or centrifuge to separate the free from bound fraction. The radioligand selected for RRA should be selective, chemically stable, radio-chemically pure and must possess a high affinity for the respective receptor [21].

A major advantage of radio-ligand binding assays is sensitivity, selectivity and ease of use. Only one labelling step is required, that allows a quick set-up for the assay. The major drawback of these assays is, however, the use of radioactivity that poses a health risk to the operator and cause of producing radioactive waste. The requirement of separation of bound from free ligand renders these assays more labour-intensive and relatively slow.

1.2.2 Scintillation Proximity Assay (SPA)

SPA is a radioactive assay which involves immobilization of a receptor on a small (5micrometer diameter) scintillant-containing microsphere and the ligand is labelled with a radioactive isotope. When this radio-isotopically labelled molecule binds to the

microsphere, the radioisotope comes in proximity to the scintillant. Energy transfer from the radioisotope to the scintillant takes place through emission of β particles to the scintillant which emits light photons as a consequence of the energy transfer. The light is detected by a phototube that in turn can be translated to the concentration of the ligand in the solution. The unbound radioactive ligand molecules lose energy in the aqueous medium without transferring it to the scintillant; hence, no photons are emitted due to unbound ligand molecules [22]. The technology has been widely utilized with a broad spectrum of applications, including mass measurement in research, pharmacological studies and cellular function screening for analytes. The isotopes of interest in the SPA technique are [^3H] and [^{125}I], with a preference for ^{125}I due to its higher specific activity [23].

The advantage of mix-and-read-format makes this scintillation proximity assay easy to automate, which enhances assay reliability [23].

- Major disadvantages include use of radioactivity making this technique very expensive and environment pollutant due to the production of radioactive waste.
- Another potential difficulty is the need to immobilize the receptor on a solid surface, where it should remain stable and maintain affinity.
- SPA is time-consuming (18 H) in comparison to a filtration assay (90 min). The time necessary to reach equilibrium for the receptor-bead interaction and to allow the beads to settle down in the microtiter plate is the major cause. The latter is necessary to avoid signals from ligand that is not bound to the beads and can be accelerated by centrifugation. The relative long incubation time may also be a problem for instable receptors.

1.2.3 Fluorescence Resonance Energy Transfer (FRET)

Most of the mix-and-measure assays use the principle of fluorescence resonance energy transfer between ligand and receptor molecule when they come in proximity. FRET uses transfer of energy from a donor molecule to an acceptor molecule, which depends on the distance between two, for detection. FRET employs sensitivity to distance for the study of molecular interactions. The transmission of energy from a donor to acceptor is radiation-free. The donor molecule is the dye or chromophore that initially absorbs the energy and the acceptor is another chromophore to which subsequently absorbs energy [24]. This resonance interaction occurs over distances greater than the interatomic distances. It occurs without conversion into thermal energy or loss due to any molecular

collision. The transfer of energy reduces the donor's fluorescence intensity and excited state lifetime which causes an increase in emission intensity of the acceptor. The kind of interaction that occurs in FRET is often referred as donor/acceptor interaction. FRET can result either in a decrease in fluorescence of the donor or an increase in fluorescence of the acceptor. The two cosequent signals are compared to extract information [25] as shown in Figure 1.4.

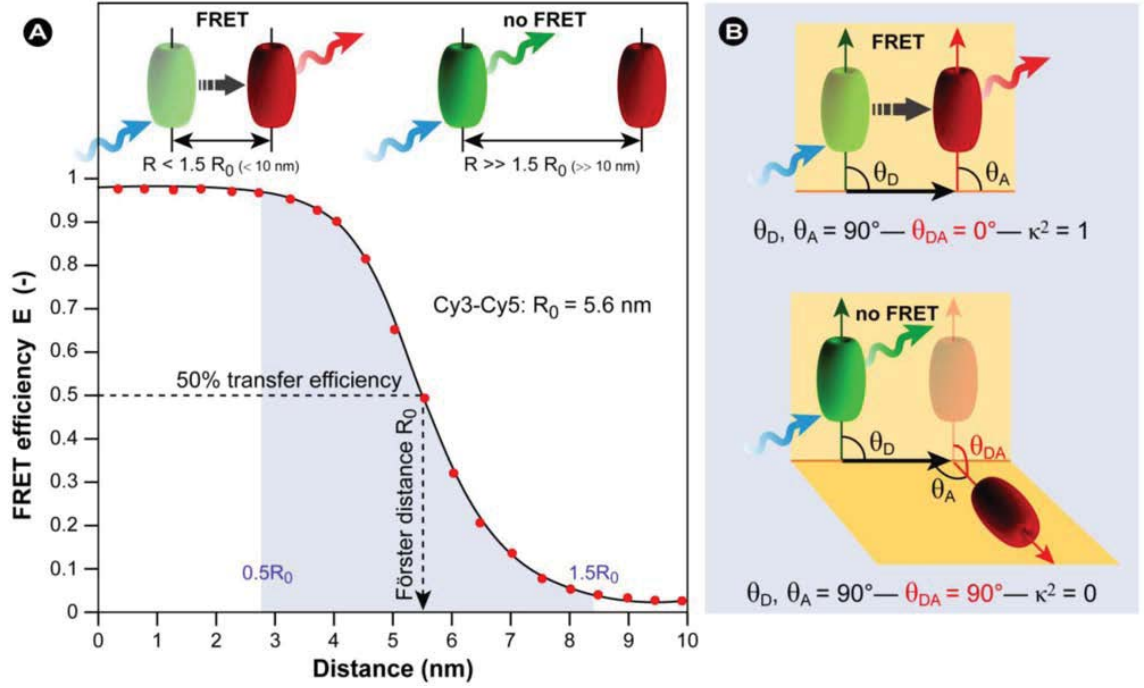


Figure 1.4 Basic concept of FRET as photophysical process. (A) The plot shows the dependence of the FRET efficiency on the proximity of the donor-acceptor pair. (B) shows the effect of angle between donor fluorochrome and acceptor molecule on FRET [25]

The advantage of this method is a measure of interaction, that is independent of the absolute concentration of the sensor [26, 27]. The disadvantage is the matter of proximity depending on the assay design, appropriate donor-acceptor pair selection, distinguishability from one another, and the requirement of enough spectral overlap for efficient energy transfer between donor and acceptor pair. The utility of this technique to measure receptor-ligand interactions in homogenous assay is also limited due to the requirement of labelling both the donor and acceptor molecule. FRET is applied to study the structure and conformation of proteins [24]; spatial distribution and assembly of proteins [26]; receptor-ligand interactions [27]; immunoassays [28]; structure and conformation of nucleic acids [29].

1.2.4 Fluorescence Polarization (FP)

Fluorescence Polarization measurements are based on the assessment of the rotational motion of the molecular species upon excitation with polarized light. This technique measures the difference in the rotational speed of the ligand molecule upon binding to its receptor during excited lifetime. The fluorescent labelled ligand is excited by polarized light, and the polarization of the emitted light is determined. Excitation of a fluorescent ligand with low molecular weight by polarized light results in depolarized light emitted in consequence of rapid rotation of ligand. When the same fluorescent ligand is bound to a high molecular weight receptor, the rotational speed of the bound molecules decrease causing the emitted light remains partially polarized.

This technique has a clear advantage of one-step labelling as compared to FRET that required two-step labelling. FP requires simple and less complicated testing setup. The disadvantages of this technique are lack of precision at low (Nanomolar) concentrations; sensitivity is dependent on the affinity of ligand, intensity of the fluorophore and quantity of the receptor. Required precision for an acceptable standard FP assay is achieved by keeping the receptor concentration at least 1pmol/mg protein and the ligand affinity below 5nM as stated by Gagne et al. [30]. The FP Assay technique has been applied to the soluble oestrogen receptor [31].

1.2.5 Fluorometric Micro volume Assay (FMAT)

This is mix-and-measure assay technique which makes use of commercially available laser scanner that measures multi-well plates. The small molecule ligand is labelled with a fluorophore and receptor is immobilized on beads in, either, 96, 384 or 864 multi-well plates with transparent bottom and opaque sidewalls of each well. The scanner scans a 1mm² area using Helium-Neon red laser (633nm) as the excitation source for fluorophore labelled ligands bound with receptor molecules. It uses two photomultiplier tubes with band pass filters for the respective labels to detect two independent red dye emissions e.g. Cy5 and Cy5.5. Multiplexing minimizes reagent consumption and increases throughput. The mix-and-measure format is achieved by discriminating between cell-associated and free fluorescence during data processing, where cell-associated fluorescence is detected as localized areas of concentrated fluorescence at the bottom of the well. To avoid interference, from auto-fluorescence of the cells, long wavelength emitting red dyes are used, which results in a very sensitive assay. Laser-

scanning imaging is an analogous technique to FMAT, which can also be used for multiplexing to measure ligand–receptor interactions [32].

1.2.6 AlphaScreen™

This is homogeneous bead-based assay also known as Amplified Luminescence Proximity Homogenous Assay. The donor used for this assay is singlet oxygen ($^1\text{O}_2$, half-life 4 μs). On excitation with a wavelength of 680 nm, photosensitizer present in the donor beads convert ambient oxygen to singlet oxygen. that can travel longer distance (200nm) allowing the assay to probe interactions over longer distance than FRET. Receptor is immobilized on donor beads whereas antibody-captured ligand is present on acceptor bead. If acceptor bead is in the close proximity to donor, i.e. less than 200nm, the singlet oxygen transfers its energy in order to return to ground state, to the acceptor bead leading to emission of light with wavelength varying between 520 to 620nm. The singlet oxygen molecule goes undetected if there is no acceptor bead present within the range of 200nm [33]. The beads used in this assay are 250nm diameter, which is much smaller than the beads used in SPA and FMAT. This property serves advantageous to avoid clogging in liquid handling devices [34].

1.2.7 Flow Cytometry

This technique sequentially sorts or counts microscopic particles suspended in a fluid by means of optical signals using fluorescence. These particles may be cells or cell sized beads of polystyrene/latex or dextran microspheres with a diameter in the micrometer range. Flow Cytometry requires that one of the interacting partners among receptor and ligand is immobilized on the bead and the other is provided with a fluorescent tag for the quantification of receptor-ligand binding. Two lasers are used to identify the bead and quantify the fluorescence associated with the immobilized partners [35]. It can measure and quantify molecular interaction in a sensitive and specific manner, combined with high throughput of samples, multiplexing and the possibility of kinetic analyses. Although these are deemed to be the advantages of flow Cytometry technique but on the other hand, it remains difficult to setup such assays which require highly skilled man power and expensive setups.

1.2.8 Fluorescence Correlation Spectroscopy (FCS)

Fluorescence correlation spectroscopy is a homogeneous assay technique that determines receptor–ligand binding by measuring intensity fluctuations consequent to the differences in diffusion rate of individual dye-labelled ligands free in solution or bound to a high-molecular-weight receptor. Binding of the ligand molecule to a receptor molecule results in an increase in the mass and hence in a reduced rate of diffusion, which leads to increased average time spent in the irradiated volume. This results in multiple photons emission from the labelled ligand/complex within a given time. As these photons are emitted from the same labelled ligand/complex moving in the fluid volume due to Brownian motion, they are correlated in time. The average correlation time is a measure of the fraction of ligand that is bound to the receptor and will be at its maximum if the fluorescent labelled ligand saturates the receptor. Since fluctuations of the fluorescent signal are governed by the number and quantum yield of the fluorescent molecules, it is necessary to reduce the irradiated volume such that individual molecules can be measured. This is achieved by using diffraction-limited laser beams and confocal detection optics, in combination with pinholes in the image plane, generating observation volumes in the order of femtoliters (μm^3) [36]. Laser systems used in FCS are based on: Helium–Neon laser with excitation wavelength of 543nm and 633nm; Argon laser with excitation wavelength of 488 and 514 nm and Argon–Krypton lasers with excitation wavelength of 568 and 647nm.

FCS displays an advantage to study receptor-ligand interactions at the molecular level on a living cell as compared to the traditional assay techniques which require extraction of a receptor from its natural membrane environment. Another advantage of FCS is that there is no need to immobilize a ligand or receptor as in the case of bead-based assays and biosensors. FCS is suitable of producing high throughput screening with an additional advantage of microliter of sample volume. On the other hand, it requires expensive setup in a laboratory environment with highly skilled workforce and extremely expensive state of the art optical and analytical equipment that is termed as a disadvantage of the technique.

1.3 Immunoassay

An **immunoassay** is a type of biochemical testing that is used to measure the concentration of a specific substance in a solution containing a complex mixture of

substances. Such testing uses the ability of very limited group of molecules called antigen to bind with an antibody. The binding between two requires high specificity just like a lock and key. The degree to which the analytical reagent can bind to its specific partner determines the specificity of the assay. The analytical reagents associated with a detectable label are required to perform immunoassay. These labels used may be radioactive, phosphorescent, fluorescent, and chemiluminescent dyes. In addition to the binding specificity, a transducer is used to produce a measurable signal in response to a specific binding of antibody-antigen pair. Four main types of transducer have been used in immunoassay technology. Electrochemical transducer (potentiometric, amperometric, conductimetric) detect changes in electrical properties of the sample. Heat transducer (calorimetric) detect changes in temperature of the sample. Mass transducer (piezoelectric, Surface Acoustic Wave (SAW)). Optical transducer (luminescent, fluorescent, reflective, refractive, ellipsometric, Surface Plasmon Resonance (SPR) Nuclear Magnetic Resonance (NMR) and waveguide) detect the change in frequency, phase shift and wave properties of the acoustic or electromagnetic radiation carrying the information after reflecting or refracting from the sample.

All immunoassays require reference to a calibrator for interpretation of the signal produced as a result of the procedure. The comparison mimics the characteristics of the sample medium. In the case of qualitative immunoassays the calibrator consists of reference with no analyte present. It is called negative sample whereas, a positive sample is one which has the lowest concentration of detectable analyte. Quantitative assays make use of additional calibrators that contain known analyte concentrations. The assay response of a real sample compared to the assay responses by the calibrators produces a signal. The strength of this signal determines the presence or concentration of analyte in the sample.

Immunosensor is a device operating on the principles of solid-phase immunoassay, with either antibody or antigen immobilized on the sensor surface. These are used to detect an extensive range of analytes like environment pollutant such as pesticides, bacteria, drugs, and medical diagnostic markers such as hormones (steroids and pituitary hormones). Advantages like, absence of labelling requirements and ability to investigate the reaction dynamics of the antibody-antigen binding, has provided these devices a leading edge over the conventional assay techniques. The basic principles of immunosensors with respect to the applied transducer systems are discussed as follows.

The development of optical techniques for monitoring of minute changes in light scatter, refractive index, phase change and absorption has provided a promising platform for the development of this technique. Optical transducers based on reflectance, ellipsometry, surface plasmon resonance and optical fiber waveguide have all been briefly described here.

1.3.1 Surface Plasmon Resonance (SPR)

This method used for the detection of antibody-antigen interaction does not require labelling. The SPR device consists of a sensor chip, a flow cell, a light source, a prism and a detector that is positioned at a fixed angle. The sensor's surface consists of a thin gold layer (~50 nm) fixed onto a glass surface with an interaction layer e.g. BSA-biotin. The carboxylic acid group on this layer can be activated to immobilize either the receptor/antibody, or the ligand/antigen covalently [37].

SPR measures changes in refractive index for a resonance angle at which polarized light is reflected from a surface. This change is related to the change in mass of the analyte or layer thickness. [38, 39]. Specific ligands can be immobilized on the upper surface of the device (sensor surface), to interact directly with the biomolecules in the sample. SPR technology is based on the excitation of the surface electrons of the metal (gold) which behave differently as compared to the bulk electrons since they can oscillate more freely in comparison to the bulk electrons. When excited, these electrons, also termed as surface plasmon, oscillate at different frequency from that in the bulk of the metal film, absorb light photons and generate an evanescent wave. In SPR system, polarized light is directed in one plane into the prism and gets totally internally reflected due to the difference of refractive indices of prism and metal surface from the metal glass interface. At the resonance angle, SPR is initiated; the absorption of light energy by the surface plasmon causes a sharp decrease in the intensity of the reflected light. The evanescent wave propagates into the metal layer which allows it to sense the metal-sample interface. The resonance angle is determined by the wavelength, polarization and refractive indices of the prism, metal and a sample layer of the system. Changes in refractive index take place when biomolecules attach to the ligand immobilized at the sensor surface. Consequent to that the resonance angle, at which drop of intensity is observed, changes. Continuous monitoring of the reflected light intensity provides a direct profile of the changes in the refractive index at the sensor surface and hence a

real-time analysis of the binding events at the sensor surface is obtained. The basic operating principle of SPR is shown in Figure 1.5

As surface plasmon resonance is dependent on changes in mass, it is advantageous to attach the molecule with the lowest molecular weight to the surface and measure binding of the higher molecular weight partner. Nevertheless, due to the possible difficulties of immobilizing low molecular weight ligands/antigen (e.g. loss in binding affinity), it might be necessary to attach the high-molecular weight receptor/antibody to the surface and work with a smaller signal [40]. The latter approach has the benefit of requiring less receptor [41], but has an important limitation in the form of denaturation of the immobilized receptor may occur upon repeated use. The sensitivity of the assay can be increased by immobilizing the ligand/antigen on the sensor surface, thereby, generating a large signal due to binding higher molecular mass receptor/antibody as described by Kroger et al. [42]

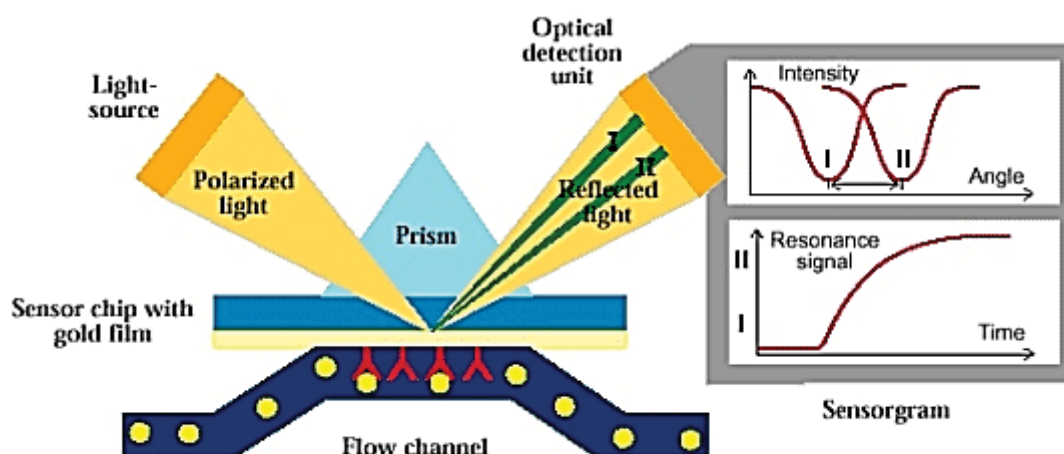


Figure 1.5 Detection principle of SPR technique[38]

The main advantage of SPR is thus the monitoring of molecular interactions in real-time without the use of labels. The major limitation is that one of the binding partners needs to be immobilized.

1.3.2 Total Internal Reflection Fluorescence (TIRF)

Total internal reflection fluorescence detection technique is based on the same principle corresponding to SPR. The difference between two is that SPR is a label-free technique whereas TIRF relies on the binding of a fluorescent-labeled ligand to an immobilized receptor on the sensor surface. The information carrying signal in TIRF is not

dependent on the mass of the ligand, but it makes use of the sensitivity of fluorescence. The evanescent wave produced due to the excitation of the surface plasmon by polarized light causes excitation in the fluorescent labels present close to the sensor surface (~100nm). The change in the intensity of the incident light is measured. Since only those fluorescent ligands that are near the surface and thus bound to the receptors are excited by the evanescent wave, the signal is not affected by the fluorescent ligand in the buffer solution [43-45]. TIRF has been used to measure estrus cycle in dairy cows by measuring the progesterone level in the bovine milk [46].

1.3.3 Ellipsometry

Ellipsometry is a sensitive optical technique to determine surfaces and thin films properties. It is used to study the binding of proteins to surfaces [47]. If a known oriented linearly polarized light reflects from a surface at an oblique angle, the polarization of the reflected light changes to elliptically polarized. The angle of incidence, the direction of polarization of light, and the properties of the incident surface determine the orientation and shape of the ellipse. The polarization of the reflected light can be measured with a quarter-wave plate followed by an analyser; the orientations of the quarter-wave plate and the analyser are varied until no light passes through the analyser. By measuring these orientations and the direction of polarization of incident light, relative phase change Δ , and the relative amplitude change ψ , can be evaluated. These properties alter when a molecule is adsorbed to the surface, and the new readings can be interpreted as change in the refractive index and coating thickness of the sensor surface. This leads to the calculation of the concentration of the bound analyte. Isoscope® ellipsometer has been used to study receptor-ligand interactions. [48].

1.3.4 Nuclear Magnetic Resonance Spectroscopy

Nuclear magnetic resonance (NMR) is a physical phenomenon which is based on the absorption and re-emission of electromagnetic radiation of a magnetic nucleus in presence of a strong magnetic field. The EM energy is absorbed, when the frequency of the applied electromagnetic field matches the natural frequency of the exposed nucleus, called resonance frequency. The resonance frequency depends on the magnetic field strength and the nuclear magnetic properties of the atom. NMR imaging relies on the observation of magnetic quantum mechanical properties of an atomic nucleus. The

resonant frequency of a material varies directly to the strength of the magnetic field applied. Superconductors are used to increase the magnetic field strength to obtain the required resolution of the image.

NMR spectroscopy is used to study the interaction of molecules at atomic level. It is also widely used to elucidate the structures of chemically synthesized compounds and biomolecules [49]. Functional group analysis, bonding connectivity and orientation, through space connectivity, Molecular Conformations, DNA, peptide and enzyme sequencing and structure are a few other applications of NMR [50].

1.3.5 Amperometric Immunosensors

These devices measure current flowing through the electrolyte in a chemical cell at a constant voltage. The current is produced as a result of the redox reaction at the sensing electrode. The current generated varies directly to the amount of oxygen or hydrogen peroxide reduced or oxidized at the electrode [51]. The system has the advantage of high sensitivity, linear concentration dependence and high selectivity. However, for intrinsically non-electroactive molecules like proteins cannot be detected by direct approach that is a demerit of this system. For such molecules, enzymes are incorporated as labels to catalyse redox reactions that facilitate the production of electroactive species that may then be able to be detected by amperometric immunosensors. For example, a multi-analyte amperometric immunosensor has been developed for measuring the human gonadotropin hormone, follicle stimulating hormone and luteinizing hormone achieving low detection limits. The device uses two horseradish peroxidase-labelled antibodies in a ferrocene-medicated system [52].

1.3.6 Conductimetric Immunosensors

Chemical reactions produce or consume ions species and therefore alter the overall electrical conductivity of the solution. Sensors designed by immobilizing a suitable enzyme over a set of chemically inert metals electrodes, and by measuring the change in the conductance of a solution containing the analyte of interest, consequent to an applied electric field, are termed as conductimetric immunosensor. For example, when urea is converted to ionic product NH_4^+ by the enzyme urease, the increase in the solution conductance measured is proportional to the concentration of urea in the solution [53]. These sensors face the problem of non-specificity of measurements because the resistance of the solution is determined by migration of all ions present.

1.3.7 Surface Acoustic Wave Immunosensors (SAW)

This technique uses oscillations of piezoelectric crystals at higher frequencies (30-200MHz), and an acoustic wave is generated by application of alternating voltage across a pattern of interlaced metal electrodes, known as interdigital transducer. The high-frequency acoustic signal is detected by another interdigital transducer separated by a small distance. The adsorption of sample to the crystals slows down the acoustic wave, and the recorded change in velocity is proportional to the analyte concentration. Such devices have successfully been used in specific areas such as environmental gas monitoring [54], chemical detection [55], rapid immunoassay of antigen present in the foodstuffs and human IgG measurements [56]. The schematics of a SAW sensing device is shown in Figure 1.6 [57].

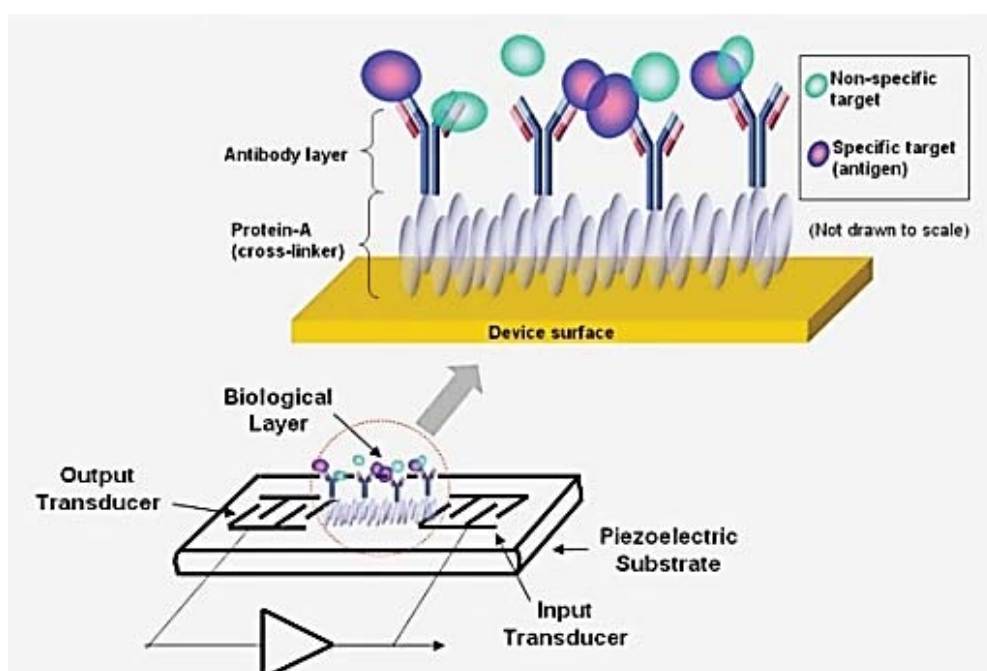


Figure 1.6 Schematics of a SAW immunosensor [57]

1.3.8 Enzyme-linked Immunosorbent Assay (ELISA)

It is a biochemical technique used to detect the presence of an antibody or an antigen in a sample. Unknown amount of antigen is immobilized in a microtiter plate by adsorption and detection antibody is added which form a binding with the antigen. The detection antibody can be covalently linked to an enzyme through bio-conjunction. Before each step the microtiter plate is washed with a mild detergent solution to remove antibodies that remain unbounded. An enzymatic substrate is added to develop the plate

to observe a visible signal, most commonly a colour change, which indicates the quantity of antigen in the sample. ELISA is used as a diagnostic tool in medicine, plant pathology, biochemical detection, and as quality control in various industries [58].

All the assay techniques and methods discussed in the preceding literature survey have their own merits and de-merits. Labelled sensors use immunoassay approach for binding the target molecule that is purely laboratory-based technique involving expensive, time-consuming and hi-tech laboratory protocols, hence, rendering impossible real-time measurements. Sensors for direct, label-free quantification of analytes are attractive to researchers for a number of reasons like direct detection of analytes with minimal or no sample preparation, cost effective, simple and real-time. These involve optical, mass-sensitive and electrochemical detection routes for measurement of analyte in bulk sample. Optical sensors are the most studied but the electrochemical sensors are relatively more sensitive and display comparatively lower detection limit capabilities with a requirement of least complicated support instrumentation. On the other hand, optical and mass-sensitive techniques claim state-of-the-art electronics and bulky instrumentation for interpretation of optical and mass variation data into comprehensible information. Table 1.2 provides the reader a crisp and comprehensive comparison of the contemporary techniques and methodologies that are applied most-frequently in today's world.

Table 1.2 Advantages and disadvantages of contemporary techniques used for biochemical analytes

Assay Format	Detection Principle	Advantages	Disadvantages
Filtration assay	Radioactive	Labelling steps does not change affinity	Requires separation, radioactivity, medium throughput
SPA/flash plate	Energy transfer	Mix-n-read, affinity does not change by labelling, high-throughput	Radioactivity, receptor immobilization, low sensitivity
Filtration assay non-radioactive	Fluorescence	Fluorescent	Require separation, labelling change affinity, medium-throughput, fluorescence interference
FRET	Energy Transfer	Mix-n-read, fluorescent	Dual labelling, distance constraints, correct dipole orientation, background noise
FP	Light polarization	Mix-n-read, one label, ratiometric measurement, ease of automation, facile to miniaturize.	Labelling alters affinity, requires suitable ligands
FMAT	Single cell measurement	Mix-n-read, multiplexing, minimal background noise, miniaturization	Requires receptor immobilization, high assay variation, expensive setup
AlphaScreen™	Energy transfer	Mix-n-read, time-resolved	Uses beads for donor and acceptor, receptor immobilization.
Flow cytometry	Single cell measurement	Mix-n-read, sensitive, minimal background noise, high throughput, multiplexing	Requires fluorescent labels and immobilization of receptor and ligand, Limitation in sample handling
FCS	Diffusion mediated intensity fluctuations	Molecular, homogenous, min. background noise, real time, time resolved, miniaturization	Limited accessibility, complex instrumentation, stringent optical requirements.
SPR	Refractive index	No labelling, sensitive, real-time, no interference, automation	Receptor or ligand immobilization, sensitivity depends on molecular weight of analyte, high cost, high protein density, correct orientation
TIRF	Refractive Index	Real-time, high sensitivity, combined with micro fluids, surface specificity	Receptor immobilization, labelling
Microarray	Optical intensity change	Multiplexing, real-time,	Labelling and immobilization of receptor and ligand.

1.4 Conclusions

Almost all contemporary analytical techniques described here are highly sensitive due to the requirement of measurement of trace levels of EDCs present in food and beverage samples. Table 1.2 compares the advantages and disadvantages of the most applied biochemical sensing techniques. Unfortunately, these are time-consuming, expensive, complicated, produce laboratory waste, need the expertise of highly trained professionals in addition to the submission of samples to laboratories, worth millions of dollars. Blood and urine are the most common matrices used for biomonitoring of EDCs in human body but the results of these biomonitoring do not provide the complete picture of EDCs intake, rather just provides the quantity of metabolites excreted, losing information about the amount of phthalates that have become the body burden. Therefore, it is necessary to have a rapid assay which may detect the quantity of phthalates present in food and beverages as initial intake via the oral route which is deemed to be the biggest source of human phthalate exposure due to the extensive use of plastics in our everyday life style. The requirement of instant screening of a batch of products manufactured at an industrial set up still requires attention of the researchers to device an assay which may be simple enough to be handled with minimal training needs and does not involve bulky and expensive support electronics. The objective of this research is to develop a low-cost real time testing system which could readily be installed in an industrial setup. Furthermore, a portable low-cost sensing system is envisaged which can be used to rapidly quantify the amount of phthalates in edible consumer products.

1.5 Research Contributions

The major contribution of this research work is the development of a smart sensing system that owns the capabilities to detect hormones and endocrine disruptor compounds in food stuffs. The smart sensing system is based on design and development of a smart sensor that can selectively quantify the analyte in real-time. Low cost and robustness are the merit points that make this system unique. This system can readily couple with any existing chemical and biochemical sensing technique.

The contributions of this research work can be summarized as follows:

- 1 Explore a novel interdigital capacitive sensor design that owns penetration depth of the fringing electric field, enough to allow bulk-sample testing.
- 2 Analyse the new sensor design by finite element analysis and select the most sensitive configuration of interdigital electrodes under given boundary conditions.
- 3 Fabricate smart sensor interdigital configuration on silicon substrate using MEMS based semiconductor fabrication technology.
- 4 Analyse and achieve stability and reproducibility in impedance measurement characteristics of the smart sensor design.
- 5 Establish automatic data acquisition setup to measure impedance characteristics of an electrochemical cell using the fabricated sensor.
- 6 Real-time detection and analysis of hormones in bulk aqueous medium by applying electrochemical impedance spectroscopy technique.
- 7 Real-time detection and analysis of two phthalate esters in polar, electrolytic and acidic media using electrochemical impedance spectroscopy technique in bulk samples.
- 8 Develop and tailor robust technique to induce selectivity for the phthalate analyte in the smart sensing system.
- 9 Explore and apply technique to immobilize analyte selective functional material on highly polished silicon substrate based smart sensor.
- 10 Analyse the performance of the selective smart sensor and compare it with commercially available detection methodology.

1.6 Organization of the Thesis

Chapter 1

The introduction part briefly describes endocrine system, hormones, and endocrine disrupting compounds and highlights the research problem to the reader. In the second part a detailed literature survey is presented to discuss the most applied and to-date available chemical and biochemical detection techniques and compare .

Chapter 2

Chapter 2 describes the methods and methodologies, merits and demerits, pros and cons of the electrochemical impedance spectroscopy (EIS) technique. The author tried to make the reader of this thesis well-versant with the equipment used, methodologies, conditions and analytical methods applied in this technique to deduce the results.

Chapter 3

This chapter discusses the details of the steps involved in design and simulation of the interdigital capacitive transducer. It explained the worked out improvements in the design of the sensor that was simulated to virtually assure the sensitivity and operation. Principal component analysis was used to analyse the effects of post-fabrication annealing process carried out to induce stability and reproducibility in its performance.

Chapter 4

This part of the presented work gives an account of the exposure of the developed system to a real world problem. Detection of progesterone and metabolite of estradiol-E1G were tested using the developed system. Electrochemical analyses of the experiments proposed that the system was able to detect both in deionized water based medium.

Chapter 5

As a next phase the developed system was exposed to endocrine disrupting compounds that mimic hormones in living beings. The system was tested not only in deionized media but also with spiked juice and energy drinks. The results proclaimed that the system is perfectly sensitive to the spiked deionized medium but in juices and drinks the sensitivity deteriorated which led the research to induce selectivity in the system.

Chapter 6

This chapter explores the methods to induce selectivity in the developed system. In order to keep the system robust and achieve real-time detection of the analyte, molecular imprinted polymer technique is discussed in detail. MIP formation and immobilization on the sensing surface is discussed in detail. MIP functionalized sensor is used to detect phthalate in aqueous medium and the results were validated by HPLC.

Chapter 7

This chapter gives an overview of the research work in conclusions and some recommendations are made for the future work.

Chapter 2 Impedance Spectroscopy and Experimental Setup

2.1 Introduction

The objective of this chapter is to introduce the measuring instruments and software programs used for the experimental setup. It provides the reader a detailed insight of, electrochemical impedance spectroscopy basics and data representation along with highlighting the methodology of measurement data collection. It explains all the hardware and software used to collect the impedance data and the models involved in analysing the acquired information. It also describes the interfacing of the measuring instruments with LabVIEW program to obtain a stand-alone automated measurement system. It provides an account of the basic applications of impedance spectroscopy method for characterization of sensors and material under test (MUT).. The objectives are to measure and characterize the developed sensors according to EIS models and methods. Mathematical methods like complex non-linear least square curve fitting were used to deduce equivalent circuit to the electrochemical cell under test. The parameters obtained from the measuring instruments are frequency, f , impedance, Z and phase angle. Mathematical methods used to interpret these into real and imaginary parts in complex plane for analysis of impedance characteristics are also discussed.

2.2 Electrochemical Impedance Spectroscopy

Electrochemical Impedance Spectroscopy (EIS) has seen huge boost in popularity in recent time due to its extraordinary sensitivity. It is used to evaluate electrical properties of materials and their interfaces with surface-modified electrodes [59]. This method have been widely used to study of electrochemistry [60, 61], biomedical applications [62, 63], material science [64] and others. J. Ross Mcdonald in [65] describes the EIS as a part of Impedance measurement using ac polarography involving electrochemical reactions. The response of an electrochemical cell to a low amplitude sinusoidal

perturbation as a function of frequency and has been reported to estimate the dielectric properties of milk [66], meat inspection [67], quality testing in leather [68], Saxophone reed inspection [69], detection of contaminated seafood with marine bio-toxin [70], food endo-toxins [71-75], evaluate electrical properties of drinks, and water [76]. EIS involves measurements and analysis of materials involving ionic conduction in solid and liquid electrolytes. Ionically conducting glasses and polymers, fused salts, and nonstoichiometric ionically bonded single crystals have been used for impedance measurements where conduction can involve motion of ion vacancies and interstitials. EIS is also conducted to study of fuel cells, rechargeable batteries, and corrosion. Other category of IS applies to dielectric materials: solid or liquid non-conductors whose electrical characteristics involve dipolar rotation, and to materials with predominantly electronic conduction [77]. System Impedance may be measured using various techniques. The most cited impedance measurement techniques are given as follows:

2.2.1 AC bridges

This is the oldest of all the techniques initially used for the measurement of double-layer parameters, principally of the hanging mercury drop electrode. It has also been used to measure the electrode impedance in a faradaic reaction to evaluate the kinetic processes at the electrode. Although this method is slow, yet provides a very good precision of measurements.

2.2.2 Lissajous Curves

Formation of elliptical figures as a result of simultaneous application of the applied ac voltage and resulting ac current to a twin beam oscilloscope is called Lissajous curves. Analyses of Lissajous curves produced on twin channel oscilloscope screens was used to perform impedance measurements and had been an accepted method for impedance spectroscopy prior to the advent of modern EIS instrumentation. The measurement time involved in using this technique (often up to many hours) is long enough for a chemical cell to cause drift in its system parameters. The cell can change through adsorption of impurities, oxidations, degradations, temperature variations etc. These curves have been used to determine the impedance, but frequency limitations and sensitivity to noise has limited the use of this technique. Figure 2.1 shows the formation of Lissajous figures as a consequence of two out of phase signals.

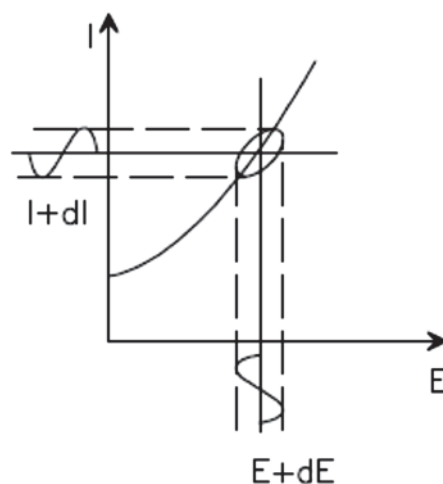


Figure 2.1 Formation of Lissajous Figure

2.2.3 Fast Fourier Transforms (FFT)

The Fast Fourier Transforms is a mathematical method to evaluate the system impedance. Taking the Fourier transform of the perturbation signal in time domain and generation of equivalent frequency domain data using a computerized algorithm is referred as FFT. FFT provides a fast and efficient algorithm for computation of the Fourier transforms. In practice, only limited length data is transformed, causing the broadening of the computer frequency spectrum, commonly called 'leakage'. Another problem called 'aliasing' is linked with the presence of the frequencies larger than one-half of the time domain sampling frequency.

2.2.4 Phase Sensitive Detections (PSD)

Phase sensitive detection is used in lock-in amplifiers interfaced with precision potentiostats for system impedance measurements. It contains one time-independent component, depending on the phase difference of two signals and proportional to the amplitude of the measured AC signal. The output signal is applied to a low-pass filter that averages the signal component having frequencies above the cut-off frequency. The disadvantage of the lock-in technique is that it retains combination of harmonic frequencies present in the input signal.

2.2.5 Frequency Response Analysis (FRA)

Frequency Response Analysers are hi precision instruments that determine the frequency response of the measured system. The operation of FRA is based on

interpreting correlation of the studied signal with the reference perturbation. The measured signal is multiplied by the sine and cosine of the reference signal of same frequency and integrated over one time period. Real and imaginary parts of the measured signal are recovered, strictly rejecting all harmonics. The advantage of the correlation process is reduction of noise, but it is achieved at the cost of attenuation of the output signal.

Among a number of methods available for impedance measurements, FRA has become a de facto standard for EIS. FRA is a single sine-wave input method in which a small amplitude (5-15mV) AC sine wave of a given frequency is overlaid on a dc bias potential, applied to the working/excitation electrode and measurement of resulting AC current is made. The system remains pseudo-linear at low-amplitude AC potential. The process is repeated for the desired frequency range, and impedance is computed for five to ten measurements per decade change in frequency. In order to ensure the system linearity, stability and repeatability, this method is rendered viable only for a stable and reversible system in equilibrium. For this reason instantaneous impedance measurements are mandatory for non-stationary systems [78]. A non-linear system will contain harmonics (noise) in the measured current response. The drift in the measured system parameters is often observed if the system loses its steady state during the measurement time. The electrochemical cell can change through adsorption, oxidation, coating degradation and temperature variations; to list, these are a few major factors affecting the steady-state condition of the system under test. EIS is used to deduce the changes taking place in the electrochemical system in general and observe the changes in the conductance and capacitance at the sensing surface, interface and layers, in particular. Next section discusses the fundamental concepts of impedance spectroscopy.

2.2.6 Electrochemical Impedance Spectroscopy; Theory and Analyses

In practice, electrochemical cells are example of non-linear complex systems. The relationship of current and voltage is highly non-linear. Pseudo-linearity of the electrochemical system is achieved by considering a small linear part of the I-V curve as shown in Figure 2.2.

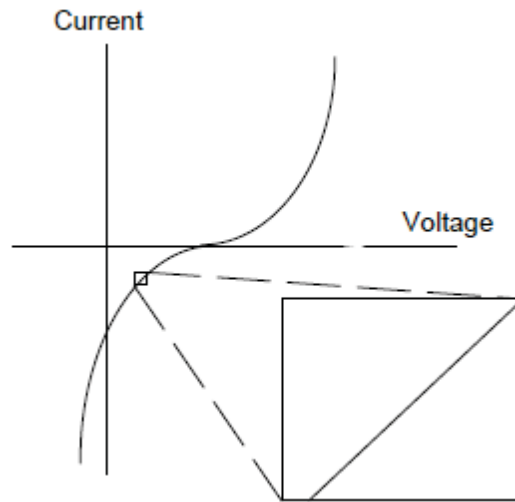


Figure 2.2 I-V curve for a non-linear system. Pseudo-linearity of the system is achieved by considering a small part of the curve

Pseudo-linearity is quite useful because; cell's large non-linear response to Direct Current (DC) potential is not observable as current is measured at excitation frequency; the measure current is independent of harmonics. If the system is non-linear, the current response of the system will be deformed by the harmonics. The system under test must remain in steady-state throughout the testing time; this is another stringent condition that may affect system linearity. With the advent of hi precision fast FRAs and computing systems this problem could be catered for. For example, it takes only 88ms for Hioki 3522-50 to measure impedance, at a particular frequency, without compromising the accuracy of 99.95% while operating at slow mode; refer to Hioki 3522-50 specification sheet shown in Table 2.1.

In a pseudo-linear electrochemical cell, impedance can be measured by applying a low-amplitude AC perturbation, E_t , and measuring the phase shift appearing in consequent alternating current flowing through the sensor with reference to the applied signal. The magnitude of the occurring phase shift depends on the impedance offered to the electron flow by nature of the electrolyte, diffusion, electrode kinetics and chemical reactions

happening inside the cell. Figure 2.3 shows a phase shift θ in the received current signal with reference to the applied potential perturbation.

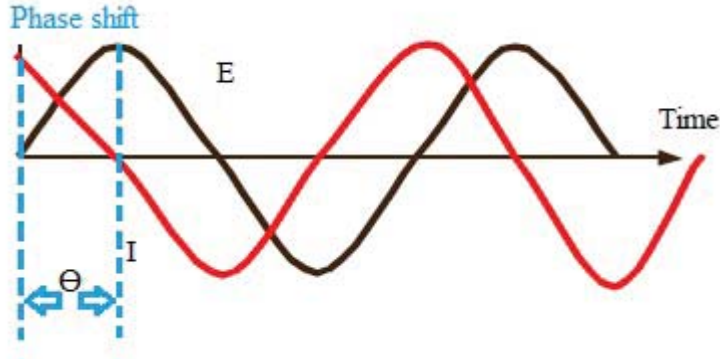


Figure 2.3 Phase shift in current I_t as a response to excitation potential E_t in a linear system

Impedance (Z) is a measure of the circuit characteristics to impede the flow of electrons through the circuit, measured in Ohm, when exposed to periodic electrical perturbations. The reciprocal of impedance is called admittance, denoted by Y and measured in Siemens (S). Mathematically, impedance is expressed as a complex number comprising of resistance and reactance. Resistance is a static property of the system, and is independent of the incident Alternating Current (AC) frequency. It is represented by the real part of the complex number, denoted as R_e , Z_{real} , or Z' . On the other hand, reactance is purely frequency dependent and appears in capacitors and inductors consequent to the applied AC frequency. Reactance is represented by the imaginary part of the complex impedance and is symbolized by R_{im} , X_c or Z_c'' for capacitive reactance and X_L or Z_L'' for inductive reactance, respectively. The basic Ohm's law in Equation 2.1 defines the resistance R in term potential, V , and current I as;

$$R = \frac{V}{I} \quad (2.1)$$

Whereas, Ohm's law for alternating current defines impedance Z in terms of time dependant alternating potential E_t , and current I_t as:

$$Z = \frac{E_t}{I_t} \quad (2.2)$$

The excitation signal can be expressed as a function of time;

$$E_t = E_0 \sin \omega t \quad (2.3)$$

Where E_t is the potential difference at time t , E_0 is the amplitude of the voltage signal at $t=0$, and ω is the angular frequency given by ($\omega = 2\pi f$) expressed in radians/second and frequency, f , in hertz.

For a linear system, the response signal I_t , has a phase shift, θ , with amplitude of I_0 which can be expressed by:

$$I_t = I_0 \sin(\omega t - \theta) \quad (2.4)$$

An expression in equation 2.2 for Ohm's Law can be used to calculate the impedance of the system given by;

$$Z = \frac{E_t}{I_t} = \frac{E_0 \sin \omega t}{I_0 \sin(\omega t - \theta)} \quad (2.5)$$

The impedance, Z , now can be expressed in term of a magnitude of Z_0 and a phase shift, θ . Equation 2.5 can also be expressed in term of Euler's relationship given by;

$$e^{j\theta} = \cos \theta + j \sin \theta \quad (2.6)$$

Where $j = \sqrt{-1}$ ('j' is preferred by electrochemists instead of 'i')

The impedance, Z , can be expressed in term of potential, E , and current response, I , given by;

$$E_t = E_0 e^{j\omega t} \quad (2.7)$$

$$I_t = I_0 e^{j(\omega t - \theta)} \quad (2.8)$$

Therefore the impedance, Z ;

$$Z(\omega) = \frac{E_t}{I_t} = \frac{E_0 e^{j\omega t}}{I_0 e^{j(\omega t - \theta)}} = Z_0 e^{j\theta} \quad (2.9)$$

$$Z(\omega) = Z_0 (\cos \theta + j \sin \theta) \quad (2.10)$$

The impedance now is in the form of real part ($Z_0 \cos \theta$) and imaginary part ($Z_0 \sin \theta$) represented as follows:

$$ReZ = Z' = Z_{real} = Z_0 \cos \theta \quad (2.11)$$

$$Z'' = Z_{imag} = Z_0 \sin \theta \quad (2.12)$$

The raw data for all measured frequencies in EIS experiments comprises of the real and imaginary components of potential difference E' and E'' and the real and imaginary components of current I' and I'' respectively. The phase shift (θ) and total impedance (Z) are the two basic parameters calculated out of the raw data using equations given in Table 2.3. For data analysis purpose, the calculated impedance characteristics are expressed as Nyquist plot and Bode plot.

2.2.7 'Nyquist' and 'Bode' plots for Impedance Data Analysis

Nyquist plot also known as Cole-Cole plot, is one of the most important and popular format for evaluating electrochemical parameters like electrolytic solution resistance (R_s), electrode polarization resistance (R_p) and double layer capacitance (C_{dl}) etc. These parameters shall be discussed in detail in the following sections. Nyquist plot represents $Z'(\omega)$ and $Z''(\omega)$ in a complex plane. Among several advantages of Nyquist plot; calculation of solution resistance by extrapolating the curve to x-axis; observable effects of solution resistance; emphasis on series circuit; comparison of the results of two or more separate experiment, are a few major advantages. One major disadvantages of Nyquist plot is that, information on frequency is lost which makes calculation of C_{dl} complicated.

Bode plot represents absolute $Z(\omega)$ and phase angle $\theta(\omega)$ in the frequency domain. Since frequency appears at one of the axes, the effect of frequencies on the impedance and phase drift is obvious. R_s , R_p , C_{dl} and frequency values, where phase shift $\theta(\omega)$ is maximum /minimum, can be evaluated using Bode plot. This format is desirable when data scatter prevents adequate fitting of the Nyquist plot. Due to these edges, researchers declare Bode plot as a clearer description of electrochemical cell's frequency-dependant behaviour compared to Nyquist plot.

A flow diagram developed by McDonald [77], shown in Figure 2.4, has been followed for analysis of the electrochemical research on detection of hormones and EDCs presented in this thesis. In order to understand the significance and methods to extract

electrochemical cell's parameters, Randle's electrochemical cell model was used to deduce equivalent circuit for the electrochemical cell under test. Complex Non-linear Least Square (CNLS) curve fitting technique was applied to extract equivalent circuit and component parameters.

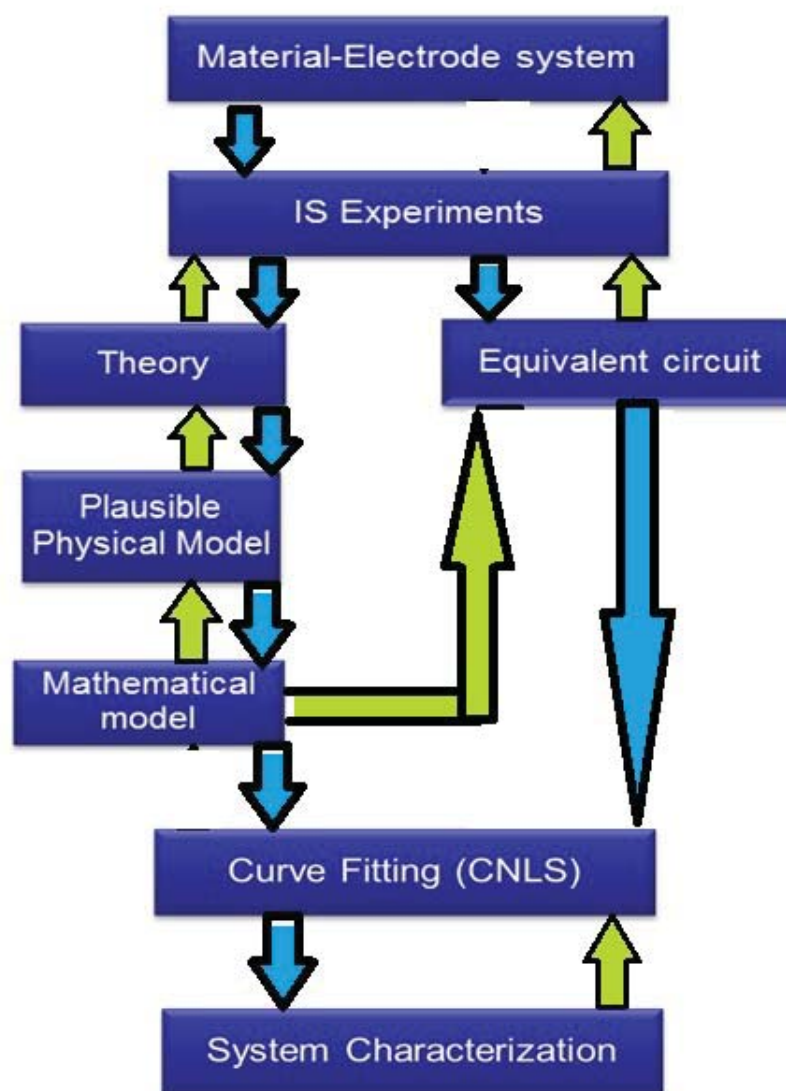


Figure 2.4 Flow chart for the measurement and characterization of a material-electrode system by EIS [77]

2.2.8 Randle's Electrochemical Cell Equivalent Circuit Model

This model was introduced by Randle in 'Discussion of the Faraday Society' in 1947 [79]. The model provides the account of mixed kinetic processes taking place at the electrode-electrolyte interface. These processes include the fast-paced mass transfer reaction, slow-paced charge transfer reaction and diffusion processes at the interface. A

double layer capacitance is observed at the interface due to the presence of Outer Helmholtz Plane (OHP) and inner Helmholtz Plane (IHP) at the electrode surface as shown in Figure 2.5.

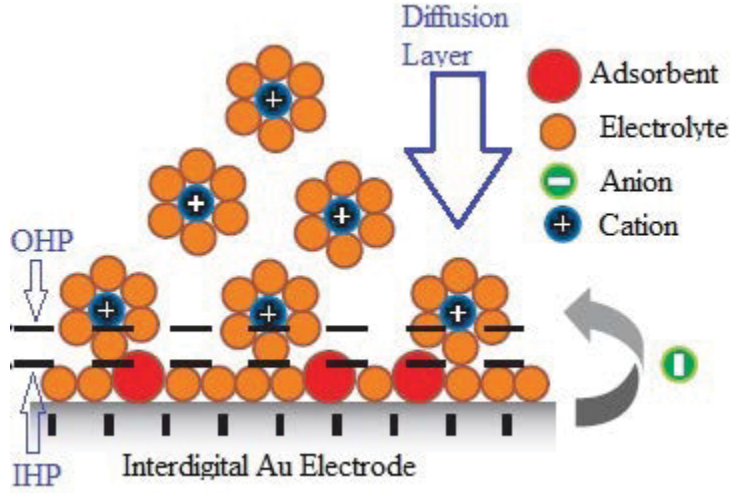


Figure 2.5 Kinetic processes taking place at electrode-electrolyte interface (Randle's cell model)

The Randle's cell includes double-layer capacitance, C_{dl} , solution resistance, R_s , charge/electron transfer resistance, R_{ct} and Z_w as shown Figure 2.6 in the electrochemical cell equivalent circuit deduced in [79].

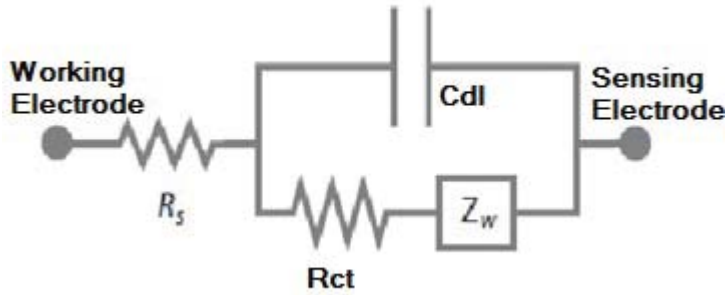


Figure 2.6 Randle's electrochemical cell equivalent circuit model

The expression for absolute impedance as a function of frequency is given as;

$$Z(\omega) = R_s + \frac{R_{ct}}{1 + \omega^2 R_{ct}^2 C_{dl}^2} - \frac{j\omega R_{ct}^2 C_{dl}}{1 + \omega^2 R_{ct}^2 C_{dl}^2} \quad (2.13)$$

Where the real part (Z') is given by;

$$Z'(\omega) = R_s + \frac{R_{ct}}{1 + \omega^2 R_{ct}^2 C_{dl}^2} \quad (2.14)$$

and the imaginary part (Z'') is given by;

$$Z''(\omega) = -\frac{\omega R_{ct}^2 C_{dl}}{1 + \omega^2 R_{ct}^2 C_{dl}^2} \quad (2.15)$$

The impedance spectra from the experimental results depicted electrode and electrolyte are related by a mixed kinetic and diffusion processes at the electrode surface which causes a polarization at the interface. R_{ct} is, therefore, sometimes referred as polarization resistance, denoted as R_p , in EIS literature. The value of ‘charge transfer resistance R_{ct} , r polarization resistance R_p ’ can be calculated from bode or Nyquist plot. The rate of an electrochemical reaction can be strongly influenced by diffusion of reactants towards, or away from the electrode-electrolyte interface. This situation can exist when the electrode is covered with adsorbed solution components, or a selective coating. An addition element called Warburg impedance, Z_w , appears in series with resistance R_{ct} . Mathematically Warburg impedance is given by;

$$Z_w = \frac{\sigma_w}{\sqrt{j\omega}} \quad (2.16)$$

Where, σ_w is called Warburg diffusion coefficient. It appears that the characteristic of the Warburg impedance is a straight line with a slope of 45° at lower frequency. This refers to low frequency diffusion control because the diffusion of reactants to the electrode surface is slow-paced process which can happen at low frequencies only. At higher frequencies, however, the reactants do not have enough time to diffuse. The slope of this line gives Warburg diffusion coefficient. The Nyquist plot in Figure 2.7 shows the diagonal line of diffusion process (Warburg impedance) at low frequency. The charge transfer process at higher frequency is illustrated by a single time constant semi-circle curve.

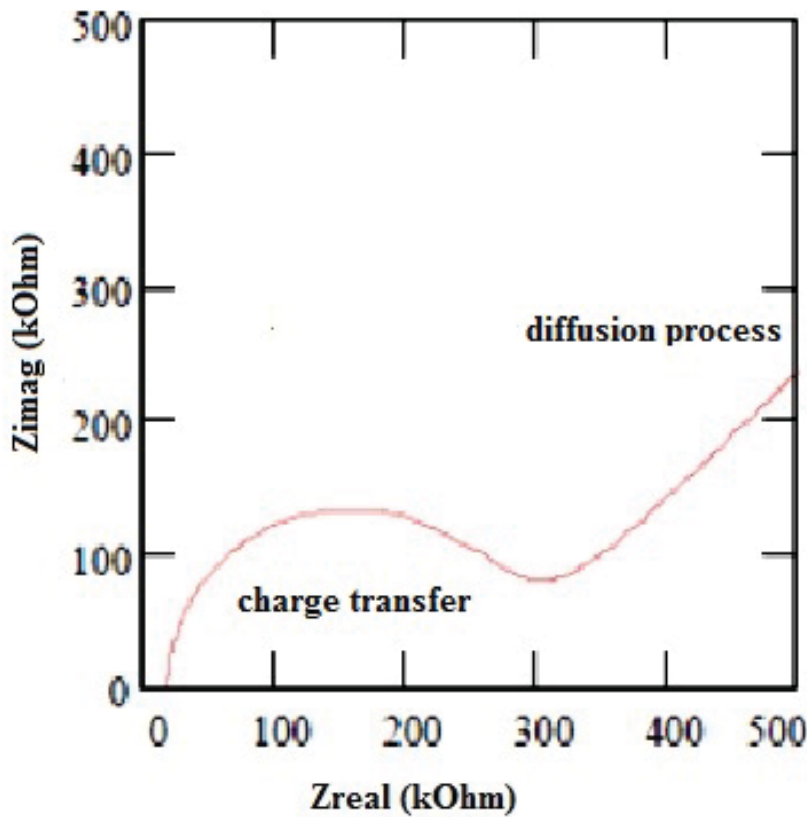


Figure 2.7 Nyquist plot for Randle's electrochemical cell model [79]

The Nyquist plot for a Randle's cell is always a semicircle due to a RC parallel equivalent circuit. The solution resistance R_s , also referred as 'uncompensated solution resistance' denoted as ' R_Ω ' in EIS literature can be calculate by high frequency intercept on the real axis. High frequency intercept lies closer to the origin of the plot. In Figure 2.7 it could be read as 25k Ω . The real axis value at the other (low frequency) intercept is the sum of solution and polarization resistance. The low frequency intercept could be read by interpolating the semi-circle to the real axis. (In Figure 2.7 it reads as 325k Ω). The diameter of the semicircle is therefore equal to the polarization resistance (300k Ω in this case). Figure 2.8 shows absolute impedance, Z , vs frequency and phase angle in degree with respect to the applied frequency, f in Hz. The two plots combined together are referred as Bode plot. Figure 2.9 shows a combined Bode plot for an electrochemical system with Z (absolute) plotted on primary y-axis and phase (degree) plotted along secondary y-axis. Frequency is plotted on x-axis. This format of Bode plot is a useful alternative to calculate solution resistance (R_s or R_Ω), polarization resistance (R_p or R_{ct}) and C_{dl} . Furthermore, the $\log(Z_{abs})$ vs $\log(\omega)$ plot sometimes allow a more effective extrapolation of the data from higher frequencies.

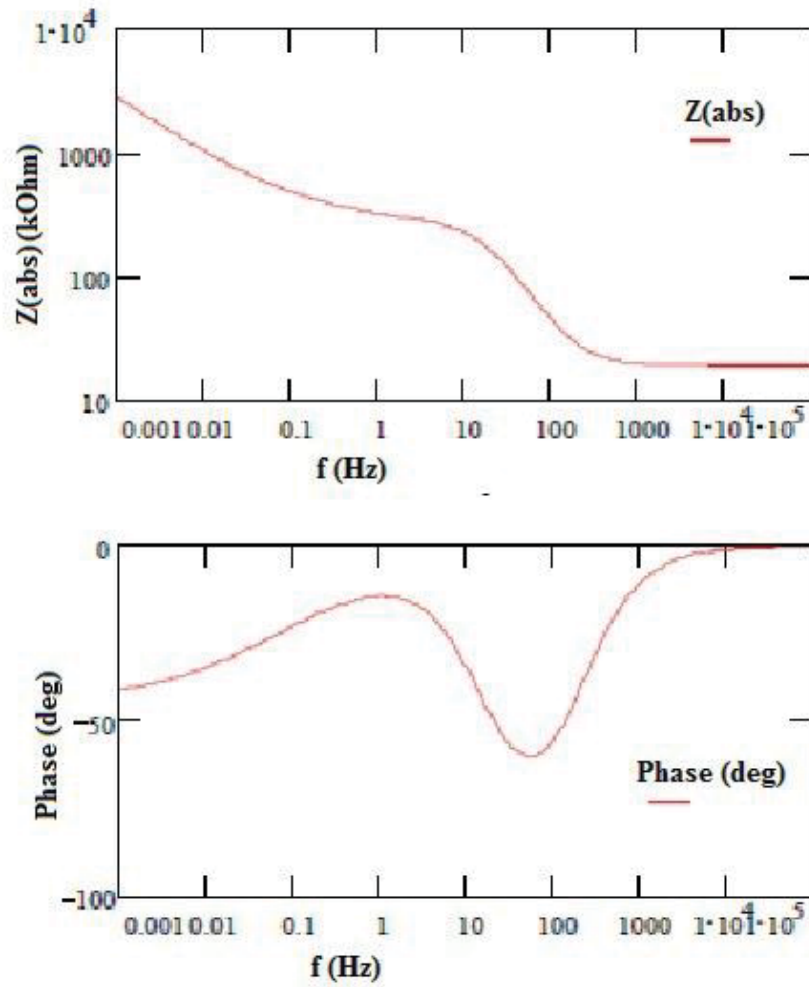


Figure 2.8 Bode plot for Randle's electrochemical cell model[79]

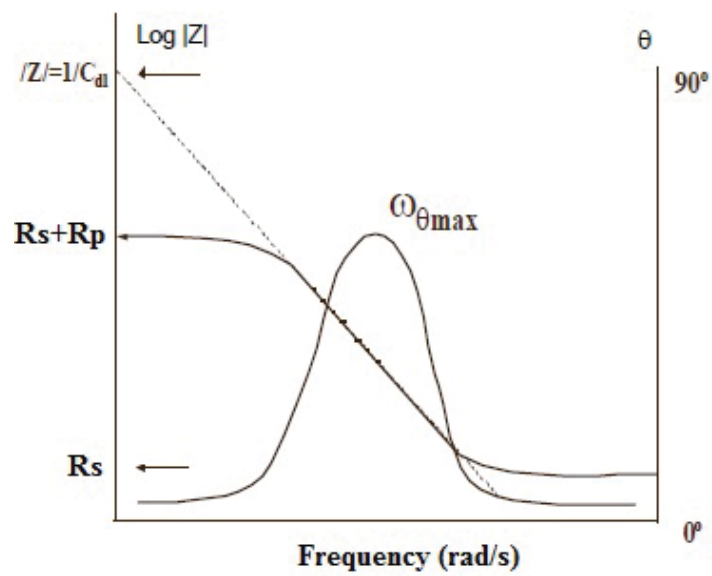


Figure 2.9 Extraction of component parameters from Bode plot[79]

2.3 Experimental Setup

The experiment setup mainly consisted of Hi-precision Hioki 3522-50 LCR meter, Hioki 4-terminal probe 9140, digital thermometer and humidity tester interfaced through RS232 to a tailor-made LabVIEW program executing on a desktop data acquisition computer. The temperature, humidity and inert atmosphere controls were achieved by placing the sensor inside a desiccator, whenever required, to perform the testing under stringent environmental conditions. MicroSuite Laboratory, a research facility available to the School of Engineering and Advanced Technology, Massey University, Palmerston North was used to conduct all set of experiments. Figure 2.10 shows the main experimental setup and the block diagram of the laboratory setup and apparatus used for this research in addition to other in-lab available facilities for heating, cooling, auto enclave, chromatography, microscopy and spectrophotometry etc.

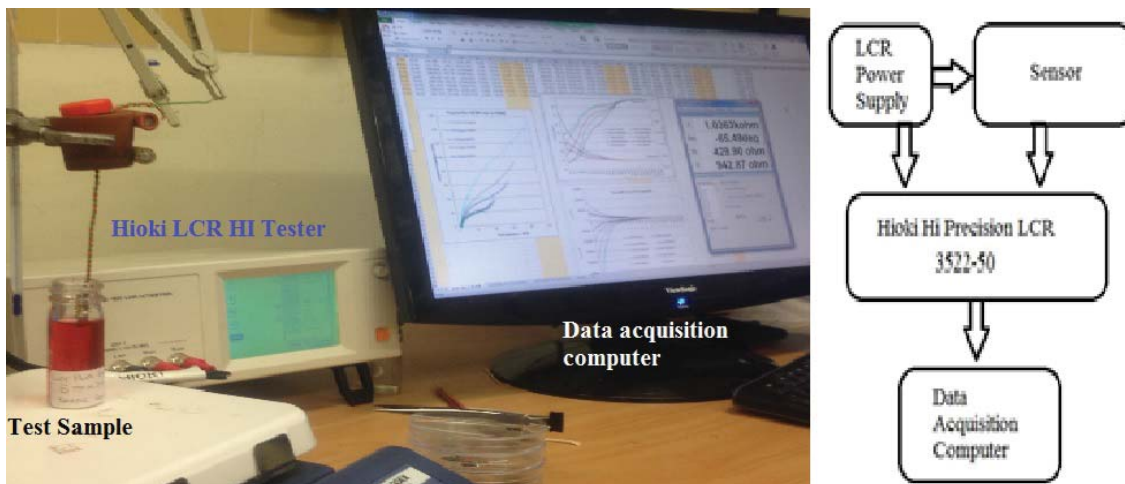


Figure 2.10 Laboratory Test bench with Hioki Hi Precision LCR and data acquisition system.

2.3.1 Equipment and Instrumentations

The high precision LCR meter Hioki 3522-50 and 3532-50 have been used to obtain test parameters' measurements in order to perform investigation electrochemical impedance spectroscopy from 1mHz to 5MHz range as required. The technical specifications of the high performance set of test equipment LCR meter Hioki 3522-50 and 3532-50 are given in Table 2.1. Figure 2.11 shows the front panel of Hioki high precision LCR meter 3522-50.



Figure 2.11 Hioki (Japan) 3522-50 LCR Hi-tester

Table 2.1 Hioki Hi Precision LCR 3522-50 and 3532-50 Specifications

Specifications		
	3522-50	3532-50
Measurement Parameters	Z , Y , θ , Rp (DCR), Rs (ESR, DCR), G, X, B, Cp, Cs, Lp, Ls, D, Q	Z , Y , θ , Rp, Rs (ESR), G, X, Cp, Cs, Lp, Ls, D, Q
Measurement Ranges: Z , R, X	10.00 m Ω to 200.00 M Ω (depending on measurement frequency and signal levels)	
θ	-180.00° to +180.00°	
C	0.3200 pF to 1.0000 F	0.3200 pF to 370.00 mF
L	16.000 nH to 750.00 kH	
D	0.00001 to 9.99999	
Q	0.01 to 999.99	
 Y , G, B	5.0000 nS to 99.999 S	
Basic Accuracy	Z: $\pm 0.08\%$ rdg. $\theta \pm 0.05^\circ$	
Measurement Frequency	DC, 1 mHz to 100 kHz	42 Hz to 5 MHz
Measurement Signal Levels	10 mV to 5 V rms /10 μ A to 100 mA rms	
Output Impedance	50 Ω	
Display Screen	LCD with backlight / 99999 (full 5 digits)	
Measurement Time (Typical Values For Displaying Z)	Fast: 5ms Normal: 16ms Slow 1: 88ms Slow 2: 828ms	Fast: 5ms Normal: 21ms Slow 1: 72ms Slow 2: 140ms
Settings In Memory	Max. 30 Sets	
Comparator Functions	HI/IN/LO settings for two measurement parameters; percentage, $\Delta\%$, or absolute value settings	
DC Bias	External DC bias ± 40 V max. (Option)	
External Printer	9442 Printer (Option)	
External Interfaces	GP-IB or RS-232C (Options), external I/O for sequencer use	
Power Source	100, 120, 220 or 240 V($\pm 10\%$) AC (selectable), 50/60 Hz	
Maximum Rated Power	40 VA Approx.	50 VA Approx.

2.3.2 Fixture and Test Probe Connections

The standard fixture is a four-wire type Hioki 9261 which can be used for all test frequencies from DC to 5MHz. Figure 3.3 shows Hioki 9140 4-terminal test probe with crocodile clip termination which can be used for testing in a range of 1mHz to 100kHz. There are two sets of terminals connecting the sensor to the test equipment. The outer set of terminals, named H_{CUR} and L_{CUR} on the front panel, are used to measure the current flowing through the sensor, whereas, the inner set of terminals, named as H_{POT} and L_{POT} , measure the potential across the sensor at any instant of time. Detail description is shown in Figure 2.12. Table 2.2 shows the details of fixture connection with shielding to device under test (DUT).

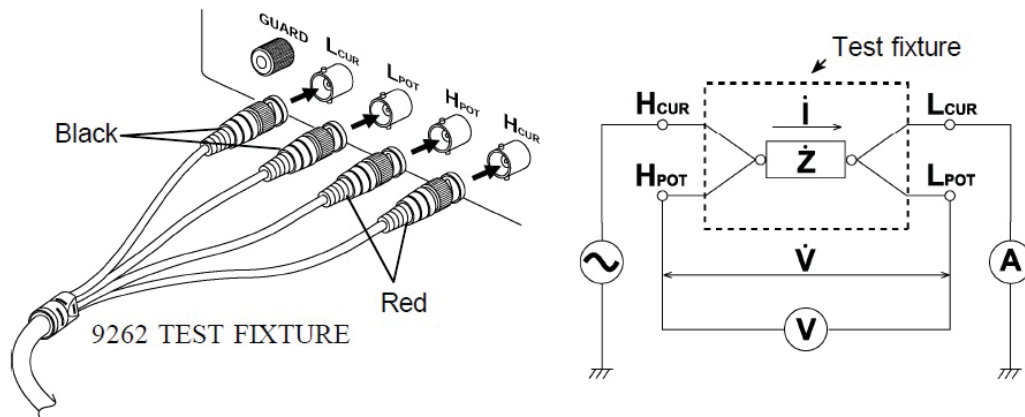


Figure 2.12 Connecting LCR3522-50/3532-50 to the 9262 Test fixture and developed interdigital sensing system

Table 2.2 Hioki Hi Precision LCR test terminals description

Test Terminal	Description
H_{CUR}	Carries the signal current source. Connected to the excitation electrodes of the interdigital sensor.
H_{POT}	Detected high voltage sense terminal. Measure potential difference at any instant of time.
L_{POT}	Detected low voltage sense terminal.
L_{CUR}	Test Current detection terminal.
GUARD	Connected to the GND input to minimize noise.

2.3.3 RS-232C Interface for 3522-50/3532-50 LCR Hi Tester

A RS-232C was used to interface Hioki LCR3522-50 to a desktop/laptop computer in order to develop an automatic data acquisition system. Use of the interface made it possible to control all the functions of the LCR3522-50/3532-50 using software algorithm. The graphical user interface was developed in Labview to input setting parameters except power on/off. The program consisted of commands and queries made by the data acquisition computer system to the interfaced instrument. A command sent is a set of instructions or data to setup the test conditions communicated to the LCR meter, whereas query is a set of data or status information requested from the LCR meter. The LCR transmitted the measured/calculated parameters in response to the queries made by the data acquisition computer. The software echoed back the received automatic measurements of the required parameters' data on the computer monitor via graphical user interface in addition to writing/saving it in Microsoft Excel worksheet in 'xls' format. Table 2.3 provides the details of the parameters measured and calculated by LCR3522-50/3532-50 using the mathematical equations mentioned against each parameter. The data acquisition computer system was used to further analyse the saved information to study the impedance characteristics of the developed sensors and material under test.

Table 2.3 LCR testing parameters and calculation equations

Parameter	Series equivalent circuit mode	Parallel equivalent circuit mode
Z		$ Z = V/I (= \sqrt{R^2 + X^2})$
Y		$ Y = 1/ Z (= \sqrt{G^2 + B^2})$
R	$R_s = ESR = Z \cos\theta $	$R_p = \left \frac{1}{ Y \cos\phi} \right (= 1/G)$
X	$X = Z \sin\theta $	-----
G	-----	$G = Y \cos\phi $
B	-----	$B = Y \sin\phi $
L	$L_s = X/\omega$	$L_p = 1/\omega B$
C	$C_s = 1/\omega X$	$C_p = B/\omega$
D		$D = 1/\tan\theta $
Q		$Q = \tan\theta = (1/D)$

2.4 Conclusions

The experimental setup, instrumentation, program and measurement methods have been discussed in this chapter. High precision LCR meter's interface with the LABVIEW program has been established in order to erect a stand-alone automatic measurement system. Details of the experimental setup, connection cables, instruments settings, and program interface were explained in the chapter. Basic theory of measurement method using Impedance Spectroscopy (IS) has also been discussed to enlighten the reader with the basic measurement methodology. The setup has been built to a stage where it could be interfaced with a smart sensing transducer that could fetch the information from the electrochemical cell, interpret it into required electrical signal so that valuable information about the kinetic processes taking place inside the cell could be extracted. Development of a sensitive, selective and reliable sensor was the most important part of this research project. The details of development of the smart sensor are discussed in the following chapter.

Chapter 3 Novel Interdigital Sensors' Development

3.1 Introduction to Interdigital Sensors

Affinity sensors are the most frequently used devices for biological and chemical sensing research and applications. These can be segregated in two major categories depending on the target binding techniques applied; labeled and label-free. Labeled sensors use immunoassay approach for binding the target molecule that is purely laboratory-based technique involving expensive, time-consuming and hi-tech laboratory protocols, hence, rendering real-time measurements impossible. Sensors for direct, label-free quantification of analytes are attractive to researchers for a number of reasons like direct detection of analytes with minimal or no sample preparation, cost effective, simple and real-time. These involve optical, mass-sensitive and electrochemical detection routes for measurement of analyte in bulk sample. Optical sensors are the most studied but the electrochemical sensors are relatively more sensitive and display comparatively lower detection limit capabilities with a requirement of least complicated support instrumentation. On the other hand, optical and mass-sensitive techniques claim state-of-the-art electronics and bulky instrumentation for interpretation of optical and mass variation data into comprehensible information.

The term 'interdigital' (ID) refers to digit-like or finger-like parallel in-plane electrodes built in a periodic pattern in order to exploit the capacitive effect produced as a result of applied alternating electric field that fringes through the material sample and carries useful information about it. This term is often replaced by 'interdigitated', 'combed' and 'microstrip' in the research literature but strictly speaking it is the name of a specialized geometric structure shown in Figure 3.1, which owns important advantages in accessing the material properties. The most important advantage is a single side access to the material under test (MUT). This advantage provides freedom of penetrating the sample with electric, magnetic or acoustic field only from one side which encourages in situ measurements and detections. Other benefits of interdigital

structures include its capability to be used for non-destructive testing which makes it more useful for process control and inline testing applications. The penetration depth of quasi-static electric field lines can be varied thus making it possible to obtain dielectric profiling and conduction properties of semi insulating materials. These dielectric properties profiling can be further helpful in evaluating other physical parameters of the material under test like density, structural integrity and chemical content in MUT [47].

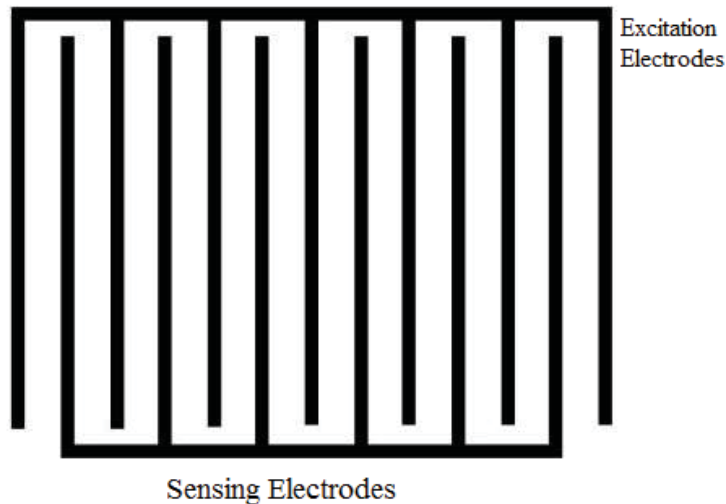


Figure 3.1 Planar interdigital sensor geometry

The technology of planar interdigital sensors is under development since last three decades. These sensors are employed in a number of applications like photosensitive detection [48-51], humidity detection [52-55], chemicals and gas sensing [56-59], moisture sensing applications [60,61] and measurement of electrolytic conductivity [62]. The dielectric characterization to evaluate the material properties is one of the most interesting areas where interdigital sensors along with meander coils are successfully employed to study the dielectric properties of meat, leather, dairy products and saxophone reeds [63-66].

Conventional interdigital sensors operate on the principle of parallel plate capacitor. Parallel plate capacitors offer uniformity of the applied electric field and the equations related to the dielectric material properties are simple, but these 3D structures do not offer single side and non-invasive testing freedom. Interdigital sensors, on the other hand, are 2D structures (coplanar geometry) and provide non-destructive, in situ and single side access to the material under test. The transformation of parallel plate capacitor to interdigital one is shown in Figure 3.2 [47].

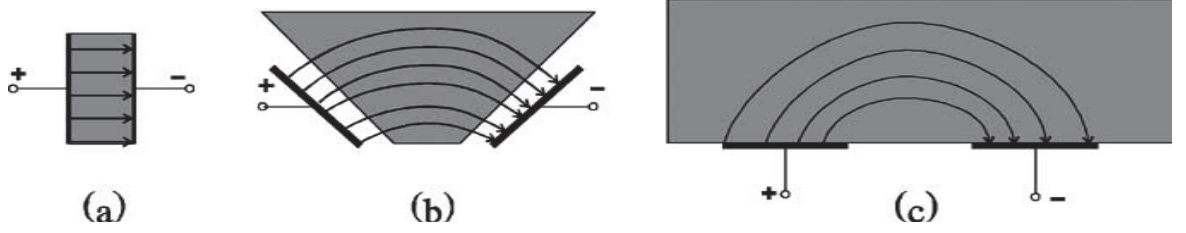


Figure 3.2 Concept of transformation (a) parallel plate capacitor (b) transformation to planar geometry (c) coplanar structure.

The transformation occurred at the cost of electric field which changed from uniform electric field to ‘fringing electric field’ penetrating through the material under test. That is the reason conventional interdigital sensors are also referred as fringing field dielectrometry sensors in literature [47]. The basic idea behind this transformation is to apply spatially periodic electric field to the material under test using single side access to the material. The penetrating field lines combined with the variation of applied excitation frequency carry useful dielectric spectroscopic information about the MUT. A change in the material dielectric properties is a function of various chemical, physical and structural properties of the material, therefore a comparative study of electrochemical impedance spectroscopy of MUT reflect the changes in material properties. The well-known expression for capacitance is given by:

$$C = \frac{\epsilon_o \epsilon_r A}{d} \quad (3.1)$$

Where C is the capacitance, ϵ_o is the permittivity of free space (8.8554×10^{-12} F/m), ϵ_r is the relative permittivity of the dielectric medium used, A is the area, and d is the spacing between the positive and negative electrode. The value of capacitance varies directly with the area A of electrodes, according to equation (3.1), and for interdigital sensors the area of electrode is sacrificed considerably due to its coplanar structure. The value of the capacitance in ID structure is reduced to an extent that it approaches the stray capacitance of the conductors connecting excitation source and electrodes. This limitation necessitates the use of repeated coplanar structures connected in parallel to keep the signal to noise ratio at an acceptable range. Important concepts related to this technology are discussed in detail in [67-70].

3.2 Novel Planar Interdigital Sensors

Depending on the application, the penetration depth of the fringing electric field is considered one of the most important parameter in design of the ID sensor structures. The penetration depth of the fringing quasi-static electric fields above the interdigital electrodes is proportional to the spacing between the centrelines of the sensing and the driven fingers and is independent of frequency [47]. This spacing is termed as spatial wavelength ' λ '. The effect of variation in the spatial wavelength is illustrated in Figure 3.3.

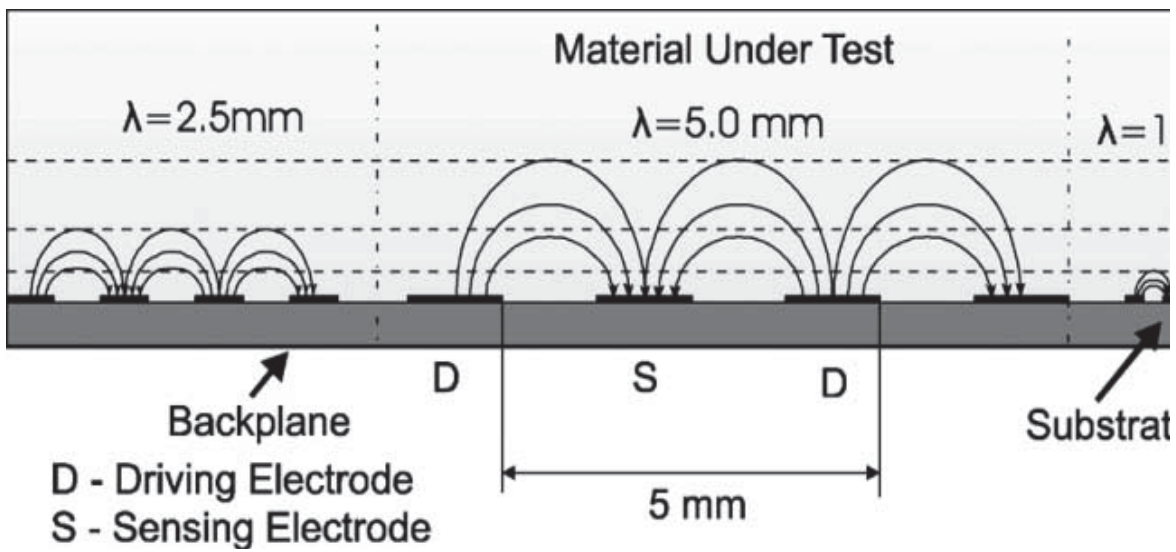


Figure 3.3 The penetration depth of electric field lines is proportional to the electrode spatial period λ

In order to increase the penetration depth, novel ID sensors were designed with more number of sensing electrodes as compared to the driving or exciting electrodes. Different geometries have been discussed in research literature [71-75]. A.R. Mohd Syaifudin et al. investigated the capacitance and penetration depth as a function of number of negative (sensing) electrodes keeping the sensing area of the ID geometry constant, and varying the substrate material. The concept of variation in penetration depth with more number of sensing electrodes is illustrated in Figure 3.4.

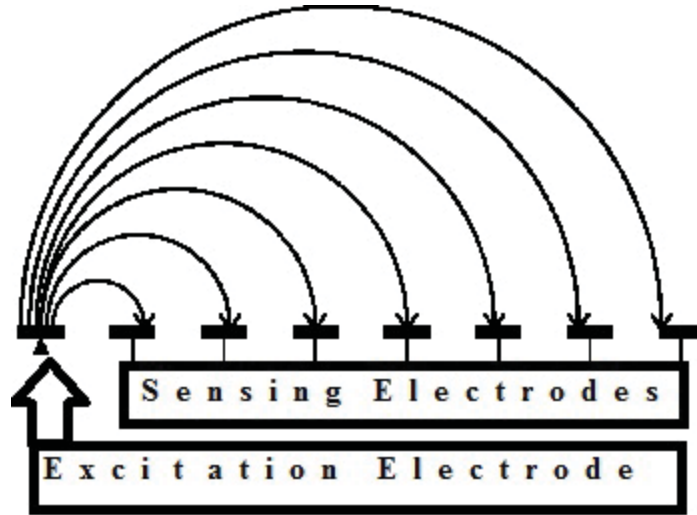


Figure 3.4 Excitation pattern for multi sensing electrode ID sensor geometry

3.3 Finite Element Modelling using COMSOL Multiphysics®

COMSOL Multiphysics is finite element analysis software designed to facilitate physicists and engineers to simulate actual environment and boundary conditions of the experiment to mathematically analyse the outcome of the proposed experiment. The FEM makes use of the solution of partial differential equations and Maxwell's equations to simulate the design and geometry of the sensor. In this research four different geometries of novel ID sensors were simulated using COMSOL. Sensing area, substrate thickness, substrate material and electrode dimensions were kept constant with a variation in the number of sensing electrodes, pitch length and spatial wavelength. To avoid confusion, it is worth mentioning that pitch length is the distance between two adjacent electrodes, whereas, spatial wavelength is the separation between two electrodes of same polarity (excitation electrodes in this case). To obtain a trade-off between capacitance value, pitch length and spatial wavelength for different geometries of the ID sensor were modelled using COMSOL Multiphysics version 4.2.

The sensors were modelled in three dimensional work space with micrometre sized electrodes and pitch length. Four sensors with different geometries and different number of sensing electrodes were modelled keeping the effective sensing area, substrate material, electrode thickness and electrode area constant. Sensing area of each electrode sensor was fixed to 2.5mm x 2.5mm, electrode thickness to 520nm and electrode area was kept constant at 25 μ m x 245 μ m. Each sensor contains different number of capacitive ID features in parallel which enables it to achieve strong sensing signal and

acceptable level of signal to noise ratio. The constant geometric parameters facilitated us in simplifying the design and were in compliance to the available feature size that could be fabricated at the MEMS fabrication facility. Pitch length and number of sensing electrodes were varied in order to get a design suitable for specific application.

Table 3.1 Geometric design parameters for all four types of modelled ID sensors

Sensor Type	Pitch Length (μm)	Number of sensing elect.	Number of excite elec.	Sensing area (mm^2)	Capacitors in ID sensor
1-5-25	25	40	9	6.25	8
1-5-50	50	30	7	6.25	7
1-11-25	25	44	5	6.25	5
1-11-50	50	33	4	6.25	3

Single crystal silicon substrate with thickness $525\mu\text{m}$ and relative permittivity (ϵ_r) 4.2 was used in the models so that the proposed models may practically be fabricated on commercially available 4 inch silicon wafer. In order to calculate capacitance, stored electric energy, penetration depth of electric field lines and field intensity the model was exposed to a dielectric medium on the top with a dielectric constant of 80 and 5.1. These are the dielectric constant values corresponding to pure MilliQ water and DEHP which were selected to observe the model response of each sensor towards the material under test. To obtain higher penetration depth and uniform electric field distribution throughout, the sensor geometry was designed with two configurations of five and eleven sensing electrodes. Figure 3.5 shows the geometric features of two ID sensors 1-5-25, 1-11-25 with pitch length of $25\mu\text{m}$. Figure 3.6 shows the geometry built in COMSOL for 1-5-50 and 1-11-50, bearing pitch length of $50\mu\text{m}$ in both cases. It should be noted that the sensor type number specifies the number of sensing electrodes and pitch length in micrometres. For example 1-5-50 illustrates: 1 excitation electrode, 5 sensing electrodes and $50\mu\text{m}$ pitch length.

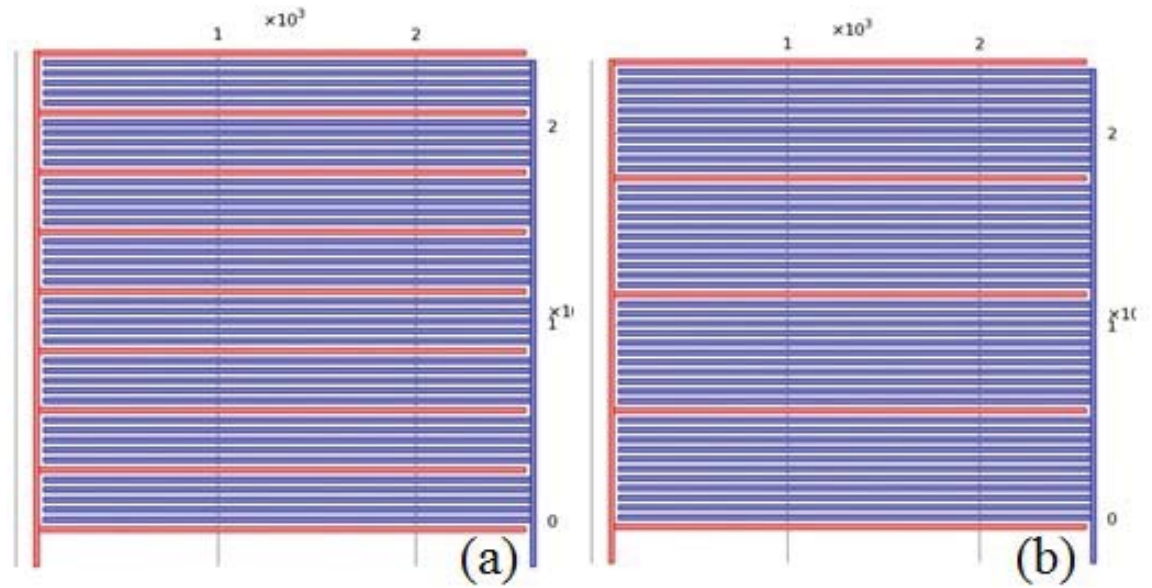


Figure 3.5 COMSOL geometric models of ID sensors with 25 μm pitch length

(a) 1 excitation, 5 sensing electrodes (b) 1 excitation, 11 sensing electrodes

The objective of modelling four different types of sensors was to obtain the best suited design for the proposed application. The models were built on a substrate and a pseudo test medium with known dielectric constant was used on the sensing side in order to figure out the sensor with best possible sensitivity for the material under test. COMSOL uses finite element meshing to evaluate potential distribution and electric field intensity not only in the material under test but in the substrate, as well, to calculate the value of capacitance and stored electrical energy for the whole structure. Figure 3.7 provides a three dimensional illustration of the ID sensor structure displaying simulated substrate and material under test. For viewing of the ID electrode structure, the material under test is rendered transparent in the figure.

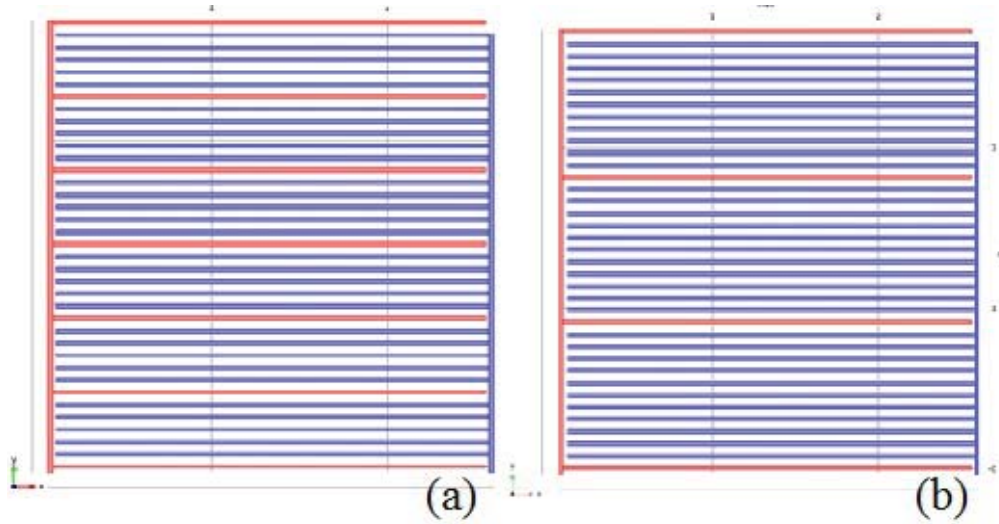


Figure 3.6 COMSOL geometric models of ID sensors with 50 um pitch length

(a) 1 excitation, 5 sensing electrodes (b) 1 excitation, 11 sensing electrodes

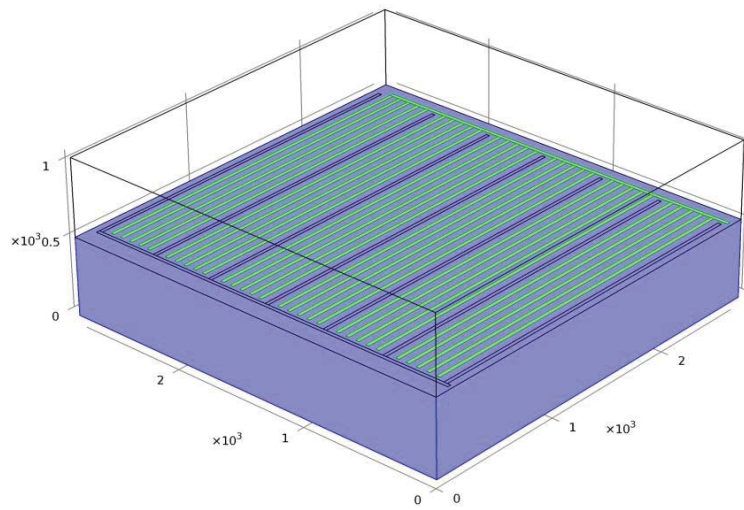


Figure 3.7 1-5-50 Sensor structure; Silicon substrate (bottom) MUT (top)

The electrostatic study of sensors model was carried out using the AC/DC module of COMSOL. Evaluation of electrostatic energy density; ' W_e ' is obtained using the COMSOL simulation. The amount of energy required to charge a capacitor equals energy of applied electrostatic field, given by;

$$W_e = \frac{Q^2}{2C} \quad (3.2)$$

The auto calculation of W_e is available in the Electrostatics application of COMSOL; FEM calculates it by integrating scalar product of electric displacement D and electric field intensity E across the electrostatic domain, $d\Omega$ is the domain boundary. Equation (2.3) shows the expression integrated over the domain to calculate energy.

$$W_e = \int_{\Omega} (D \cdot E) d\Omega \quad (3.3)$$

The capacitance, C , is related to the total charge accumulated on the two conductive plates, Q , and the voltage difference between them, ΔV , by;

$$C = \frac{Q}{\Delta V} \quad (3.4)$$

The calculation of C is carried out from the stored electric energy, W_e .

The voltage across the two plates, ΔV , and is given by;

$$C = \frac{Q^2}{2W_e} = \frac{C^2 \Delta V^2}{2W_e} \Rightarrow C = \frac{2W_e}{\Delta V^2} \quad (3.5)$$

Where W_e is the stored electrostatic energy density and V_0 is the applied voltage to the excitation electrode. The sensing electrode is kept at 0 V.

The analyses conducted using COMSOL were used to evaluate the electric field distribution and electric field intensity for all four sensors. COMSOL simulated electric potential distribution in the sensors is shown in Figure 3.8. and Figure 3.9. For the sake of simplification of the problem, voltage applied to the excitation electrodes of sensor models, V_0 in simulation is kept at 1 volt but the actual experiments were carried out at 100mv-1volt in order to avoid capacitive effects and stray inductance of the connecting wires.

Further analysis was conducted to evaluate the distribution of electric field and intensity for all the four types of sensors. The model calculated the capacitance value and total electrical energy stored for both sensors for anticipated material used for practical testing. For this purpose analyses were carried out for material with dielectric constant 80 (MilliQ) first and then for material with dielectric constant 5.1 (DEHP) keeping the dielectric constant of the substrate 4.2 (single crystal silicon) constant throughout the analyses.

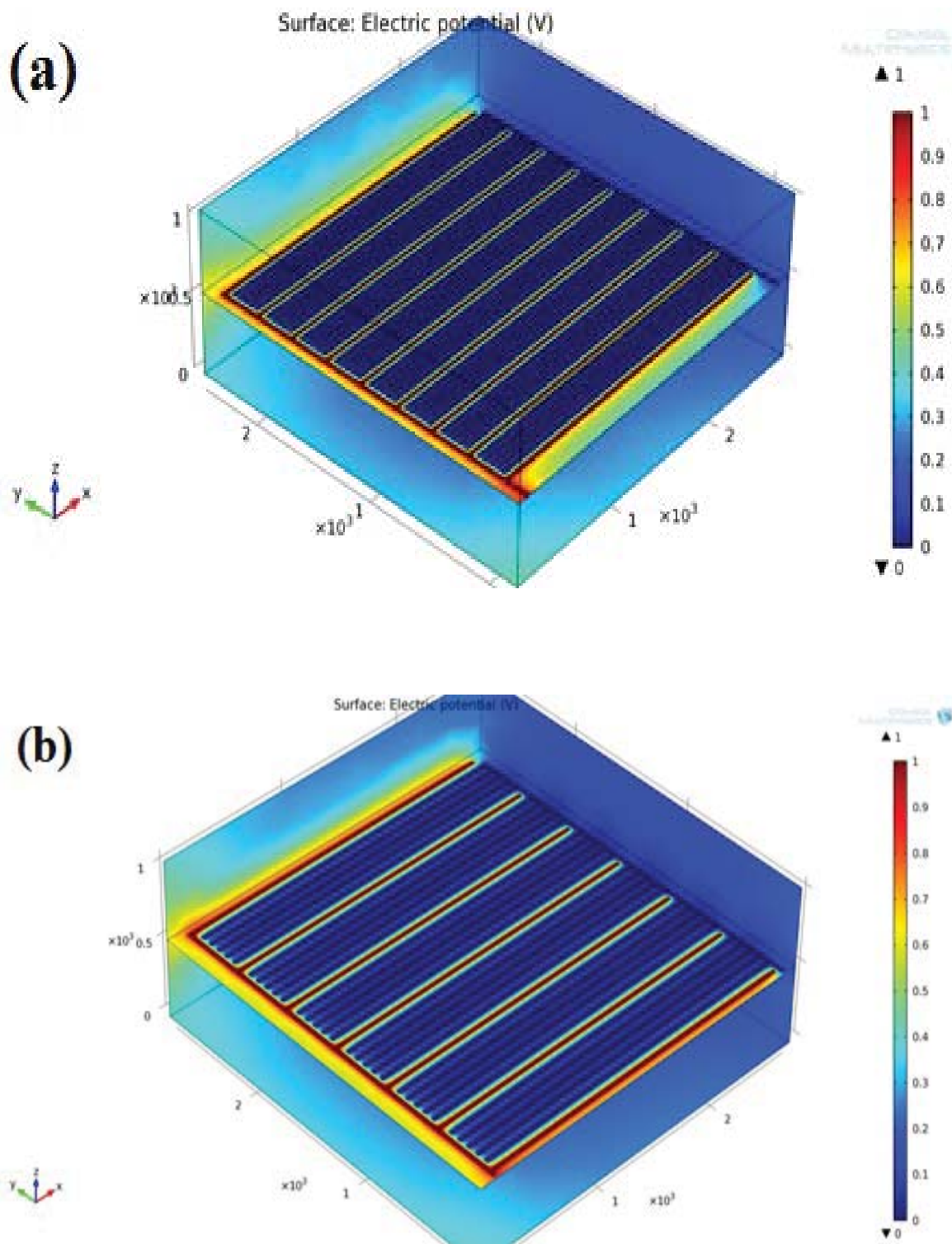


Figure 3.8 Potential distribution modelling in COMSOL for (a) 1-5-25, (b) 1-5-50

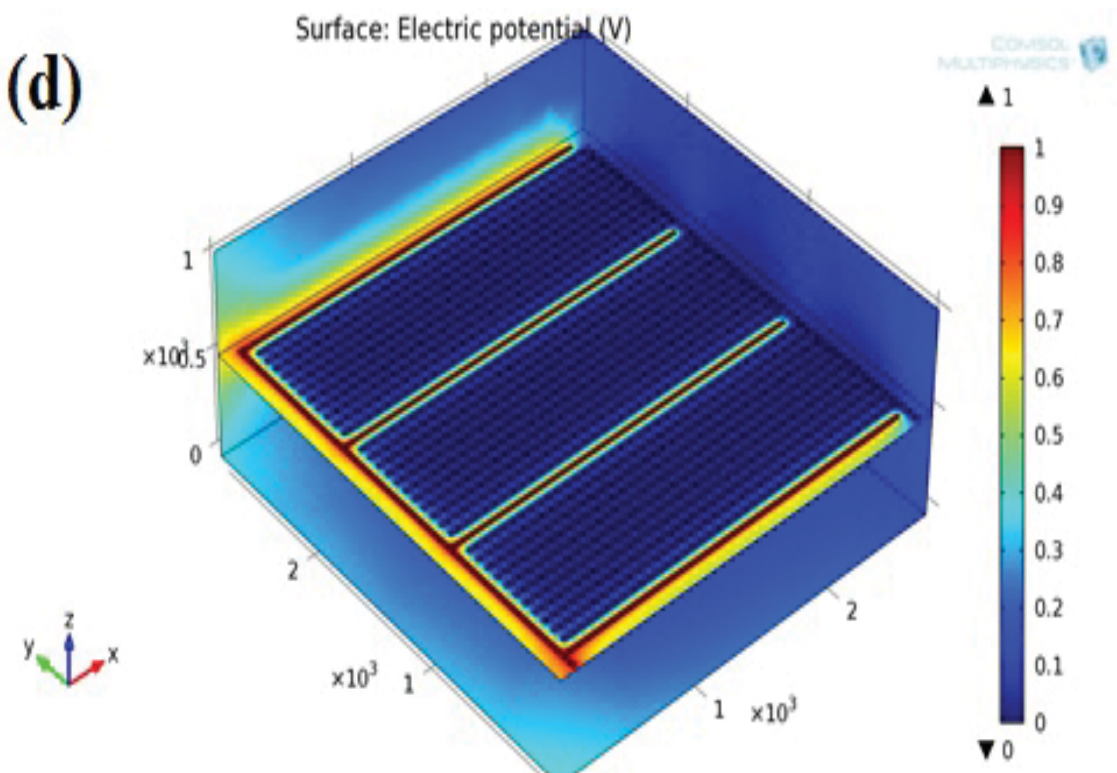
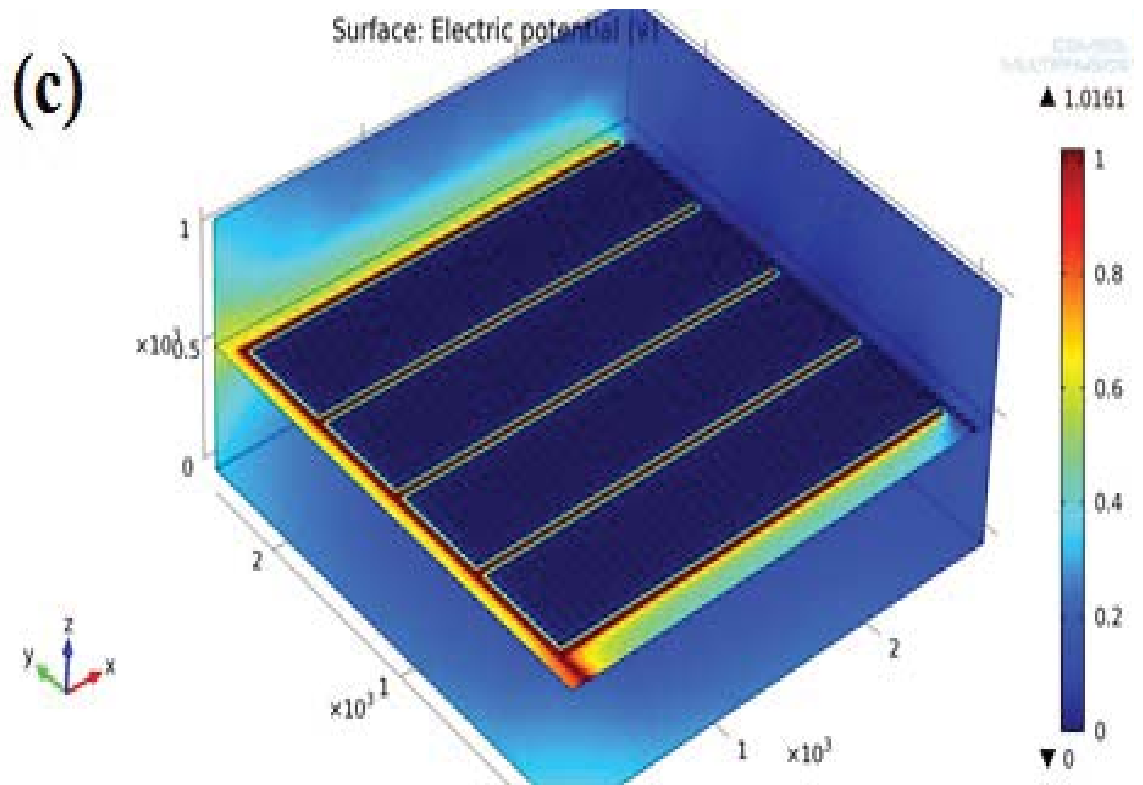


Figure 3.9 Potential distribution modelling in COMSOL for (c) 1-11-25 and (d) 1-11-50 ID sensors

The calculated values for capacitance and total electrical energy stored in are presented in Table 3.2 which provides necessary information to choose the right sensor for fabrication.

Table 3.2 Calculated values of capacitance and total electrical energy stored for all four sensors using COMSOL Multiphysics®

Sensor Type	Milli Q. $\epsilon_r = 80$		DEHP $\epsilon_r = 5.1$	
	Capacitance (F)	Energy (J)	Capacitance (F)	Energy (J)
1-5-25	2.1564e-12	1.0782e-12	2.3915e-12	1.1958e-12
1-5-50	1.3942e-11	6.9712e-12	1.5243e-12	7.6213e-13
1-11-25	1.2619e-11	6.3097e-12	1.376e-12	6.8799e-13
1-11-50	8.4627e-12	4.2314e-12	9.2558e-13	4.6279e-13

The plot in Figure 3.10 shows the capacitance value calculated for all four ID sensors using COMSOL Multiphysics for proposed dielectric medium to be tested i.e. MilliQ and DEHP. The plot shows that sensor 1-5-25 displays least response towards DEHP as it shows nearly same values for both kinds of dielectric mediums.

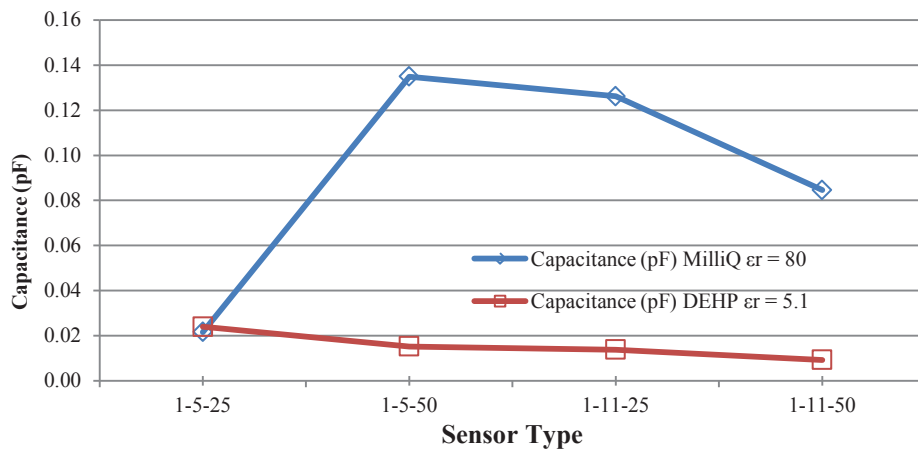


Figure 3.10 Modelled Capacitance for ID sensors

It should be noted that each sensor has different number of parallel ID capacitor features as shown in Table 3.1. The plot for capacitance of single ID capacitor feature is shown in Figure 3.11.

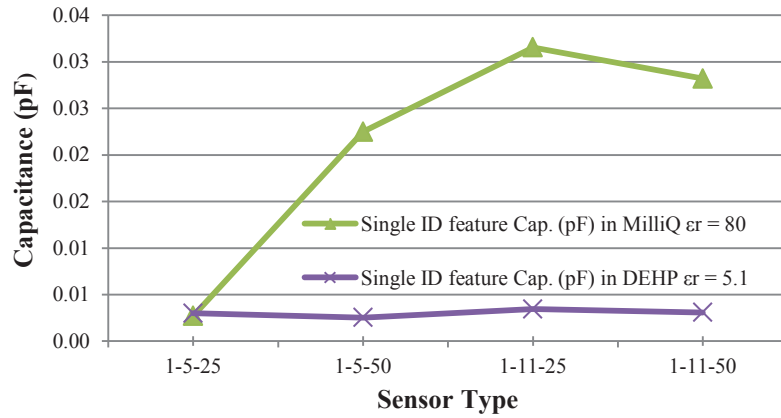


Figure 3.11 Modelled Capacitance of single ID capacitor feature on each sensor

The plot in Figure 3.11 explicitly depicts that 1-11-25 displays most responsive behavior for a medium such as DEHP whereas 1-11-50 should perform comparably well in the detection of DEHP in water. 1-5-50 has an intermediate response whereas 1-5-25 is completely irresponsive to the change of dielectric properties of the material under test. The electric field intensity and penetration depth of electric flux lines simulated in the modeled sensors using COMSOL Multiphysics are shown in the Figure 3.12. Electric field intensity is a measurement of electric field (V/m) along the z-axis. The electric fields simulated on the potential distribution plots provide a clear visualization for the idea of the fringing electric field penetrating through the material under test as described earlier in the literature survey on the topic. It is also worth noting that the electric field penetrates through the substrate material, as well, which contributes toward the numerical calculations of the capacitance and the stored electric energy in the device. For a good comparison of the performance of all four sensors, therefore, the parameter of substrate dielectric constant is not varied throughout the sensor design.

Minimum electric field intensity is observed for 1-5-25, whereas a maximum value for 1-11-50 is clearly displayed in Figure 3.12. The average penetration depth for 1-5-25 is calculated to be 137.5 μm , for 1-5-50 is 212.5 μm , for 1-11-25 is 287.5 μm and for 1-11-50 it has a maximum value of 437.5 μm which is evident in the images from the COMSOL models given in Figure 3.12 and Figure 3.13. The thickness of the test medium was therefore, kept constant at 525 μm throughout the simulation.

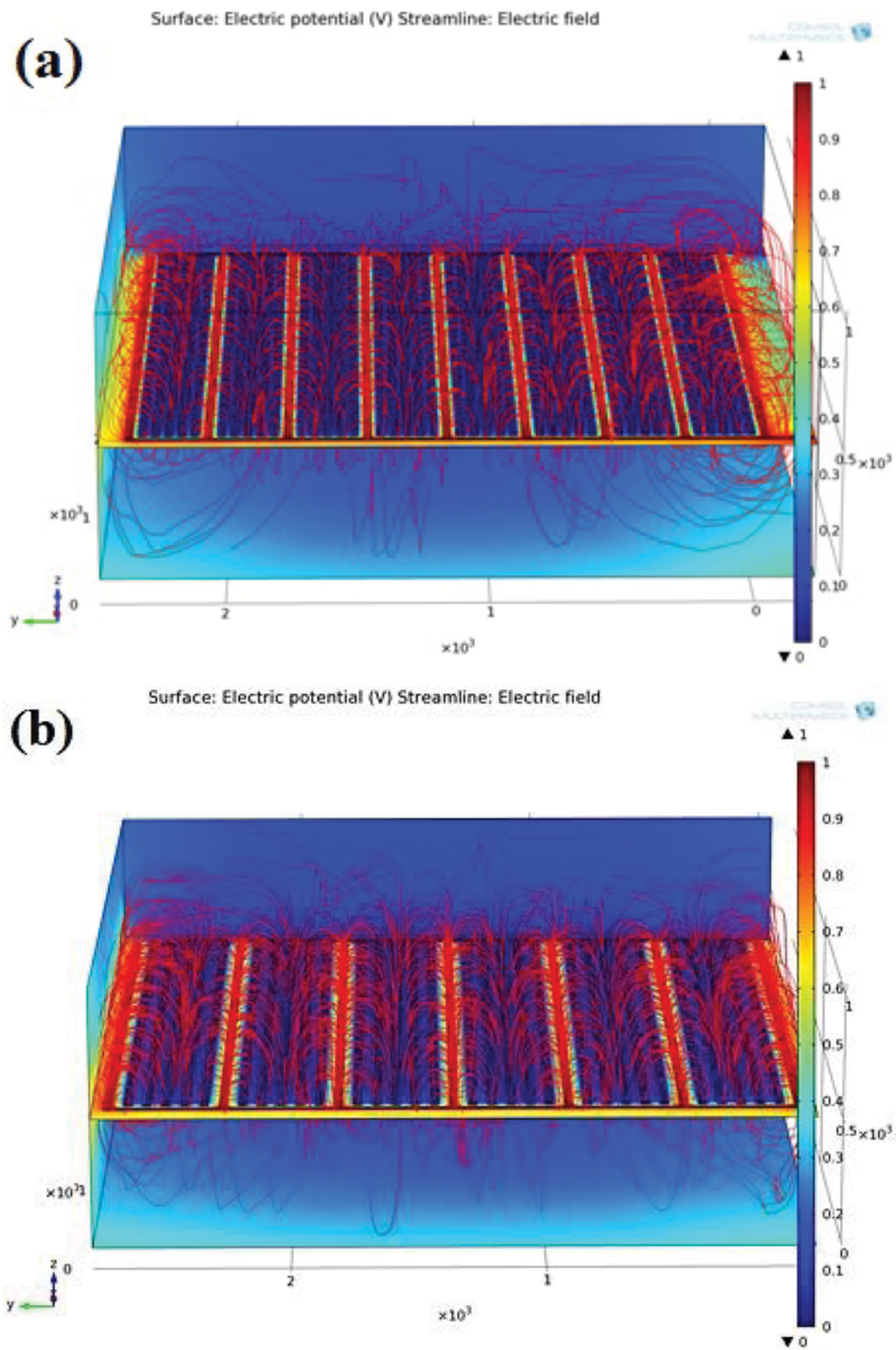


Figure 3.12 Electric field and penetration depth simulation using COMSOL (a) 1-5-25, (b) 1-5-50

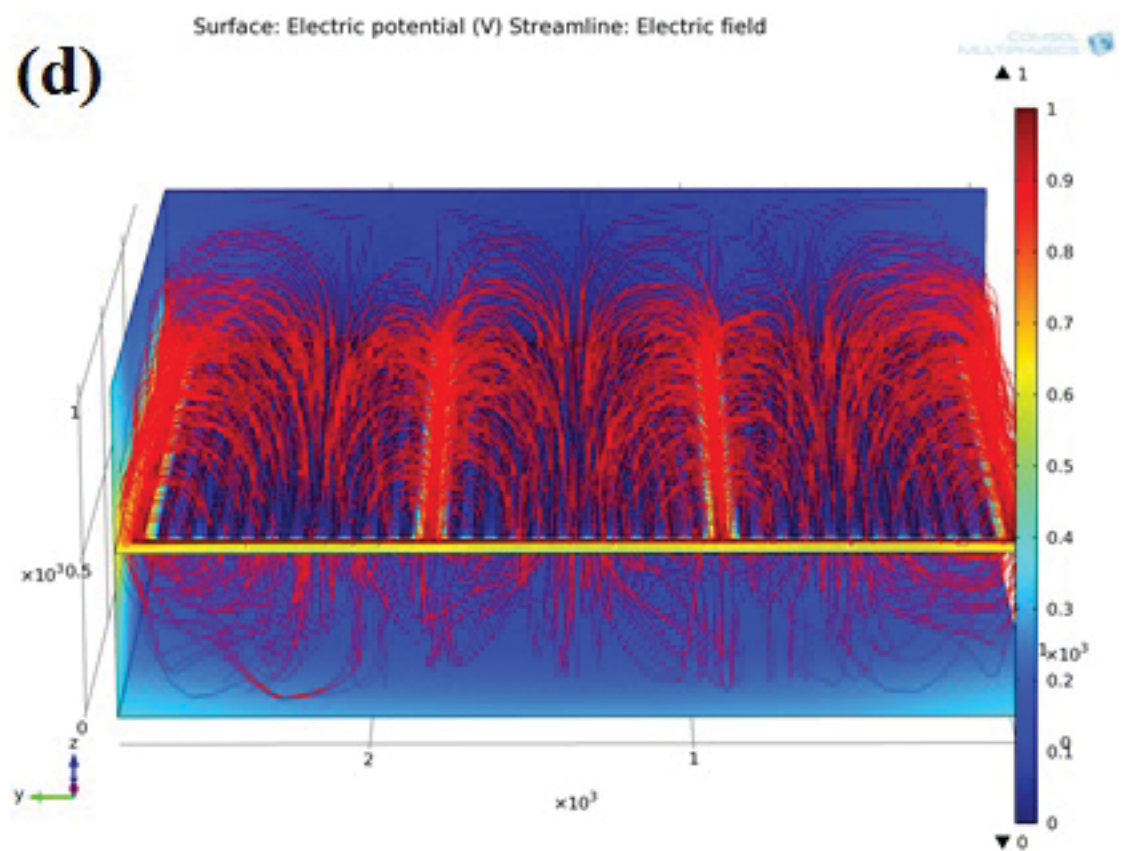
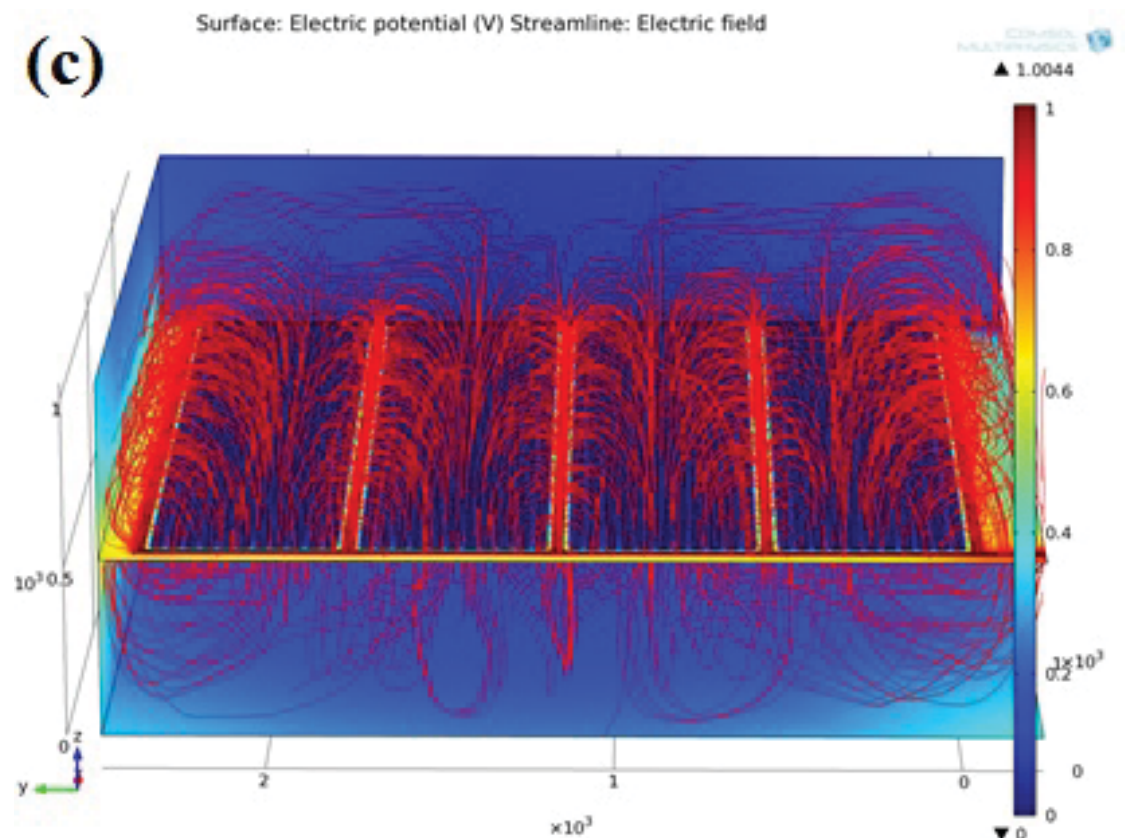


Figure 3.13 Electric field and penetration depth simulation using COMSOL (c) 1-11-25 and (d) 1-11-50 ID sensors

3.4 Sensors' Fabrication

The fabrication of the sensors was realized at King Abdullah University of Science and Technology, Saudi Arabia as a result of academic collaboration between the former and School of Engineering and Advanced Technology, New Zealand. The sensors were fabricated with two pitch lengths, 25 μ m and 50 μ m, respectively. Each type of sensor was fabricated for two repeated patterns of 1 excitation, 5 sensing electrodes and 1 excitation and 11 sensing electrodes coded as 1-5 and 1-11, respectively. This variation was carried out due to the fact that the optimum number of sensing electrodes between excitation electrodes contributes towards the sensitivity of the device. Therefore, four electrode geometries were fabricated for practical performance analysis stated in this research thesis. The wafers fabricated with the said sensor geometries were further coated with polymer layers. All areas except the electrodes and bonding pads were covered with coating. Since the sensing area is kept open, a molecular-selective coating can be applied directly on the electrodes and the sensing area. This approach helped target analytes to be attracted and adsorb as close as possible to the sensing (electrode) surface leading to high detection signals. Two different materials namely; parylene C and Silicon Nitride (Si_3N_4), were used for coating purpose on different wafers of fabricated sensors. Parylene C is a polymeric material that provides pinhole-free isolation for the sensor from the corrosive test samples, but is relatively softer material as compared to Si_3N_4 . Therefore, a coating thickness of 1 μ m was used for parylene C, whereas, Si_3N_4 was coated to 200nm only.

Planar interdigital (PID) thin film electrode structures were fabricated by DC magnetron sputtering process on a single crystal, p-doped, 4 inch diameter, 525 μ m thick and single side polished silicon wafer. Commercially available photolithography and etching techniques were used for the fabrication process. This type of sensors own advantage of noncontact measurements due to fabrication on a rigid substrate which maintains well-defined geometry of the electrode structure essentially required to implement model-based parameter estimation algorithms effectively. 'Coventorware® software was used to design the patterns of the ID structures. 36 workable sensors each with dimensions of 10mm x 10mm and sensing area of 6.25mm² were patterned on a wafer over native grown SiO_2 layer. The width of electrodes was set to a constant value of 25 μ m with sensing area dimensions as 2.5mm x 2.5mm respectively as shown in Figure 3.14. The four ID structure geometries are shown in Figure 3.15.

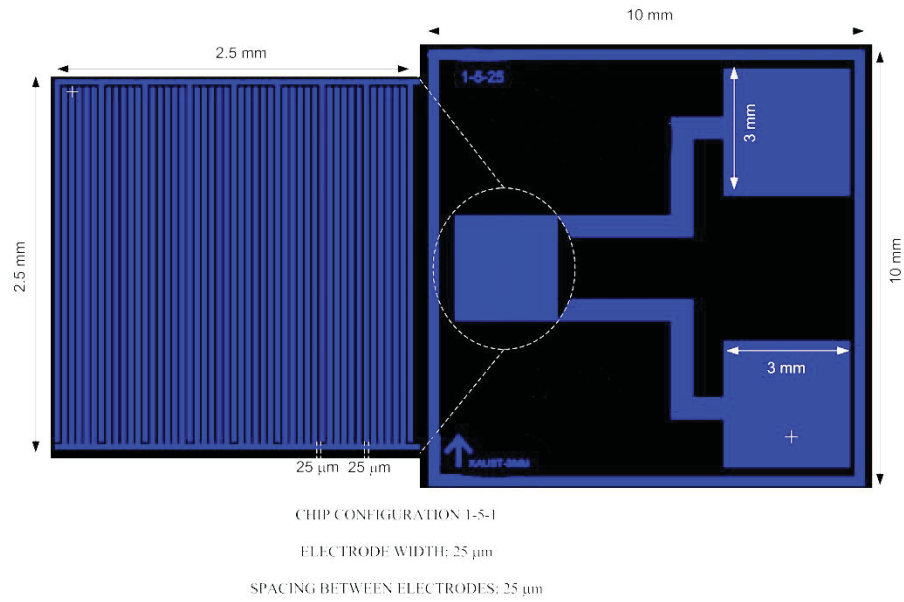


Figure 3.14 1-5-25 sensor: basic design geometry and dimensions

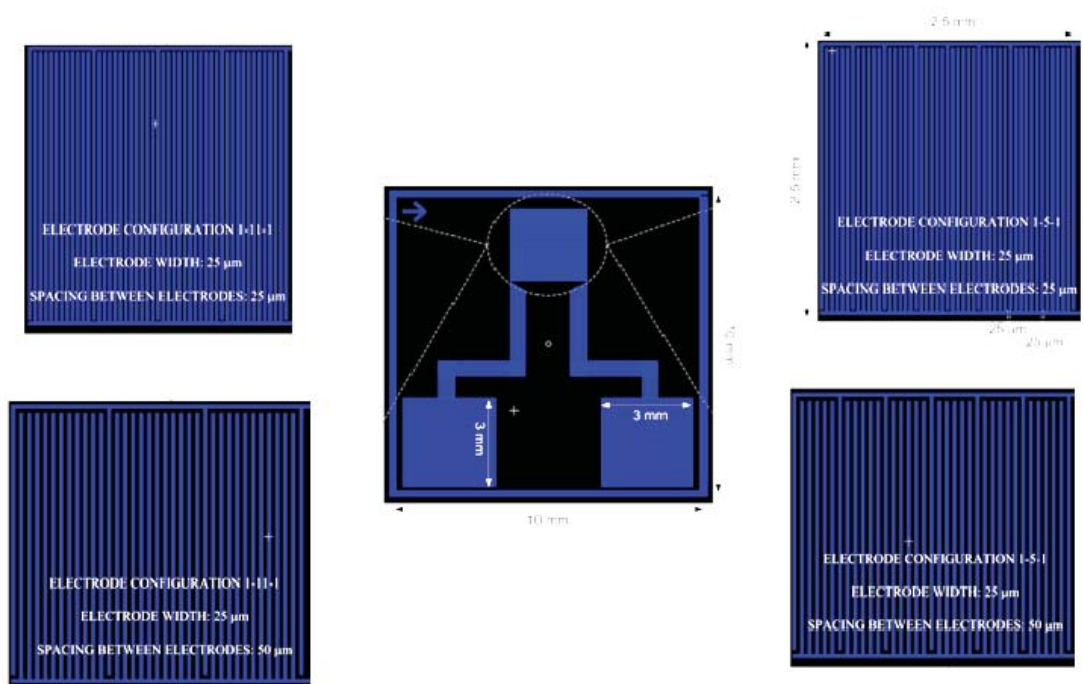


Figure 3.15 Interdigital electrode fabrication configurations

All patterns were printed on a 5 inch soda lime transparent mask using a laser mask writer. Pre-baking was performed at 150°C on the wafer substrate so photoresist attached better to the surface. A spin coater was used to coat 4 μm of positive photoresist (EC13027) on a 4 inch wafer.

An oven was used to post bake the wafer at 100°C for 1 minute. A UV light exposure tool was used to transfer the ID patterns to photoresist of the wafer. A constant dose of 200mJ/cm³ was used at a separation of 30µm between the wafer and the mask. The wafer was then developed for one minute under a solution Tetra-Methyl Ammonium Hydroxide (TMAH) based solution (AZ 726).

Plasma etching at 70°C was used to perform a "Descum" process to remove residual photoresist in the trenches. Following this, 20nm of Chromium (Cr) and 500nm of Gold (Au) where the latter acts as a barrier layer for good adhesion, were sputtered on to the wafer substrate by DC magnetron sputtering. Gold electrodes have the advantage of being inert and flexible.

Argon gas was used at a pressure of 30mTorr and the DC power was set to 800W. Lift-off was then performed under a solution of acetone. Figure 3.16 shows the steps involved in the fabrication process of the sensors.

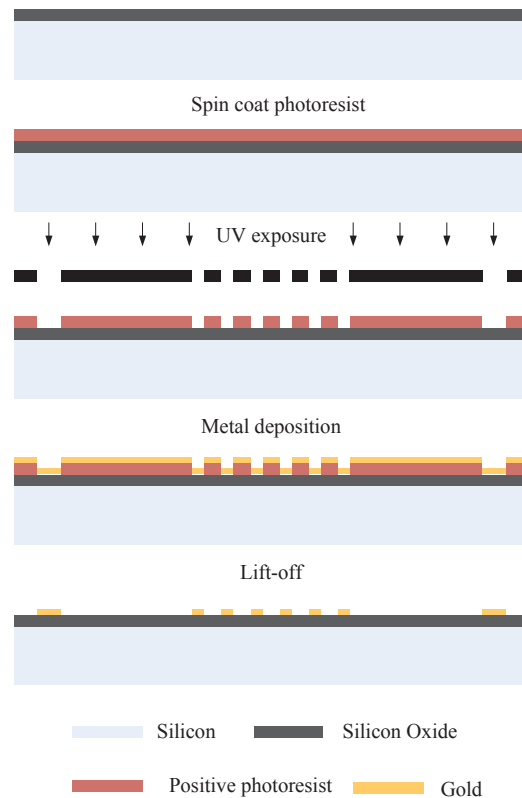


Figure 3.16 Fabrication process for all four types of sensors

After lift-off, the wafer was coated with a 1 µm layer of Parylene C. Figure 3.17 shows the coating procedure with Parylene C. The passivation layer is required to protect the sensing area from corrosion by the solutions used during experimentation. Furthermore,

it prevents moisture diffusion into the Si/SiO₂ substrate that could influence its dielectric properties which would affect sensor response. The electrodes and conducting connecting lines were covered except parts of the bonding pads. Parylene C is an ideal passivation layer since has a favorable combination of electrical and physical properties as well as a very low permeability to moisture and other corrosive substances. Furthermore, parylene can withstand continuous exposure to air at temperatures of up to 100°C for ten years while under vacuum or inert atmospheric conditions the temperature limit increases to 220°C.

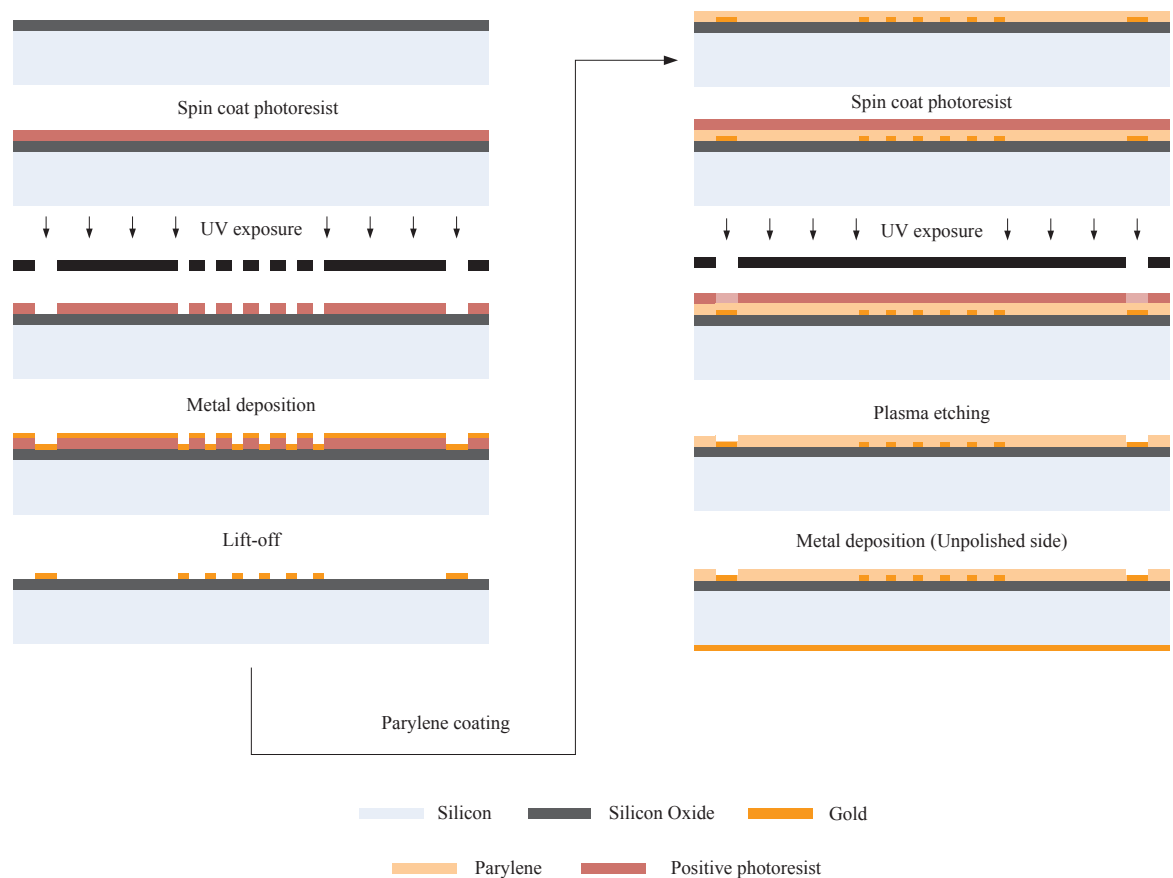


Figure 3.17 Steps involved in coating 1 μm passivation layer of Parylene C

A conformal parylene coater was used to coat the wafer with parylene. The deposition of parylene C is void and pinhole free and it does not edge, bridge or gap and the wafer in the chamber gets uniformly coated since the vapour deposition process is not in line of sight. After the parylene coating 4μm of positive photoresist (EC13027) was coated on the wafer. A UV light exposure tool was used to soften the resist over the bonding pad windows. After development plasma etching was used to etch the parylene and open via to the bonding pads at RF power 800W, temperature (chamber and substrate) 100°C, pressure 500 mTorr and O₂ 100sccm. Figure 3.18 shows 4 inch Silicon substrate

fabricated with all four types of sensors and individual sensor against scale for dimension observation.

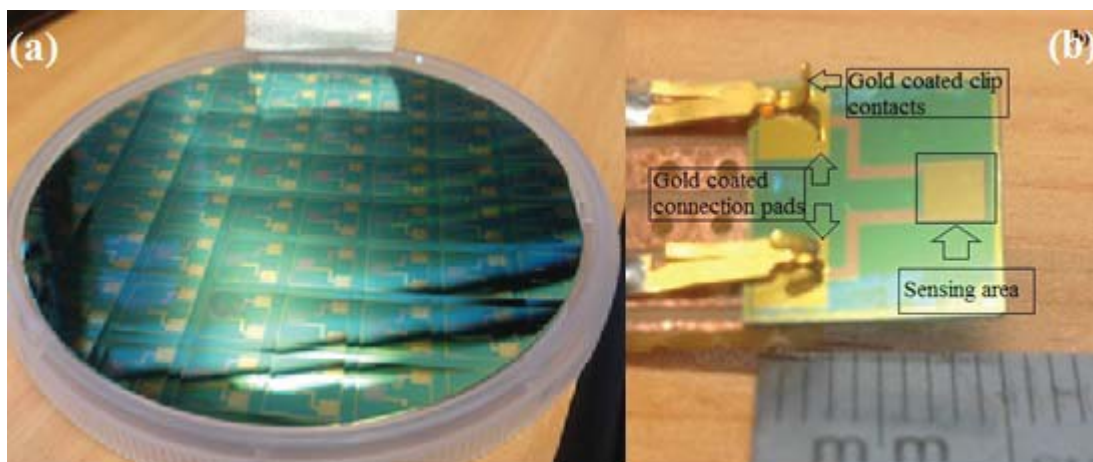


Figure 3.18 (a) 36 Workable sensors fabricated on one wafer (b) Individual sensor shown against scale

An improved design of the silicon sensors were coated with different but relatively harder material, Silicon Nitride. After fabrication steps, as in Figure 3.16, the wafer was coated with a 200nm layer of (Si_3N_4) by Plasma Enhanced Chemical Vapour Deposition (PECVD). Si_3N_4 has been used in many micro-devices as a passivation layer. The silicon nitride film thickness can be easily controlled and modified by varying its deposition methods. Above all, Si_3N_4 thick film can withstand continuous exposure to air and corrosive materials at high temperatures for long periods of time. The deposition of Si_3N_4 using the PECVD technique results in film that owns better adhesion, better isolation and insulation, good step coverage and uniformity. All areas except the electrodes and bonding pads were covered with Si_3N_4 .

3.5 Sensors' Profiling and Problem Definition

Capacitive affinity sensors and transducers could be constructed by fabricating the thin film electrodes with a choice of materials on a number of substrates; and immobilizing analyte recognition compounds in form of thin layers on the sensing surfaces, electrodes or between the electrodes. EIS is used to deduce the changes taking place in the electrochemical system in general and observe the changes in the conductance and capacitance at the sensing surface, interface and layers, in particular. The consequent changes in the dielectric properties or capacitive variations when an analyte binds to the molecular recognition sites could be measured [80, 81]. In order to ensure the system

linearity, stability and repeatability this method is rendered viable only for a stable and reversible system in equilibrium. For this reason instantaneous impedance measurements are mandatory for non-stationary systems [78]. The electrode-electrolyte interface capacitance dominates at low incident frequency, therefore, the system displays high sensitivity towards biochemical-recognition events induced capacitive variations at electrode-electrolyte interface which seems to be a merit point for the applied technique [82].

Unfortunately, high scale of sensitivity renders poor reproducibility and temperature instabilities to the system which changes its parameters even in the testing duration [83-85]. Among many factors like humidity, pH, and test time, etc. it was observed that temperature and surface roughness of the electrode surface are the most vital factors causing instability and there is a dire requirement of inducing immunity in the sensor against these parameters in order to produce stability, reproducibility and robustness in the sensing system for practical applications [81].

3.5.1 Connection Pads Soldering

Soldering connecting wires to connection pads of the sensors revealed that the sensors' profile change as soon as the sensor is exposed to an amount of heat above the eutectic temperature of gold and chromium. This proved to be an irreversible change in the impedance reading capability of the transducer. At 300 °C large fraction of Chromium diffuses into gold thin layer and the soldering temperature approaches that limit with 60:40 composition of Tin (Sn) and Lead (Pb), respectively, in solder [86, 87].

In order to investigate the problem, a selected sensor was profiled for impedance characteristics in air and deionized water. Later, it was re-profiled in same test samples after soldering wires to the connection pads. An average of three sets of impedance measurement was plotted in each case and all the experiments were carried out at identical humidity (44%) and temperature (23.3°C) conditions for all experiments. The Cole-Cole plot in Figure 3.19 shows the shift in the impedance measurements for the same sensor before and after soldering. This initial investigation on the problem led to a detailed study of the fabrication process and understanding the Physics of thin film fabrication by magnetron sputtering [88]. Next section provides a detailed account of the research and development in order to achieve stability in the impedance measurements.

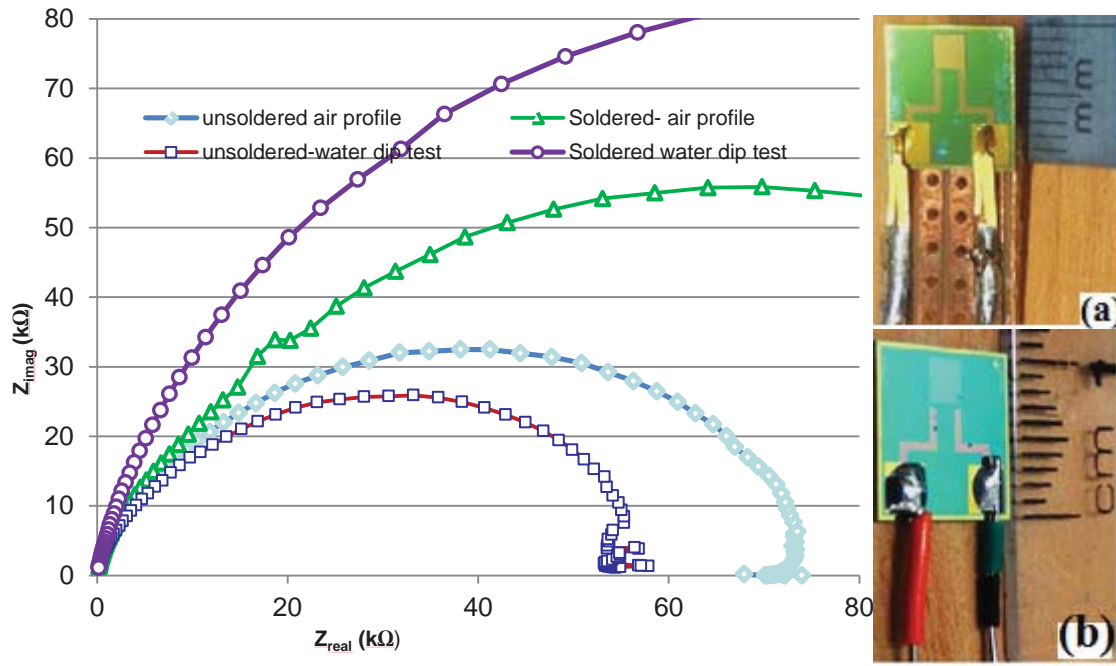


Figure 3.19 Impedance characteristics using same sensor before (a) and after (b) soldering

3.6 Performance Evaluation

3.6.1 Experimental Evaluation

Two sensors 1-1-50A and 1-1-50B were selected from the fabricated wafer for time series profiling in air under same temperature and humidity conditions. Both sensors were identical in terms of design; fabricated with repeated patterns of single excitation and single sensing electrodes and spatial wavelength of 50 μm . The connection pads were clipped in gold plated clipping pins to form connection with the Hioki 3522-50 LCR Hi Tester as shown in Figure 3.18(b). Figure 3.20 shows the inconsistency in impedance measurements by 1-1-50B at different times in presence of identical atmospheric conditions at all times in a lab setup. Figure 3.21 shows the Nyquist plot for sensor 1-1-50A at 44% humidity and 23.3°C temperature at different times mentioned against each measurement. Same unreliability of measurements can be seen this case too that was observed for 1-1-50B shown in Figure 3.20.

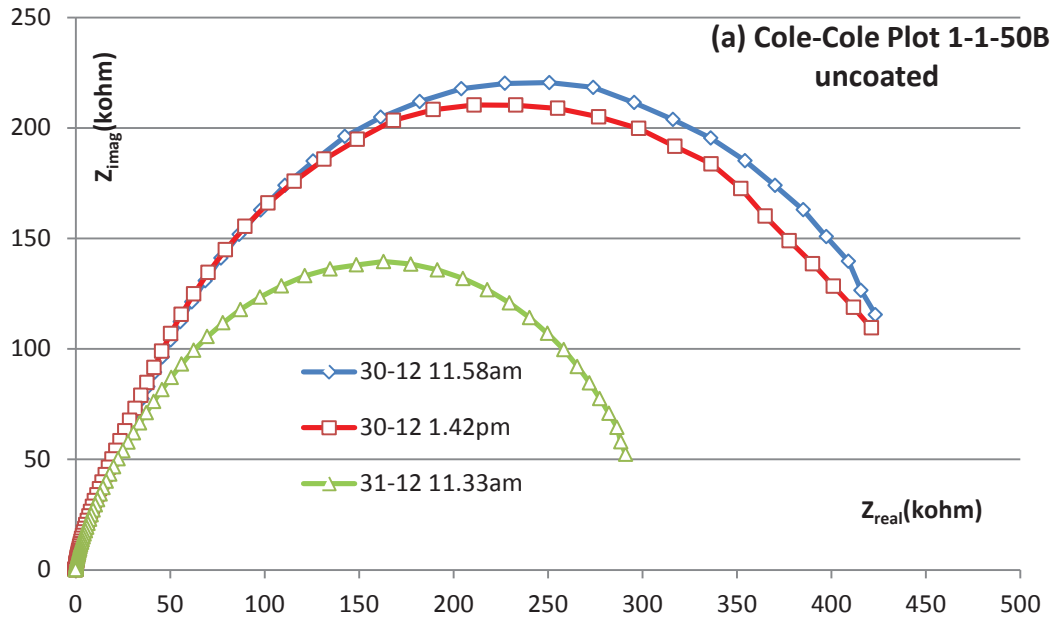


Figure 3.20 Cole-Cole plot for 1-1-50B ‘as is’ fabricated sensor’s test in air at 44% humidity and 23.3°C temperature at different times

It is obvious from the plots that despite of the constant testing parameters the fabricated sensors are not stable in measuring impedance.

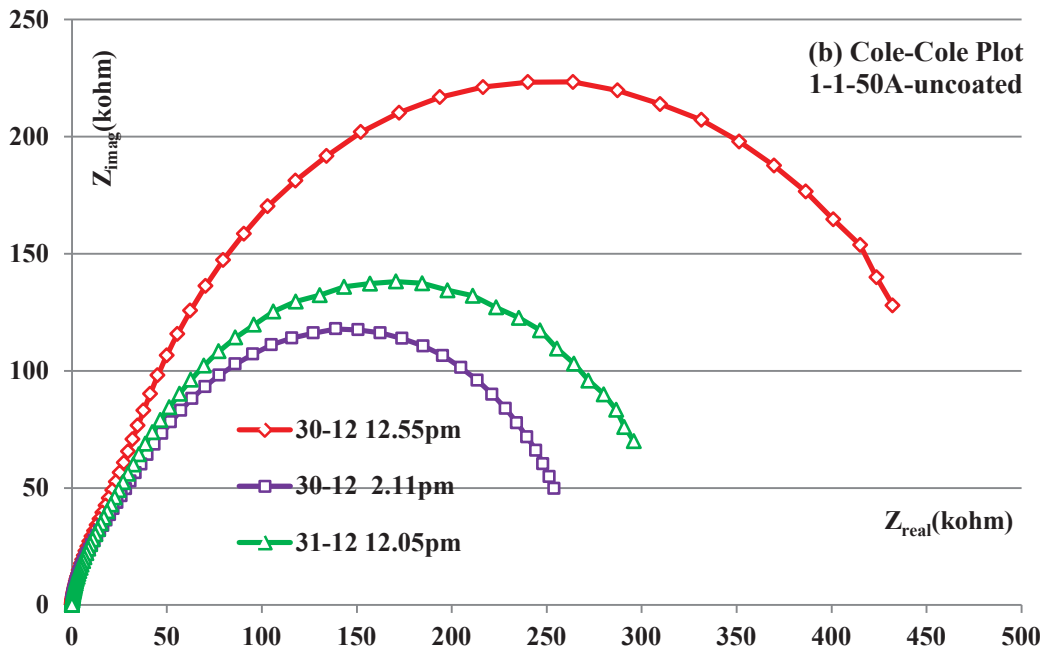


Figure 3.21 Cole-Cole plot for 1-1-50A sensor’s test in air at 44% humidity and 23.3°C temperature at different times

It should be noted that each plot is an average of three measurements and the test equipment was setup to operate in slow mode to keep the measurement error less than 0.05%. Test leads' stray capacitance error was normalized by using device's built-in open and short calibration algorithm. The algorithm measures the test leads capacitance in open and short circuit configurations and use this information to eliminate the noise from the measured values using mathematical methods and accuracy equations as mentioned in the device manual [89]. The impedance plots so obtained verify the stability and reproducibility issues as pointed out in section 3.5 of this manuscript. These kind of challenges have limited the commercial use of the impedimetric sensors and despite two decades of research efforts and hundreds of publications not any product, based on impedance spectroscopy, has achieved widespread commercial success [90, 91]. Serious efforts are lately being made to overcome the dilemma of stability and reproducibility [84, 88].

3.7 Achieving Stability in Sensors' Performance

In this part of presented research, the stability and reproducibility issue of the printable thin film interdigital electrodes has been addressed by looking into the physical and material aspects of the thin film deposition protocols of electrodes. Surface energies and morphology of the deposited/printed thin film electrodes play an important role in the application of electrochemical impedance spectroscopy technique [78, 79, 92]. [92] refers to the early EIS experiments conducted primarily to measure the capacitance of an ideally polarizable mercury electrode in the form of a hanging mercury droplet. Being a liquid metal, the spherical droplet of mercury takes its shape by achieving a balance between the inter-atomic forces and surface energies. This energy balance is responsible for the presence of perfect smooth surface of the mercury droplet. The absence of unbalanced surface and activation energies renders defect-less surface and bulk lattice structure of the mercury electrode, hence providing stability to the EIS measurements. Stability in the EIS measurement is a function of surface morphology which in turn depends on the surface energies and defect-less lattice structure of the thin film printed electrodes. Scanning Electron Microscopy (SEM) was used in requirement to understand the surface morphology of the DC magnetron Argon sputtered gold electrodes for fabricated sensor. Figure 3.22 shows the SEM image of the bare electrode showing grains of the sputtered gold on the electrode surface. Usually, gold does not

display a good adhesion on the silicon substrate. Gold, on the other hand, is the most commonly used electrode material for sensing application due to its excellent physiochemical stability, biological affinity, low electrical resistivity inevitable for impedance spectroscopy measurements and high reflectivity required for optical sensors. In order to deposit Gold on Si substrate, the deposition of a seed layer such as Chromium is required in order to provide better adhesion of Gold on Si wafer. DC magnetron sputtering of Gold over the seed layer of Chromium deposits Gold in form of grains forming the electrode surface. The grain size depends on the rate of sputtering of Gold due to Argon [93]. Even at extremely slow rates of argon flow the sputtered metal deposits in form of grains which is the major cause of surface defects and unbalanced surface energies at the electrode surface [94].

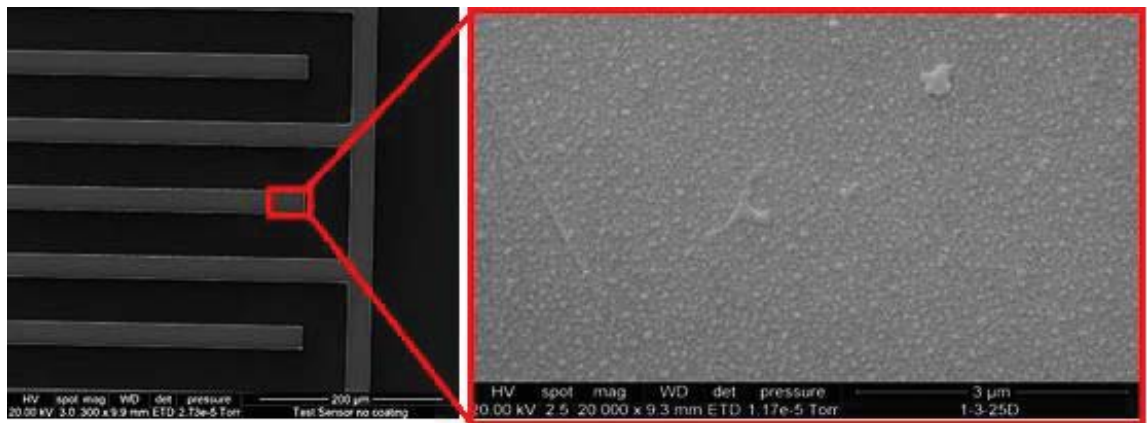


Figure 3.22 SEM image of the fabricated electrode shows roughness of electrodes due to DC magnetron sputtering process

The use of Argon plasma sputtering for gold deposition is a low cost method most commonly used in the semiconductor fabrication industry.

3.7.1 Post-fabrication Anneal of ID Sensor

Owing to the physics of the deposition procedure, lattice structure defects are created within the sputtered gold thin film electrodes [94]. Semiconductor industries follow a long set of procedures to fabricate an electronic device including multiple cleaning, annealing and sintering processes. These necessary procedures help to remove the lattice defects automatically during the fabrication processes. In this case, the sensor fabrication procedure does not involve any annealing step; therefore, the defects in the lattice structure of the gold electrodes are not removed which affect the performance of the sensor. A remedial post-fabrication heat treatment was applied to the sensor to

achieve improvement in its performance, but keeping the fabrication cost to the bare minimum level. A combination of sputtered gold electrodes deposition and post annealing procedure served dual purpose of low cost and better performance of the sensor.

In order to equalize the surface energies and remove the defects from the electrode surface, temperature annealing is the most cited method in material science research [87, 93]. The energy required to eliminate a defect on an electrode surface held at a constant potential is the difference in surface tension per defect on a surface with defect γ_d and surface without defect γ_0 . The work done required to eliminate a defect at the solid interface at constant potential is given by:

$$E_{d(\phi)} = E_d^0 - \lim_{\rho \rightarrow 0} \frac{1}{\rho} \left\{ \int_{\phi_{pz}}^{\phi} (\sigma_d^+(\phi') - \sigma_d(\phi')) d\phi' \right\} \quad (3.6)$$

Where, ϕ is the electrode potential, σ is the surface charge density and ρ is the density of defects on the surface. Analog to Equation 3.6 the activation energy required to transport atom on the surface is given as:

$$E_{d(\phi)} = E_d^0 - \lim_{\rho \rightarrow 0} \frac{1}{\rho} \left\{ \int_{\phi_{pz}}^{\phi} (\sigma_d^+(\phi') - \sigma_d(\phi')) d\phi' \right\} \quad (3.7)$$

$\sigma_d^+(\phi')$ is the charge density on the surface with defects in the activated transition state. Generalizing surface charge densities around a particular potential ϕ_0

$$\sigma_d(\phi) = \sigma_d(\phi_0) + C_d(\phi_0)(\phi - \phi_0) \quad (3.8)$$

$$\sigma_0(\phi) = \sigma_0(\phi_0) + C_0(\phi_0)(\phi - \phi_0) \quad (3.9)$$

$C_d(\phi_0)$ and $C_0(\phi_0)$ are the differential capacitance of the surface with and without defects. Using Equations 3.6, 3.8 and 3.9:

$$E_{d(\phi)} = E_d^0 - \lim_{\rho \rightarrow 0} \frac{1}{\rho} \left\{ \sigma_d(\phi_0) - \sigma_0(\phi_0)(\phi - \phi_0) + \frac{1}{2} (C_d(\phi_0) - C_0(\phi_0)(\phi - \phi_0)^2) \right\} \quad (3.10)$$

At a small potential, the defect energies behave as linear function of potential difference. This holds good for the activation energies required for defect transport process too [95, 96].

The annealing temperature and time are the most important parameters in this regards. Annealing temperature was set to reach 210°C in seven steps of 30°C each considering presence of both Gold and Chromium thin films on the sensor surface. At 300°C large fraction of chromium diffuses into gold thin layer, consequently increasing the resistivity of the electrodes that may lead to poor circuit characteristics [86]. 210°C was set as a trade-off between electrode surface defects' removal and avoid unwanted diffusion of Cr into gold to keep the resistivity of the electrodes to a minimal level. In order to observe the changes in the sensing characteristics with temperature the sensor was set in the vacuum oven and the oven was programed to start from 30°C, anneal the sensor for one hour and raise the temperature to 60°C at a rate of 10°C per minute. Anneal again for one hour and increase temperature to 90°C at the same rate and so on. At the end of each annealing step, impedance measurements were taken twice before the oven moves to next temperature range. Annealing process of the sensor was carried out in vacuum oven in order to avoid oxidation of electrodes and silicon surface.



Figure 3.23 Annealing sensors in vacuum oven in Micro-Suit

3.7.2 Results' Validation

The plot of all the impedance measurements during anneal procedure is given in Figure 3.24. Consequent to the annealing procedure, the sensor was tested again under initial humidity condition in order to observe its behaviour. The impedance measurements were taken in duplicate at different times and temperatures in a pre-heated oven. A

maximum of 90°C was reached to avoid oxidation at higher temperature. Figure 3.25 shows the impedance plot for the annealed sensor at 30, 60 and 90°C.

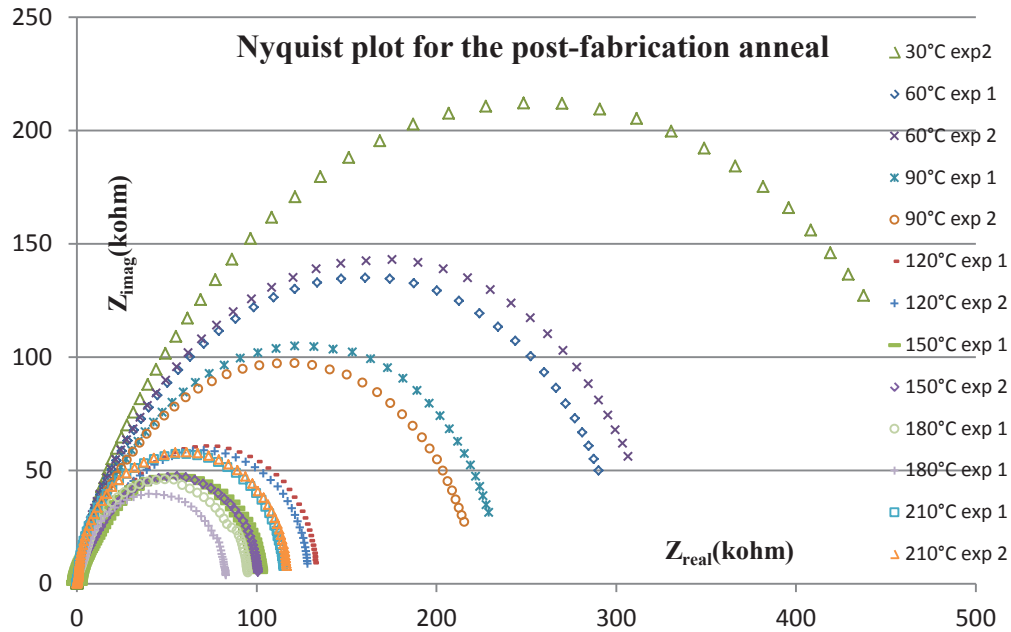


Figure 3.24 Nyquist plot for EIS during annealing process at 30, 60, 90, 120, 150, 180, and 210 ° C

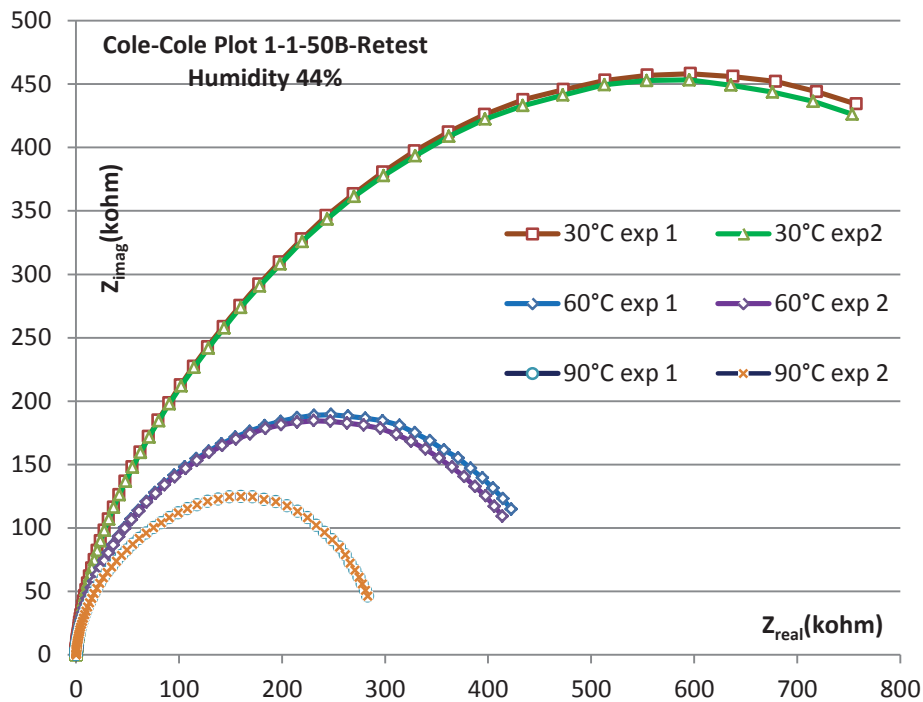


Figure 3.25 Nyquist plot for improved performance annealed sensors at initial temperature and humidity conditions

It is obvious from Figure 3.25 that annealing has affected the profile of the sensor in a drastic manner. The sensor behaves identically under same temperature and humidity

conditions while profiled at two different times at a lapse of one hour, which is quite promising in terms of stability and repeatability of the impedimetric measurements. The SEM image of the electrode surface, after annealing, shows highly smooth electrode surface as displayed in Figure 3.26 SEM image of electrode before (a) and after (b) anneal(b). It should be noted that a dust particle was focused in the image to provide depth and contrast to observe surface smoothness. For comparison, the SEM image of same part of the electrode surface is given in Figure 3.26 (a). It is obvious from the figures that even at a resolution of 40,000 the electrode surface appears smooth without any grains and grain boundaries.

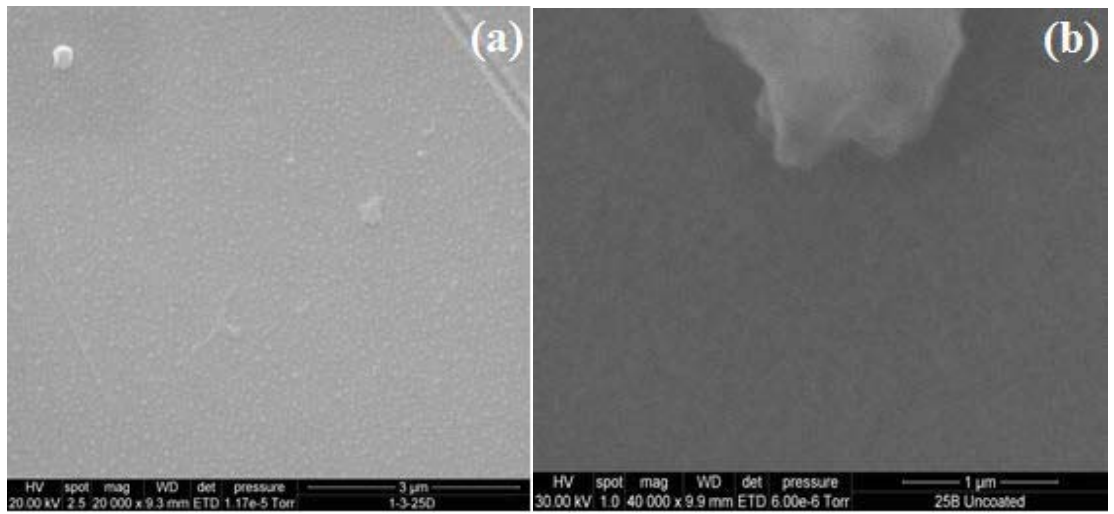


Figure 3.26 SEM image of electrode before (a) and after (b) anneal

3.7.3 Complex Nonlinear Least Squares Curve Fitting

Electrochemical spectrum analyser algorithm was used to deduce the equivalent circuit and component parameters by fitting the experimental data on its theoretically estimated response based on Randle's model. The algorithm performs statistical analysis to calculate the residual mean square $r_{amplitude}^2$ for experimentally observed values in measured spectra by complex nonlinear least square using following relation [75, 97].

$$r_{amplitude}^2 = \sum_{i=1}^N \frac{(Z'_{iobs} - Z'_{icalc})^2 + (Z''_{iobs} - Z''_{icalc})^2}{Z'_{iobs}^2 + Z''_{iobs}^2} \quad (3.11)$$

Where Z'_{iobs} is the observed real impedance.

Z'_{icalc} is the calculated real impedance.

Z''_{iobs} is the observed imaginary impedance.

Z''_{icalc} is the calculated imaginary impedance.

$r_{amplitude}^2$ determines the deviation of the experimentally observed data from the optimal solution. Table 3.3 shows components' parameters for optimal curve fitting of the experimental data averaged over three fittings. An interesting observation made was that the sensor's response to the fitted circuit model changed with the change in annealing temperature.

Table 3.3 Component parameters for the best fit circuit

$$(r_{amplitude}^2 = 1E - 4)$$

Temp	30°C	60°C	90°C	120°C	150°C	180°C	210°C
C1 (nF)	0.768	0.818	0.533	1.07	1.80		
C2 (nF)				1.28	0.92		
R1 (Ω)	2.88E-06	2.68E-10	1.96E-13	1.39E+01	3.12E-01	3.54E-02	6.84E-02
R2 (Ω)	0.226M	0.108M	0.056M	6.33	0.217k	3.93k	9.51k
R3 (Ω)	0.176	7.17	3.15	2.40k	4.99k	15.52k	17.6k
W1(Ω)	5.43E-12	3.26E-13	4.10E-14	1.15E-15	2.19E-18	5.19E-12	1.49E-13
W2 (MΩ)				1.49	2.06		
CPE1	1.50E-08	1.59E-08	8.42E-09	2.93E-05	4.40E-05	4.85E-09	2.98E-08
CPE2						3.80E-09	3.80E-09

It followed one circuit model in the temperature range 30°C to 90°C, another model for 91°C to 150°C and a third model for 151°C to 210°C. Figure 3.27, Figure 3.29, and Figure 3.31 show the equivalent circuits EC1, EC2, and EC3 suggested by the CNLS algorithm for temperature range 30°C to 90°C, 91°C to 150°C and for 151°C to 210°C respectively. Figure 3.28, Figure 3.30, and Figure 3.32 show the fitted Nyquist plots for EC1, EC2, and EC3 by the CNLS algorithm for temperature range 30°C to 90°C, 91°C to 150°C and for 151°C to 210°C respectively. It should be noted that $r_{amplitude}^2$ for each fitting is of the order of magnitude 10^{-4} achieved with 300 iterations.

The analysis shows that the annealing of the sensor is driving the profile of the electrodes from a single time constant circuit to a circuit of twin time constants, which could be attributed to the migration of defects on the electrode surface caused by gradually created balance between the inter-atomic forces and surface energies in the thin film electrodes. At high temperature, the Si semiconductor substrate becomes more conductive due to increased rate of electron hole pairs formation inside the single crystal silicon substrate. It behaved as conducting plate of a parallel plate capacitor with an insulative oxide layer of SiO₂ acting as dielectric between electrodes giving rise to capacitive constant phase element. Constant Phase Elements (CPE1 and CPE2) behave

as two capacitors connected in series separated by an insulation layer of SiO_2 present on both sides of the sensor. The SiO_2 layers behave as R_2 and R_3 as shown in the equivalent circuit.



Figure 3.27 EC1 CNLS equivalent circuit for 30-90°C

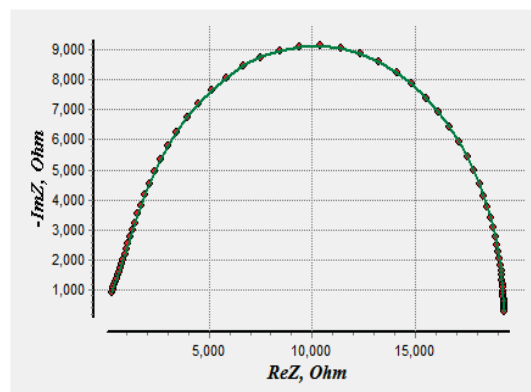


Figure 3.28 EC1 fitted curve (30-90°C)

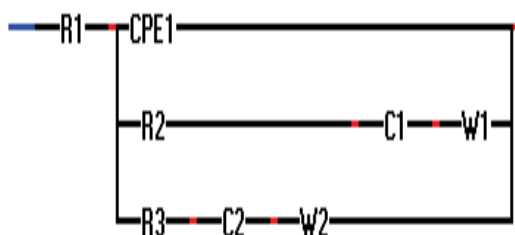


Figure 3.29 EC2 CNLS equivalent circuit for 91-150°C

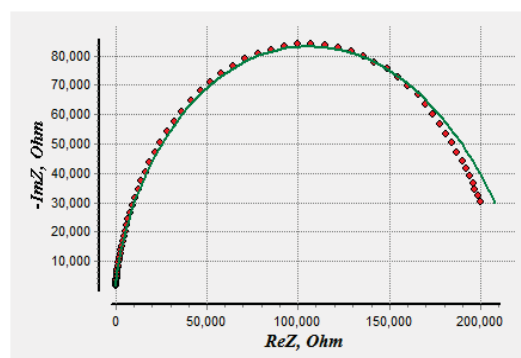


Figure 3.30 EC2 fitted curve (91-150°C)

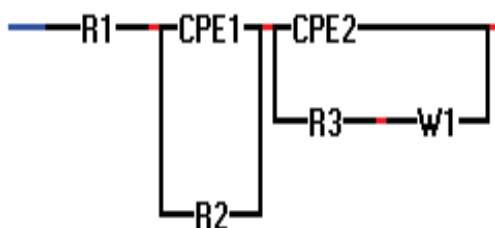


Figure 3.31 EC3 CNLS equivalent circuit for 151-210°C

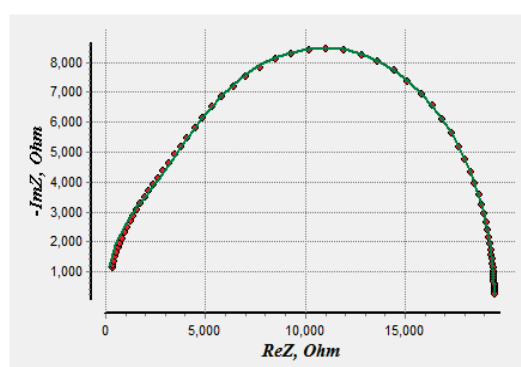


Figure 3.32 EC3 fitted curve (151-210°C)

3.7.4 Principal Component Analysis (PCA)

Traditional analysis method requires separate examination between different circuit variable, for example, between constant phase element (CPE) parameter and time or resistance parameter and time on a two-dimensional plot, which can be misleading in determination of valuable abstract mathematical correlations hidden in the impedance parameters. A better approach of PCA explores the orthogonal linear combinations of the original variables. These combinations, termed as principal components, represent different aspects of system variables and are helpful by eliminating redundancy and reduce noise in the data [75, 98, 99].

Principal component analysis is a statistical tool based on multivariate data analysis, introduced in 1901 by Pearson [100]. Later, Hotelling in 1933, further developed PCA independently [101]. PCA is a technique that reduces the dimensionality of a data set by linearly combining the original variables, in order to generate new axes known as principal components[102]. Each linear combination defines the variance in the data set and then all linear combinations are uncorrelated to others. Eigenvalue associated with each principal component is a measure of variation in a data set. Eigenvectors, usually expressed as a percentage of the total variation, are just linear combinations of the original variables (in the simple or rotated factor space) that described how variables "contribute" to each factor axis. Therefore, the PCA can be executed in five steps; Subtract the mean to produce a data set whose mean is zero; calculate the covariance matrix (or correlation); calculate the eigenvectors and eigenvalues of the covariance matrix; choose components and form a feature vector; and derive the new data set of less number of variables with redundant variables being truncated. PCA has been used to minimize dimensionality of data in impedance spectroscopy analyses by eliminating redundancy of data and without loss of information and without requiring physical knowledge of test conditions for the impedance system under investigation [75, 103, 104].

IBM-SPSS PCA was applied to analyse various quality states of the system during annealing.

3.7.5 PCA analysis – ECI (30°C – 90°C) anneal

Complex nonlinear least squares curve fitting algorithm suggested Equivalent circuit 1 (EC1) by fitting the experimental data on hypothetically calculated electrical circuit

representing electrochemical processes taking place inside the electrochemical cell. The suggested circuit displays six circuit components shown in Figure 3.27. The variance in Table 3.4 displays 99.13% cumulative eigenvalues for the system, explained by four principal components, pointing out the system scattering. The component plot shown in Figure 3.33 displayed high variance and weak correlations of equivalent circuit components.

Table 3.4 Table of variance ECI (30°C – 90°C) anneal

PCA Comp.	Initial Eigenvalues			Extraction Sums of Squared Loadings		
	Total	% Variance	Cumulative %	Total	% Variance	Cumulative %
1	3.321	55.347	55.347	3.321	55.347	55.347
2	1.191	19.842	75.190	1.191	19.842	75.190
3	0.820	13.673	88.863	0.820	13.673	88.863
4	0.616	10.272	99.135	0.616	10.272	99.135
5	0.052	0.865	100.000	0.052	0.865	100.000
6	-1E-013	-1E-013	100.000	1E-013	1E-013	100.000

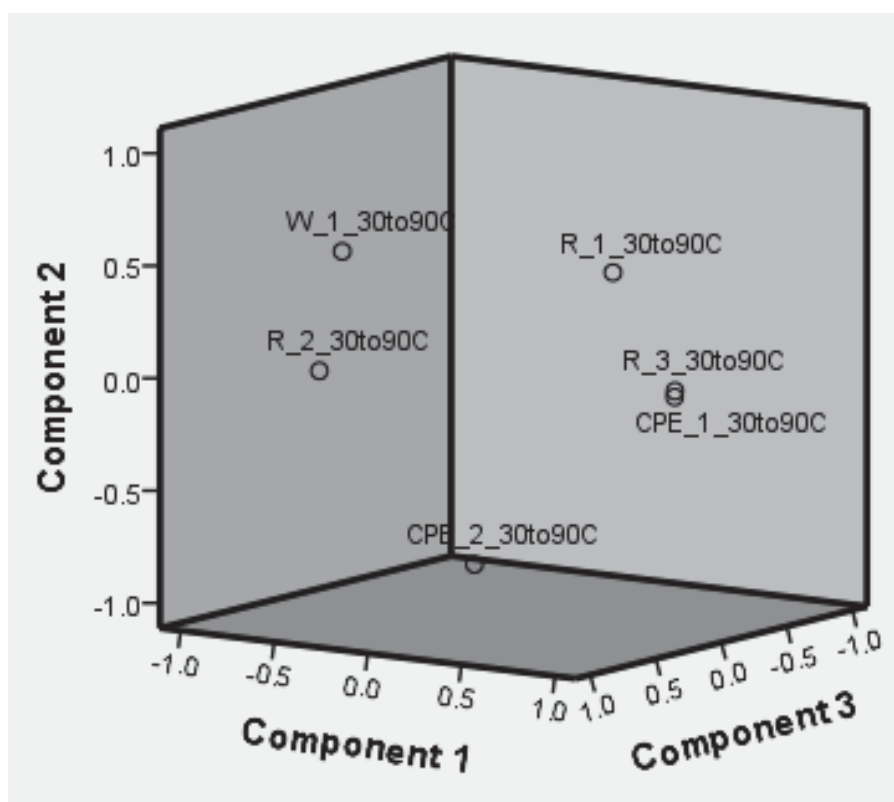


Figure 3.33 Component Plot ECI (30°C – 90°C) anneal

Physically, the instability observed in the impedance measurements executed by the as-is fabricated sensor depicts the system scattering evaluated by the PCA in the lower temperature range. The scree plot for EC1 is given in Figure 3.34.

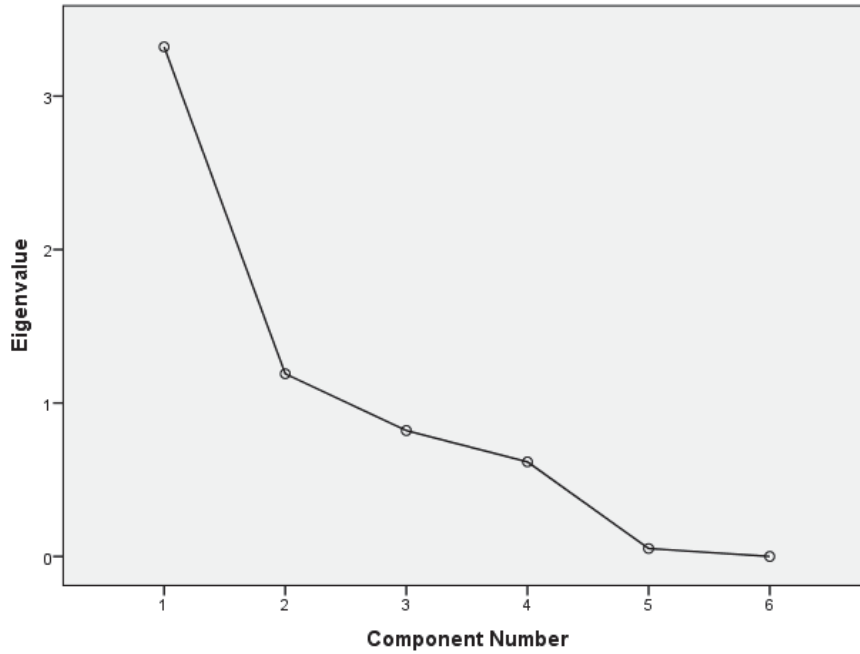


Figure 3.34 Scree Plot ECI (30°C – 90°C) anneal

Principal component analysis of equivalent circuit I, that was deduced from the experimental results obtained at temperatures 30, 60 and 90°C, portrays a system with high scattering. The system variables were scattered in four directions with a maximum convergence of 55.3% observed in the first eigen vector. The second vector displayed a convergence of 19.8%, third showing 13.67% and fourth one showed only 10.2%. Due to the scattering of the system variables the system did not display stability in the impedance measurements when tested with a sample ad depicted in the test results of 1-1-50A and 1-1-50B shown in Figure 3.20 and Figure 3.21 respectively. Interpreting these results in terms of Physics and surface morphology of the electrodes, the PCA results show that although the system has absorbed energy, yet it is not enough to remove the defects in the electrodes caused by sputtering and the electrodes surface still have grains and grain boundaries.

3.7.6 PCA analysis – EC2 (91°C – 150°C) anneal

Equivalent circuit 2 (EC2) displays eight circuit components shown in Figure 3.29. The variance in Table 3.5 displays 98.422% cumulative eigenvalues for the system,

explained by three principal components. The system still displays scattering but is reduced compared to the scattering displayed by equivalent circuit 1.

Table 3.5 Table of variance EC2 (91°C – 150°C) anneal

PCA Comp.	Initial Eigenvalues			Extraction Sums of Squared Loadings		
	Total	% of Variance	Cumulative %	Total	% of Variance	Cumulative %
1	3.840	63.996	63.996	3.840	63.996	63.996
2	1.310	21.834	85.830	1.310	21.834	85.830
3	.756	12.593	98.422	.756	12.593	98.422
4	.072	1.196	99.619	.072	1.196	99.619
5	.021	.349	99.968	.021	.349	99.968
6	.002	.032	100.000	.002	.032	100.000

The PCA component plot is shown in Figure 3.35 that displays moderate variance and stronger correlations of equivalent circuit components. The analysis pronounces the system to drift from scattering to stability of parameters.

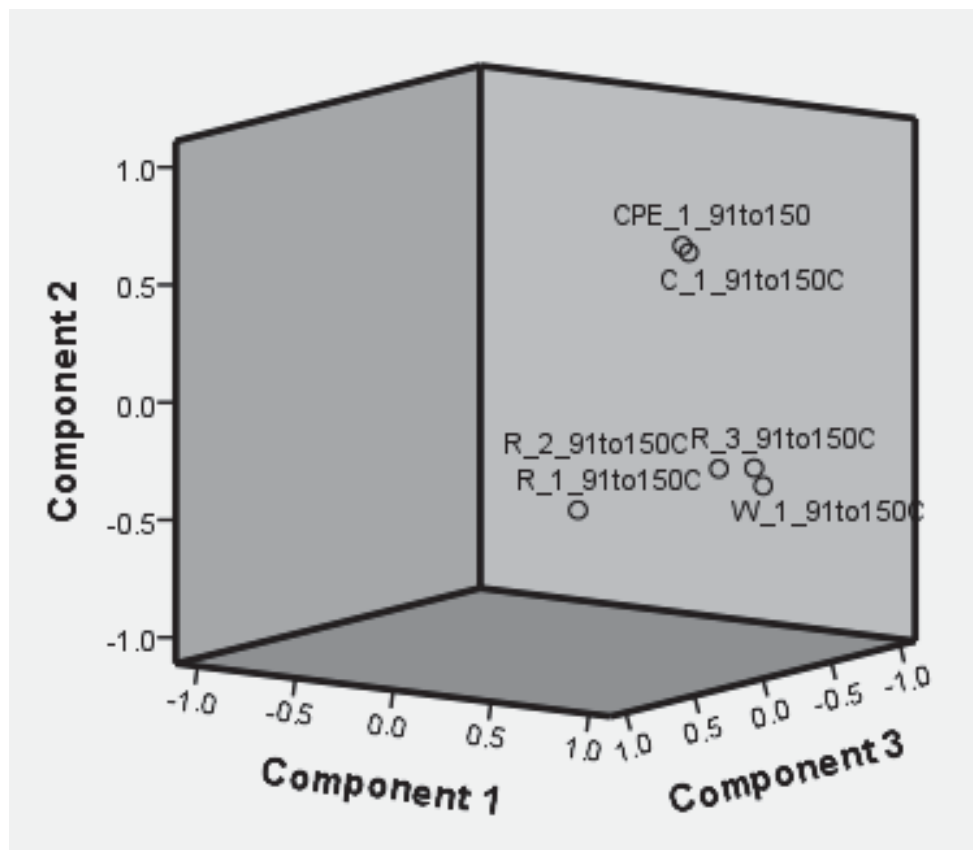


Figure 3.35 Component Plot EC2 (91°C – 150°C) anneal

The analysis defines three orthogonal eigenvectors to describe the system. PCA component 1 in EC2, only, is now defining 63.996% of all the defined components as compared to the EC1 that displayed 55.34%. The scree plot for EC2 is given in Figure 3.36 that now defines only three components to explain 99.422% of system parameters, compared to EC1 which was just 88.863% of the system variables clustered in three components. Though the entropy of the system is rising due to heat, yet the system is gaining stability in terms of electrical parameters. The physics of the system behaviour could be explained on the basis of energy balances gained due to the equalization of the bulk and surface energies [95].

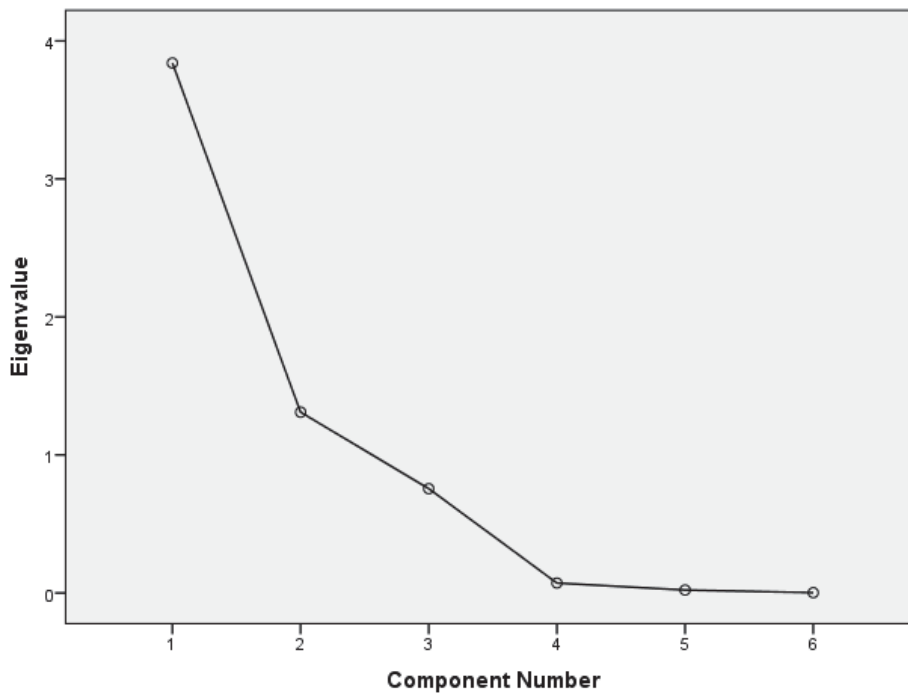


Figure 3.36 Scree Plot EC2 (91°C – 150°C) anneal

Principal component analysis of equivalent circuit II, that was deduced from the experimental results obtained at temperatures 120 and 150°C portrays a system with medium scattering. The system variables have now converged into three eigen vectors with a percentage of variance 63.99, 21.83 and 12.59% respectively. The system still displays scattering but relatively less as compared to untreated sensors.

3.7.7 PCA analysis – EC3 (151°C – 210°C) anneal

Equivalent circuit 3 (EC3) displays six components with a two time constant circuit shown in Figure 3.31. The variance in Table 3.6 displays 97.258% cumulative eigenvalues for the system, explained by only two principal components with first

component explaining 85.11% system parameter depicting system convergence to stability. The component plot is shown in Figure 3.37 depicting the clustered components.

Table 3.6 Table of variance EC3 (151°C – 210°C) anneal

PCA Comp.	Initial Eigenvalues			Extraction Sums of Squared Loadings		
	Total	% of Variance	Cumulative %	Total	% of Variance	Cumulative %
1	5.107	85.111	85.111	5.107	85.111	85.111
2	.729	12.147	97.258	.729	12.147	97.258
3	.118	1.960	99.218			
4	.046	.769	99.987			
5	.001	.013	100.000			
6	1.000E-013	1.005E-013	100.000			

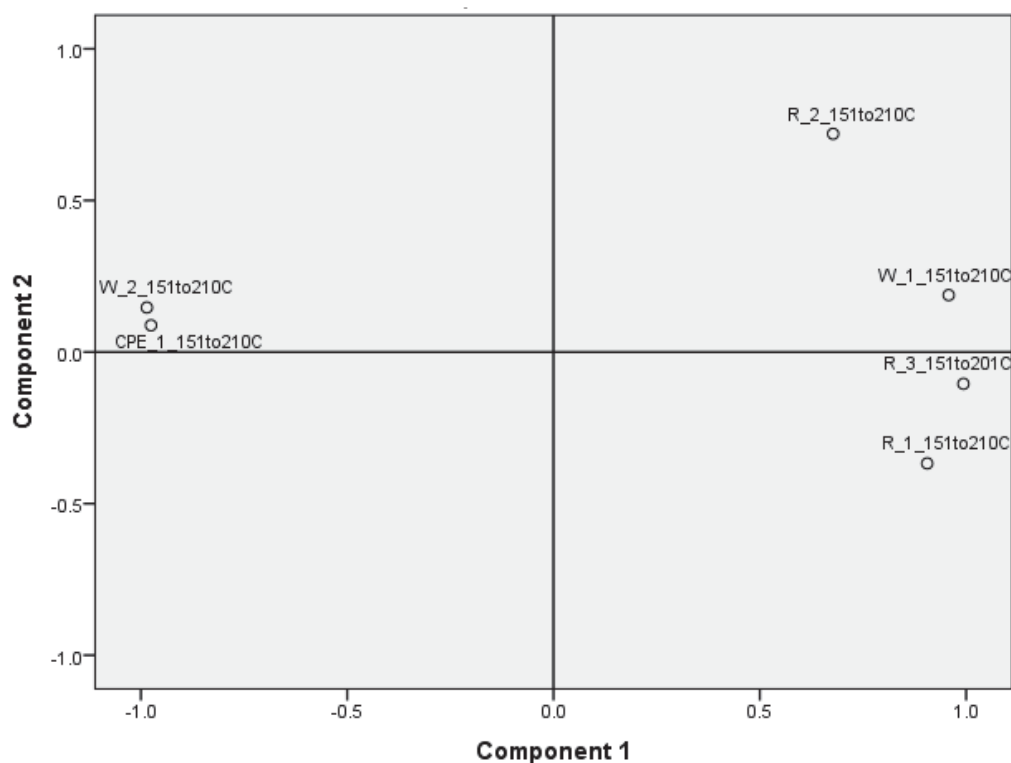


Figure 3.37 Component Plot EC3 (151°C – 210°C) anneal

The scree plot for EC1 is given in Figure 3.38.

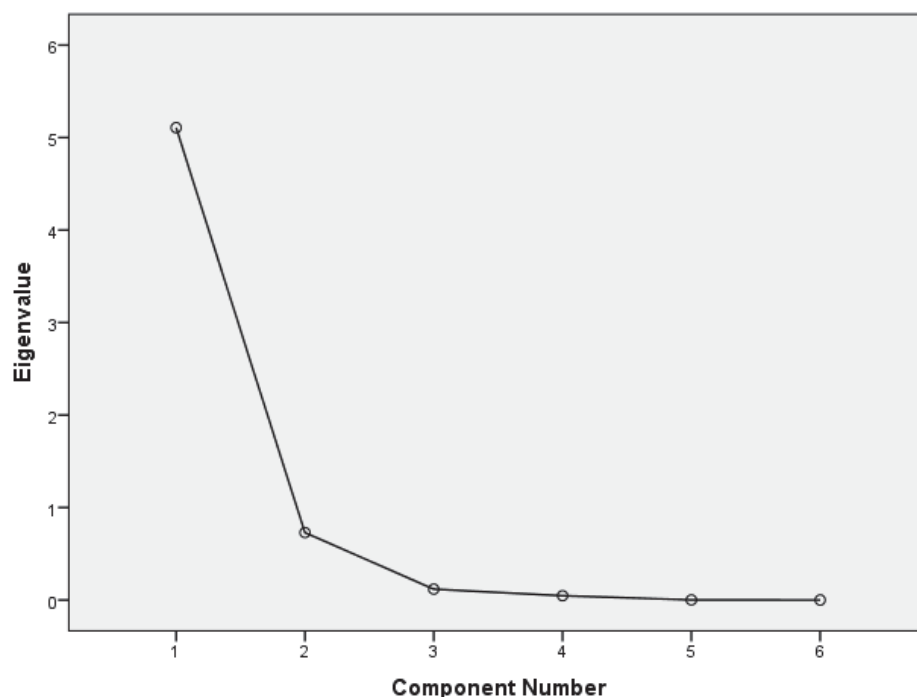


Figure 3.38 Scree Plot EC3 (151°C – 210°C) anneal

It is a proven result that in a set of m eigenvectors of an eigen matrix, the eigen vectors corresponding to the largest eigen values, minimize the mean square reconstruction error over all choices of m orthonormal basis vectors. Such set of eigen vectors defines a new uncorrelated dimensions of a coordinate system. Therefore, the first principal component with the largest eigen values is the most discriminant one [98, 105]. The results obtained as an outcome of the principal component analysis depict that annealing results in dramatic changes in the electrodes' gold layer morphology and improved surface smoothness. This objective was achieved by providing enough thermal energy to facilitate migration of defects on the gold surface and creating a balance between the surface and bulk energies in the gold lattice.

V. Švorčík et. al. [96] studied the effects of annealing on the gold structures sputtered onto glass substrate using AFM, UV-VIS and electrical measurements. They reported formation of structures on the gold surface at 300°C which is different in the presented case since the annealing temperature reached is 210°C, which is merely enough to achieve a balance in surface and bulk energies.

The fabricated post-annealed sensors are currently employed as biosensor to detect food pathogens and bacteria in meat [75] and as chemical sensor to detect the presence of endocrine disrupting compounds (EDCs) in beverages up to a trace level as low as one parts per million [106]. The achieved stability in impedance measurements used in

conjunction with the characteristic high sensitivity of the sensor declares it a potential candidate for the commercial applications.

3.8 Conclusions

An enormous interest is found in the industrial sector for impedance spectroscopy due to its sensitivity. This requires an innovative approach to select samples, execute impedance measurements and perform data analysis. A reliable transducer is required to interpret this sensitive technique to gain stability in measurements. The applied approach of designing, simulation and fabrication of interdigital sensors provided a reliable and novel tool for testing and achieving stability and reproducibility in the impedance spectroscopy results. This objective was achieved by providing enough thermal energy to facilitate migration of defects on the gold surface and creating a balance between the surface and bulk energies in the gold lattice.

The next phase of this work was to evaluate the sensitivity of the designed sensor. COMSOL simulations discussed in this chapter declared the highest level of sensitivity for the sensors with multiple (5 and 11) sensing electrodes and pitch length of 50 μ m. The practical sensitivity of the designed sensor could be determined only if the system is exposed to the in-field tests and investigations. Experiments and analyses conducted in this respect are discussed in the next two chapters. Chapter 4 is dedicated to the test and analyses of the hormones pertaining to the reproductive cycle of the mammals and chapter 5 discusses the detection of endocrine disrupting compounds and reproductive toxins.

Chapter 4 Electrochemical Detection of Hormones

4.1 Introduction

The objective of this chapter is to investigate the capability of the designed sensors, and to explore the analytical powers of electrochemical impedance spectroscopy, in detection of different hormones. The target hormones are related to the reproductive cycle of mammals. ‘Non-invasiveness of methodology’ and ‘real-time measurements of samples’ were the prime objectives of this research project. These characteristics of the presented research make this work unique in comparison to all available contemporary methodologies. Apart from that, it was envisaged that execution of the hormone quantification assay should be simple enough to be adapted by a common user without requiring a necessary scientific background.

The first part of this chapter discusses the application of the proposed system to detect estrone glucuronide, an excretory metabolite of estradiol, commonly known as E1G. This hormone plays a major role in the reproductive fertility of human female. The information on the quantity of excretion of this hormone metabolite is useful in determining the window of fertility for human female. The handy availability of this information is extremely important to achieve conception or contraception in human reproductive cycle.

The second part of the chapter deals with the sensor’s response in detection of progesterone hormone excreted in the milk of dairy cows. Obtaining urine samples, to gather the fertility information, is not feasible in the case of dairy animals. Though, milk owns a complex chemical matrix, yet it is the easiest and most non-invasive method to achieve the information on ‘window of fertility’ for the animal.

Electrochemical impedance analyses making use of bode plots, Nyquist plots, CNLS curve fitting, electrochemical equivalent circuit parameters and sensitivity of the sensor toward the analytes are discussed in this chapter.

4.2 Detection of Ovarian Hormone Estrone Glucuronide (E1G)

4.2.1 Motivation

The reproductive fertility of human male stays active for nearly all his adult life whereas woman's fertility is periodic and disappears completely at the later age of her life. The 'window of fertility' is termed for a part of ovulatory menstrual cycle of woman in which she owns the potential to conceive and reproduce. This period begins up to six days before and ends one day after ovulation. It is clinically determined by a series of ultrasound scans of ovary or by a series of blood analysis comparing patterns of secretions of ovarian hormones estradiol, progesterone and luteinizing hormone (LH) [107, 108]. Analysis of the rate of excretion of hormonal metabolites, estrone glucuronide (EG) and pregnanediol glucuronide (PG) in urine has an advantage of being non-invasive over the serum analysis and has proved to be more closely correlated to the hormonal concentration in ovary. A marked rise of estradiol production occurs 36 hours before ovulation followed by a peak of LH secretion which occurs 17 hours before ovulation at average [108]. Classic mean curves for each hormone plotted after a hormonal study of 25 women is shown in Figure 4.1 [107].

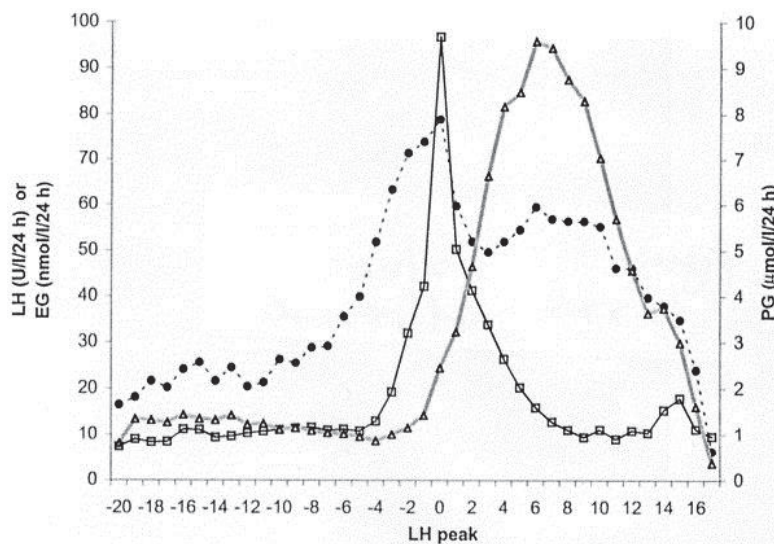


Figure 4.1 Mean hormonal values of estrone glucuronide (E1G) (-.-.), LH (-□-), and pregnanediol glucuronide (PG) (-△-) by cycle day throughout 78 ovulatory cycles from 25 women [107]

It is clinically agreed that the first rise in one out of three urinary metabolite of estrogen, E1G, is a natural marker for start of fertility window; it is not accepted widely the best maker for beginning of fertility by the researchers, though [109, 110].

Presently, Radioimmunoassay (RIA) is the most widely used method among the existing laboratory based techniques to measure E1G and LH in urine samples in order to detect the beginning of the fertility in women. With an advantage of being the most accurate, this assay has major drawbacks of producing radioactive waste, expensive, time consuming along with a requirement of trained professionals carrying out the immunoassay in laboratory environment under stringent conditions.

4.2.2 Point-of-care Methods

The other methods currently in practice for the detection of fertility include Basal Body Temperature (BBT), Billings Ovulation Method, Symptothermal Method (STM) and Ovarian Monitor use. These methods serve as a tool to predict the window of fertility information in human females. The gathered information is equally useful for family planning as well as conception and pregnancy.

4.2.3 Basal Body Temperature method (BBT)

During ovulation the body temperature elevates by 0.2°C for three days in comparison to the preceding six days of mensuration cycle. A special thermometer measures the BBT throughout each cycle to predict fertility starting from the 1st day of elevated temperature [111]. This data recording helps to estimate the window of fertility in women.

4.2.4 Billings Ovulation Method

This is a track and record method of checking the amount and quality of cervical mucus. Ovulation occurs within one or two days of the peak day of abundant wet and stretchy cervical mucus [112]. This method does not involve any scientific hormonal measurement yet provides training to predict fertility by track and record [111].

4.2.5 Symptothermal Method (STM)

This method is a combination BBT and Billings Ovulation Method to predict probable fertility window during each cycle [111]. Data is recorded after checking the amount and quality of cervical mucus in addition to the tracking of the elevated body temperature by basal body temperature measurements throughout the ovulation period. This method involves the scientific body temperature measurements and track and

record of the amount and thickness of the cervical mucus in order to predict window of fertility in human females.

4.2.6 Ovarian Monitor

The Ovarian Monitor is used to measure E1G and PdG in urine samples. It uses pre-coated assay tubes following the principle of homogeneous enzyme immunoassay in a home or in a point-of-care environment. In this immunoassay, an antibody to a ligand specifically inhibits the enzyme activity of an enzyme-ligand conjugate to measure the E1G in the urine sample. [113-115]. The Ovarian Monitor system uses a specially designed piece of electronic hand held device that is a rate colorimeter thermostatted at 40° C with timer settings for the warm-up and enzyme reactions. The display read-out is given in three digits and is related to light transmission $\times 1000$. The device provides single instrument solution for single assay that is tailored for home or point-of-care use. For multiple assays, a 48 assay tubes accommodative heating block fitted with a thermostat is supplied. The electronic read-out and measuring device is used as a colorimeter and the assay timings are manually performed using a stop watch. This setup allows up to 48 E1G assays or 20 PdG assays in a single run that can be clinically used. Validation study of Ovarian Monitor has found its results comparable to the laboratory standards [115] and is viewed as an alternative to more costly laboratory testing, but it requires timed urine samples (over three hour minimum), dilution of urine test samples, takes around 40 minutes for E1G testing and lack of reusability of the sensor (assay tube).

In the presented research, the author used Electrochemical Impedance Spectroscopy based approach to measure E1G by using a new planar ID capacitive sensor for rapid results without involving any timed samples. The hormonal metabolites could be quantified, without any additional steps of sample preparation, in mere five minutes. The applied sensor can be reused for the next measurement after wash and dry cycle.

4.2.7 Materials and Methods to Detect E1G

Four concentrations of E1G, 8.33nmol/L, 16.66nmol/L, 33.33nmol/L, and 55.55nmol/L were prepared in a buffer solution. Non-spiked buffer solution was used as control reference for testing E1G samples. The samples were tested immediately after preparation in the laboratory environment at 47% humidity and 23°C temperature. The samples were kept refrigerated at 4°C for further testing. The sensor was immersed in

the 2 ml of control buffer solution to create a control reference for the measurement. Special care was taken to immerse only the sensing part of the sensor in the solution. Figure 4.2 demonstrates the dip testing procedure. The samples were tested in reverse order i.e. lowest to highest concentration in order to avoid saturation of the sensor. The sensor was cleaned with 99.7% ethanol, rinsed with distilled water and dried with nitrogen after each test. Sensor's profile test in air was carried out after cleaning procedure and the results were compared with the reference in order to validate the cleaning procedure and to reset the sensor to its initial conditions.

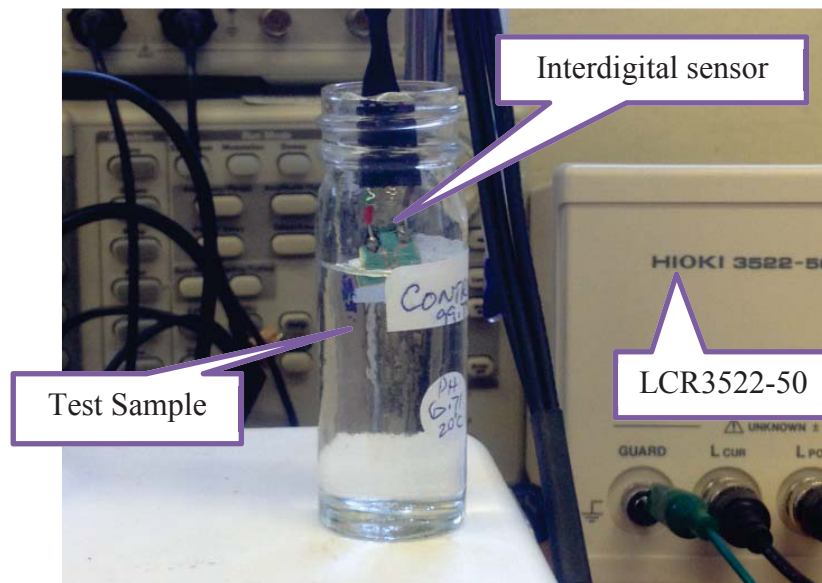


Figure 4.2 Dip test method for EIG testing

EIS experiments were carried out using Hioki 3522-50 LCR Hi precision Tester (Japan) at laboratory ambient temperature (23°C) at a controlled humidity level. All experiments were performed using slow mode of the testing equipment as to achieve error rate of less than 0.05% specified by the manufacturer. A sinusoidal signal of $1V_{rms}$ was applied to the sensor with a frequency sweep of 1 Hz to 10 kHz with 20 data points per decade on the log scale. LabView® data acquisition program was used to write the measured values in Microsoft excel® file for post-processing and analysis of the experimental data on the attached desktop computer. An average of three experiments was used to ensure reproducibility and reliability of the tests' results. Figure 4.3 shows the test bench setup for the experiments.

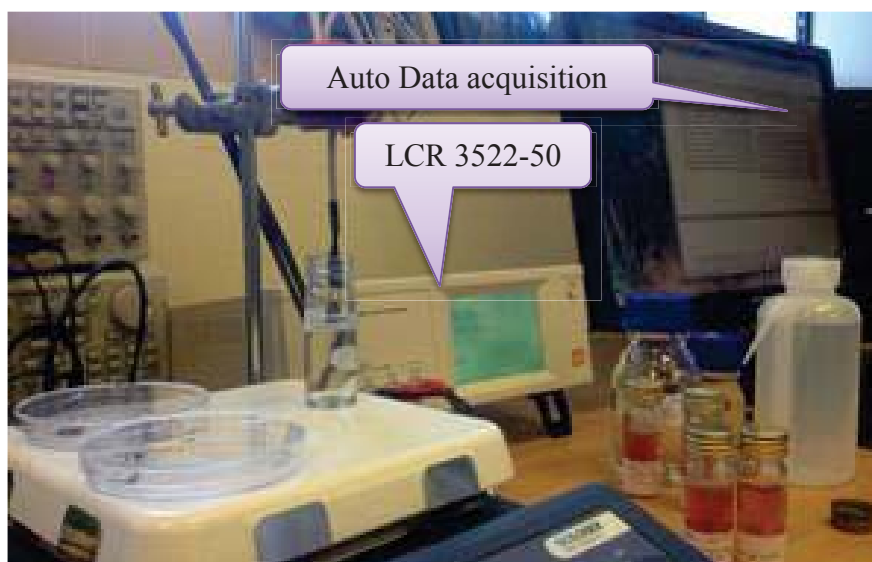


Figure 4.3 Laboratory test bench for EIG testing

4.2.8 Results and Discussions

The impedance Z of the sample is determined by applying a small signal perturbation as a function of frequency and consequent analysis of the resultant current through the system in terms of amplitude and phase shift compared to voltage-time function. The complex value of impedance can thus be interpreted in terms of its real and imaginary parts at different frequencies. The samples were evaluated for real part (R_e) and Reactance (X) imaginary part of the impedance and were plotted against the excitation frequency for reference and sample solutions as shown in Figure 4.4. The primary axis shows the average real R_e impedance in $k\Omega$. The real impedance of the sample reads the ionic concentration in the test samples as compared to the control buffer. It is obvious from the plot that as the concentration of E1G increases in the sample solution, the real impedance drops as compared to the preceding concentration. This happens due to higher concentration of ions in the following sample of higher concentration of E1G. The secondary axis shows the reactance X ($k\Omega$) of the sample solutions plotted against frequency. The change in this parameter is a measure of the dielectric properties of the E1G molecule. The results of an impedance measurement can be graphically demonstrated using bode and Nyquist plot for all applied frequencies with real part of impedance Z plotted along X-axis and Imaginary part plotted along Y-axis in the later.

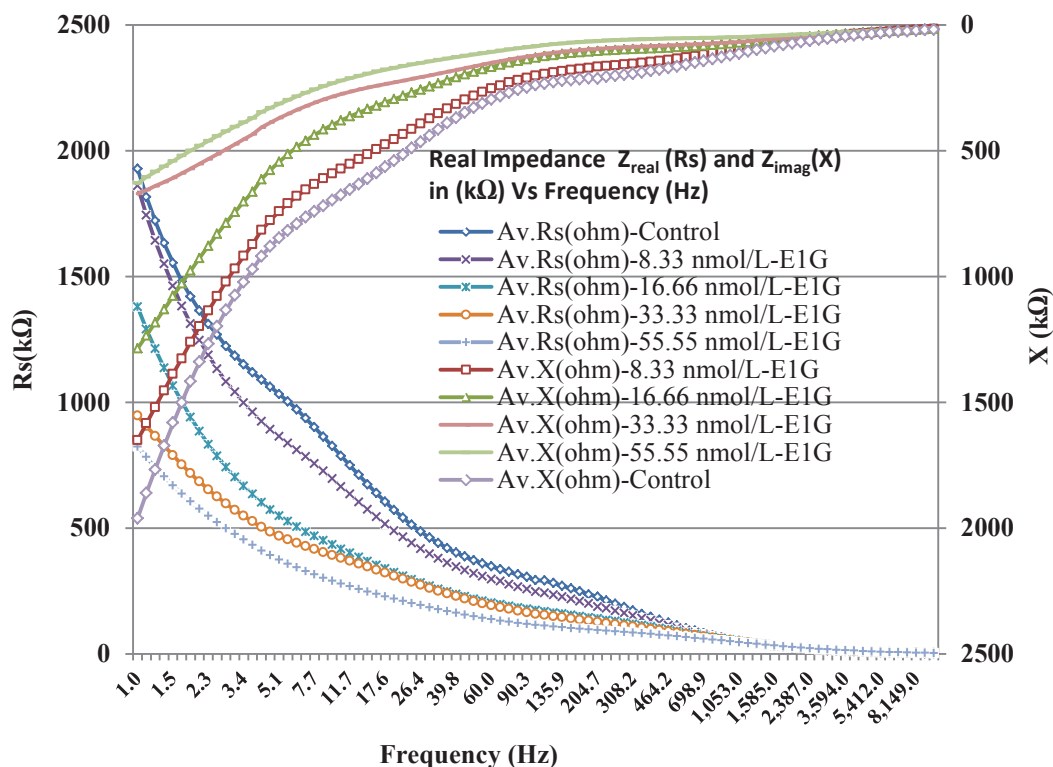


Figure 4.4 Real and imaginary parts of the measured impedance for E1G

The Nyquist plot for the equivalent circuit comprises of a semi-circular region followed by a straight line as shown in Figure 4.5. The straight line at an angle of 45° represents a faster mass-transfer limited process at lower frequencies, whereas, the semi-circular portion describes a relatively slower charge transfer limited process at higher frequencies. It can be seen from the plot that the diameter of the curve reduces with growing concentration of E1G, indicating an increase in the conductance of the samples. The values of the charge transfer resistance decreased with the increasing concentration of the analyte, which is responsible for the increase in the double layer capacitance appearing at the electrode-electrolyte interface.

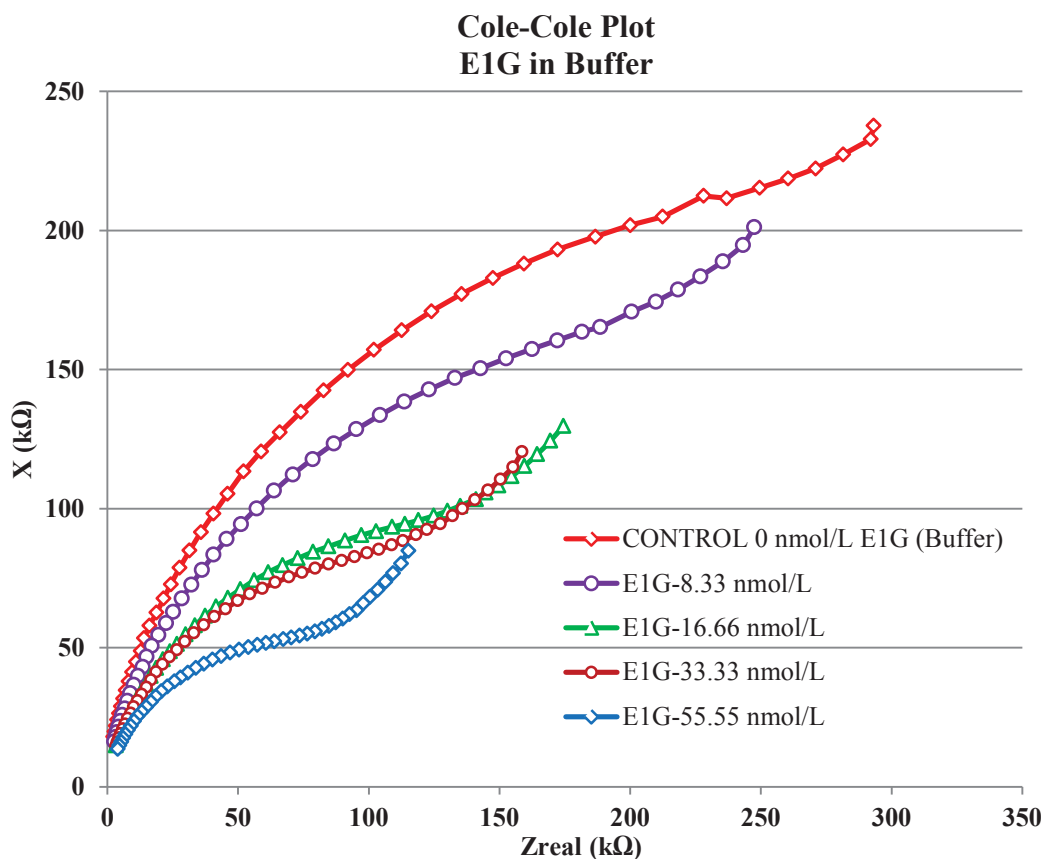


Figure 4.5 Nyquist (Cole-Cole) plot for the impedance measurements of E1G

4.2.9 Electrochemical Impedance Spectroscopy Analyses for E1G

The experimental data is used for characterization of surface, layers and concentrations with a detailed insight to the system kinetics. This is achieved by analysing the impedance spectrum on basis of an equivalent series/parallel circuit commonly consisting of resistances and capacitances representing the different electrochemical and physiochemical properties of the system under analysis [90].

Figure 4.6 shows the equivalent circuit obtained as interpretation of the experimental findings by using complex nonlinear least squares curve fitting (CNLS) technique. The experimental impedance spectrum not only interprets the exchange and diffusion processes taking place in the electrochemical cell but it provides necessary characterization of surface, layers and concentrations when analysed on basis of Randle's model by CNLS algorithm. It shows uncompensated solution resistance R_s in series to a parallel combination of double layer capacitance C_{dl} to the charge transfer resistance R_{ct} in series with Warburg impedance Z_w [116].

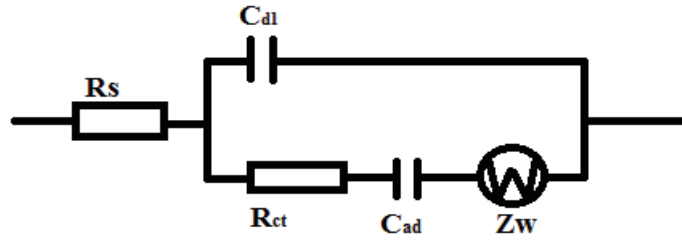


Figure 4.6 Electrochemical equivalent circuit extracted by CNLS curve fitting

C_{dl} can be calculated from the frequency at the maximum of semi-circular region in the Nyquist plot using $\omega = 2\pi f = 1/R_{ct}C_{dl}$, whereas, R_{ct} is calculated by extrapolating the semicircle to real impedance axis. Using Randle's cell model, the real and imaginary impedance at the electrode-solution interface could be derived as shown by the Equation 4.1.

$$Z(\omega) = R_s + \frac{R_{ct}}{1 + \omega^2 R_{ct}^2 C_{dl}^2} - \frac{j\omega R_{ct}^2 C_{dl}}{1 + \omega^2 R_{ct}^2 C_{dl}^2} \quad (4.1)$$

The equivalent circuit was estimated using theoretical calculations by electrochemical spectrum analyser algorithm. The algorithm performs statistical analysis to calculate the residual mean square for experimentally observed values in measured spectra. The results are compared to the calculated values based on the theoretical response of suggested equivalent circuit. The fitted Nyquist plot is shown in Figure 4.7.

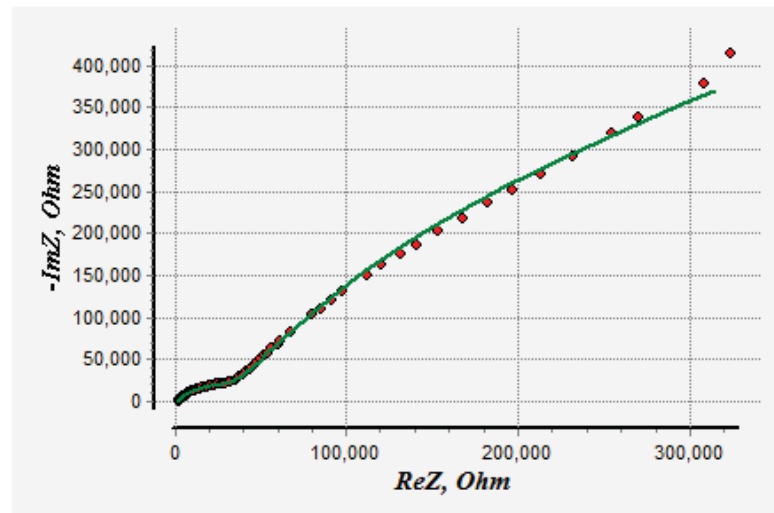


Figure 4.7 CNLS curve fitting of Nyquist plot by spectrum analyser for the highest concentration of EIG 33.33nmol/L.

The bold line curve displays the modelled behaviour of the equivalent circuit whereas; the markers represent the experimentally observed response from the electrochemical cell. The optimization of the calculated data is achieved by the number of iterations it takes to solve the mathematical model for the proposed equivalent circuit. It took 500 iterations to extract the equivalent component values for the equivalent circuit shown in Figure 4.6. The table of values at different concentrations of E1G is given in Table 4.1

Table 4.1 Equivalent circuit components' parameters deduced by CNLS curve fitting technique for electrochemical spectrum analysis

Component	Concentration of E1G solution in buffer		
Parameter (unit)	8.33nmol/L	16.66nmol/L	33.33nmol/L
C_{ad} (F)	1.825E-07	1.45E-07	1.58E-07
R_s (Ω)	1.14E+02	1.01E+02	0.30E+02
R_{ct} (Ω)	1.7304E05	1.61E+05	1.57E+05
Z_w (Ω)	2.4431E06	1.90E+06	1.79E+06
C_{dl} (F)	6.95E-09	8.69E-09	9.20E-09

It should be noted that CNLS was applied to three concentrations of E1G only.

4.2.10 E1G Sensitivity Analysis

Characterization of each sensor was performed on the basis of Bode and Nyquist plots. The sensitivity of the sensor was calculated by using the real impedance and reactance data using following relations.

$$Z_{real}Sensitivity = \frac{Z_{real}(control) - Z_{real}(sample)}{Z_{real}(control)} \times 100 \quad (4.2)$$

$$X_{imag}Sensitivity = \frac{X(control) - X(sample)}{X(control)} \times 100 \quad (4.3)$$

The sensitivity was plotted against concentration with reference to the control solution for five chosen values of frequency to observe its effect at minimum and maximum values. These values were chosen one frequency per decade with a minimum of 1Hz

through to 10 kHz. The sensitivity plots for reactance and real impedance are shown in Figure 4.8 and Figure 4.9, respectively. The plots show that the sensor is fairly sensitive in a frequency range of 10 to 100 Hz. This is due to the fact that the sensor owns capacitive properties due to the electrode geometry and the thin film passivation layer of Si_3N_4 ; therefore, its capacitance value is higher during this range as simulated and predicted by Finite Element Modelling as discussed in 3.3. At higher frequencies, its capacitive response to the periodic perturbation reduces as it behaves as a high pass filter at those frequencies.

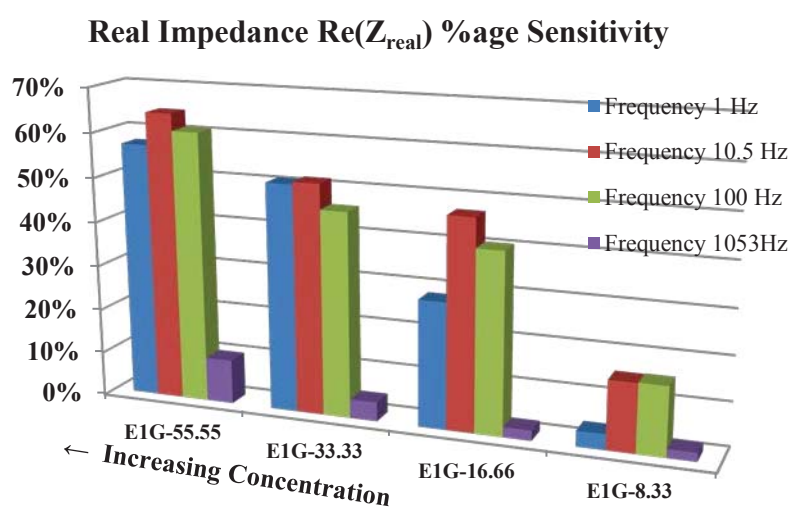


Figure 4.8 %age sensitivity of the real part of impedance (Re).

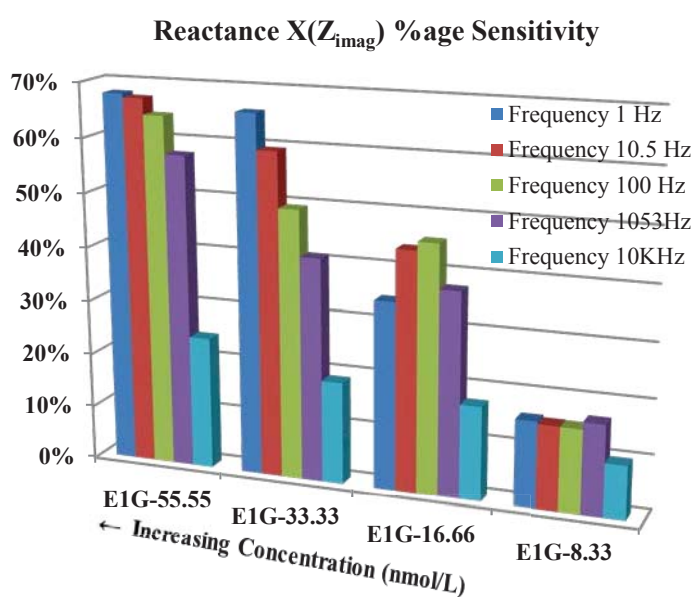


Figure 4.9 %age sensitivity of capacitive reactance (X).

Comparing the sensitivities of Re and X, it is concluded that the imaginary part of impedance (X) provides better sensitivity, in terms of magnitude and incident frequency band, for the detection of the hormone metabolite E1G [117].

4.3 Electrochemical detection of Progesterone Hormone

4.3.1 Motivation

Poor reproductive performance of dairy cattle is one of the most difficult and expensive problems for dairy and livestock producers. The profitability of the dairy industry is mainly dependent upon the satisfactory reproductive management of the herd. An ideal model followed in dairy farming states that a dairy herd is termed reproductively efficient when it follows a calving interval of 365 days, in a 10 week period 90% of cows calve and when 5% or fewer animals are culled due to reproductive failure [118, 119]. Statistics show that even in well managed dairy farms in New Zealand, reproductive failure rate is much higher than 5%. The main problem faced in this context is poor detection of estrus. Estrus is a phase in the reproductive cycle of the dairy cow prior to ovulation when it is reproductively receptive ('in heat'). Figure 4.10 shows the progesterone concentration level during 21 days reproductive cycle of dairy cows dictating the estrus window targeted in this research. Extended calving intervals, veterinary costs, milk loss, etc. are the major adverse outcomes of incorrect detection of estrus which causes loss of profit in the dairy business.

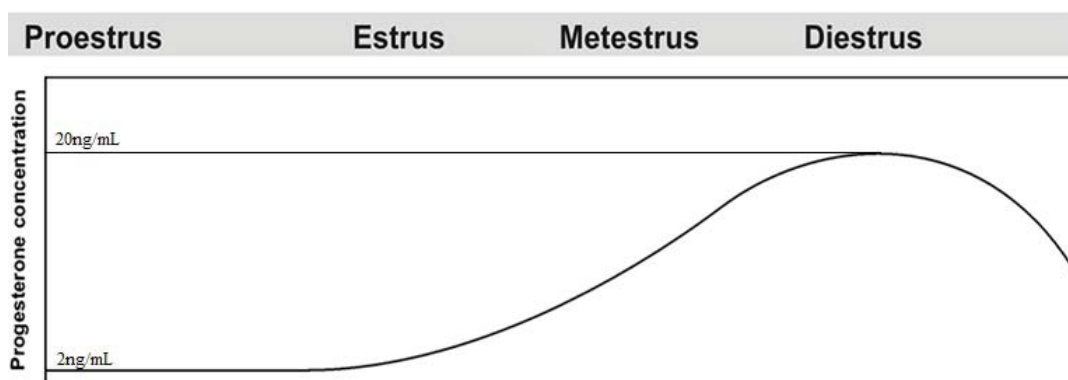


Figure 4.10 Progesterone concentration level during 21 days reproductive cycle of dairy cows [12]

Measurements of progesterone concentration in the blood or milk are an accurate indicator of estrus [22, 120, 121], but monitoring progesterone level in milk rather than

blood has an advantage of easy sampling method. The concentration of progesterone in the blood is correlated closely with its concentration in milk. In fact, since progesterone is a steroid hormone, it has an affinity for milk fat: thus progesterone in milk is somewhat in higher concentration than in blood [122]. Elevated progesterone concentrations indicate luteal dominance, while low amounts of progesterone are associated with estrus [122].

Methods used presently for estrus detection such as pedometry, teaser bull or visual behavior of cow, are not precise and accurate. Farmers often achieve a heat detection rate of only 35% to 70% and up to 20% of cows presented for insemination are not in heat [123]. Progesterone detection test based on enzyme-linked immunoassays (ELISA) is available as kits on farm use [22], but most of these tests are manual, indicative and designed for qualitative measurement to confirm estrus and determination of pregnancy or non-pregnancy only. These tests are unable to quantify the precise concentration of progesterone in sample therefore; can only be used for 'estrus confirmation', not for 'estrus detection'. Various other immunoassay formats have been proposed for progesterone detection in bovine milk such as BIAcore™ biosensor based on surface plasmon resonance (SPR) [124], Heap et al.[125] quantified progesterone concentration using radioimmunoassay (RIA), a rapid enzyme immunoassay (EIA) based on horseradish peroxidase was developed by Claycomb et al. [126], a competitive immuno-chromatographic assay of milk progesterone was developed by Laitinen and Vuento [127] and Total internal reflection fluorescence based detection of milk progesterone [46]. All these methods are expensive, time consuming, require highly skilled personnel and need laboratory environment to perform. Moreover, livestock producer are not much benefited from these techniques as the farmers have to invest extra effort, resources and time in order to get access to these methods. Above all, these techniques cannot be used for continuous monitoring of milk progesterone in bovine milk for estrus detection.

According to Senger [118] an ideal system for detection of estrus in dairy animal should: (i) have continuous surveillance characteristics; (ii) automatically detect estrus; (iii) operative during whole productive life-time of a cow; (iv) have minimal labor requirements; (v) be highly accurate and efficient (95%). Unfortunately, there is no such detection system available at farm level, which may scientifically detect and inform the farm manager, the right time for artificial insemination (AI), for better reproductive efficiency of the dairy animals. Farmers, to-date, have to rely on centuries

old methods for this important parameter of their industry. This inadequacy had provided necessary motivation to apply the fabricated interdigital capacitive sensor and impedance spectroscopy technique for real time measurement of progesterone in aqueous media to mimic bovine milk whey, which is normally used for such kind of detection and quantification. Another objective of this research was to develop a rapid real time assay technique by applying impedance spectroscopy based novel interdigital sensor technology; and to model and evaluate the performance of the proposed system.

4.3.2 Materials and Methods for Progesterone Detection

Research grade progesterone hormone was procured from Sigma-Aldrich, GmbH, Germany for testing. The hormone is not water soluble, therefore, 20mg of progesterone was dissolved in 0.5ml of 99.6% Ethanol and the solution was poured in 999.5ml of purified Milli-Q water to make the stock solution. Concentration of progesterone in stock solution is 20 μ g/ml. Using series dilution method 200ng/ml, 20ng/ml, 2ng/ml and 0.02ng/ml concentration of progesterone was achieved in successive steps. The samples were tested immediately after preparation in the laboratory environment at 47% humidity and 23°C temperature. The samples were kept refrigerated at 4°C for further testing. A control solution was prepared with 999.5ml MilliQ and 0.5ml 99.6% ethanol for calibration of sensors and to obtain a reference for sensitivity calculations. The sensing part of the sensor was immersed in the 2 ml of control solution to create a control reference for the measurement. EIS experiments were carried out using Hioki 3522-50 LCR Hi precision Tester (Japan). All experiments were performed using slow mode of the testing equipment as to keep error rate less than 0.05% as specified by the manufacturer in the specification. A constant voltage sinusoidal signal of 1V_{rms} was applied to the sensor with a frequency sweep of 10Hz to 200kHz with 20 data points per decade on the log scale. Experiments were conducted to analyse the performance of 1-11-50 parylene coated sensor at different concentration levels of progesterone in deionized water. The concentration levels tested for detection of progesterone in MilliQ water are given in Table 4.2 and results for sample-B, sample-C and sample-D are plotted as bode and Nyquist plots. Sample-C and sample-D were chosen due to the target range of progesterone concentration in bovine milk whereas; sample-B was tested to figure out the limit of detection (LOD) for progesterone. To ensure removal of any residual hormone from the sensing surface, it was cleaned with ethanol and dried under nitrogen flow before the next run. To make sure that the sensor has attained its initial

conditions, the sensor was profile in air. Each test was run three times and average of three sets was taken for all applied frequencies.

Table 4.2 Progesterone in deionized water- Samples' nomenclature and concentration

Sample Name	Progesterone concentration
Sample-B	0.02ng/ml
Sample-C	2ng/ml
Sample-D	20ng/ml
Sample-E	200ng/ml

4.3.3 Electrochemical Impedance Analyses for Progesterone

Characterization of each sample was performed on the basis of Bode and Nyquist plots. The plot of real and imaginary impedance vs frequency for 1-11-50 sensor in Figure 4.11 showed the relative change in impedance varying with different concentration levels of progesterone. This change was prominent at lower frequencies as compared to the higher frequency range.

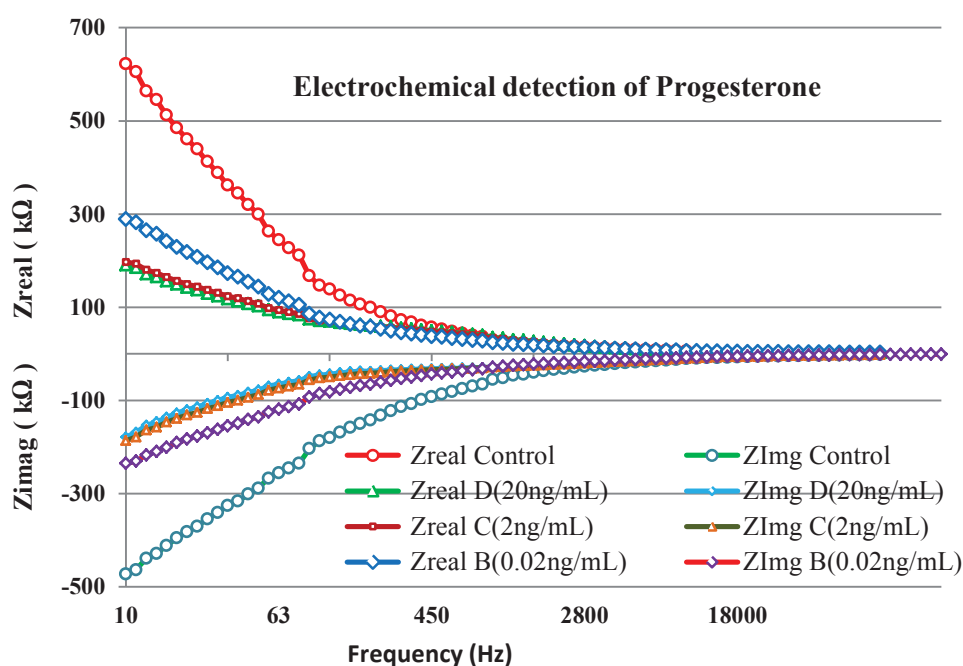


Figure 4.11 Real and Imaginary Impedance (reactance) characteristics

With increasing concentration of progesterone the imaginary impedance decreases which could be attributed to the conductance of the progesterone molecule in the solution. This dictates the capacitive behaviour of the sensor at low frequencies. The

real part of the impedance which is the dissipative part changes in considerable amount providing a direct relationship for the conductivity of the medium to the increasing concentration levels of progesterone in the solution.

Figure 4.12 shows the Bode Plot impedance spectra. It was observed that the change in absolute impedance occurred, even, for 0.02ng/ml concentration and is read by the sensor. It provided close agreement to the Bode plot for a system where electrode polarization is due to kinetic processes taking place at the electrodes' surface. This can be validated by modelling an equivalent circuit. The measured impedance value applied to the equivalent circuit can generate a fitting impedance spectrum to match the experimental observations.

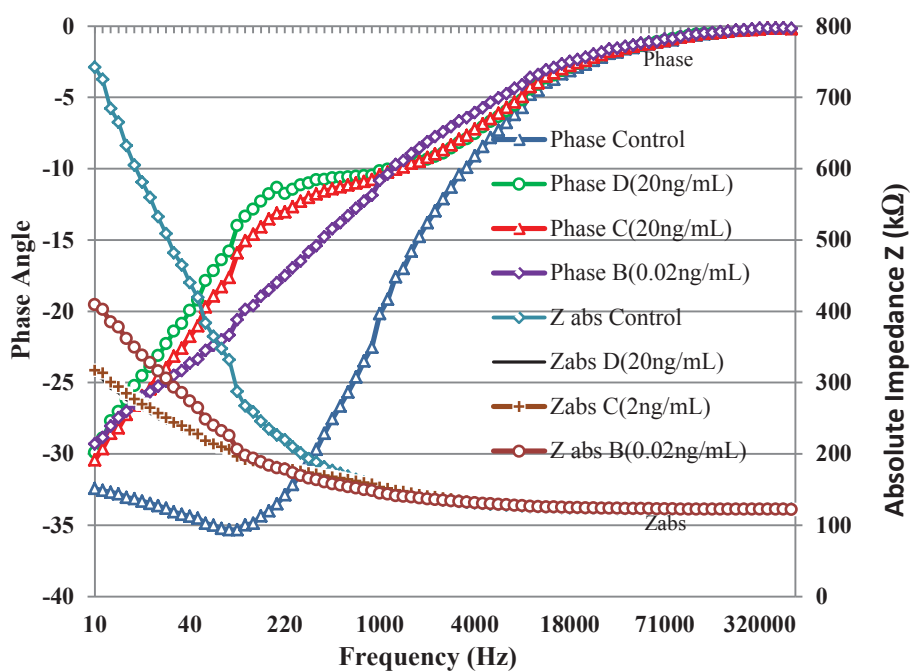


Figure 4.12 Bode plot for progesterone detection in deionized water

Figure 4.13 shows Nyquist plot for the electrochemical impedance spectra of the sensor at different concentration levels of progesterone hormone samples. The plot depicts that a 45° line starts appearing with the plots as soon as the concentration of hormone increases in the solution. This line represents the presence of ionic concentration with the increasing concentration of the hormone in the sample. The decrease in reactance with increasing concentration of progesterone is due to the dielectric properties of the hormone, therefore, it could be concluded that the concentration could be correlated with reactance or conductance of the progesterone hormone. However, reactance is the more dominating part of impedance change.

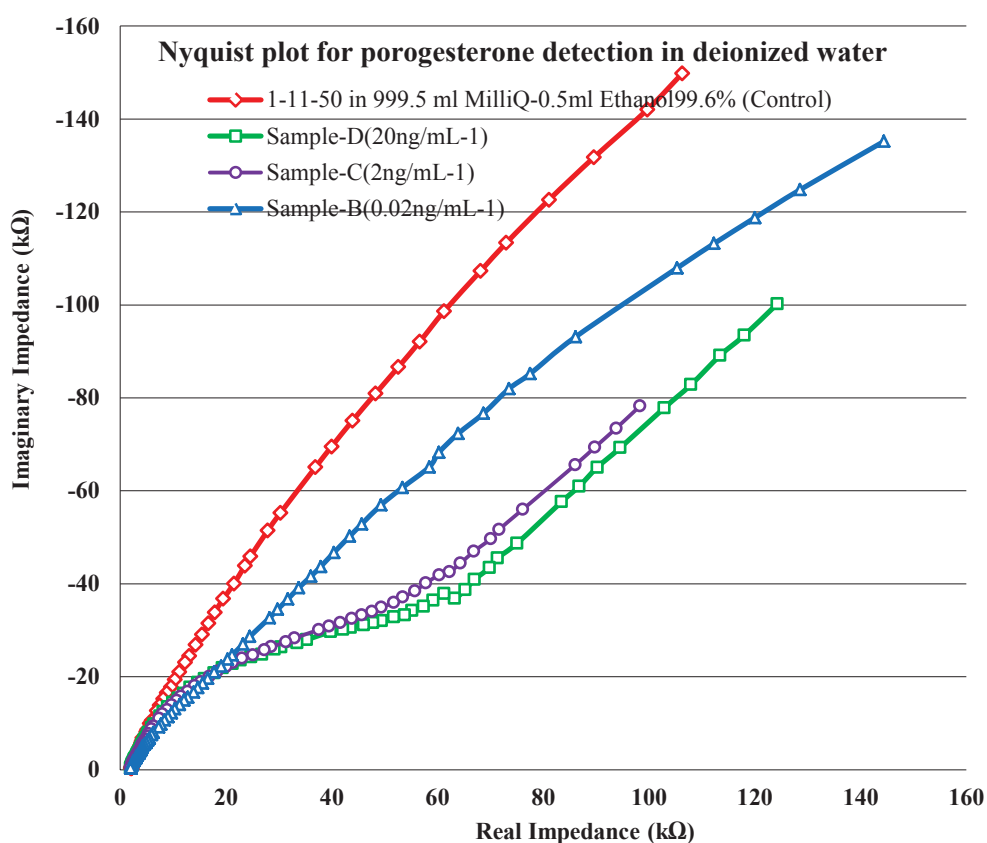


Figure 4.13 Nyquist plot for progesterone detection in DI water

It is noticed from Figure 4.13 that each of three impedance spectra includes a semicircle and a linear line portion at an angle of 45° . The diameter of the semicircle represents the electron transfer resistance at the surface of the electrodes whereas; the linear portion corresponds to a diffusion process leading to Warburg resistance at the electrode-solution interface. It was observed that the sensor can distinctively distinguish between concentrations of progesterone especially at low frequencies. This feature defines the sensitivity of the sensor for progesterone concentration in the solution as observed in Figure 4.14. The sensitivity curves (Figure 4.14 and Figure 4.15) were plotted using Equation 4.2 and 4.3 respectively which calculated the sensitivity values with reference to the control solution. The results display that the reactance percentage sensitivity stays till considerable range of frequency whereas conductance percentage sensitivity approaches lower values in the smaller part of the incident spectrum.

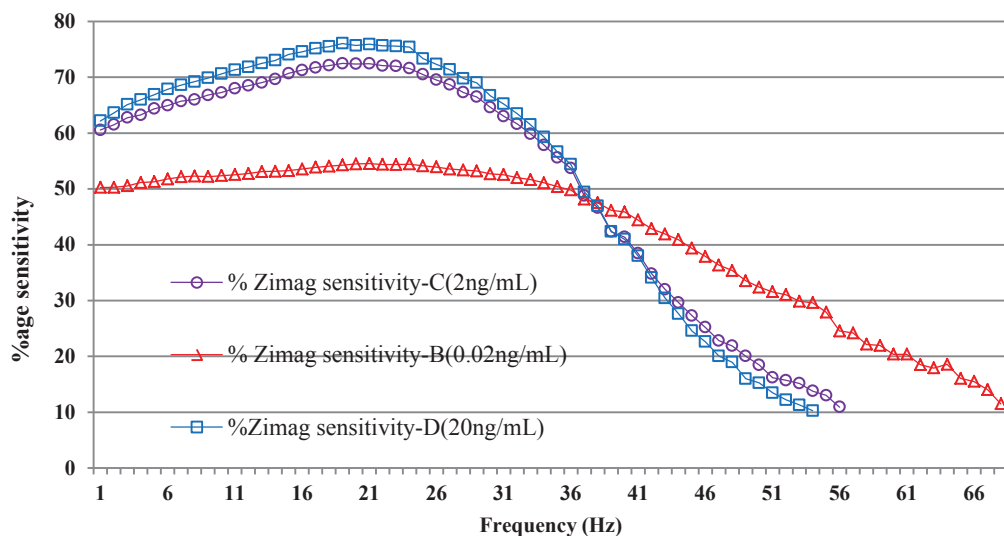


Figure 4.14 $Z_{imag}(X)$ %Sensitivity

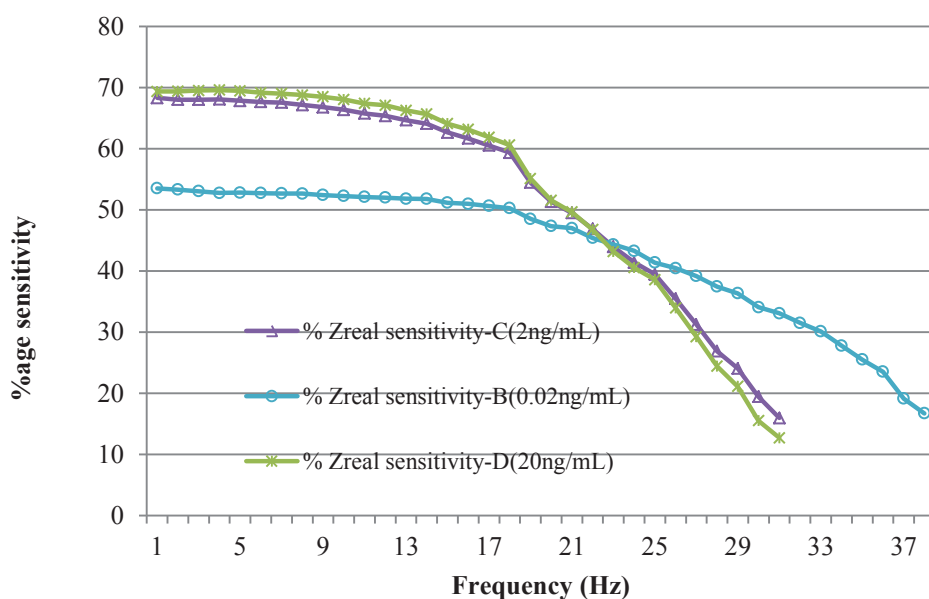


Figure 4.15 $Z_{real}(R_s)$ %Sensitivity

In view to the response of the sensor at low frequencies, the sensitivity of the sensor was plotted in a frequency range of 1Hz to 50Hz to figure out the most sensitive frequency value. The sensor displayed the sensitivity value well above 50% to the progesterone concentration as low as 0.02ng/ml in the deionized water [128].

4.4 Conclusions

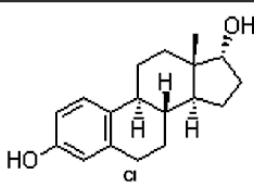
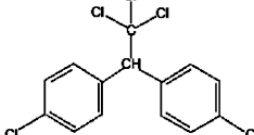
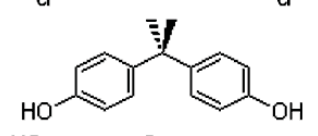
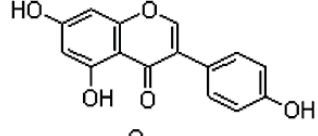
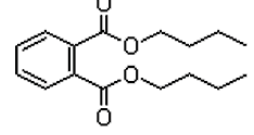
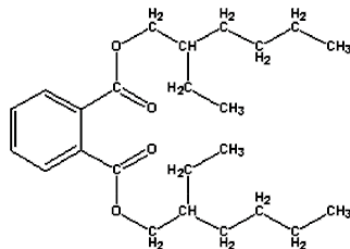
The response of the proposed sensing system was analysed for progesterone hormone and hormone metabolite E1G. The analyses depicted that the sensing system had enough potential to detect the presence of analytes in deionized aqueous medium. The sensitivity analyses for both types of molecules proclaimed the capability of the sensor and sensing system to differentiate between different concentrations of the analytes. It should be noted that the tested analyte concentrations were just trace level and detecting such minute quantities was quite promising for further research and developments in the project. In the next phase of this research endeavour, couple of endocrine disrupting compound were tested for rapid detection using the developed sensing system and electrochemical analyses were carried out to deduce meaningful information.

Chapter 5 Detection of Endocrine Disrupting Compounds

5.1 Introduction

Endocrine disrupting compounds are exogenous chemicals or mixture of chemicals that interfere the normal functioning of the endocrine system and cause hormonal imbalances in living organisms. These hormonal imbalances can cause cancers, birth defects, developmental disorders, nutritional malfunctions and impotency especially in males. EDC can block the receptor cells by stopping them to respond or can cause an adverse response by getting attached to the receptor in place of a hormone cell. Table 5.1 shows molecular structures of the most ubiquitous endocrine disruptors on earth.

Table 5.1 List of the most ubiquitous EDCs

Compound	Structure	Description
Estradiol		Endogenous Estrogen
DDT		Pesticide
BPA		Plastics Component
GEN		Phytoestrogen
DBP		Phthalate
DEHP		Phthalate

Phthalates, chemically known as 1-2-Benzenedicarboxylic acid esters, are internationally recognized as key industrial chemicals with a large number of commercial uses, such as additives, solvents and plasticizers due to their low cost [1]. Phthalates with higher molecular weight i.e. DINP (Diisononyl phthalate) and DEHP constitute about 80% of the phthalate production for the reason of their use as plasticizer in almost every plastic product including food and beverage packaging and medical applications, while low molecular weight phthalates, such as diethyl phthalate (DEP) and dimethyl phthalate (DMP), are used in cosmetics, insecticides, paints and pharmaceutical applications [129]. Phthalates added as plasticizers; do not covalently bond to the molecular structure of the resulting product, therefore, their potential for non-occupational exposure to the environment is high. They leach and migrate into packed food and beverages, gas out in the atmosphere or enter directly into human body fluids through medical products [130]. Human exposure to phthalates is a major concern for adverse human health risk. Phthalates have been characterized as environmental endocrine-disrupting compounds (EDCs) by many health monitoring agencies in the world due to their observed reproductive and developmental defects in rodents [131]. It was concluded that DEHP poses highest toxicity threat to human race, especially to children under 12 months of age and pregnant and nursing mothers [1]. A number of recent researches have suggested declining trend in the reproductive hormones levels in male adults [5] and elevated risk of breast cancer in females [7].

Human beings come in contact with phthalates in environment by three major routes; Dermal, Inhalation and oral (dietary) intake [132]. Oral route is the most important among all as it contributes the highest phthalate exposure rates to the human beings. Dietary exposures occur by accumulating phthalates either during the food processing and packaging from processing equipment or leaching into fatty foods, including dairy products, and from packaging during storage. Dairy products consumption by children per kilogram body weight is higher as compared to the adults, posing greater risk of reproductive and developmental toxicities for young children [7]. Polymer toys softened with DINP were estimated exposures ranged from 5-44 µg/kg body weight/day with 99th percentiles up to 183 µg/kg body weight/day for infants via mouthing activities [8]. Due to the leach-ability several researchers reported migration of phthalates from food packaging [9], PET (PETE, polyethylene terephthalate) bottled beverages and mineral water [2] and from corks of glass bottles [10]. World Health Organization (WHO) and European Union have limited DEHP in their water policy by

setting the guideline value at 8.0 µg/L in fresh and drinking waters in a published list of priority compounds posing endocrine disrupting hazard to human [12]. Table 5.2 shows risk assessment of phthalates by agencies in EU, US and Canada.

Table 5.2 Risk assessment of phthalates by world agencies [130].

Phthalate type	Risk assessment of Phthalates			
	Country, region	Committee/year	mg/kg bodyweight/day	MRL ¹ /TDI ² /RfD ³
DEHP	USA	US-EPA, 1993b	0.02	RfD
DEHP	USA	ATSDR, 2002	0.1	MRL
DEHP	Canada	Health Canada, 1994	0.044	TDI
DEHP	EU	CSTEE, 1998a,b	0.050	TDI
DINP	EU	CSTEE, 1998a,b	0.25	TDI
DEP	USA	ATSDR, 1995	7	MRL
DBP	USA	ATSDR, 2001	0.5	MRL
DBP	USA	US-EPA, 1990	0.1	RfD

¹ minimal risk level; ² tolerable daily intake; ³ reference dose levels

5.2 Impedimetric Detection of DEHP and DINP

In May 2011, Ministry of Health Taiwan reported illegitimate addition of phthalates by a drink manufacturing company into its products to make the juice look cloudy [133]. DEHP was added as a clouding agent in the drink. Later, on investigations, phthalates were found in certain medicines, foods and beverages manufactured in Taiwan. DEHP has legitimately been used as plasticizers in PVC food contact packaging material, but its use as food additive has never been allowed due to its health risk. It should be noted that the Tolerable Daily Intake (TDI) limit for DEHP in Taiwan and Hong Kong is 1.5ppm [134]. Long-time ingestion of DEHP with food at levels above the TDI can create hormonal imbalance in the human body that may result in the decrease of male reproductive ability, and female precocious puberty, breast cancer and loss of gender uniqueness [7, 8, 135, 136]. This incident created a huge wave of suspicion for all packed beverages throughout the world. Importers demanded testing certifications from the manufacturing companies which caused huge workload on the test laboratories. Due to expensive and time consuming testing, manufacturers had to face production loss and paid additional costs.

Phthalates' detection and measurement is purely a laboratory based procedure. The ubiquitous presence of this compound as a contaminant seriously limits its minimal

detection level. Even in most controlled laboratory setup it cannot generally be accurately quantified below about 2ppb [13]. Gas chromatography (GC) is the most commonly used technique for detection and quantification of phthalates metabolites [137]. High performance liquid Chromatography (HPLC) is used to measure phthalate concentrations in blood plasma and urine sample at low detection limits [11, 14]. Chromatography technique is used to separate complex mixtures of organic compounds with each compound quantified by its specific detector. DEHP is measured using Electron Capture Detector (ECD) [137] and Flame Ionization Detector (FID) [138]. Liquid Chromatography (LC) coupled with mass spectrometry (MS) or ultra violet (UV) detection are also a few commonly used techniques for detection of phthalates.

5.2.1 Motivation

Almost all contemporary analytical techniques used to detect phthalates in food products and beverages require laboratory environment with stringent conditions over sampling procedures. There is a paramount requirement for a low cost real time testing system which could be used for instant screening of food and beverage products to detect the presence of phthalates that could readily be installed in an industrial setup. The discussed design and methodology of the developed sensing technique possesses properties of speed, in situ testing with an additional benefit of low cost. The objective of this part of research was to test the detection response of the fabricated sensor for the two phthalate esters; di(2-ethylhexyl) phthalate (DEHP) and diisononyl phthalate (DINP). The molecular structures of DEHP and DINP are shown in Figure 5.1 and Figure 5.2 respectively.

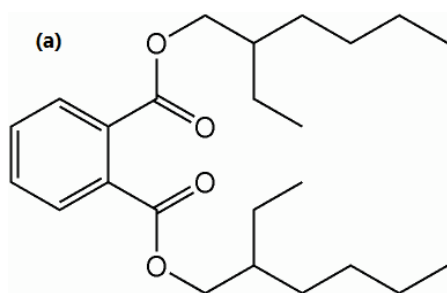


Figure 5.1 Molecular structure DEHP

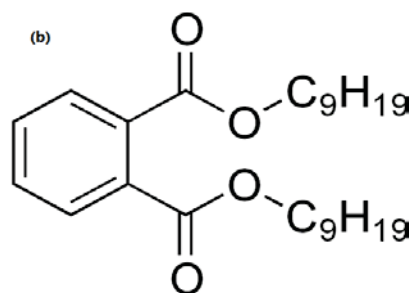


Figure 5.2 Molecular structure DINP

5.2.2 Materials and Methods

Gravimetrically prepared 99.5 % pure solutions of DEHP and DINP at a concentration of 100 μ g/mL (100 ppm) in ethanol were procured from ChemService[®] USA. Two set of working solutions of these compounds were prepared by serial dilution method. The first set was prepared with deionized water MilliQ[®] (MILLIPORE USA) at concentration of 0.002 through 2ppm concentration levels of DEHP. The second set of samples was prepared at a concentration level of 0.1, 0.5, 1 and 20ppm of DINP in ethanol. 20ppm concentration from this set was used as stock solution. 99.7% pure research grade ethanol was used to serial dilute the stock to achieve lower concentrations. pH of control and working solutions were tested using IQ Scientific Instrument Inc. USA after calibration with the buffer solutions provided by the manufacturer.

Hioki 3522-50 LCR Hi precision Tester (Japan) was used for the EIS experiments. The equipment was interfaced with a desktop computer through RS-232C hardware interface device. Automatic data acquisition software programmed in Lab view[®] was used to generate Microsoft excel[®] data file in real time. The LCR tester was calibrated with built-in open circuit and short circuit tests in order to offset any stray capacitance appearing due to the testing leads. Figure 5.3 shows the test bench setup and Figure 5.4 shows bulk sample testing using dip-test method.

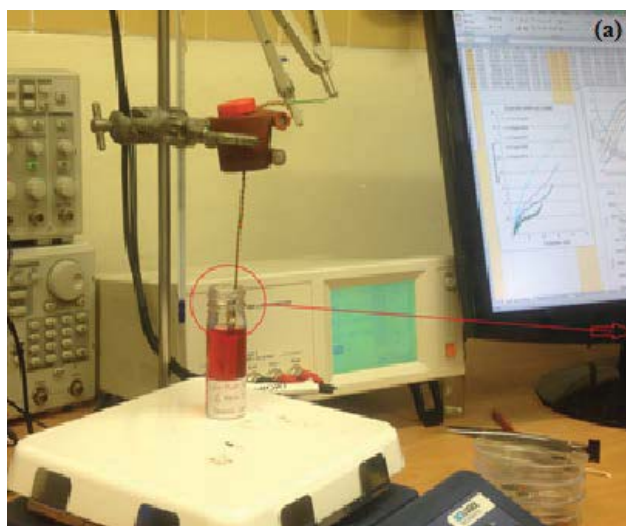


Figure 5.3 Test bench setup



Figure 5.4 Dip-test (bulk)

All experiments were performed using slow mode of testing to achieve error rate of <0.05%. For reliable results the device was set to write an average of 8 readings of

impedance values at each single frequency applied to the sensor. A 1V_{rms} sinusoidal signal was applied to the sensor with a frequency sweep of 10Hz to 100kHz with 20 data points per decade on log scale. An average of three experiments was used to further ensure reproducibility and reliability of the results. The sensor was cleaned with acetone, rinsed with deionized water and dried in nitrogen in before next test.

5.2.3 DEHP Detection Test in Deionized Water

Deionized Milli-Q water (18M Ω cm) with 2ppm ethanol (99.7% purity) was used as control solution. The pH of the control was 7.3 at 23°C in the laboratory environment. 2ppm concentration of DEHP was used as stock solution to obtain the lower concentrations of 0.2ppm, 0.02ppm and 0.002ppm by serial dilution of the stock solution. This range of the DEHP concentration in the test-samples was chosen to check the response of the sensing system for the trace level detection of DEHP. The pH of the stock solution was measured to be 6.95 at 23°C. Experiments were conducted immediately after sample preparation at 23°C with a humidity level of 47% in laboratory environment. Figure 5.5 shows the plot for imaginary and real part of impedance vs. frequency for all the four concentrations of DEHP.

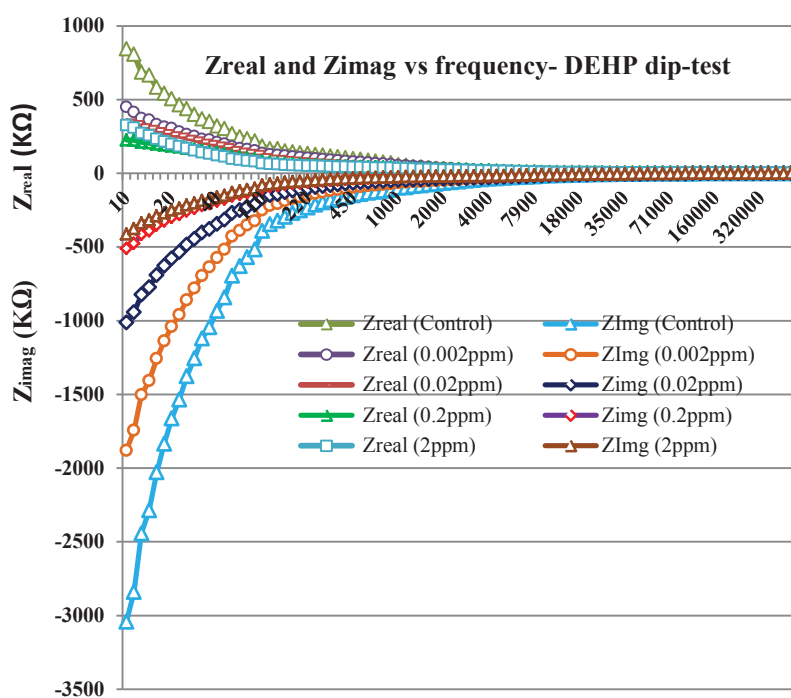


Figure 5.5 Imaginary and real parts of impedance measurements for DEHP dip-test

The capacitive reactance (Z_{imag}) showed a good variation with changing concentrations of DEHP especially at lower frequency range (10Hz-400Hz). At higher frequencies (500Hz to 5kHz) the rate of change in impedance was observed to be extremely low. This change is described in terms of sensitivity in the analysis discussed in later part of this chapter. The corresponding change in Z_{real} was not dominant and its rate of change was much less in comparison to its counterpart; capacitive reactance (Z_{imag}). This showed the increase in capacitance of the sensor with increase in DEHP concentration which was due to the inherent dielectric properties of the target DEHP molecule. The real part represented the static resistance of the solution appearing due to the ionic currents passing through the electrochemical cell. The coated polymer stopped the ion exchange through the electrode surface. The Nyquist plot shown in Figure 5.6 demonstrates; a mass transfer process in form of a straight line at 45° which corresponded to the Warburg resistance and a charge transfer process displayed as a semi-circular region of different diameters. Each semi-circle corresponded to the DEHP concentrations in test solutions.

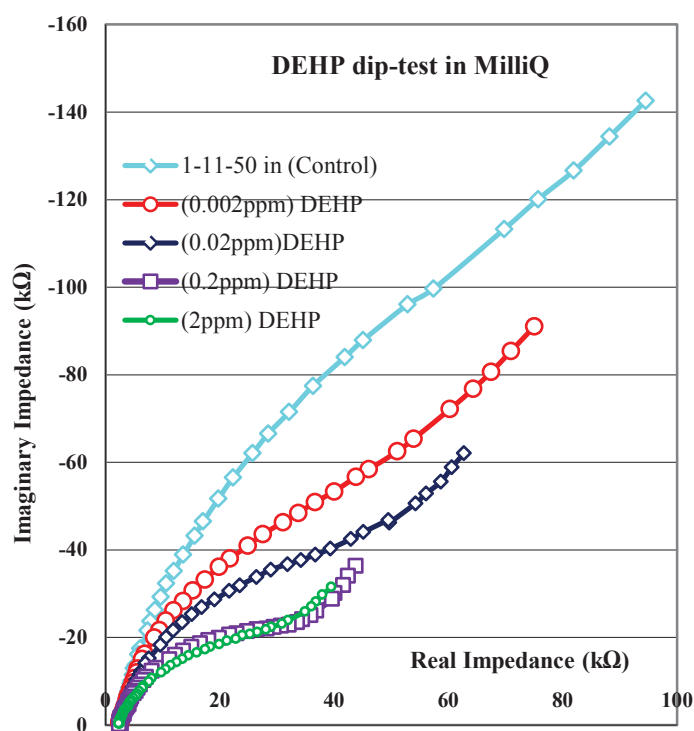


Figure 5.6 Nyquist plot for detection of DEHP in DI water

The diameter of the semicircle dictated the value of the charge transfer resistance R_{ct} . Correspondingly, R_{ct} changes the double layer capacitance C_{dl} , at the electrode-solution

interface which showed the ability of the sensor to monitor the variation of DEHP as low as 0.002ppm in the deionized water.

5.2.4 Experimental Data Analyses by CNLS Curve Fitting

The equivalent circuit was estimated using theoretical calculations by electrochemical spectrum analyser algorithm. The circuit parameters were estimated by non-linear least square fitting technique which fits the measured impedance data on theoretically estimated values. The algorithm performs statistical analysis to calculate the residual mean square $r_{amplitude}^2$ for experimentally observed values in measured spectra against the calculated values based on the theoretical response of suggested equivalent circuit. $r_{amplitude}^2$ determines the deviation of the experimentally observed data from the optimal solution. The optimization of the calculated data is achieved by the number of iterations it takes to solve the mathematical model for the proposed equivalent circuit. The value of $r_{amplitude}^2$ in the range of 10^{-4} shows optimal fitting with an error rate of less than 5% in calculating the values of equivalent circuit components. Figure 5.7 shows the equivalent circuit interpreting the kinetics of the electrochemical model obtained in consequence of non-linear least square fitting. Figure 5.8 depicts the fitting plot for absolute value of Z. Figure 5.9 shows curve fitting for Nyquist plot and Figure 5.10 displays the curve fitting for the phase shift. It should be noted that the solid line in all curve fitting plots sketches the theoretically calculated values and the markers display the plot of the experimentally observed values respectively [106].

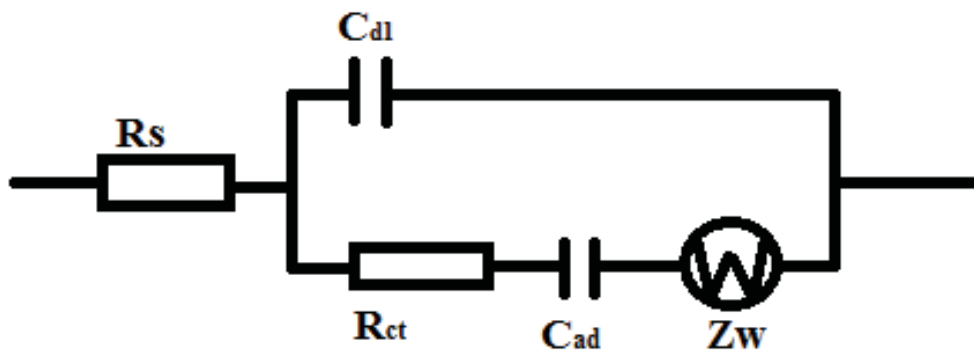


Figure 5.7 Equivalent circuit proposed by CNLS curve fitting

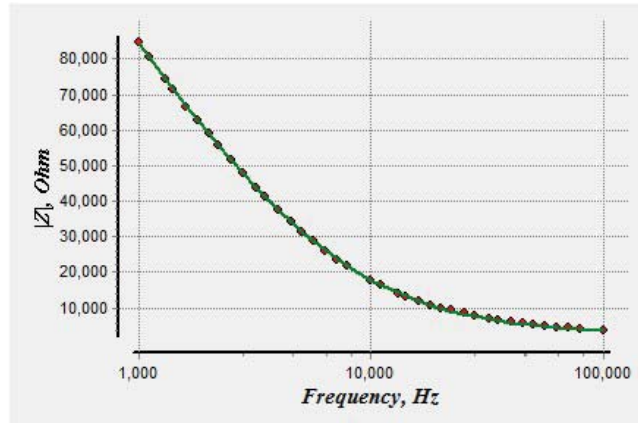


Figure 5.8 CNLS curve fitting plot for absolute value of Impedance.

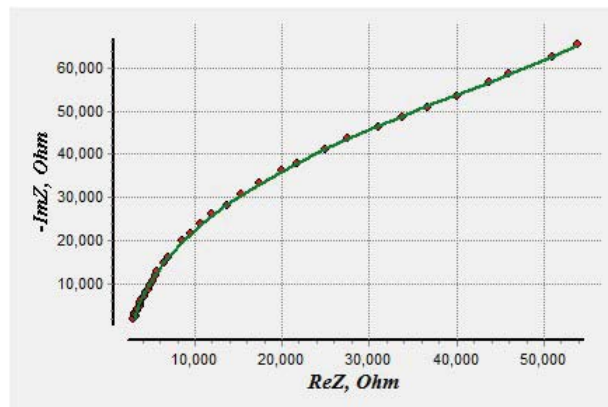


Figure 5.9 CNLS curve fitting plot for imaginary value of Impedance.

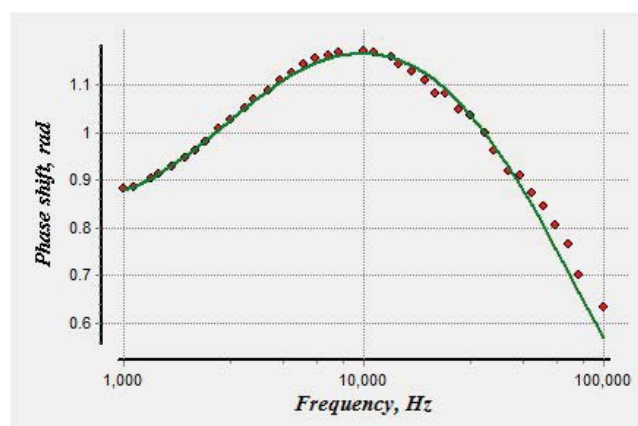


Figure 5.10 CNLS curve fitting plot for phase shift (ϕ)

Table 5.3 presents the equivalent circuit components' parameters, error %ages, and residual mean square values obtained from non-linear least square fitting for DEHP concentrations from 0.002 ppm to 2 ppm in 1 kHz to 100 kHz frequency range.

Table 5.3 Equivalent circuit parameters evaluated by CNLS algorithm

Equivalent Circuit Parameters	Units	DEHP concentrations in deionized water							
		0.002ppm DEHP		0.02ppm DEHP		0.2 ppm DEHP		2ppm DEHP	
		Value	Error (%)	Value	Error (%)	Value	Error (%)	Value	Error (%)
C_{dl}	F	1.58E-9	0.322	1.7E-9	0.93117	2.3134E-9	0.42549	1.003E-8	0.52117
C_{ad}	F	5.88E-9	2.72	1.326E-8	4.057	1.2799E-8	2.4528	1.148E-8	4.0362
R_{ct}	Ω	91152	0.57	64578	1.2952	42339	0.41634	48805	0.68871
Z_w	Ω	2.18E+6	1.61	1.7024E+6	3.4118	5.1313E+5	2.6064	2.915E+5	4.4795
R_s	Ω	2889.9	2.826	2845.7	4.4782	2681.6	1.9857	2021.1	3.1013
$r_{amplitude}^2$		0.00075375		0.0009797		0.0003502		0.0002925	
Iterations		300		300		300		300	

The analysis showed that the double layer capacitance C_{dl} increased from 1.5pF to 10pF with increasing concentration of DEHP which verified the inherent dielectric properties of DEHP molecule present in the sample solutions. The charge transfer resistance R_{ct} decreased from 91.1k Ω to 48.8k Ω . Same kind of decrease is observed in Warburg impedance Z_w that reduced from 2.1M Ω to 0.29M Ω with increasing molecular density of DEHP in the sample solutions. The solution resistance R_s value, which depends on the ionic concentration in the sample solution, also fell from 2.8k Ω to 2k Ω indicating increase in conductivity of the sample solutions with increasing concentration of DEHP. Another parameter C_{ad} was observed to build up with increasing concentration of DEHP in samples from 5.8nF to 11.4nF which is attributed to the formation of adsorbed layer of DEHP on gold electrode surface. It is caused by the diffusion of ions from the electrode surface into the solution as a result of transfer of charges (electrons) into the electrode from the bulk solution [139].

5.2.5 Sensitivity Analysis – DEHP

The sensitivity of the sensor was evaluated on the basis of capacitive reactance which is dominant over change in the real part of the measured impedance spectra. The real part was unable to provide useful information on impedance change induced by DEHP concentration. This occurred due to the fact that DEHP is a dielectric material, therefore did not contain any ionic concentration in the test samples.

The calculated values of sensitivity (%) plotted in Figure 5.11.

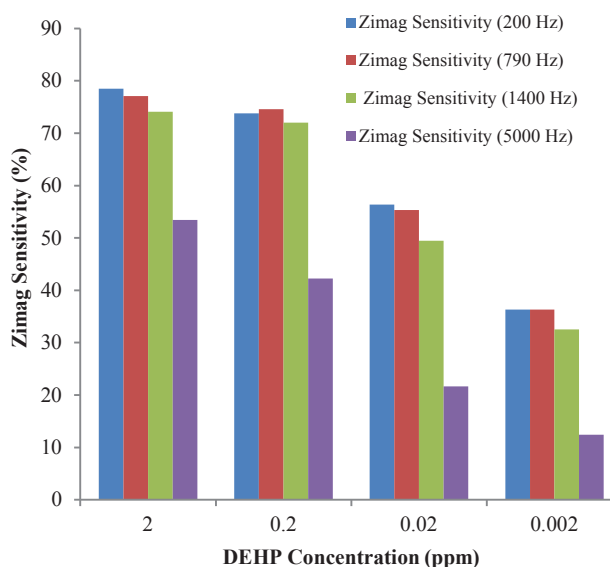


Figure 5.11 Reactance percentage sensitivity for DEHP in DI water

The plot depicted that the sensor remains sensitive to the DEHP concentration in MilliQ during a fair range of frequency i.e. 10 Hz to 1400 Hz. Figure 5.11 accounts for the calculated percentage sensitivity values using Equation 4. plotted for different concentrations of DEHP in the test solutions at 200, 790, 1400 and 5000 Hz frequencies. The sensitivity deteriorates drastically after 5 kHz.

5.2.6 DEHP Detection in Commercially Sold Energy Drink

Due to the strict control by Ministry of Health in New Zealand, it was assumed that the beverages available in the local New Zealand markets are phthalate free. The sensor's response was tested with added DEHP in one of the locally available energy drink, branded "Lift Plus Extra". This drink is supplied in glass bottle packaging. PET bottled drink was not selected for test due to the uncertainty of leached phthalate in the drink. Figure 5.12 shows the test bench used to test DEHP-spiked energy drinks.

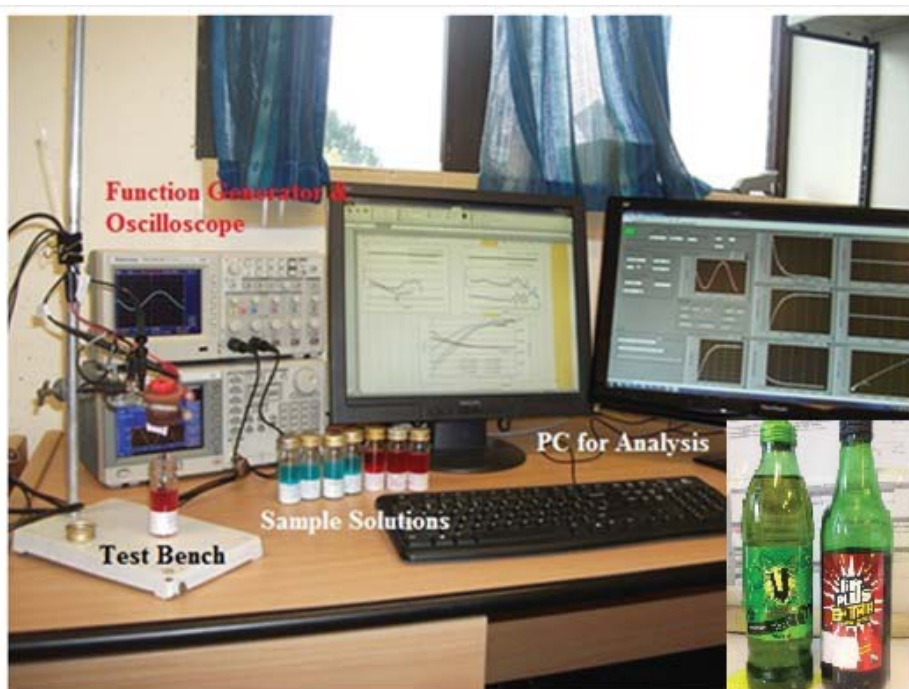


Figure 5.12 Test bench setup for DEHP-spiked energy drinks

Three spiked working solutions with 2, 6 and 10 ppm concentrations of DEHP were prepared at 23°C temperature and were tested immediately after sample preparation. These concentration levels were selected to note the detection response of the sensor below and above the MRL limit set by ATSDR, USA. Un-spiked original drink was used as the control reference solution for comparison [140].

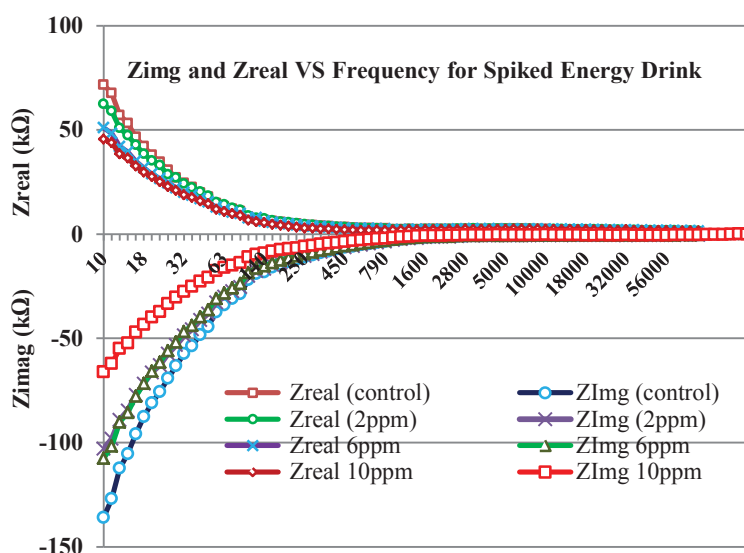


Figure 5.13 Z_{real} and Z_{imag} for DEHP dip-test of spiked energy drink

The sensor displays change of impedance in the capacitive reactance dominating the corresponding real impedance (Z_{real}) change through a frequency range of 10Hz to

1.3kHz. Figure 5.13 shows the plot for real and imaginary part of impedance spectra for the energy drink spiked with DEHP as compared to the un-spiked drink. Figure 5.14 displays the bode plot for DEHP spiked drink in the said frequency range.

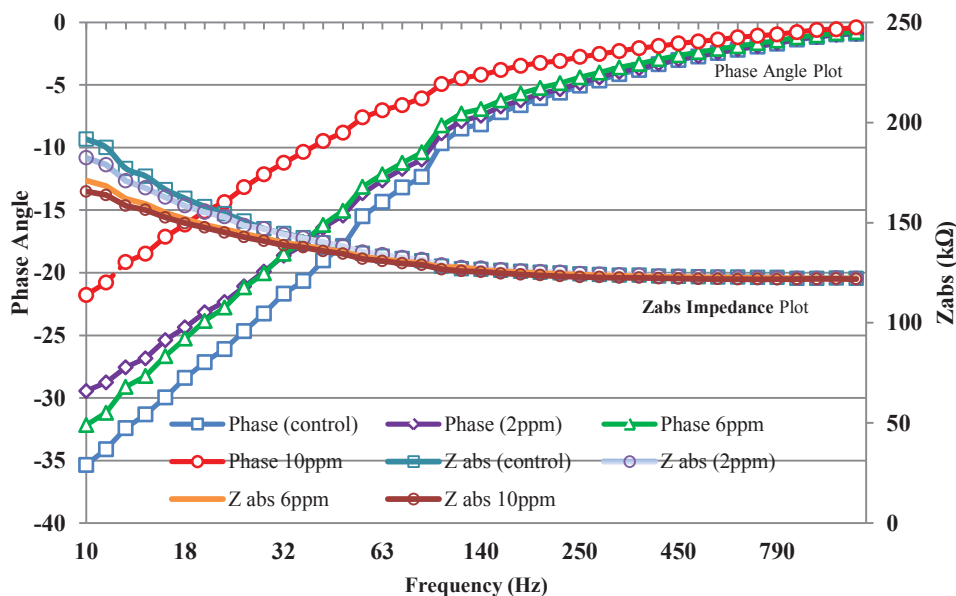


Figure 5.14 Bode plot showing measured spectra for the spiked drink

It has been observed that the change in the absolute Impedance Z_{abs} is visible only at the lower frequency range, whereas, the phase shift is distinctive for pure and spiked samples, especially for DEHP concentration as high as 10ppm. The magnitude of change in imaginary impedance for 2ppm and 6ppm of spiked energy drink did not show much difference due to the fact that energy drink contains many other chemicals apart from the spiked DEHP, that also contribute in the impedance measurements. The solution to this problem required the selectivity characteristics to be induced in the sensor for the specific analyte molecule (DEHP in this case).

5.2.7 Impedance Measurements of DINP-spiked Ethanol Samples

All phthalates including DINP are synthetic oily compounds that do not dissolve in aqueous medium. On the other hand, are soluble in all organic solvents. Experiments were conducted to investigate the capability of the sensing system for phthalate detection in alcohol based beverages. Although, alcohol based drinks are supplied in glass bottles yet research has declared that the cork stopper used in glass bottled drinks leach phthalates and the migration is even faster in this case by virtue of the solubility properties of alcohol [10].

Four different concentrations of DINP-in-Ethanol; 0.1, 0.5, 1 and 20ppm were tested at room temperature using the designed real-time detection system.

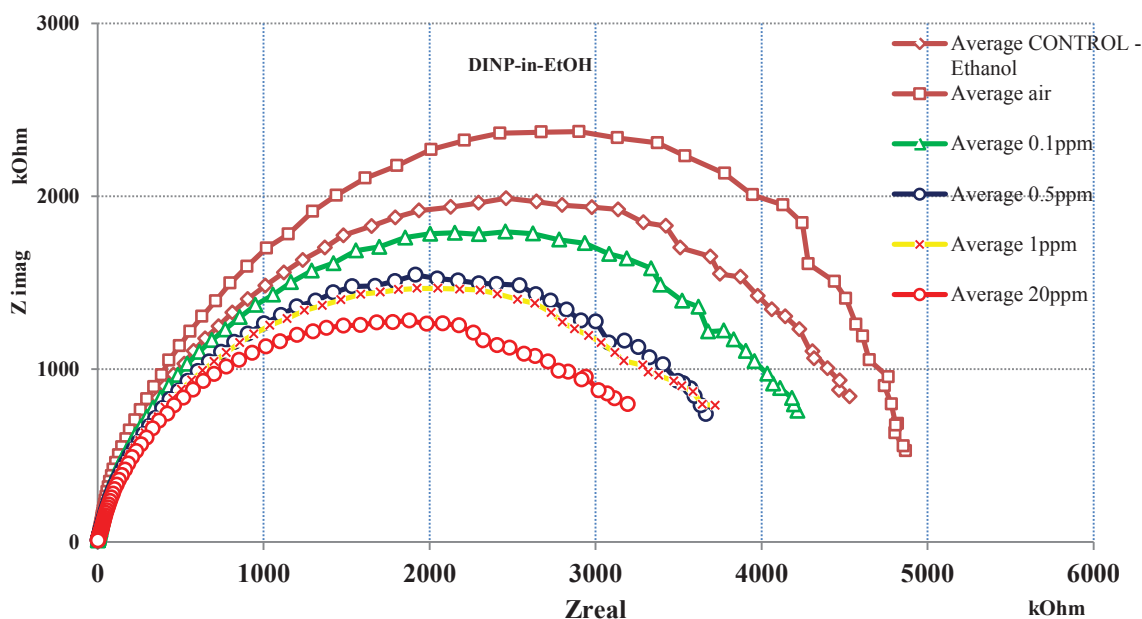


Figure 5.15 Nyquist plot for DINP concentration test in EtOH

Control solution is 99.6% pure ethanol with pH 6.71. It was observed that addition of DINP in the working solutions did not alter their pH level and their average pH value observed was 6.52 at 20°C. The sensor was profiled in air before its exposure to the different DINP concentrations. Figure 5.15 shows the Nyquist plot for the impedance spectrum obtained. It was observed that the plot did not display diffusion-limited process (Warburg Resistance) in the selected frequency range which is attributed to Si_3N_4 coating on the sensing area and absence of redox-active compound in the solution [16]. The high value of charge transfer resistance (R_{ct} is $5\text{M}\Omega$ for air and control) calculated from the plot depicts the charge transfer process. The double layer capacitance (C_{dl}) appears due to the layer of charges formed at the electrode-solution interface, at this point, it had a value of 0.115nF for air and 0.113nF for the control solution. The corresponding values of C_{dl} for 0.1, 0.5, 1 and 20ppm DINP concentrations are calculated to be 7.7nF , 96.95nF , 100nF and 113.2nF respectively. The change in the value of the C_{dl} corresponded to the change in the concentration of DINP in ethanol. It is observed that the sensor is highly sensitive at low frequencies (6 to 100Hz). The reactance (imaginary Impedance) of the sensor dominates the real impedance showing its capacitive behaviour.

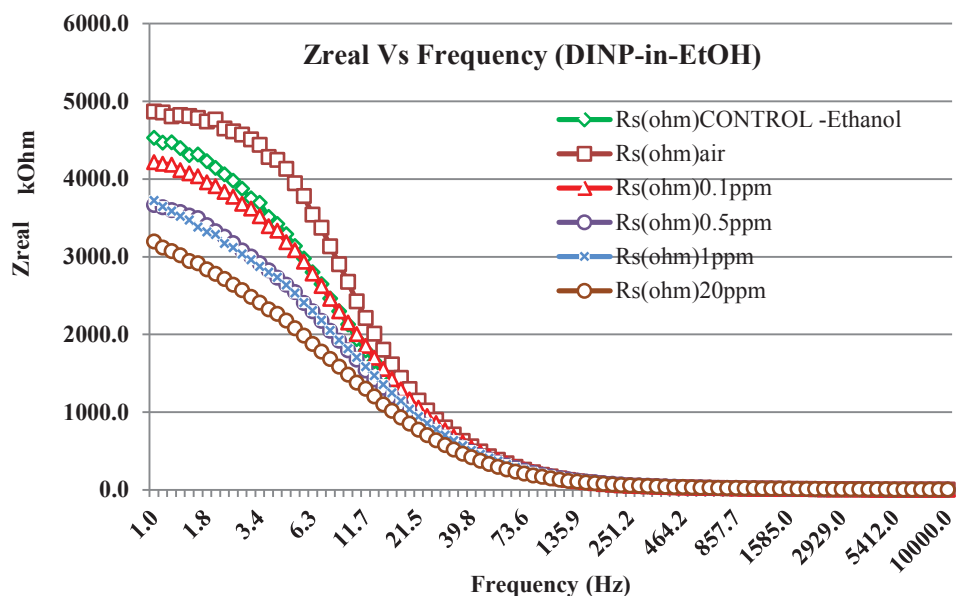


Figure 5.16 Real part of impedance for DINP-in-EtOH

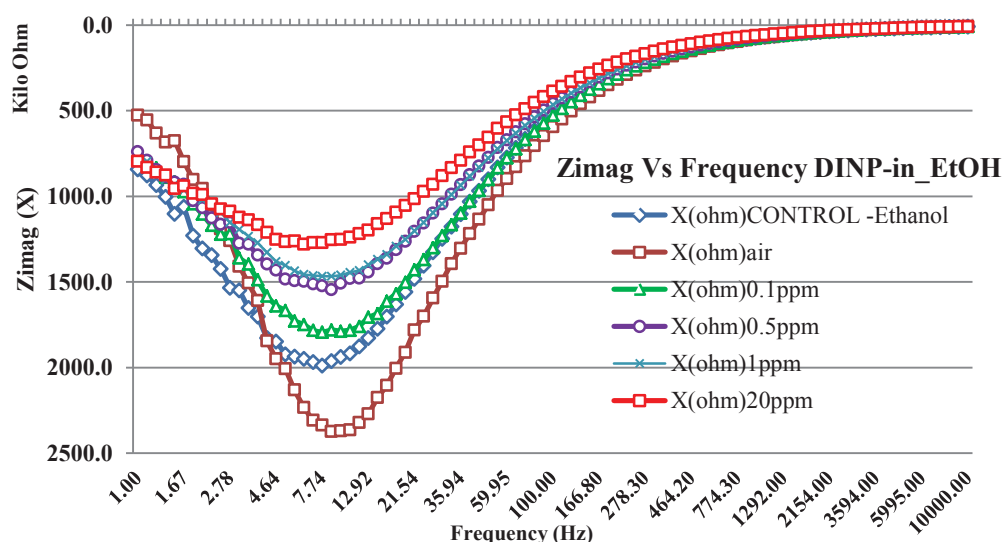


Figure 5.17 Imaginary Part of Impedance for DINP-in-EtOH

Figure 5.16 and Figure 5.17 show the real and imaginary impedance plotted against frequency respectively. A sequential decrease in the reactance is observed with the increasing concentration of DINP in EtOH as shown in Figure 5.17.

5.2.8 Impedance Measurements of DINP-Spiked Orange Juice

Assuming that glass bottled juices are phthalate-free in New Zealand, 5, 10 and 20ppm DINP was added to a locally available orange juice (average pH of 3.47 at 20°C). Control for this set of samples was un-spiked (no added DINP) juice [76].

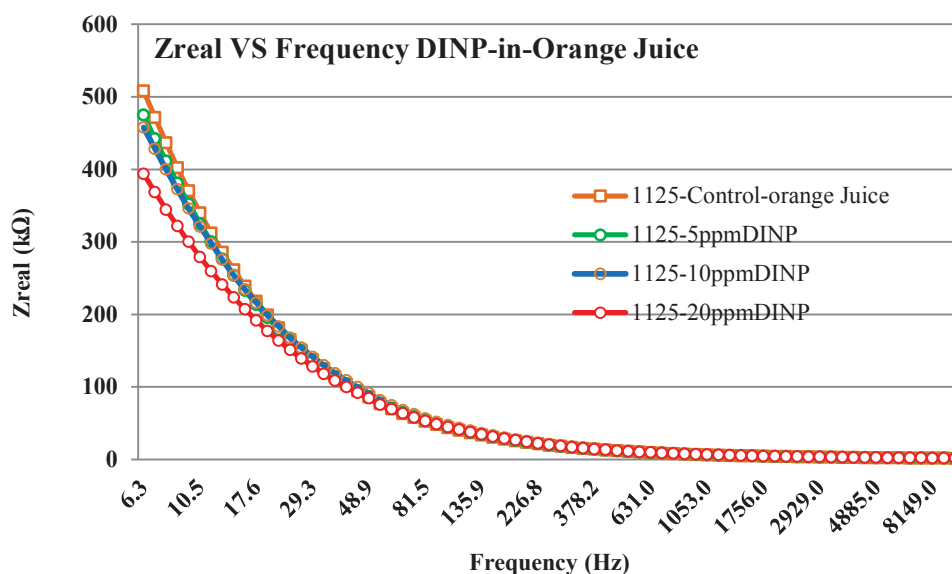


Figure 5.18 Real part of measured impedance for DINP in orange juice

Figure 5.18 shows the real impedance plot for the results which show that the sensor was able to translate the DINP concentration in the samples in terms of reactance. It was observed that the acidic medium has reduced the solution resistance ten folds as compared to the test in ethanol medium. It happened due to the presence of ionic concentration in the medium; therefore, the process of ionic diffusion takes place in the solution at the electrode-solution interface on the application of electrical perturbations. Consequently, it caused a drastic decrease in the solution resistance. Figure 5.19 shows the imaginary part of impedance measured in testing spiked orange juice with the proposed detection system.

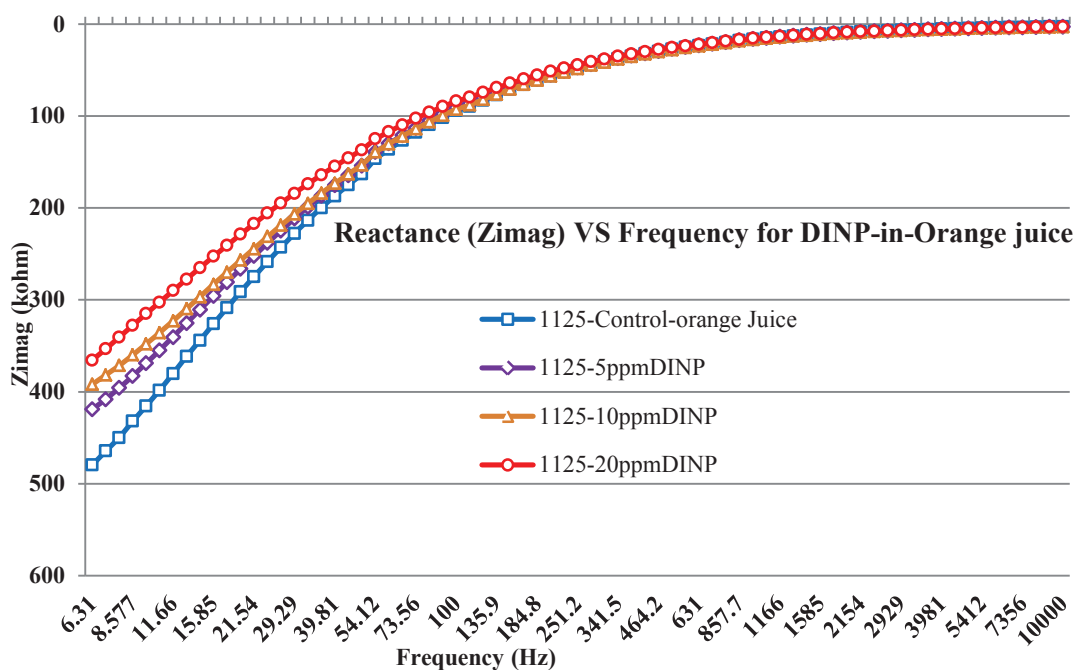


Figure 5.19 Reactance plot for DINP-in-Orange juice

The presence of other chemicals in the complex matrix like orange juice has drastically affected the sensitivity of the sensor, which can be seen from the plotted imaginary impedance curves for different concentrations of DINP in orange juice. The range of frequency for which the sensor has shown presence of DINP (6.31Hz to 39.81Hz) has reduced; additionally, the magnitude of change in reactance of the sensor has eroded. The test results of DINP in orange juice were not too different to the test results of DEHP in energy drink. The system was unable to detect the trace level concentrations of phthalates in complex solutions like drinks and juices.

5.2.9 Conclusions

The developed sensor and sensing system was employed to detect two types of phthalates spiked in different types of mediums. The tests were performed in real-time and the sensor performed successfully in the detection of phthalates in pure polar medium. The system was able to detect the presence of DEHP and DINP even to a trace level in the polar medium but the outcomes of the investigation made for electrolytic and acidic media were not up to the mark. Although, the sensitivity analysis of the system displayed high level of sensitivity in pure aqueous and organic solvent media yet, the system sensitivity deteriorated drastically in complex solutions. This led the sensing system research to the next stage of development. In order to adapt the sensor and sensing system for complex chemical matrices like beverages, milk and urine, selectivity for analyte molecules was an utmost requirement. Different options to pave the way to selective adsorption of phthalates on the sensing surface have been explored. Published research provides a number of methods to selectively detect analyte from a complex matrix by extraction, absorption, adsorption, biological separation and filtration. Unfortunately, all these techniques are laboratory based and require certain skills and expertise to perform. On the other hand these techniques are extremely delicate and require certain environmental conditions to execute.

One of the main objectives of this research was to develop an assay system that is robust enough to have an in-field application without any technical expertise requirement for the user. To achieve this objective a robust assay technique was tailored and applied to induce selectivity in the designed sensing system. The discussion on inducing selectivity for specific molecules is carried out in the next chapter of this thesis.

Chapter 6 Inducing Analyte Selectivity in the Sensing System

6.1 Introduction

The need for the development of fast, sensitive and highly selective chemical and biochemical sensors for applications related to complex matrices of medical, environmental and industrial interests has been a subject of ultimate research and development recently. A number of chemical and biochemical sensors have been designed by making use of enzymes, antibodies, membranes, carbon nanotubes, magnetic nanoparticles and supramolecular assemblies to realize the sensing elements for chemical and biochemical analytes [141-143]. However, the availability of biocomponent required, or the mandatory requirement of stability and reproducibility in chemical and biochemical recognition remained unachieved. Therefore, all the techniques and assays developed stayed restrained to laboratories. The aim of rapidness and robustness in chemical and biochemical recognition had been an ambition for the researchers in this field.

Recent studies in polymer science demonstrated that use of analyte (organic template) could create imprinted cavities in cross-linked polymers and has proved to be the most efficient way of polymerizing synthetic materials bearing selective molecular recognition sites for the analyte. Since the chemical, physical and electrical properties of the polymers may be tailored over a wide range of characteristics, sophisticated and hi-tech electronic and electrical sensing devices have a huge potential of placing polymers at a permanent collaborative position in the field of chemical and biochemical sensing [144, 145].

The developed methodology is based on chemical, physical or electrical interaction of the analyte, called print molecule or template, with a functional monomer to polymerize together. A rigid, cross-linked, macro-porous polymer is formed that contains the analyte packed in the synthesized polymer. On removal of the print molecule by elution, specific sites are left behind that are complementary to the print molecule in shape and arrangement with an outstanding capability of rebinding the template and structurally

related analytes. The polymer with the “memory” of the analyte hence gets the name of ‘Molecular Imprinted Polymers’ (MIP) [146-148]. Molecular imprinted polymers (MIPs) are specially designed polymerized materials owing valuable molecular recognition capabilities. These possess specific cavities designed for a target molecule, privileged by unique advantages like high selectivity, physiochemical stability and specific recognition of analyte and structurally related compounds.

Molecular Imprinted polymers could be synthesized by applying a number of approaches like precipitation, bulk, suspension, swelling, miniemulsion and core-shell polymerizations depending on the application [147]. Figure 6.1 shows the steps involved in the synthesis of MIP and Figure 6.2 shows the extraction process making molecular recognition sites available in the polymer matrix for selective extraction.

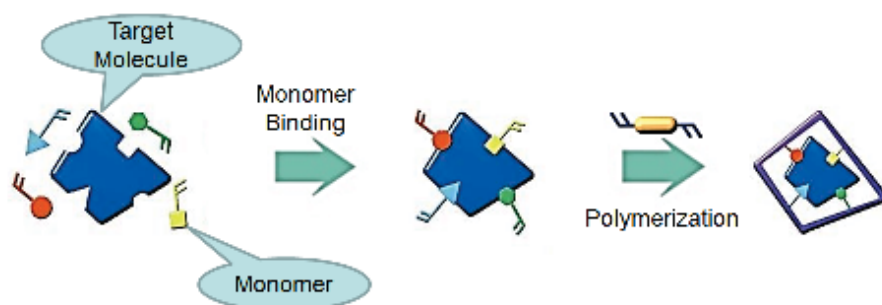


Figure 6.1 Synthesis process of Molecular Imprinted Polymer

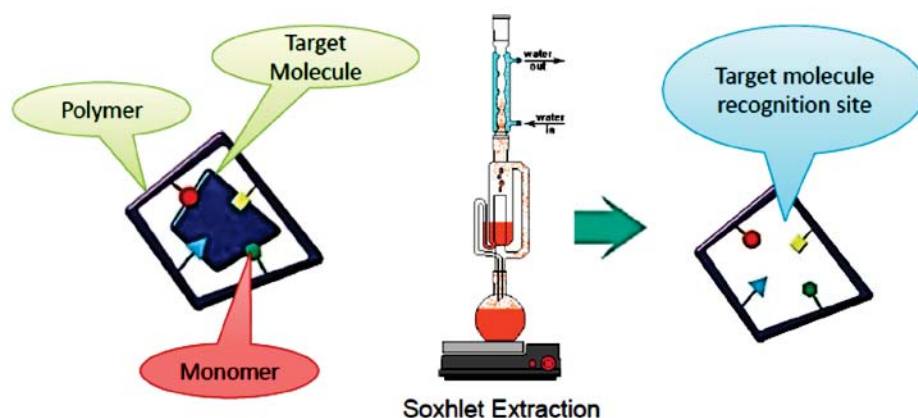


Figure 6.2 Extraction of template molecule forming molecular recognition site in MIP

Latest research depicts that molecular imprinting technique has rigorously been used to extract the phthalate analytes from the samples as an application for sample clean-up to

quantify DEHP by using gas chromatography [17, 149, 150]. The entrapment of target molecules is achieved by two established strategies using covalent or non-covalent interactions of the target molecule with the functional monomer. Non-covalent approach makes use of instinctive intermolecular forces present between the target and monomer molecule. This molecular recognition selectivity has proved to be an attractive predominant advantage for separation and analyses of complicated samples and has been applied in several contexts e.g. solid phase extraction (SPE) [15, 150], chromatography [151], electro-chromatography [152], membrane filtration and sensing. It has obvious advantages over biological receptors and antibodies of more number of target molecule capturing sites [151]. MIPs are intrinsically stable robust and reusable. These relatively weak forces could be hydrogen bonding, ion pair, dipole-dipole interactions or van der Waals forces between the two molecules. This is the most commonly used approach since it requires minimal effort to remove the entrapped molecules from the molecular recognition sites whereas the covalent bonding requires additional steps to release the entrapped molecules [153]. Molecular imprinted micro and nano-spheres applied for DEHP determination have been reported as a product of precipitation polymerization for MIP [16]. The microspheres exhibited a strong DEHP molecular affinity and the authors evaluated an imprinted factor (IF) of higher than 8 in their reported research [16]. Yan et al. reported the synthesis of a new imprinted microsphere for DINP by precipitation polymerization and determined the PAEs in plastic bottled beverages as an application. The average recovery of the five PAEs at three different spiking levels was found to be ranging from 84.3% to 96.2% for different phthalate molecules [154].

In the presented research, a selective MIP for DEHP was synthesized by the process of suspension polymerization with the use of methacrylamide as a functional monomer. DEHP molecule was used as template with N,N-methylene-bis-acrylamide behaving as a cross-linker molecule to polymerize the MIP. The adsorbed DEHP was extracted using soxhlet extraction method through methanol. The MIP was air dried and immobilized on the ID sensor for rapid quantification of DEHP in aqueous medium by electrochemical impedance spectroscopy application studies.

6.1.1 Materials and Methods

Di(2-ethylhexyl) phthalate (DEHP). N,N-methylene-bis-acrylamide, methacrylamide, ammonium persulfate, Methanol, ethanol, acetonitrile, chloroform, dimethyl

formamide (DMF), dichloromethane and 3-aminopropyltriethoxysilane (APTES) were procured from Sigma Aldrich, Germany. Deionized (DI) water MilliQ[®] was obtained from MILLIPORE water system (USA)- 18 MΩ cm. Gravimetrically prepared di (2-ethylhexyl) phthalate (DEHP) solution at a concentration of 200μg/mL (200ppm) in ethanol (99.5% purity) was ordered and received from ChemService[®] USA. Other working solutions of lower concentrations were achieved by serial dilution method in the deionized water MilliQ[®]. Pure deionized water with a 100ppm concentration of ethanol was used as control solution for the experiments. pH meter from IQ Scientific Instrument Inc. USA was used to measure pH levels of the spiked and control solutions. The device was calibrated with buffer solutions provided by the manufacturer.

6.1.2 Synthesis of DEHP imprinted polymer

A DEHP selective molecular imprinted polymer was synthesized by suspension polymerization using methacrylamide as a functional monomer attaching itself to DEHP molecule via hydrogen bonds. N,N-methylene-bis-acrylamide was used as crosslinker for polymerization reaction. Ammonium persulfate was used as initiator for synthesis of the polymer.



Figure 6.3 Polymerisation reaction

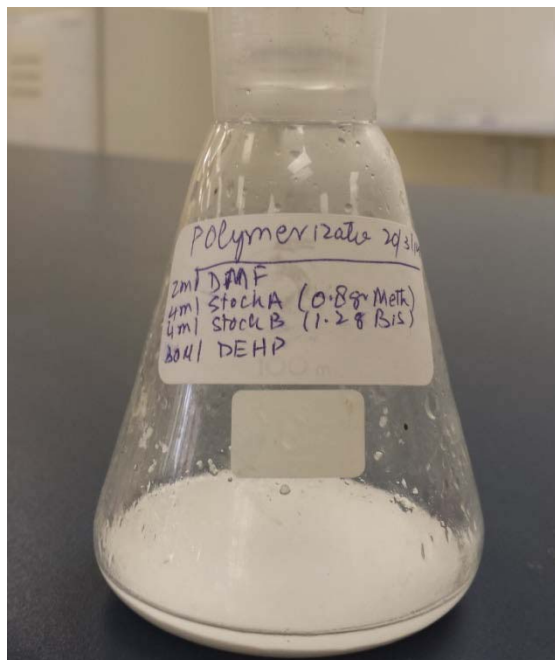


Figure 6.4 Polymerized MIP

A solution of 2.5ml DMF, 7.5ml MilliQ water, 14.5mmol methacrylamide and 1ml DEHP was prepared in an ice bath and functional monomer and template (DEHP)

molecules were allowed to generate hydrogen bonds between DEHP and methacrylamide (monomer) in the presence of nitrogen atmosphere. 5.3mmol N,N-methylene-bisacrylamide (cross linker) and 0.7mmol ammonium persulfate (initiator) were added to the mixture and stirred until dissolved in the solution in a flask installed with a reflux condenser and a magnetic stirrer as shown in Figure 6.3. The cold water circulation in the reflux condenser was used to avoid any evaporation from the polymerization flask. The solution was kept at 50°C for 8 hours in order to complete the polymerization reaction.

MIP was filtered, washed with deionized water and dried under nitrogen flow (Figure 6.4). MIP was ground and sieved to obtain 90µm particle size. DEHP (template) was extracted out of the MIP powder encapsulated in 0.22µm filter caplet by Soxhlet extraction in 12 hours with methanol as shown in Figure 6.5. Extraction of DEHP in 0.22µm filter is shown in Figure 6.6.

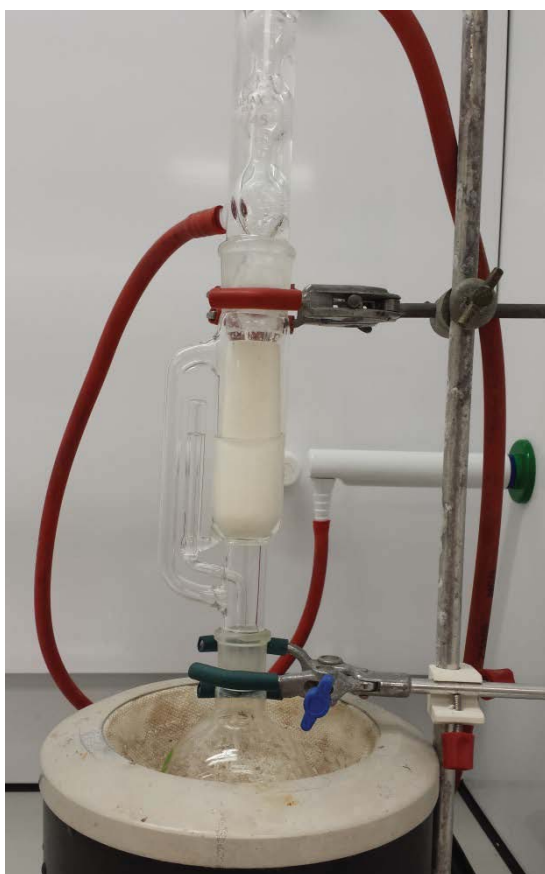


Figure 6.5 Soxhlet Extraction



Figure 6.6 Filter caplet 0.22µm

MIP powder was dried under nitrogen at room temperature. Self-assembled monolayer of 3-aminopropyltriethoxysilane (APTES) was used to immobilize MIP functional

coating on the sensing surface of the sensor by dip coating method. 2g MIP powder was mixed with 2.5ml APTES and 1.5ml of DI water to prepare a coating suspension. The sensor was dipped in the suspension and was withdrawn at a slow rate of 2.5mm per minute to achieve a uniform coating on the sensing surface. The dip coated sensor was dried for 18 hours in nitrogen at room temperature prior to testing. Figure 6.7 shows the MIP in 90 μ m sieved powdered form after extraction of template (DEHP).

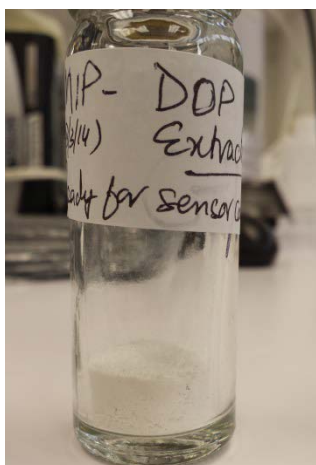


Figure 6.7 DEHP extracted MIP

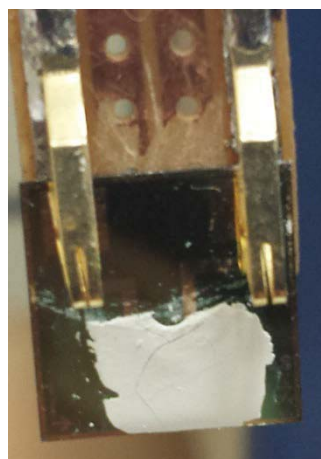


Figure 6.8 MIP coated sensor using SAM of APTES

The coating was observed under optical microscope for surface morphology and porosity. Figure 6.9 shows confocal micrograph image of MIP coated sensor depicting that the MIP embedded SAM coating on the sensing surface is uniform and porous.

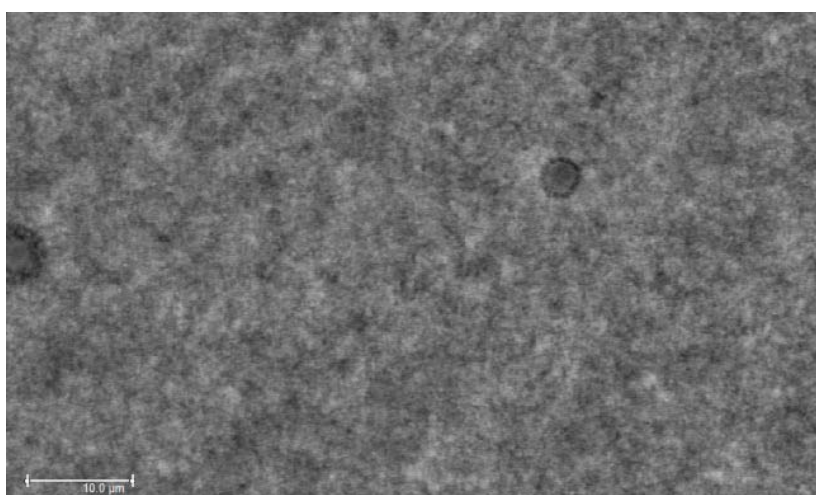


Figure 6.9 Confocal micrograph image of MIP coated sensor

Two identical sensors 1-11-50A and 1-11-50B were coated and profiled in inert atmosphere at 24% humidity and 23.3°C temperature. Figure 6.10 shows the dip coating process of the sensors and Figure 6.11 shows drying under inert atmosphere for 18 hours in a desiccator.



Figure 6.10 Dip Coating process



Figure 6.11 Drying in nitrogen flow

6.1.3 EIS for detection of DEHP in MilliQ

Electrochemical Impedance Spectroscopy technique owns high sensitivity with limitation of stable and reversible system in equilibrium. Therefore for non-stationary systems instantaneous impedance measurements are mandatory. In case of non-compliance, system linearity, stability and repeatability could not be ensured. In order to overcome these challenges all experiments were conducted under identical temperature, humidity, and pH boundary condition in controlled laboratory environment. The sensor was connected to Hioki 3522-50 LCR Hi precision tester (Japan) by gold contact clamp pin connector. The device was run with built in open and short calibration tests to nullify any stray capacitance due to connecting leads. LCR tester was set to slow mode of testing to achieve error rate of $<0.05\%$ as recommended by the manufacturer. The sensor setup was formed in a desiccator to achieve the required controls of 24% humidity and inert atmosphere. To obtain a reference, the sensor was profiled in air for a frequency sweep of 2MHz to 42Hz with ten measurements per decade change in frequency at the log scale. Three different concentrations of DEHP - 1, 10, and 50mgL⁻¹ (ppm) in deionized water were tested at

initial temperature (23.3°C) and humidity (24%) conditions. Control solution was 18MΩ cm deionized MilliQ water with pH 6.71. It was observed that addition of DEHP in the working solutions did not alter pH level and average pH value measured was 6.52 at 23.3°C. The sensor was profiled in air before its exposure to the different DEHP concentrations to create an experimental reference curve for sensor performance. The immobilized MIP sensor was pipetted with 10μl of MilliQ water and the test was run to generate control reference curve, later the MIP functionalized sensor was pipetted with 10μl 1ppm solution. A seven minutes time period was allowed for polymer to entrap DEHP molecules from the test sample. Figure 6.12 shows the lab test bench set up for MIP coated sensor testing.

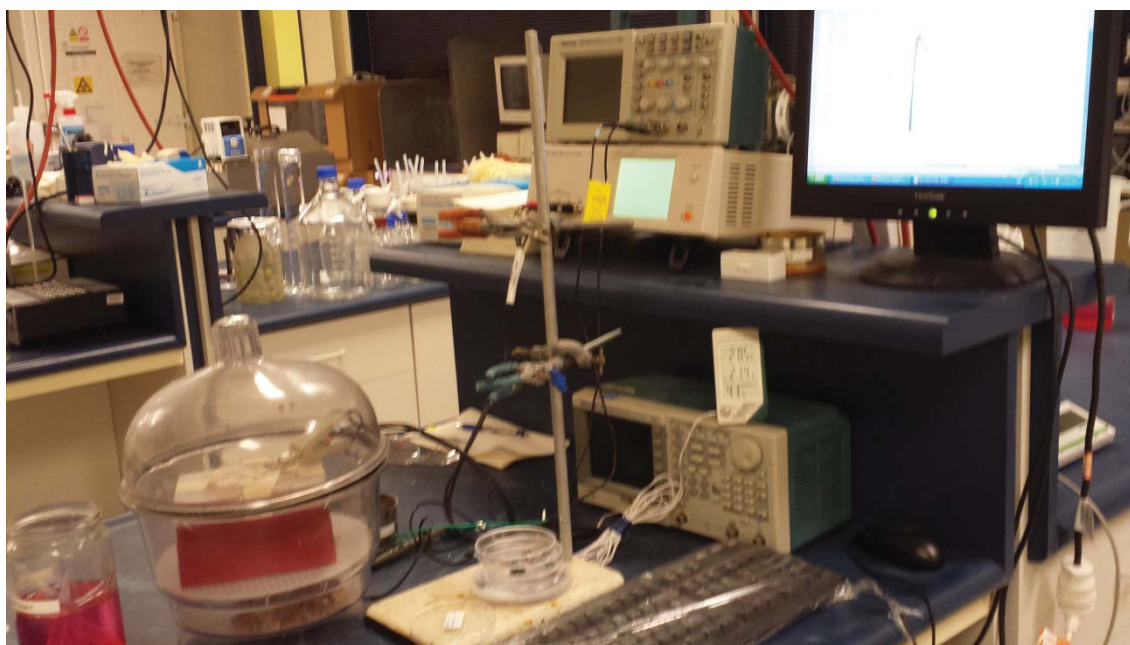


Figure 6.12 Laboratory test bench setup for MIP coated sensor

The MIP was washed with acetone and rinsed with distilled water in order to remove excess/un-bound DEHP molecules and the EIS testing was executed thrice under same initial temperature and humidity conditions. The MIP coated sensor was sonicated in dichloromethane for half an hour to remove the entrapped DEHP molecules and regenerate the functionalized MIP coating. The eluent was preserved and later tested with HPLC for validation of DEHP entrapment. The sensor surface was dried with nitrogen and profiled in air in order to evaluate and ensure achievement of initial conditions of the EIS testing system before each run. Each concentration was tested with the proposed system following the described procedural steps. The control

reference was plotted by executing experiment after pipetting 10 μ l control solution on the MIP functionalized sensing area of the sensor.

6.1.4 Results and Discussions

Molecular imprinted polymers (MIP) are specially designed polymer materials owing valuable target molecules recognition sites, privileged by unique advantages like high selectivity, physiochemical stability, robustness, longer shelf life, reusability and specific recognition of analyte and structurally related compounds. This molecular recognition selectivity has proved to be an attractive predominant advantage over biological receptors and antibodies for more number of target molecule capturing sites [151]. MIPs have been applied in solid phase extraction (SPE), chromatography, electro-chromatography, membrane filtration and sensing [155, 156]. Lately molecular imprinting technique has rigorously been applied to extract phthalate analytes as a sample clean up prior to quantification of DEHP by gas chromatography[149]. The analyte could be entrapped by MIP either by covalent or non-covalent bonding, which is accepted as a well-established technique for analyte capture for sample clean-up [152]. Non covalent bonding makes use of relatively weak forces like hydrogen bonding, ion pair, dipole-dipole interactions or van der Waal forces to entrap target molecules. This approach is more appreciated because it requires minimal efforts to remove the target molecules from the recognition sites, whereas, covalent entrapment requires energy transfers to break the bond in order to remove the analyte [149, 157, 158].

6.1.5 Adsorption studies of DEHP to MIP

The extraction of adsorbed DEHP from the sensor's functionalized coating was carried out in an equal volume (2ml) of dichloromethane by sonication process of 15 minutes at all instances. The solvent was evaporated and 50 μ l dichloromethane was used for HPLC testing of the eluent. Luna C18 column was used in DIONEX HPLC system to test the samples at a wavelength of 224nm for diode array detector (DAD) with a mobile phase of methanol/acetonitrile (1:9 v/v). The binding isotherms of DEHP to MIP were determined in the concentration range of 1-100 μ gml⁻¹. Adsorption studies helped us to determine two important parameters about the functionalized coating on the sensing surface. Firstly, we can determine the highest concentration that could be adsorbed by the immobilized MIP and secondly, time of adsorption could be determined for the amount of MIP immobilized on the sensing surface. Highest adsorption concentration

can be studied by static adsorption investigation (section 6.1.6) whereas, uptake kinetic studies (section 6.1.7) can provide the information about the time of adsorption which is an important parameter to know for quasi-static electrochemical cell in order to keep the system in steady-state for EIS measurements.

6.1.6 Static Adsorption of DEHP to MIP

The static adsorption of MIP was calculated using Equation 6.1.

$$Q = \frac{(C_i - C_f)V}{m} \quad (6.1)$$

Where Q (mg g^{-1}) is the mass of DEHP adsorbed per gram of MIP, C_i (mg l^{-1}) is the initial concentration of DEHP; C_f (mg l^{-1}) is final concentration of DEHP after adsorption. $V(\text{l})$ is the total volume of the adsorption mixture and $m(\text{g})$ is the mass of the polymer used. The isotherm for the static adsorption studies of DEHP to MIP is shown in Figure 6.13.

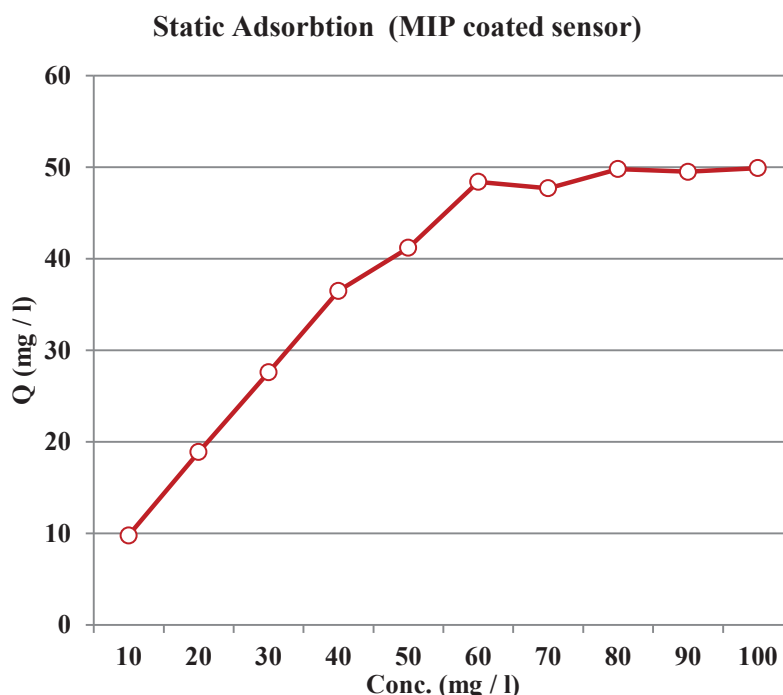


Figure 6.13 Isotherm for the static adsorption studies of DEHP to MIP

The plot depicts that the amount of DEHP bound to the polymer increases with the increase in concentration of the DEHP in the test samples below a concentration level of 50 mg l^{-1} (ppm). The polymer saturates as the concentration level increases above the said limit and the curve becomes parallel to concentration axis. This is due to the fact that

the miniature size of sensor allows very less MIP immobilized on the sensing surface. Since the targeted range of detection is lower to the saturation limit therefore, it is deemed acceptable [159].

6.1.7 Uptake Kinetics of MIP Coated Sensor to DEHP

Figure 6.14 presents the plot for adsorption uptake kinetics of DEHP to MIP. This study was helpful to determine the adsorption time required by DEHP present in the sample to get trapped at the molecular recognition sites in the MIP. The coated sensor was dipped in 5ml test solution with a concentration of $50\mu\text{gml}^{-1}$.

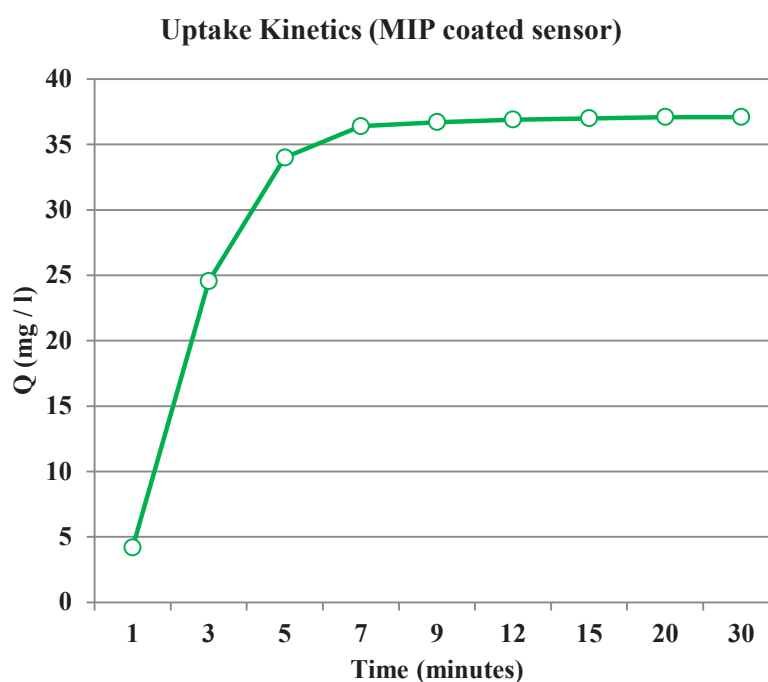


Figure 6.14 Isotherm for adsorption uptake kinetics of DEHP to MIP

The concentration level was chosen in the light of static adsorption studies undertaken in section 6.1.6. The results showed that the molecular imprinted polymer owns fast entrapment kinetics, and the binding equilibrium was reached in almost 7 minutes. The rapid adsorption capability of the MIP is an advantage for using the polymer with electrochemical impedance spectroscopy where rapid impedance measurements are mandatory for non-stationary systems.

6.1.8 Data Analyses Using Non-linear Least Square Curve fitting

Figure 6.15 shows the Nyquist plot for the experimentally obtained real and complex impedance. The decreasing diameter of the Nyquist plot indicates the increasing concentration of the phthalate in the sample. It is observed that the sensor is sensitive to the adsorbed phthalate molecules at low frequencies. The mass transfer of ions in the electrode surface is a fast kinetic process which is taking place at low frequency range, on the other hand the capacitive behaviour of the sensor is observed at relatively high frequency range. The semi-circular portion describes a relatively slower charge transfer limited process at higher frequencies. C_{dl} can be calculated from the frequency at the maximum of semi-circular region in the Nyquist plot using $\omega = 2\pi f = 1/R_{ct}C_{dl}$ whereas, R_{ct} is calculated by extrapolating the semicircle to Z_{real} axis.

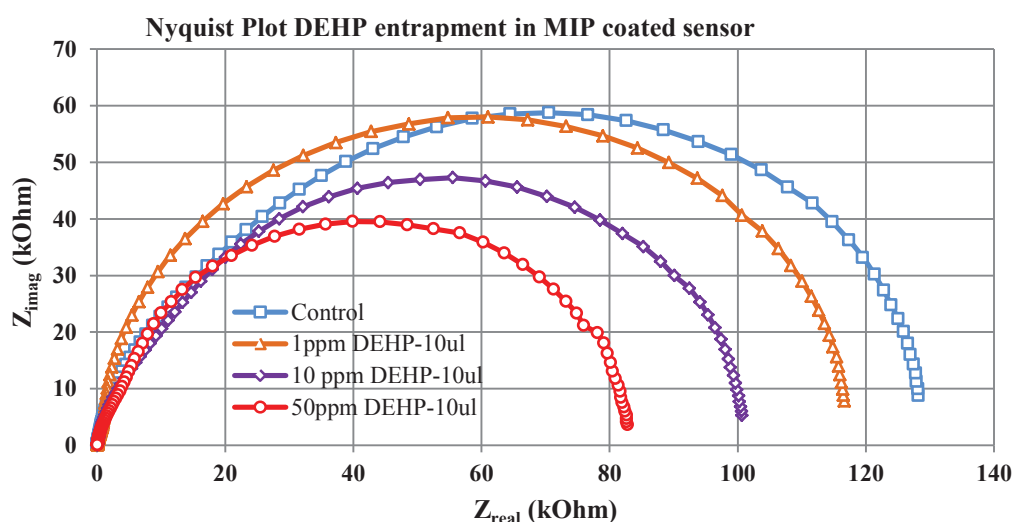


Figure 6.15 Nyquist plot for EIS testing of MIP coated Sensor

The double layer capacitance C_{dl} and charge transfer resistance R_{ct} are the key electrical parameters in determination of impedance change for analytical studies of the system kinetics in detection of the phthalates. The values of R_{ct} decreases from 130k Ω to 80k Ω as the concentration of DEHP increases from 0ppm to 50ppm as shown in Figure 6.15. The equivalent circuit was estimated using theoretical calculations by electrochemical spectrum analyser algorithm shown in Figure 6.16.

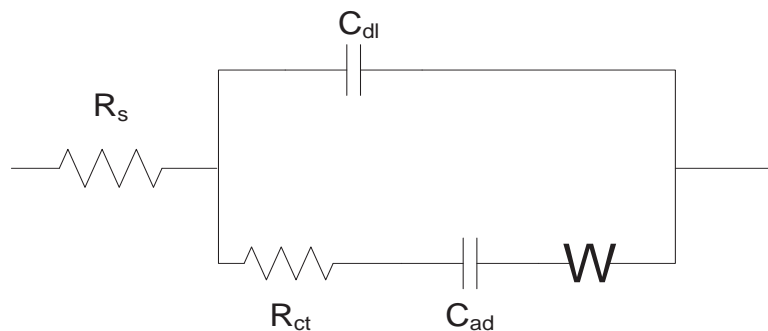


Figure 6.16 Equivalent circuit estimated by CNLS analysis

The circuit parameters were estimated by complex non-linear least square fitting technique which fits the measured impedance data on theoretically estimated values. The algorithm performs statistical analysis to calculate the residual mean square $r_{amplitude}^2$ for experimentally observed values in measured spectra against the calculated values based on the theoretical response of suggested equivalent circuit.

Table 6.1 CNLS curve fitted equivalent circuit parameters

Parameter (unit)	DEHP Test samples in DI water					
	1 ppm		10 ppm		50 ppm	
	Value	Error	Value	Error	Value	Error
		(%)		(%)		(%)
C_{ad} (F)	3.37E-08	2.4318	3.77E-08	2.7215	5.50E-08	1.9596
R_s (Ω)	7.2	3.4286	6.00	2.6131	1.32	2.441
R_{ct} (Ω)	1.29E+05	3.9552	9.97E+04	4.0774	8.42E+04	4.422
Z_w (Ω)	1.78E-06	13.9593	1.57E-06	14.6884	9.52E-05	15.4408
C_{dl} (F)	1.01E-09	3.6404	9.03E-10	3.7977	7.07E-10	18.971
r^2	5.859E-04		4.395E-04		6.782E-04	

The results of curve fitting show that the adsorption capacitance increases with the increase in concentration of the analyte in the test samples whereas; the charge transfer resistance is decreasing with the increasing concentration. The new results with selective coating are in compliance to the earlier experiments with DEHP in aqueous medium. The Warburg resistance has reduced to zero due to the self-assembled monolayer of APTES embedded with MIP particles. APTES provides good adhesion with the silicon dioxide layer present at the sensing surface. Since ionic concentration in the test sample is not present and the SAM of APTES provides good insulation between the

sensing surface and the electrolyte, therefore the existence of Warburg resistance is nominal which proves that the capacitive characteristics of the sensor have enhanced due to the coating of MIP.

6.1.9 Results validation by HPLC

The eluent collected after the extraction of adsorbed DEHP from sensing surface was filtered with 0.22 μ m filter, solvent was evaporated and 50 μ l methanol was used for HPLC testing of the eluent. Luna C18 column was used in DIONEX HPLC system to test the samples at a wavelength of 224nm for diode array detector (DAD) with a mobile phase of methanol/acetonitrile (1:9 v/v) in order to validate the EIS results. Figure 6.17 shows the DIONEX HPLC apparatus in the Micro-suite laboratory which is a programmable self-injecting semi-automatic piece of equipment.

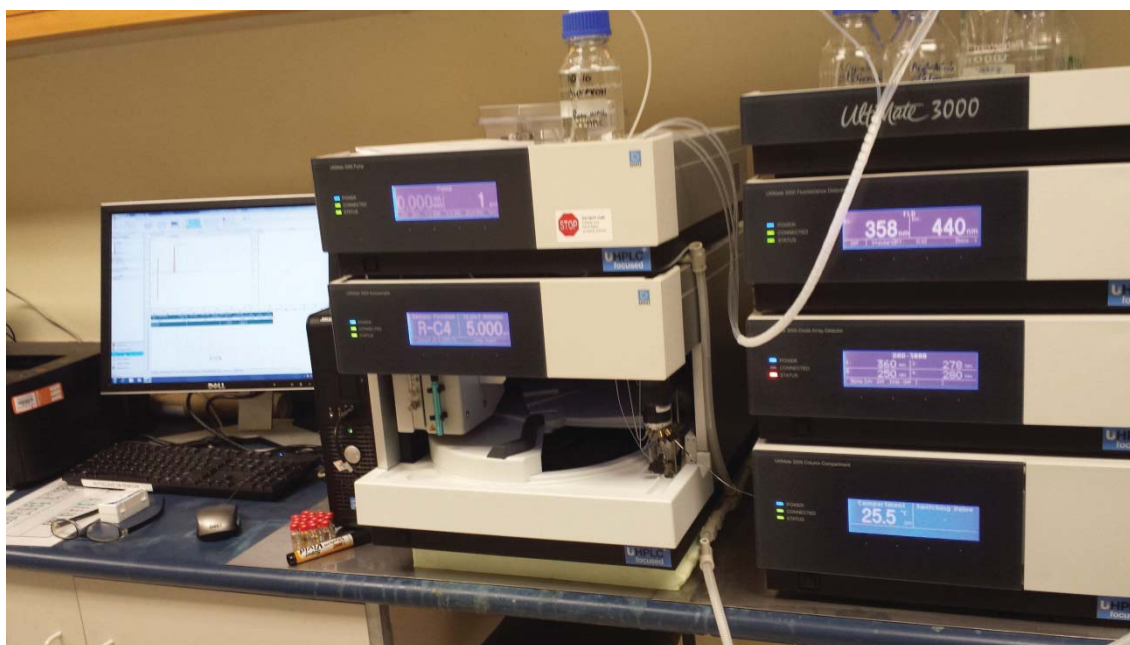


Figure 6.17 DIONEX-Ultimate 3000 HPLC apparatus

Figure 6.18 shows the peak absorption wavelength in absorption spectrum of DEHP.

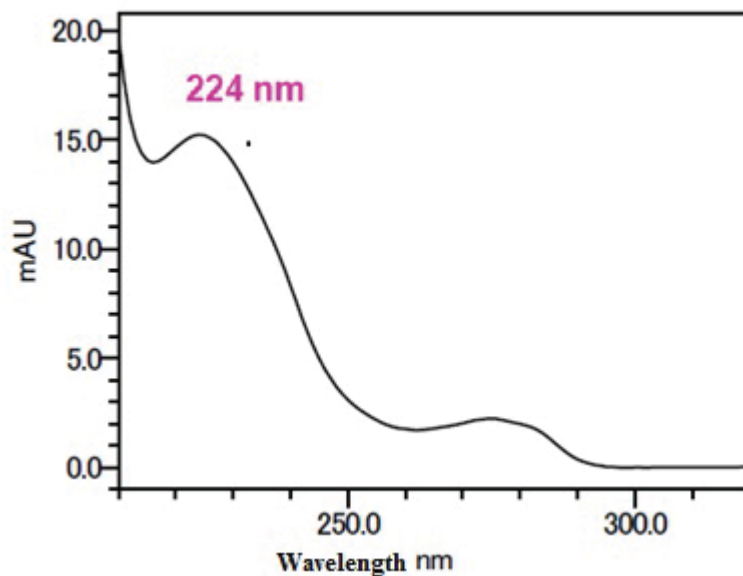


Figure 6.18 Absorption spectrum of DEHP

The HPLC peak was observed at 6.19 minutes with C18 (150X4.6mm) column at a flow rate of 1mL/min of the mobile phase. Un-spiked methanol was used as a control reference for detecting concentrations of 1mg/L to 100mg/L in methanol. The plots for the observed DEHP peaks are shown in Figure 6.19. The area under the peaks determined the concentration of DEHP in the sample.

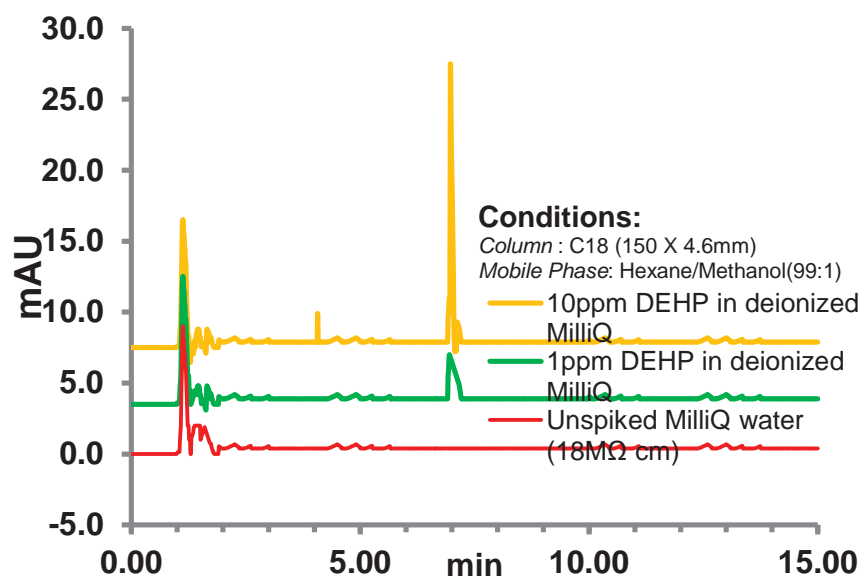


Figure 6.19 MIP eluent tested with HPLC for EIS results validation

The chromatograph shows a few peaks at 1.2 minutes which correspond to the solvent. The DEHP concentrations read by HPLC in the eluent are marked in Figure 6.20

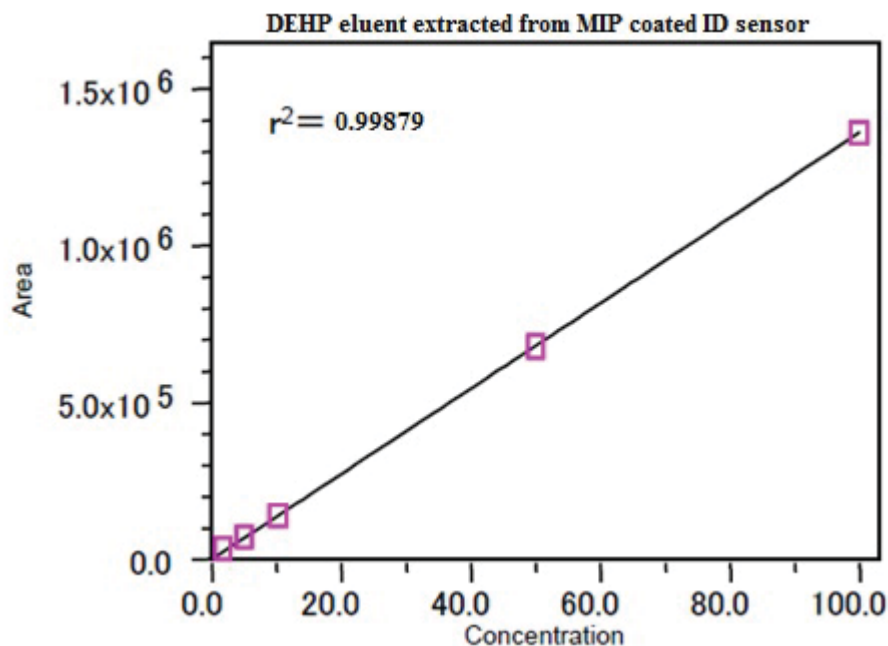


Figure 6.20 DEHP eluent extracted from MIP immobilized on ID sensor

The calibration curve shown in Figure 6.20 was plotted using samples of known concentration in MeOH. The square marks shown on the plot represent the concentration read by the HPLC.

6.1.10 DEHP in Energy Drink – MIP Coated Sensor

Commercially available energy drink (Lift Plus) was spiked with DEHP at a concentration of 1, 5, and 10ppm. The drink is sold in New Zealand markets in glass bottle packaging therefore, possibility of addition of leached DEHP from the packaging was ruled out. The spiked drink samples were tested with MIP functionalized interdigital sensor by electrochemical impedance spectroscopy and the eluent after extraction of DEHP from the sensor's coating was injected to HPLC for validation.

Figure 6.21 shows the Nyquist plot for the impedance data measured by the MIP functionalized sensor. It should be noted that all the steps in the test procedure were identical to the test with spiked deionized water as explained in section 6.1.3.

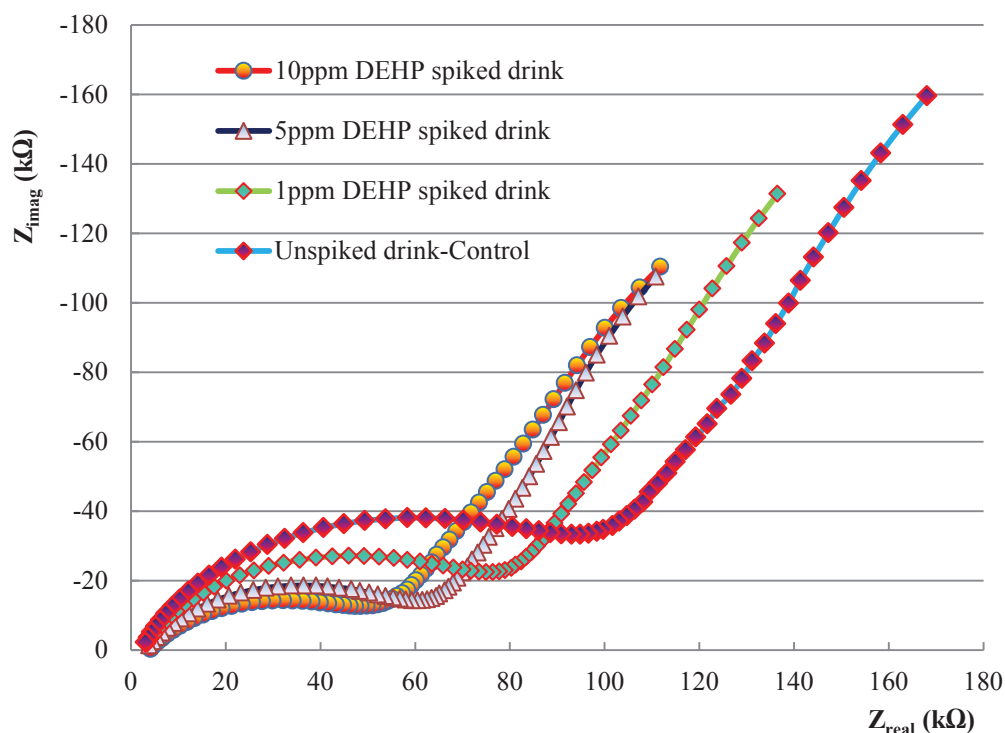


Figure 6.21 Nyquist plot for DEHP spiked drink by MIP coated sensor

The change in the impedance read by the developed EIS system showed that the concentration of the analyte is changing in the spiked drink. The 45° tail line with the semi-circular curve in the plot showed the presence of Warburg resistance in the equivalent circuit. The appearance of Warburg resistance strictly dictated the presence of ions in the spike samples that is attributed to the electrolytes present in the energy drink. The current flowing through the circuit due to conductive medium dictated the value of the resistance. The equivalent circuit parameters are shown Table 6.2.

Table 6.2 Equivalent circuit parameters evaluated by CNLS fitting for DEHP detection in ‘Lift Plus’ drink by MIP functionalized sensor

Eq. Circuit Parameters (unit)	DEHP spiked energy drink- MIP functionalized sensor		
	1ppm	5ppm	10ppm
C_{ad} (F)	1.813E-07	1.359E-07	1.466E-07
R_s (Ω)	1.145E+02	1.33E+02	1.58E+02
R_{ct} (Ω)	8.2304E04	6.21E+04	5.57E+04
Z_w (Ω)	2.431E06	1.92E+06	1.64E+06
C_{dl} (F)	7.95E-09	8.79E-09	9.25E-09

The smart system results were validated by HPLC analysis. The chromatogram in Figure 6.22 shows DEHP peaks at 6.91 minutes. The peaks that appeared before DEHP peak are due to the presence of other chemicals in the eluent. These might get attached to the MIP due to its porous nature. This problem could be rectified by increasing the density of the DEHP recognition sites in the MIP matrix by adding more template molecules. The quantity of the template compound added in the pre-polymerization complex determines the density of the recognition sites formed in resulting MIP.

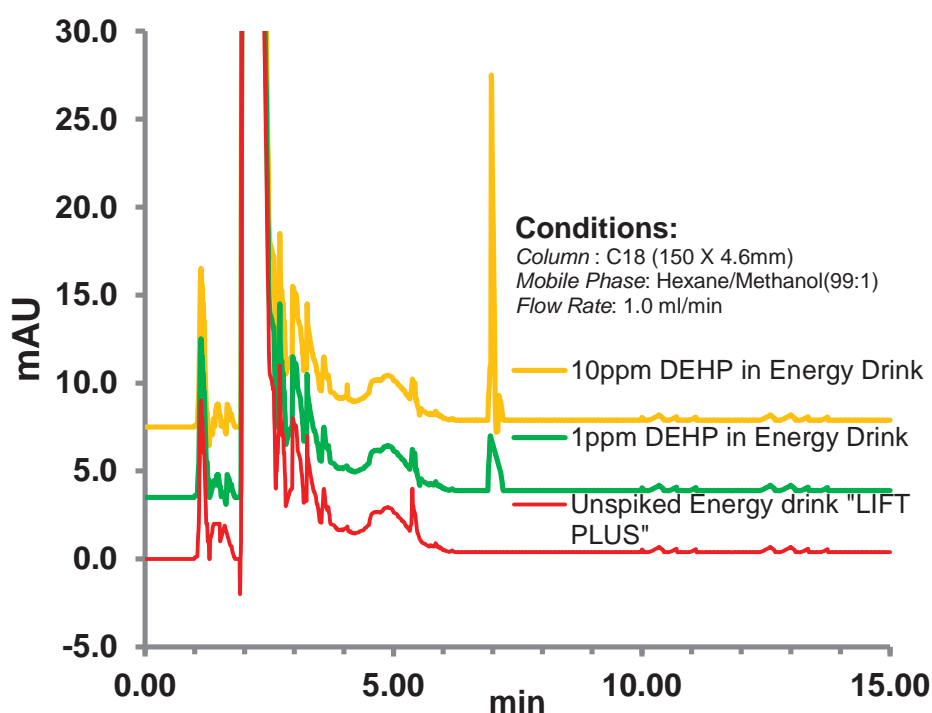


Figure 6.22 HPLC chromatogram showing the DEHP peaks in the eluent extracted out of the functionalized MIP

6.1.11 Conclusions

Non-invasive, real time detection technique for ubiquitous environmental endocrine-disrupting compounds in water has been discussed. Optimization of design for MEMS based interdigital sensors has been achieved on basis of mathematical modelling using finite element modelling software COMSOL Multiphysics®. Optimized designs of sensors have been fabricated using thin film semiconductor device fabrication techniques. The sensing surface was functionalized by a self-assembled monolayer of 3-aminopropyltriethoxysilane (APTES) with embedded molecular imprinted polymer

(MIP) to introduce selectivity for the di (2-ethylhexyl) phthalate (DEHP) molecule. Various concentrations (1, 10 and 50 ppm) of DEHP in deionized MilliQ water were tested using the functionalized sensing surface to capture the analyte. Frequency response analyzer (FRA) algorithm was used to obtain impedance spectra so as to determine sample conductance and capacitance for evaluation of phthalate concentration in the sample solution. Spectrum analysis algorithm interpreted the experimentally obtained impedance spectra by applying complex nonlinear least square (CNLS) curve fitting in order to obtain electrochemical equivalent circuit and corresponding circuit parameters describing the kinetics of the electrochemical cell. The results obtained by the testing system were validated using commercially used HPLC-DAD.

Chapter 7 Conclusions and Future Research

7.1 Conclusions

This thesis contributed in the impedance spectroscopy research for the development of novel interdigital sensors by applying this technique to hormone and chemical detection. The research work required to do a substantial addition to the existing knowledge includes, but not limited to the literature surveys in this and allied fields, design and design developments, simulations and fabrications, experimentation and analyses, measurements and hypothesis, functionalization and immobilization, selectivity and sensitivity, detailed mathematical and statistical analyses and result validations. The presented research work has successfully been applied to develop an exciting transducer that could not only selectively detect its target but is capable enough to quantify harmful synthesized organic impurities in our food stuffs. This research work has not only provided a real-time tool to perform week-long chemical and biochemical assays in minutes yet, it had been operating as a source of community awareness about the said chemicals that we keep ingesting knowing or unknowingly. Consequently, these teratogenic, endogenic and carcinogenic chemicals become our body burden and we fall prey to some incurable diseases that cause to shorten our life span.

The research work executed in this capacity, is a set of sequential moves to this accomplishment, described as follows.

The first chapter defines and highlights the problem and its gravity. In the introduction part it briefly describes the good and the bad; hormones, that are the good chemicals generated by a living body naturally, to help it grow, nurture and nourish and endocrine disrupting compounds, the bad chemicals that when enter the living body, mimic hormones, damage and destroy the natural balances and cause devastating malfunctions in body metabolisms. The author then tried to find some way to detect these silent killers in the existing human knowledge-base by reviewing the up-to-date research published in this context. The basic objective of the author in this search was to find out some method that may be smart enough to identify these chemicals to a trace level of parts per million to parts per billion, in addition to a rapid and real-time execution of the investigation. During this endeavour the author came across a few excellent approaches to the solution of the problem but unfortunately none of those could qualify the

condition of rapid detection. Over and above, all these technologies required stringent test conditions and bulky machines worth millions of dollars. These methodologies may be affordable to the elite class of the community but an average member may afford it once in a blue moon only. At the end of the chapter a comprehensive comparison of all the applied technologies have been discussed in order to emphasize the scarcity of a sensitive and rapid technique for chemical and biochemical assay

The next milestone to this journey was to search out some technique that may have the throbbing potential to fulfil the targeted conditions but has not yet been so developed to cater for it. Chapter 2 described the methods and methodologies, merits and demerits, dos and don'ts, pros and cons of the electrochemical impedance spectroscopy (EIS) technique. The author selected it to proceed further on researching it because it had enough potential for sensitivity, rapidness and did not require any bulky test equipment due to which it was one of the lowest cost technologies ever known. The author tried to make the reader of this thesis well-versed with the equipment used, methodologies, conditions and analytical methods applied in this technique to deduce the results in chapter 2.

After explanation to build a standalone EIS data acquisition system that may work semi-automatically using a computer, the author started working on the development of a transducer that could interpret the material information extracted by EIS in to readable electrical signals. This transducer was supposed to be the heart and soul of the detection system. Therefore, it had to be highly sensitive, precisely selective, carefully designed and thoroughly tested and tried.

Planar interdigital capacitive sensors have been under extensive research and development for last two decades. They have shown high level of accuracy and excellent sensitivity of measurements in the evaluation of near-surface properties like permeability, conductivity, dielectric properties of materials, non-invasive testing, label-free detection of biological species and analysis of chemical compounds. The coplanar structure provides freedom of in-situ and single side access feature for the sensor along with acceptable signal-to-noise ratio in measurements. The capacitance and conductance between the sensors' electrodes is dependent on the material, geometry and dielectric properties of the analyte. When these sensors operate in conjunction with the Electrochemical Impedance Spectroscopy (EIS) technique, applied alternating electromagnetic perturbations fringe through the material sample producing capacitive

effects as a result of the presence of analyte molecule in the sample under test. The impedance Z of a system is determined as a function of frequency and by analysing the resultant current through the system in terms of amplitude and phase shift compared to voltage-time function.

Chapter 3 detailed the steps involved in design and simulation of the interdigital capacitive transducer. It explained the worked out improvements in the design of the sensor that was simulated to virtually assure the sensitivity and operation. Smart fruitful collaborative partnerships were established to fabricate these sensors at King Abdullah University of Science and Technology, Saudi Arabia. These sensors were fabricated on single crystal silicon wafer widely used in the ICs fabrication in semiconductor fabrication industry. The sensors were designed simulated in miniature size with multiple configurations of sensing electrode structures. Silicon based sensors provided low cost fabrication opportunity where 36 sensors could be fabricated on a single 4 inch silicon wafer. High sensitivity, low impedance and better sensing signal to low noise ratio were the most important characteristics requirements for these sensors.

The details of fabrication and initial testing with known materials are discussed. A remedial post-fabrication heat treatment was applied to the sensor to achieve improvement in its performance, but keeping the fabrication cost to the bare minimum level. A combination of sputtered gold electrodes deposition and post annealing procedure served dual purpose of low cost and better performance of the sensor. The shortcomings marked out in testing and the remedial actions taken to overcome those shortcomings have been discussed in chapter 3.

The objective of Chapter 4 was to investigate the capability of the designed sensors, and to explore the analytical powers of electrochemical impedance spectroscopy, in detection of different hormones. The target hormones are related to the reproductive cycle of mammals. 'Non-invasiveness of methodology' and 'real-time measurements of samples' were the prime objectives of this research project. These characteristics of the presented research make this work unique in comparison to all available contemporary methodologies. Apart from that, it was envisaged that execution of the hormone quantification assay should be simple enough to be adapted by a common user without requiring a necessary scientific background.

The first part of this chapter discussed the application of the proposed system to detect estrone glucuronide, an excretory metabolite of estradiol, commonly known as E1G.

This hormone plays a major role in the reproductive fertility of human female. The information on the quantity of excretion of this hormone metabolite is useful in determining the window of fertility for human female. The handy availability of this information is extremely important to achieve conception or contraception in human reproductive cycle.

The second part of the chapter dealt with the sensor's response in detection of progesterone hormone excreted in the milk of dairy cows. Obtaining urine samples, to gather the fertility information, is not feasible in the case of dairy animals. Though, milk owns a complex chemical matrix, yet it is the easiest and most non-invasive method to achieve the information on 'window of fertility' for the animal.

Electrochemical impedance analyses making use of bode plots, Nyquist plots, CNLS curve fitting, electrochemical equivalent circuit parameters and sensitivity of the sensor toward the analytes were discussed in chapter 4.

Endocrine disrupting compounds are exogenous chemicals or mixture of chemicals that interfere the normal functioning of the endocrine system and cause hormonal imbalances in living organisms. These hormonal imbalances can cause cancers, birth defects, developmental disorders, nutritional malfunctions and impotency especially in males. EDC can block the receptor cells by stopping them to respond or can cause an adverse response by getting attached to the receptor in place of a hormone cell.

In chapter 5 the developed sensor and sensing system was employed to detect two types of phthalates spiked in different types of mediums. The tests were performed in real-time and the sensor performed successfully in the detection of phthalates in pure polar medium. The system was able to detect the presence of DEHP and DINP even to a trace level in the polar medium but the outcomes of the investigation made for electrolytic and acidic media were not up to the mark. Although, the sensitivity analysis of the system displayed high level of sensitivity in pure aqueous and organic solvent media yet, the system sensitivity deteriorated drastically in complex solutions. This led the sensing system research to the next stage of development. In order to adapt the sensor and sensing system for complex chemical matrices like beverages, milk and urine, selectivity for analyte molecules was an utmost requirement. Different options to pave the way to selective adsorption of phthalates on the sensing surface have been explored. Published research provides a number of methods to selectively detect analyte from a complex matrix by extraction, absorption, adsorption, biological separation and

filtration. Unfortunately, all these techniques are laboratory based and require certain skills and expertise to perform. On the other hand these techniques are extremely delicate and require certain environmental conditions to execute.

One of the main objectives of this research was to develop an assay system that is robust enough to have an in-field application without any technical expertise requirement for the user. To achieve this objective a robust assay technique was tailored and applied to induce selectivity in the designed sensing system. The discussion on inducing selectivity for specific molecules was carried out in the next chapter of this thesis.

Non-invasive, real time analyte-selective detection technique for ubiquitous environmental endocrine-disrupting compounds in water has been discussed in chapter 6. The sensing surface was functionalized by a self-assembled monolayer of 3-aminopropyltriethoxysilane (APTES) with embedded molecular imprinted polymer (MIP) to introduce selectivity for the di (2-ethylhexyl) phthalate (DEHP) molecule. Various concentrations (1, 10 and 50 ppm) of DEHP in deionized MilliQ water were tested using the functionalized sensing surface to capture the analyte. Frequency response analyser (FRA) algorithm was used to obtain impedance spectra so as to determine sample conductance and capacitance for evaluation of phthalate concentration in the sample solution. Spectrum analysis algorithm interpreted the experimentally obtained impedance spectra by applying complex nonlinear least square (CNLS) curve fitting in order to obtain electrochemical equivalent circuit and corresponding circuit parameters describing the kinetics of the electrochemical cell. The results obtained by the testing system were validated using commercially available high performance liquid chromatography diode array detection at an incident wavelength at 224nm. DEHP spiked energy drink was also investigated by the developed technology in order to confirm its operation in the real world scenario.

7.2 Future Work

7.2.1 Sensitivity and selectivity Improvement

A satisfactory performance of the sensing system has been achieved though, still a few of following improvements in the sensor and sensing system can make it even better.

- 1 The sensitivity may be improved by trying different polymerising materials with higher densities of recognition sites.
- 2 By improving the coating method with spin coating or electro-spin coating methods.
- 3 Specific coating thickness and uniform layers of cross-linker may be explored.
- 4 Uniform/patterned distributions of molecular recognition sites to achieve known density of molecular trapping site.
- 5 Better analyses of results by CNLS can provide more insight in the electrochemical cell.
- 6 Conducting EIS experiments at a wider range of frequencies starting from mHz range can provide better sensitivity.
- 7 Change in sensor design is suggested as in Figure 7.1. This design change will reduce the capacitive effect caused between the connecting lines that will help improve sensitivity.
- 8 Increasing the length of the sensor will allow soldering flexible wires to the connection pads as shown in Figure 7.1. That will help keep the sensing part away from the solder heat.
- 9 Annealing the substrate at 210°C for two hours should be added as a post-fabrication step in the fabrication process so that all the defects caused in the electrodes' surface due to gold sputtering get removed.

7.2.2 Thick Film Electrodes

The sensors may be fabricated using thick film electrodes. The available sensors' electrodes are formed by sputter coating 500nm gold over a chromium seed layer of 20nm thickness. New sensors with electrode thickness as much as 5µm should be fabricated and tested. Thick electrode will be able to provide a uniform electric field as high as 5µm between the electrodes. The availability of a uniform electric field along with fringing field will increase the sensitivity many folds. The analyte molecules

adsorbed to the silicon surface between the electrodes will contribute more to the C_{ad} and C_{dl} .

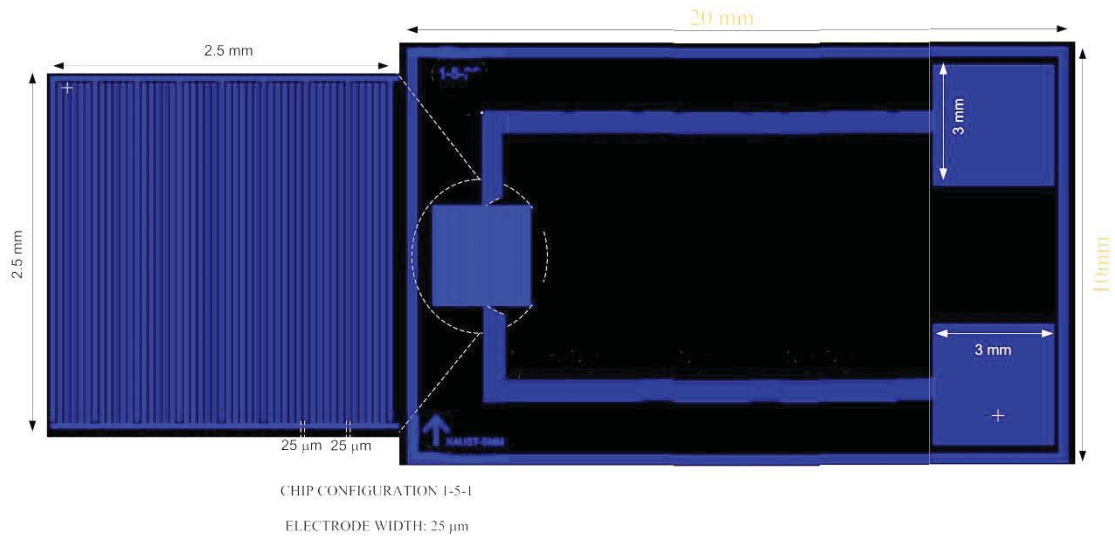


Figure 7.1 New sensor design to overcome heat and stray capacitance problems

7.2.3 Substrate Type

The Si substrate used for the fabrication, presently, is single crystal Si wafer without any doping concentration. It is suggested that p-type and n-type doped Si wafers may also be used for sensor fabrication. The interdigital electrodes should be deposited on silicon dioxide insulation layer. The partially conductive substrate will provide a conductive path to the electric field through the substrate material on the rear side of the sensor. This will help reduce noise in the EIS measurements. Presently a back Au plane at ground potential serves the purpose.

Bibliography

- [1] T. Schettler, "Human exposure to phthalates via consumer products," *International journal of andrology*, vol. 29, pp. 134-139, 2005.
- [2] P. Montuori, E. Jover, M. Morgantini, J. M. Bayona, and M. Triassi, "Assessing human exposure to phthalic acid and phthalate esters from mineral water stored in polyethylene terephthalate and glass bottles," *Food Additives and Contaminants*, vol. 25, pp. 511-518, 2008.
- [3] R. Green, R. Hauser, A. M. Calafat, J. Weuve, T. Schettler, S. Ringer, K. Huttner, and H. Hu, "Use of di (2-ethylhexyl) phthalate-containing medical products and urinary levels of mono (2-ethylhexyl) phthalate in neonatal intensive care unit infants," *Environmental health perspectives*, vol. 113, p. 1222, 2005.
- [4] P. Foster, "Disruption of reproductive development in male rat offspring following in utero exposure to phthalate esters," *International journal of andrology*, vol. 29, pp. 140-147, 2006.
- [5] J. D. Meeker, A. M. Calafat, and R. Hauser, "Urinary metabolites of di (2-ethylhexyl) phthalate are associated with decreased steroid hormone levels in adult men," *Journal of andrology*, vol. 30, p. 287, 2009.
- [6] J. A. Colacino, T. R. Harris, and A. Schecter, "Dietary intake is associated with phthalate body burden in a nationally representative sample," *Environmental health perspectives*, vol. 118, p. 998, 2010.
- [7] L. Lopez-Carrillo, R. U. Hernandez-Ramirez, A. M. Calafat, L. Torres-Sanchez, M. Galvan-Portillo, L. L. Needham, R. Ruiz-Ramos, and M. E. Cebrian, "Exposure to Phthalates and Breast Cancer Risk in Northern Mexico," *Environmental health perspectives*, vol. 118, pp. 539-544, Apr 2010.
- [8] J. A. Colacino, A. S. Soliman, A. M. Calafat, M. S. Nahar, A. Van Zomeren-Dohm, A. Hablas, I. A. Seifeldin, L. S. Rozek, and D. C. Dolinoy, "Exposure to phthalates among premenstrual girls from rural and urban Gharbiah, Egypt: A pilot exposure assessment study," *Environmental Health*, vol. 10, p. 40, 2011.
- [9] M. R. Lee, F. Y. Lai, J. Dou, K. L. Lin, and L. W. Chung, "Determination of Trace Leaching Phthalate Esters in Water and Urine from Plastic Containers by Solid-Phase Microextraction and Gas Chromatography-Mass Spectrometry," *Analytical Letters*, vol. 44, pp. 676-686, 2011.
- [10] R. Sendón, A. Sanches-Silva, J. Bustos, P. Martín, N. Martínez, and M. E. Cirugeda, "Detection of migration of phthalates from agglomerated cork stoppers using HPLC-MS/MS," *Journal of Separation Science*, vol. 35, pp. 1319-1326, 2012.
- [11] Z. Guo, D. Wei, M. Wang, and S. Wang, "Determination of six phthalic acid esters in orange juice packaged by PVC bottle using SPE and HPLC-UV: Application to the migration study," *Journal of chromatographic science*, vol. 48, pp. 760-765, 2010.
- [12] Who, "WHO | Guidelines for drinking-water quality, fourth edition," World Health Organization 2012-02-21 18:58:44 2011.
- [13] X. L. Cao, "Determination of phthalates and adipate in bottled water by headspace solid-phase microextraction and gas chromatography/mass spectrometry," *Journal of Chromatography A*, vol. 1178, pp. 231-238, 2008.
- [14] J. Li, Y. Cai, Y. Shi, S. Mou, and G. Jiang, "Analysis of phthalates via HPLC-UV in environmental water samples after concentration by solid-phase

- extraction using ionic liquid mixed hemimicelles," *Talanta*, vol. 74, pp. 498-504, 2008.
- [15] F. Tamayo, E. Turiel, and A. Martín-Esteban, "Molecularly imprinted polymers for solid-phase extraction and solid-phase microextraction: Recent developments and future trends," *Journal of Chromatography A*, vol. 1152, pp. 32-40, 2007.
 - [16] J.-P. Lai, M.-L. Yang, R. Niessner, and D. Knopp, "Molecularly imprinted microspheres and nanospheres for di (2-ethylhexyl) phthalate prepared by precipitation polymerization," *Analytical and bioanalytical chemistry*, vol. 389, pp. 405-412, 2007.
 - [17] P. Qi, J. Wang, Y. Li, F. Su, J. Jin, and J. Chen, "Molecularly imprinted solid-phase extraction coupled with HPLC for the selective determination of monobutyl phthalate in bottled water," *Journal of Separation Science*, vol. 34, pp. 2712-2718, 2011.
 - [18] M. Wagner and J. Oehlmann, "Endocrine disruptors in bottled mineral water: total estrogenic burden and migration from plastic bottles," *Environmental Science and Pollution Research*, vol. 16, pp. 278-286, 2009.
 - [19] C. Giam, H. Chan, and G. Neff, "Rapid and inexpensive method for detection of polychlorinated biphenyls and phthalates in air," *Analytical chemistry*, vol. 47, pp. 2319-2320, 1975.
 - [20] D. A. Vignali, "Multiplexed particle-based flow cytometric assays," *Journal of immunological methods*, vol. 243, pp. 243-255, 2000.
 - [21] J. Šmisterová, K. Ensing, and R. De Zeeuw, "Methodological aspects of quantitative receptor assays," *Journal of pharmaceutical and biomedical analysis*, vol. 12, pp. 723-745, 1994.
 - [22] R. Nebel, "On-farm milk progesterone tests," *Journal of dairy science*, vol. 71, pp. 1682-1690, 1988.
 - [23] N. D. Cook, "Scintillation proximity assay: a versatile high-throughput screening technology," *Drug Discovery Today*, vol. 1, pp. 287-294, 1996.
 - [24] T. Jonsson, C. D. Waldburger, and R. T. Sauer, "Nonlinear free energy relationships in Arc repressor unfolding imply the existence of unstable, native-like folding intermediates," *Biochemistry*, vol. 35, pp. 4795-4802, 1996.
 - [25] H. C. Ishikawa-Ankerhold, R. Ankerhold, and G. P. Drummen, "Advanced fluorescence microscopy techniques—Frap, Flip, Flap, Fret and flim," *Molecules*, vol. 17, pp. 4047-4132, 2012.
 - [26] B. S. Watson, T. L. Hazlett, J. F. Eccleston, C. Davis, D. M. Jameson, and A. E. Johnson, "Macromolecular arrangement in the aminoacyl-tRNA. cntdot. elongation factor Tu. cntdot. GTP ternary complex. A fluorescence energy transfer study," *Biochemistry*, vol. 34, pp. 7904-7912, 1995.
 - [27] W. Berger, H. Prinz, J. Striessnig, H.-C. Kang, R. Haugland, and H. Glossmann, "Complex molecular mechanism for dihydropyridine binding to L-type Ca²⁺-channels as revealed by fluorescence resonance energy transfer," *Biochemistry*, vol. 33, pp. 11875-11883, 1994.
 - [28] P. L. Khanna and E. F. Ullman, "4', 5'-Dimethoxy-6-carboxyfluorescein: A novel dipole-dipole coupled fluorescence energy transfer acceptor useful for fluorescence immunoassays," *Analytical biochemistry*, vol. 108, pp. 156-161, 1980.
 - [29] R. M. Clegg, A. Murchie, and D. Lilley, "The solution structure of the four-way DNA junction at low-salt conditions: a fluorescence resonance energy transfer analysis," *Biophysical journal*, vol. 66, pp. 99-109, 1994.

- [30] A. Gagne, P. Banks, and S. Hurt, "Use of fluorescence polarization detection for the measurement of Fluopeptide™ binding to G protein-coupled receptors," *Journal of Receptors and Signal Transduction*, vol. 22, pp. 333-343, 2002.
- [31] T. J. Kowski and J. J. Wu, "Fluorescence polarization is a useful technology for reagent reduction in assay miniaturization," *Combinatorial chemistry & high throughput screening*, vol. 3, pp. 437-444, 2000.
- [32] P. Zuck, Z. Lao, S. Skwish, J. F. Glickman, K. Yang, J. Burbaum, and J. Inglese, "Ligand-receptor binding measured by laser-scanning imaging," *Proceedings of the National Academy of Sciences*, vol. 96, pp. 11122-11127, 1999.
- [33] E. F. Ullman, H. Kirakossian, A. Switchenko, J. Ishkanian, M. Ericson, C. Wartchow, M. Pirio, J. Pease, B. Irvin, and S. Singh, "Luminescent oxygen channeling assay (LOCI): sensitive, broadly applicable homogeneous immunoassay method," *Clinical chemistry*, vol. 42, pp. 1518-1526, 1996.
- [34] M. B. Meza, "Bead-based HTS applications in drug discovery," *Drug Discovery Today*, vol. 5, pp. 38-41, 2000.
- [35] B. Bohn, "Flow cytometry: a novel approach for the quantitative analysis of receptor-ligand interactions on surfaces of living cells," *Molecular and cellular endocrinology*, vol. 20, pp. 1-15, 1980.
- [36] M. Eigen and R. Rigler, "Sorting single molecules: application to diagnostics and evolutionary biotechnology," *Proceedings of the National Academy of Sciences*, vol. 91, pp. 5740-5747, 1994.
- [37] U. Jönsson, L. Fägerstam, S. Löfas, E. Stenberg, R. Karlsson, A. Frostell, F. Markey, and F. Schindler, "Introducing a biosensor based technology for real-time biospecific interaction analysis," in *Annales de biologie clinique*, 1992, pp. 19-26.
- [38] U. Jönsson, L. Fägerstam, B. Ivarsson, B. Johnsson, R. Karlsson, K. Lundh, S. Löfås, B. Persson, H. Roos, and I. Rönnberg, "Real-time biospecific interaction analysis using surface plasmon resonance and a sensor chip technology," *Biotechniques*, vol. 11, pp. 620-627, 1991.
- [39] S. Subrahmanyam, S. A. Piletsky, and A. P. Turner, "Application of natural receptors in sensors and assays," *Analytical chemistry*, vol. 74, pp. 3942-3951, 2002.
- [40] W. D. Wilson, "Analyzing biomolecular interactions," *Science*, vol. 295, pp. 2103-2105, 2002.
- [41] J. E. Gestwicki, H. V. Hsieh, and J. B. Pitner, "Using receptor conformational change to detect low molecular weight analytes by surface plasmon resonance," *Analytical chemistry*, vol. 73, pp. 5732-5737, 2001.
- [42] D. Kröger, F. Hucho, and H. Vogel, "Ligand binding to nicotinic acetylcholine receptor investigated by surface plasmon resonance," *Analytical chemistry*, vol. 71, pp. 3157-3165, 1999.
- [43] E. L. Schmid, A.-P. Tairi, R. Hovius, and H. Vogel, "Screening ligands for membrane protein receptors by total internal reflection fluorescence: the 5-HT3 serotonin receptor," *Analytical chemistry*, vol. 70, pp. 1331-1338, 1998.
- [44] D. Axelrod, T. P. Burghardt, and N. L. Thompson, "Total internal reflection fluorescence," *Annual review of biophysics and bioengineering*, vol. 13, pp. 247-268, 1984.
- [45] D. Axelrod, E. H. Hellen, and R. M. Fulbright, "Total internal reflection fluorescence," in *Topics in fluorescence spectroscopy*, ed: Springer, 2002, pp. 289-343.

- [46] N. D. Käppel, F. Pröll, and G. Gauglitz, "Development of a TIRF-based biosensor for sensitive detection of progesterone in bovine milk," *Biosensors and Bioelectronics*, vol. 22, pp. 2295-2300, 2007.
- [47] U. Jönsson, M. Malmqvist, and I. Ronnberg, "Adsorption of immunoglobulin G, protein A, and fibronectin in the submonolayer region evaluated by a combined study of ellipsometry and radiotracer techniques," *Journal of colloid and interface science*, vol. 103, pp. 360-372, 1985.
- [48] M. Stenberg and H. Nygren, "A receptor-ligand reaction studied by a novel analytical tool—the isoscope ellipsometer," *Analytical biochemistry*, vol. 127, pp. 183-192, 1982.
- [49] B. Meyer and T. Peters, "NMR spectroscopy techniques for screening and identifying ligand binding to protein receptors," *Angewandte Chemie International Edition*, vol. 42, pp. 864-890, 2003.
- [50] C. A. Lepre, J. M. Moore, and J. W. Peng, "Theory and applications of NMR-based screening in pharmaceutical research," *Chemical reviews*, vol. 104, pp. 3641-3676, 2004.
- [51] B. R. Eggins, *Chemical sensors and biosensors* vol. 28: John Wiley & Sons, 2008.
- [52] D. Pritchard, H. Morgan, and J. Cooper, "Simultaneous determination of follicle stimulating hormone and luteinising hormone using a multianalyte immunosensor," *Analytica chimica acta*, vol. 310, pp. 251-256, 1995.
- [53] L. Watson, P. Maynard, D. Cullen, R. Sethi, J. Brettle, and C. Lowe, "A microelectronic conductimetric biosensor," *Biosensors*, vol. 3, pp. 101-115, 1988.
- [54] C. G. Fox and J. F. Alder, "Surface acoustic wave sensors for atmospheric gas monitoring. A review," *Analyst*, vol. 114, pp. 997-1004, 1989.
- [55] M. Nieuwenhuizen, A. Nederlof, M. Vellekoop, and A. Venema, "Preliminary results with a silicon-based surface acoustic wave chemical sensor for NO₂," *Sensors and Actuators*, vol. 19, pp. 385-392, 1989.
- [56] E. Gizeli, N. J. Goddard, C. R. Lowe, and A. C. Stevenson, "A Love plate biosensor utilising a polymer layer," *Sensors and Actuators B: Chemical*, vol. 6, pp. 131-137, 1992.
- [57] P. J. Edmonson, W. D. Hunt, D. D. Stubbs, and S.-H. Lee, "Analogies between digital radio and chemical orthogonality as a method for enhanced analysis of molecular recognition events," *International journal of molecular sciences*, vol. 9, pp. 154-168, 2008.
- [58] A. Voller, D. E. Bidwell, and A. Bartlett, *The enzyme linked immunosorbent assay (ELISA). A guide with abstracts of microplate applications*: Dynatech Europe, Borough House, Rue du Pre., 1979.
- [59] E. J. Olson and P. Buhlmann, "Minimizing hazardous waste in the undergraduate analytical laboratory: a microcell for electrochemistry," *Journal of Chemical Education*, vol. 87, pp. 1260-1261, 2010.
- [60] M. Khafaji, S. Shahrokhian, and M. Ghalkhani, "Electrochemistry of Levo-Thyroxin on Edge-Plane Pyrolytic Graphite Electrode: Application to Sensitive Analytical Determinations," *Electroanalysis*, vol. 23, pp. 1875-1880, 2011.
- [61] J. Fischer, H. Dejmekova, and J. Barek, "Electrochemistry of pesticides and its analytical applications," *Current Organic Chemistry*, vol. 15, pp. 2923-2935, 2011.

- [62] C. Valero Vidal and A. Igual Muñoz, "Effect of physico-chemical properties of simulated body fluids on the electrochemical behaviour of CoCrMo alloy," *Electrochimica Acta*, vol. 56, pp. 8239-8248, 2011.
- [63] C. Wolner, G. E. Nauer, J. Trummer, V. Putz, and S. Tschegg, "Possible reasons for the unexpected bad biocompatibility of metal-on-metal hip implants," *Materials Science and Engineering: C*, vol. 26, pp. 34-40, 2006.
- [64] C. Xhoffer, K. Van den Bergh, and H. Dillen, "Electrochemistry: a powerful analytical tool in steel research," *Electrochimica Acta*, vol. 49, pp. 2825-2831, 2004.
- [65] J. R. Macdonald, "Impedance spectroscopy," *Annals of biomedical engineering*, vol. 20, pp. 289-305, 1992.
- [66] S. C. Mukhopadhyay, C. P. Gooneratne, G. S. Gupta, and S. N. Demidenko, "A low-cost sensing system for quality monitoring of dairy products," *Instrumentation and Measurement, IEEE Transactions on*, vol. 55, pp. 1331-1338, 2006.
- [67] S. C. Mukhopadhyay and C. P. Gooneratne, "A novel planar-type biosensor for noninvasive meat inspection," *Sensors Journal, IEEE*, vol. 7, pp. 1340-1346, 2007.
- [68] S. Mukhopadhyay, S. D. Choudhury, T. Allsop, V. Kasturi, and G. Norris, "Assessment of pelt quality in leather making using a novel non-invasive sensing approach," *Journal of biochemical and biophysical methods*, vol. 70, pp. 809-815, 2008.
- [69] S. C. Mukhopadhyay, G. S. Gupta, J. D. Woolley, and S. N. Demidenko, "Saxophone reed inspection employing planar electromagnetic sensors," *Instrumentation and Measurement, IEEE Transactions on*, vol. 56, pp. 2492-2503, 2007.
- [70] M. S. A. Rahman, S. C. Mukhopadhyay, P. L. Yu, J. Goicoechea, I. R. Matias, C. P. Gooneratne, and J. Kosel, "Detection of Bacterial Endotoxin in Food: New Planar Interdigital Sensors based Approach," *Journal of Food Engineering*.
- [71] M. Rahman, S. B. Abdul, S. C. Mukhopadhyay, and P. L. Yu, "Novel Sensors for Food Inspections," *Sensors & Transducers (1726-5479)*, vol. 114, 2010.
- [72] A. Mohd Syaifudin, S. Mukhopadhyay, P. Yu, C. H. Chuang, H. P. Wu, C. P. Gooneratne, and J. Kosel, "Characterizations and performance evaluations of thin film interdigital sensors for Gram-negative bacteria detection," 2011, pp. 181-186.
- [73] A. Mohd Syaifudin, S. Mukhopadhyay, P. Yu, M. J. Haji-Sheikh, C. H. Chuang, and H. P. Wu, "Detection of natural bio-toxins using an improved design interdigital sensors," 2011, pp. 1028-1031.
- [74] A. Mohd Syaifudin, S. Mukhopadhyay, and P. Yu, "Modelling and fabrication of optimum structure of novel interdigital sensors for food inspection," *International Journal of Numerical Modelling: Electronic Networks, Devices and Fields*, vol. 25, pp. 64-81, 2012.
- [75] M. S. Abdul Rahman, S. C. Mukhopadhyay, P.-L. Yu, J. Goicoechea, I. R. Matias, C. P. Gooneratne, and J. Kosel, "Detection of bacterial endotoxin in food: New planar interdigital sensors based approach," *Journal of Food Engineering*, vol. 114, pp. 346-360, 2013.
- [76] A. I. Zia, A. R. Mohd Syaifudin, S. C. Mukhopadhyay, I. H. Al-Bahadly, P. L. Yu, C. P. Gooneratne, J. Kosel, and T.-S. Liao, "MEMS based impedimetric sensing of phthalates," in *Instrumentation and Measurement Technology Conference (I2MTC), 2013 IEEE International*, 2013, pp. 855-860.

- [77] E. Barsoukov and J. R. Macdonald, *Impedance spectroscopy: theory, experiment, and applications*: Wiley-Interscience, 2005.
- [78] B.-Y. Chang and S.-M. Park, "Electrochemical impedance spectroscopy," *Annual Review of Analytical Chemistry*, vol. 3, pp. 207-229, 2010.
- [79] J. E. B. Randles, "Kinetics of rapid electrode reactions," *Discussions of the Faraday Society*, vol. 1, pp. 11-19, 1947.
- [80] X. B. Li, S. D. Larson, A. S. Zyuzin, and A. V. Mamishev, "Design principles for multichannel fringing electric field sensors," *Sensors Journal, IEEE*, vol. 6, pp. 434-440, 2006.
- [81] S. E. Creager, L. A. Hockett, and G. K. Rowe, "Consequences of microscopic surface roughness for molecular self-assembly," *Langmuir*, vol. 8, pp. 854-861, 1992.
- [82] S. M. Radke and E. C. Alocilja, "A microfabricated biosensor for detecting foodborne bioterrorism agents," *Sensors Journal, IEEE*, vol. 5, pp. 744-750, 2005.
- [83] D. Grieshaber, R. MacKenzie, J. Voros, and E. Reimhult, "Electrochemical biosensors - Sensor principles and architectures," *Sensors*, vol. 8, pp. 1400-1458, Mar 2008.
- [84] L. Ianeselli, G. Grenzi, C. Callegari, M. Tormen, and L. Casalis, "Development of Stable and Reproducible Biosensors based on Electrochemical Impedance Spectroscopy: Three-Electrode versus Two-Electrode Setup," *Biosensors and Bioelectronics*, 2013.
- [85] M. Kitsara, D. Goustouridis, S. Chatzandroulis, M. Chatzichristidi, I. Raptis, T. Ganetsos, R. Igreja, and C. Dias, "Single chip interdigitated electrode capacitive chemical sensor arrays," *Sensors and Actuators B: Chemical*, vol. 127, pp. 186-192, 2007.
- [86] J. Rairden, C. Neugebauer, and R. Sigsbee, "Interdiffusion in thin conductor films—chromium/gold, nickel/gold and chromium silicide/gold," *Metallurgical Transactions*, vol. 2, pp. 719-722, 1971.
- [87] V. Švorčík, O. Kvítek, O. Lyutakov, J. Siegel, and Z. Kolská, "Annealing of sputtered gold nano-structures," *Applied Physics A*, vol. 102, pp. 747-751, 2011.
- [88] A. Zia, S. Mukhopadhyay, P. Yu, I. Al-Bahadly, C. Gooneratne, and J. Kosel, "Post Annealing Performance Evaluation of Printable Interdigital Capacitive Sensors by Principal Component Analysis," *Sensors Journal, IEEE*, vol. PP, pp. 1-1, 2014.
- [89] E. C. Hioki, "HIOKI 3532-50 LCR HITESTER Instruction Manual [Z]," *JAPAN. HIOKI EE CORPORATION*, 2001.
- [90] F. Lisdat and D. Schäfer, "The use of electrochemical impedance spectroscopy for biosensing," *Analytical and bioanalytical chemistry*, vol. 391, pp. 1555-1567, 2008.
- [91] Y. X. Wang, Z. Z. Ye, and Y. B. Ying, "New Trends in Impedimetric Biosensors for the Detection of Foodborne Pathogenic Bacteria," *Sensors*, vol. 12, pp. 3449-3471, Mar 2012.
- [92] D. D. Macdonald, "Reflections on the history of electrochemical impedance spectroscopy," *Electrochimica Acta*, vol. 51, pp. 1376-1388, 2006.
- [93] D. Hyman and M. Mehregany, "Contact physics of gold microcontacts for MEMS switches," *Components and Packaging Technologies, IEEE Transactions on*, vol. 22, pp. 357-364, 1999.

- [94] J. M. Delgado, J. M. Orts, J. M. Pérez, and A. Rodes, "Sputtered thin-film gold electrodes for in situ ATR-SEIRAS and SERS studies," *Journal of Electroanalytical Chemistry*, vol. 617, pp. 130-140, 2008.
- [95] M. Giesen, G. Beltramo, S. Dieluweit, J. Müller, H. Ibach, and W. Schmickler, "The thermodynamics of electrochemical annealing," *Surface science*, vol. 595, pp. 127-137, 2005.
- [96] V. Švorčík, J. Siegel, P. Šutta, J. Mistrík, P. Janíček, P. Worsch, and Z. Kolská, "Annealing of gold nanostructures sputtered on glass substrate," *Applied Physics A*, vol. 102, pp. 605-610, 2011.
- [97] A. I. Zia, M. S. A. Rahman, S. C. Mukhopadhyay, P.-L. Yu, I. Al-Bahadly, C. P. Gooneratne, J. Kosel, and T.-S. Liao, "Technique for Rapid Detection of Phthalates in Water and Beverages," *Journal of Food Engineering*, 2013.
- [98] A. Miszczyk and K. Darowicki, "Multispectral impedance quality testing of coil-coating system using principal component analysis," *Progress in Organic Coatings*, vol. 69, pp. 330-334, 2010.
- [99] M. A. M. Yunus, S. C. Mukhopadhyay, and S. Ibrahim, "Planar electromagnetic sensor based estimation of nitrate contamination in water sources using independent component analysis," *Sensors Journal, IEEE*, vol. 12, pp. 2024-2034, 2012.
- [100] K. Pearson, "LIII. On lines and planes of closest fit to systems of points in space," *The London, Edinburgh, and Dublin Philosophical Magazine and Journal of Science*, vol. 2, pp. 559-572, 1901.
- [101] H. Hotelling, "Analysis of a complex of statistical variables into principal components," *Journal of educational psychology*, vol. 24, p. 417, 1933.
- [102] I. Jolliffe, *Principal component analysis*: Wiley Online Library, 2005.
- [103] H.-R. Tränkler, O. Kanoun, M. Min, and M. Rist, "Smart sensor systems using impedance spectroscopy," *Proc. Estonian Acad. Sci. Eng*, vol. 13, pp. 455-478, 2007.
- [104] A. Mohd Syaifudin, S. C. Mukhopadhyay, P.-L. Yu, M. J. Haji-Sheikh, C.-H. Chuang, J. D. Vanderford, and Y.-W. Huang, "Measurements and performance evaluation of novel interdigital sensors for different chemicals related to food poisoning," *Sensors Journal, IEEE*, vol. 11, pp. 2957-2965, 2011.
- [105] C. A. Olivati, A. Riul Jr, D. T. Balogh, O. N. Oliveira Jr, and M. Ferreira, "Detection of phenolic compounds using impedance spectroscopy measurements," *Bioprocess and biosystems engineering*, vol. 32, pp. 41-46, 2009.
- [106] A. I. Zia, M. S. A. Rahman, S. C. Mukhopadhyay, P.-L. Yu, I. Al-Bahadly, C. P. Gooneratne, J. Kosel, and T.-S. Liao, "Technique for rapid detection of phthalates in water and beverages," *Journal of Food Engineering*, vol. 116, pp. 515-523, 2013.
- [107] M. a. E. Allende, "Mean versus individual hormonal profiles in the menstrual cycle," *Fertility and sterility*, vol. 78, pp. 90-95, 2002.
- [108] L. F. Blackwell, J. B. Brown, and D. Cooke, "Definition of the potentially fertile period from urinary steroid excretion rates. Part II. A threshold value for pregnanediol glucuronide as a marker for the end of the potentially fertile period in the human menstrual cycle," *Steroids*, vol. 63, pp. 5-13, 1998.
- [109] W. H. Organization, "Temporal relationships between indices of the fertile period," *Fertility and sterility*, vol. 39, pp. 647-654, 1983.
- [110] W. P. Collins, "The evolution of reference methods to monitor ovulation," *Am J Obstet Gynecol*, vol. 165, pp. 1994-6, 1991.

- [111] G. Freundl, I. Sivin, and I. Batár, "State-of-the-art of non-hormonal methods of contraception: IV. Natural family planning," *The European Journal of Contraception and Reproductive Health Care*, vol. 15, pp. 113-123, 2010.
- [112] M. C. Weissmann, L. Foliaki, E. Billings, and J. Billings, "A trial of the ovulation method of family planning in Tonga," *The Lancet*, vol. 300, pp. 813-816, 1972.
- [113] J. Brown, L. Blackwell, J. Holmes, and K. Smyth, "New assays for identifying the fertile period," *Supplement to International journal of gynecology and obstetrics*, vol. 1, p. 111, 1989.
- [114] J. B. Brown, J. Holmes, and G. Barker, "Use of the Home Ovarian Monitor in pregnancy avoidance," *Am J Obstet Gynecol*, vol. 165, pp. 2008-11, 1991.
- [115] L. F. Blackwell, J. B. Brown, P. Vigil, B. Gross, S. Sufi, and C. d'Arcangues, "Hormonal monitoring of ovarian activity using the Ovarian Monitor, Part I. Validation of home and laboratory results obtained during ovulatory cycles by comparison with radioimmunoassay," *Steroids*, vol. 68, pp. 465-476, 2003.
- [116] M. I. Prodromidis, "Impedimetric immunosensors--A review," *Electrochimica Acta*, vol. 55, pp. 4227-4233, 2010.
- [117] A. Zia, S.C. Mukhopadhyay, P.L.Yu, I. H. Al Bahadly, "Ovarian Hormone Estrone Glucuronide (E1G) Quantification- Impedimetric Electrochemical Spectroscopy Approach," in *Sensing Technology (ICST), 2013 Seventh International Conference on*, 2013, pp. 22 - 27.
- [118] P. Senger, "The estrus detection problem: new concepts, technologies, and possibilities," *Journal of dairy science*, vol. 77, pp. 2745-2753, 1994.
- [119] E. Strandberg and P. A. Oltenacu, "Economic consequences of different calving intervals," *Acta Agriculturae Scandinavica*, vol. 39, pp. 407-420, 1989.
- [120] J. Laing and R. Heap, "The concentration of progesterone in the milk of cows during the reproductive cycle," *The British veterinary journal*, vol. 127, pp. xix-xxii, 1971.
- [121] G. Otava, C. Mircu, H. Cernescu, and V. Igna, "Comparative relations between progesterone blood concentration and appearance of oestrus in cows," *Veterinarski glasnik*, vol. 61, pp. 37-42, 2007.
- [122] R. Koelsch, D. Aneshansley, and W. Butler, "Milk progesterone sensor for application with dairy cattle," *Journal of agricultural engineering research*, vol. 58, pp. 115-120, 1994.
- [123] M. G. Diskin and J. M. Sreenan, "Expression and detection of oestrus in cattle," *Reprod. Nutr. Dev*, vol. 40, pp. 481-491, 2000.
- [124] Y. Wu, J. Mitchell, C. Cook, and L. Main, "Evaluation of progesterone-ovalbumin conjugates with different length linkers in enzyme-linked immunosorbant assay and surface plasmon resonance-based immunoassay," *Steroids*, vol. 67, pp. 565-572, 2002.
- [125] H. RJ, G. JE, L. JA, and W. DE, "Pregnancy diagnosis in the cow from milk progesterone concentration," *British Veterinary Journal*, vol. 132, pp. 445-464, 1976.
- [126] R. W. Claycomb, M. J. Delwiche, C. J. Munro, and R. H. BonDurant, "Rapid enzyme immunoassay for measurement of bovine progesterone," *Biosensors and Bioelectronics*, vol. 13, pp. 1165-1171, 1998.
- [127] M. Laitinen and M. Vuento, "Affinity immunosensor for milk progesterone: identification of critical parameters," *Biosensors and Bioelectronics*, vol. 11, pp. 1207-1214, 1996.

- [128] A. I. Zia, A. Mohd Syaifudin, S. Mukhopadhyay, P. Yu, I. Al-Bahadly, J. Kosel, and C. Gooneratne, "Sensor and instrumentation for progesterone detection," in *Instrumentation and Measurement Technology Conference (I2MTC), 2012 IEEE International*, 2012, pp. 1220-1225.
- [129] U. Heudorf, V. Mersch-Sundermann, and J. Angerer, "Phthalates: toxicology and exposure," *International journal of hygiene and environmental health*, vol. 210, pp. 623-634, 2007.
- [130] R. Hauser, S. Duty, L. Godfrey-Bailey, and A. M. Calafat, "Medications as a source of human exposure to phthalates," *Environmental health perspectives*, vol. 112, p. 751, 2004.
- [131] Usepsc, "Toxicity Review of DEHP," Bethesda, MD, USA2010.
- [132] V. Triantafyllou, K. Akrida-Demertzi, and P. Demertzis, "A study on the migration of organic pollutants from recycled paperboard packaging materials to solid food matrices," *Food Chemistry*, vol. 101, pp. 1759-1768, 2007.
- [133] J. Yang, R. Hauser, and R. H. Goldman, "Taiwan food scandal: The illegal use of phthalates as a clouding agent and their contribution to maternal exposure," *Food and Chemical Toxicology*, vol. 58, pp. 362-368, 2013.
- [134] A. Schecter, M. Lorber, Y. Guo, Q. Wu, S. H. Yun, K. Kannan, M. Hommel, N. Imran, L. S. Hynan, and D. Cheng, "Phthalate concentrations and dietary exposure from food purchased in New York State," *Environmental health perspectives*, vol. 121, p. 473, 2013.
- [135] J. D. Meeker, A. M. Calafat, and R. Hauser, "Di (2-ethylhexyl) phthalate metabolites may alter thyroid hormone levels in men," *Environmental health perspectives*, vol. 115, p. 1029, 2007.
- [136] H. M. Koch, R. Preuss, and J. Angerer, "Di (2-ethylhexyl) phthalate (DEHP): human metabolism and internal exposure—an update and latest results1," *International journal of andrology*, vol. 29, pp. 155-165, 2006.
- [137] A. D. LaFleur and K. A. Schug, "A review of separation methods for the determination of estrogens and plastics-derived estrogen mimics from aqueous systems," *Analytica chimica acta*, vol. 696, pp. 6-26, 2011.
- [138] S. Hird, "Mass Spectrometry in Food Safety: Methods and Protocols Methods in Molecular Biology, Vol. 747 Jerry Zweigenbaum (Editor): Springer Verlag, New York ISBN: 978-61779-135-2 PRICE: \$139.00: 416 pages," *Rapid Communications in Mass Spectrometry*, vol. 26, pp. 1162-1164, May 15 2012.
- [139] Z. Kerner and T. Pajkossy, "Measurement of adsorption rates of anions on Au (111) electrodes by impedance spectroscopy," *Electrochimica Acta*, vol. 47, pp. 2055-2063, 2002.
- [140] A. I. Zia, A. M. Syaifudin, S. Mukhopadhyay, P. Yu, I. Al-Bahadly, C. P. Gooneratne, J. Kosel, and T.-S. Liao, "Electrochemical impedance spectroscopy based MEMS sensors for phthalates detection in water and juices," *Journal of Physics: Conference Series*, vol. 439, p. 012026, 2013.
- [141] K. Cammann, B. Ross, A. Katerkamp, J. Reinbold, B. Gründig, and R. Renneberg, "Chemical and biochemical sensors," *Ullmann's Encyclopedia of Industrial Chemistry*, 1994.
- [142] M. E. Tess and J. A. Cox, "Chemical and biochemical sensors based on advances in materials chemistry," *Journal of pharmaceutical and biomedical analysis*, vol. 19, pp. 55-68, 1999.
- [143] S. Shtykov and T. Y. Rusanova, "Nanomaterials and nanotechnologies in chemical and biochemical sensors: capabilities and applications," *Russian Journal of General Chemistry*, vol. 78, pp. 2521-2531, 2008.

- [144] B. Adhikari and S. Majumdar, "Polymers in sensor applications," *Progress in polymer science*, vol. 29, pp. 699-766, 2004.
- [145] T. Panasyuk-Delaney, V. M. Mirsky, M. Ulbricht, and O. S. Wolfbeis, "Impedometric herbicide chemosensors based on molecularly imprinted polymers," *Analytica chimica acta*, vol. 435, pp. 157-162, 2001.
- [146] A. Merkoci and S. Alegret, "New materials for electrochemical sensing IV. Molecular imprinted polymers," *TrAC Trends in Analytical Chemistry*, vol. 21, pp. 717-725, 2002.
- [147] V. B. Kandimalla and H. Ju, "Molecular imprinting: a dynamic technique for diverse applications in analytical chemistry," *Analytical and bioanalytical chemistry*, vol. 380, pp. 587-605, 2004.
- [148] C. Alexander, H. S. Andersson, L. I. Andersson, R. J. Ansell, N. Kirsch, I. A. Nicholls, J. O'Mahony, and M. J. Whitcombe, "Molecular imprinting science and technology: a survey of the literature for the years up to and including 2003," *Journal of molecular recognition*, vol. 19, pp. 106-180, 2006.
- [149] H. Shaikh, N. Memon, H. Khan, M. Bhangar, and S. Nizamani, "Preparation and characterization of molecularly imprinted polymer for di (2-ethylhexyl) phthalate: Application to sample clean-up prior to gas chromatographic determination," *Journal of Chromatography A*, 2012.
- [150] K. Yongfeng, D. Wuping, L. Yan, K. Junxia, and X. Jing, "Molecularly imprinted polymers of allyl- β -cyclodextrin and methacrylic acid for the solid-phase extraction of phthalate," *Carbohydrate Polymers*, vol. 88, pp. 459-464, 2012.
- [151] L. Ye and K. Mosbach, "Molecular Imprinting: Synthetic Materials As Substitutes for Biological Antibodies and Receptors†," *Chemistry of Materials*, vol. 20, pp. 859-868, 2008.
- [152] A. Bossi, F. Bonini, A. Turner, and S. Piletsky, "Molecularly imprinted polymers for the recognition of proteins: the state of the art," *Biosensors and Bioelectronics*, vol. 22, pp. 1131-1137, 2007.
- [153] A. Mayes and M. Whitcombe, "Synthetic strategies for the generation of molecularly imprinted organic polymers," *Advanced Drug Delivery Reviews*, vol. 57, pp. 1742-1778, 2005.
- [154] H. Yan, X. Cheng, and G. Yang, "Dummy Molecularly Imprinted Solid-Phase Extraction for Selective Determination of Five Phthalate Esters in Plastic Bottled Functional Beverages," *Journal of agricultural and food chemistry*, vol. 60, pp. 5524-5531, 2012.
- [155] G. Díaz-Díaz, D. Antuña-Jiménez, M. Carmen Blanco-López, M. Jesús Lobo-Castañón, A. J. Miranda-Ordieres, and P. Tuñón-Blanco, "New materials for analytical biomimetic assays based on affinity and catalytic receptors prepared by molecular imprinting," *TrAC Trends in Analytical Chemistry*, vol. 33, pp. 68-80, 2012.
- [156] G. Sun, P. Wang, S. Ge, L. Ge, J. Yu, and M. Yan, "Photoelectrochemical sensor for pentachlorophenol on microfluidic paper-based analytical device based on molecular imprinting technique," *Biosensors and Bioelectronics*, 2014.
- [157] J. Wolska and M. Bryjak, "Sorption of phthalates on molecularly imprinted polymers," *Separation science and technology*, vol. 47, pp. 1316-1321, 2012.
- [158] J. He, R. Lv, J. Zhu, and K. Lu, "Selective solid-phase extraction of dibutyl phthalate from soybean milk using molecular imprinted polymers," *Analytica chimica acta*, vol. 661, pp. 215-221, 2010.

- [159] A. I. Zia, S. C. Mukhopadhyay, P.-L. Yu, I. Al-Bahadly, C. P. Gooneratne, and J. Kosel, "Rapid and molecular selective electrochemical sensing of phthalates in aqueous solution," *Biosensors and Bioelectronics*, vol. 64, pp 342-349, 2014.